Mechanisms underlying potentiation of murine airway smooth muscle contraction by activation of postjunctional M2 muscarinic receptors

A thesis submitted to the

School of Health and Science,

Dundalk Institute of Technology

For the degree of **Doctor of Philosophy**

By

Srijit Ghosh M.S. (Pharm)

March 2026

Under the supervision of **Professor Gerard P. Sergeant** &

Co-supervision of **Professor Keith Thornbury**,

Smooth Muscle Research Centre, Dundalk Institute of Technology

Declaration

We, the undersigned declare that this thesis entitled “Mechanisms underlying potentiation of murine airway smooth muscle contraction by activation of postjunctional M2 muscarinic receptors”, is entirely the author’s own work and has not been taken from the work of others, except as cited and acknowledged within the text.

The thesis has been prepared according to the regulations of Dundalk Institute of Technology and has not been submitted in whole or in part for an award in this or any other institution.

Author Name: Srijit Ghosh

Author Signature: 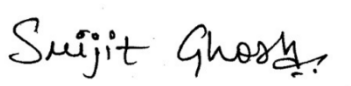

Date: 13/04/2026

Supervisor Name: Prof. Gerard P. Sergeant

Supervisor Signature: 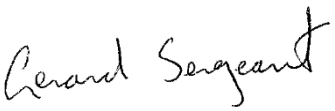

Date: 13/04/2026

Table of contents

Acknowledgements

I am grateful for the opportunity to thank the contributions of many people who have been inspirational and encouraging during my career and have provided me with the most valuable knowledge to help me succeed in my endeavours, as well as for making my PhD journey unique and memorable.

First of all, I would like to thank my PhD supervisor, Prof. Gerard P. Sergeant, for his guidance, support and encouragement throughout this research journey. His patience and continuous trust in me and in the project have been key to the successful completion of this work. I would also like to thank Prof. Keith Thornbury and Prof. Mark Hollywood for their valuable advice and suggestions during the course of this project.

I would like to say thank you to Billie McIlveen for her technical help and support at SMRC. I am grateful to our postdoc, Dr. Kaneez Rabab, for her help and insightful discussions and for teaching molecular biology techniques. A special thanks to Dr. Caoimhin Griffin and Dr. Bernard Drumm for their expertise, guidance and support.

I am deeply thankful to my colleagues Sai Neeraj Palakurthy, Mitchell Mercer, Alexandru Mircea, Zainab Baig and Neha Gupta for all the fun and motivation. You were like a family over the last three years. Sharing the lab with you was truly enjoyable. I still remember the late night funny arguments and discussions about patching and Kv7 channels with Mitchell and Neeraj in the lab. In the later years, Shubhendu and Denzel joined the lab and also became great friends, and I am thankful for the many productive discussions and good times we shared. I would also like to thank all past students at SMRC, especially Dr. Tuleen Alkawadri, for teaching me essential techniques and introducing me to the field of airway smooth muscle.

This DCU-DkIT graduate programme was funded by HEA TUTF Ireland, and I sincerely appreciate the financial support provided to complete my research studies. I am also grateful to the DkIT Research Office for its contributions.

I am also thankful to my supportive parents and grandparents for their constant encouragement, even from miles away. Eventually, I am profoundly grateful to my fiancée, Debleena Mitra, who has stood beside me through every high and low. Your support, motivation and belief in me never wavered. You have held my hand through the triumphs and challenges of the past three years, always ready to encourage or reassure when needed. I will never find enough words to express my gratitude for your love and support. You have made this chapter of my life truly memorable. Therefore, I dedicate this thesis to my family.

Above all, I am grateful to the Almighty for giving me strength, good health and knowledge to complete my work. Finally, I owe my sincere gratitude to all the innocent animals who sacrificed their lives for the sake of mankind.

Abbreviations

$[Ca^{2+}]_i$	Intracellular Calcium Concentration
4-DAMP	1,1-Dimethyl-4-diphenylacetoxypiperidinium iodide
6-MB cAMP	6-Monobutyryl Cyclic AMP
α-SMA	Alpha Smooth Muscle Actin
µl	Microlitre
µM	Micromolar
τ	Deactivation Time Constant
ACh	Acetylcholine
AChE	Acetylcholinesterase
AHR	Airway Hyperresponsiveness
ANO1	Anoctamin 1
ANOVA	Analysis Of Variance
ASM	Airway Smooth Muscle
AT1	Angiotensin II Receptor Type 1
AT2	Angiotensin II Receptor Type 2
AUC	Area Under Curve
BH_4	Tetrahydrobiopterin
BK_{Ca}	Large Conductance Calcium-Activated Potassium Channel
BSA	Bovine Serum Albumin
Ca^{2+}	Calcium Ion
CaCC	Calcium-Activated Chloride Channel
cAMP	Cyclic AMP
CCB	Calcium Channel Blocker
CCh	Carbachol
CCL2	C-C Motif Chemokine Ligand 2
CCR3	C-C Chemokine Receptor 3
cDNA	Complementary DNA
cGMP	Cyclic GMP
CHO	Chinese Hamster Ovary Cells
Cl^-	Chloride Ion
CO_2	Carbon Dioxide
COPD	Chronic Obstructive Pulmonary Disease
COX	Cyclooxygenase

CPI-17	Protein Kinase C Potentiated Inhibitor 17
CRAC	Calcium Release Activated Calcium Channels
CSE	Cigarette Smoke Extract
CysLT	Cysteinyl Leukotrienes
DAG	Diacylglycerol
DMEM	Dulbecco Modified Eagle Medium
DMSO	Dimethyl Sulfoxide
dNTP	Deoxynucleotide Triphosphate
EC	Endothelial Cell
ECM	Extracellular Matrix
ECP	Eosinophil Cationic Protein
EDN	Eosinophil-Derived Neurotoxin
EDTA	Ethylenediaminetetraacetic Acid
EFS	Electrical Field Stimulation
E_{Cl}	Chloride equilibrium potential
E_K	Potassium Equilibrium Potential
E_m	Membrane Potential
eNOS	Endothelial Nitric Oxide Synthase
EPAC	Exchange Protein Activated by Camp
EPO	Erythropoietin
FAD	Flavin Adenine Dinucleotide
FBS	Fetal Bovine Serum
FEV1	Forced Expiratory Volume in One Second
FMN	Flavin Mononucleotide
FRC	Functional Residual Capacity
FVC	Forced Vital Capacity
G	Conductance
GC	Guanylyl Cyclase
GEF	Guanine Nucleotide Exchange Factor
G_{max}	Maximum Conductance
GOI	Gene Of Interest
GOLD	Global Initiative for Obstructive Lung Disease
H1R	Histamine H1 Receptor
HEK293	Human Embryonic Kidney 293 Cells

Hz	Hertz
IFN gamma	Interferon Gamma
IgE	Immunoglobulin E
IKCa	Intermediate Conductance Calcium-Activated Potassium Channel
IL	Interleukin
iNOS	Inducible Nitric Oxide Synthase
IP_3	Inositol Trisphosphate
IP_3R	Inositol Trisphosphate Receptor
K^+	Potassium Ion
KCl	Potassium Chloride
KCNE	Potassium Channel Ancillary Subunit
KO	Knockout
LABA	Long Acting Beta Agonist
LAMA	Long Acting Muscarinic Antagonist
LTCC	L-Type Calcium Channel
M2R	Muscarinic M2 Receptor
M3R	Muscarinic M3 Receptor
MBP	Myelin Basic Protein
mICAT	Muscarinic Receptor-Induced Calcium-Activated Transient
MLC	Myosin Light Chain
MLCK	Myosin Light Chain Kinase
mN	Millinewton
MUC5AC	Mucin 5AC
mV	Millivolt
MYPT	Myosin Phosphatase Target Subunit
Na^+	Sodium Ion
nAChR	Nicotinic Acetylcholine Receptor
NANC	Non Adrenergic Non Cholinergic
NET	Norepinephrine Transporter
NO	Nitric Oxide
NPY	Neuropeptide Y
NTC	No Template Control
O_2	Oxygen
°C	Degree Celsius

PBS	Phosphate Buffered Saline
PD	Pore Domains
PDGF	Platelet Derived Growth Factor
PFA	Paraformaldehyde
PIP_2	Phosphatidylinositol 4,5-Bisphosphate
PKA	Protein Kinase A
PKC	Protein Kinase C
PKG	Protein Kinase G
PLB	Phospholamban
PLC beta	Phospholipase C Beta
pS	Picosiemens
PTX	Pertussis Toxin
qPCR	Quantitative PCR
qRT-PCR	Quantitative Reverse Transcription PCR
R	Resistance
R_a	Access Resistance
R_m	Membrane Resistance
ROCK	Rho Associated Protein Kinase
ROS	Reactive Oxygen Species
RPM	Revolutions Per Minute
R_s	Series Resistance
RyR	Ryanodine Receptor
s	Seconds
SBB	Superficial Buffer Barrier
scRNA-seq	Single Cell RNA Sequencing
SEM	Standard Error of Mean
SERCA	Sarcoplasmic/Endoplasmic Reticulum Calcium ATPase
SKCa	Small Conductance Calcium-Activated Potassium Channel
SOCE	Store Operated Calcium Entry
SR	Sarcoplasmic Reticulum
STIM-Orai	STIM-Orai Calcium Entry Pathway
TGF beta	Transforming Growth Factor Beta
TNF alpha	Tumour Necrosis Factor Alpha
TRPA	Transient Receptor Potential Ankyrin

TRPC	Transient Receptor Potential Canonical
TRPM	Transient Receptor Potential Melastatin
TRPN	Transient Receptor Potential No Mechanoreceptor Potential C
TRPNL	Transient Receptor Potential Mucolipin
TRPV	Transient Receptor Potential Vanilloid
TRPY	Transient Receptor Potential Yeast
TSLP	Thymic Stromal Lymphopoietin
TTX	Tetrodotoxin
$V_{1/2}$	Half Activation Voltage
V_{com}	Command Voltage
VDCC	Voltage Dependent Calcium Channel
V_m	Membrane Potential
V_p	Peak Voltage
VSD	Voltage Sensing Domain
VSMC	Vascular Smooth Muscle Cell
WT	Wild Type
XE991	10,10-Bis(4-pyridinylmethyl)-9(10H)-anthracenone dihydrochloride

Abstract

Mechanisms underlying potentiation of murine airway smooth muscle contraction by activation of postjunctional M2 muscarinic receptors

Srijit Ghosh

Postjunctional M2 muscarinic receptors (M2Rs) on airway smooth muscle (ASM) outnumber M3 receptors (M3Rs) by approximately 4:1 in most species, yet M3Rs are classically considered the primary mediators of acetylcholine (ACh)-induced bronchoconstriction. Recent research, however, suggests that M2R stimulation can markedly potentiate ASM contractility. The present study investigated the cellular and ionic mechanisms underlying M2R-dependent potentiation of nerve-evoked contractions of murine ASM using pharmacological and electrophysiological approaches. In contrast to the role of M3Rs, which drive IP_3-dependent Ca^{2+} release from sarcoplasmic reticulum (SR), we demonstrated that M2R-mediated contractions were abolished by the L-type Ca^{2+} channels (LTCC) blocker nifedipine indicating that M2R activation enhanced cholinergic contractions predominantly through Ca^{2+} influx via LTCCs. Further analysis revealed that M2R-LTCC pathway was facilitated by inhibition of Kv7 channels and SR Ca^{2+}-ATPase (SERCA) activity, along with activation of Ano1 Ca^{2+}-activated Cl^- channels.

Potassium channel subtypes Kv7.4 and Kv7.5 were prominently expressed in ASM and M2R activation suppressed Kv7.4 and Kv7.5 currents via depletion of PIP_2 and downregulation of cAMP/PKA, respectively. Inhibition of SERCA pumps with thapsigargin mimicked and potentiated M2R-mediated responses. These effects were also abolished by nifedipine, indicating that M2R activation likely inhibited SERCA activity, reducing subplasmalemmal Ca^{2+} buffering of Ca^{2+} entry via LTCC. Inhibition of Ano1 with Ani9 suppressed M2R responses, indicating an important role for these channels in M2R-dependent contractions. Collectively, these findings provide first comprehensive evidence that M2R activation enhances ASM excitability through a coordinated mechanism involving the inhibition of Kv7 channels and SERCA pumps, as well as the activation of LTCCs and Ano1. This integrated pathway sustains depolarisation and Ca^{2+} influx, contributing to airway hyperresponsiveness. The study identifies Kv7.4/7.5 and SERCA2 as potential therapeutic targets and establishes a mechanistic framework linking M2R signalling to cholinergic airway contraction, offering new avenues for intervention in asthma and chronic obstructive pulmonary disease (COPD).

Publications

Data presented in the study have been communicated as posters and oral presentations in various scientific meetings, as well as published in several scientific journals.

Scientific Journals:

1. Ghosh, S., Alkawadri, T., McGarvey, L. P., Hollywood, M. A., Thornbury, K. D., & Sergeant, G. P. (2025). Role of voltage-gated Ca^{2+} channels and Ano1 Ca^{2+}-activated Cl^- channels in M2 muscarinic receptor-dependent contractions of murine airway smooth muscle. American journal of physiology. Lung cellular and molecular physiology, 328(2), L301–L312. https://doi.org/10.1152/ajplung.00188.2024
2. Ghosh, S., Alkawadri, T., Hollywood, M. A., Thornbury, K. D., & Sergeant, G. P. (2025). Unravelling the Role of Post-Junctional M2 Muscarinic Receptors in Cholinergic Nerve-Mediated Contractions of Airway Smooth Muscle. International journal of molecular sciences, 26(12), 5455. https://doi.org/10.3390/ijms26125455
3. Ghosh, S., Hollywood, M. A., Thornbury, K. D., & Sergeant, G. P. (2025). M2 muscarinic receptor-dependent contractions of airway smooth muscle are mediated by inhibition of Kv7 channels. American Journal of Physiology-Cell Physiology 330(4), C926–C942. https://doi.org/10.1152/ajpcell.00752.2025

Conference Abstracts:

1. Ghosh, S., Alkawadri, T., McGarvey, L. P., Hollywood, M. A., Thornbury, K. D., & Sergeant, G. P. (2024). Mechanisms underlying potentiation of nerve-evoked contractions of airway smooth muscle by activation of postjunctional M2 muscarinic receptors. Command and Control: Unveiling the Regulation of Smooth Muscle Function (Dundalk Institute of Technology, Ireland) Proc Physiol Soc 58, C19.
2. Ghosh, S., Alkawadri, T., McGarvey, L. P., Hollywood, M. A., Thornbury, K. D., & Sergeant, G. P. (2024). Postjunctional M2 muscarinic receptor activation disrupts buffering of calcium entry by SERCA, inducing airway smooth muscle contraction. 17th International Meeting of the European Calcium Society, Homerton College, University of Cambridge.
3. Ghosh, S., Hollywood, M. A., Thornbury, K. D., & Sergeant, G. P. (2025). Role of Kv7 channels in postjunctional M2 muscarinic receptor-dependent contractions of airway smooth muscle. 40th IUPS (International Union of Physiological Sciences) Congress, Frankfurt, Germany (Oral presentation, September 11-14, 2025).

Chapter 1

Review of the Literature

1.1. Respiratory Physiology

The respiratory system plays a pivotal role in maintaining homeostasis by orchestrating the precise exchange of oxygen (O_2) and carbon dioxide (CO_2). This intricate process engages multiple physiological components, encompassing respiratory muscles, pulmonary structures and neural regulatory mechanisms [1]. Respiration is comprised of three main components which include the initial transportation of respiratory gases across the gas exchange surface from the environment, the subsequent transfer of O_2 and CO_2 across the respiratory epithelium and, finally, the circulation of oxygenated and carbon dioxide-laden blood from the lungs to the tissues followed by diffusion of these gases at the cellular level [2, 3].

The respiratory system can be segmented into the upper and lower respiratory tracts. The upper respiratory tract includes the nasal passages, oral cavity, larynx, and pharynx, while the lower respiratory tract is made up of the tracheobronchial tree and the alveoli (figure 1.1) [4]. The tracheobronchial tree constitutes an intricate network responsible for conveying gases from the trachea to the acini, which are the fundamental gas exchange units within the lungs [5]. This system is characterised by various branching levels, extending from the trachea to the ultimate terminal bronchioles. The airways serve solely as conduits from the trachea to the terminal bronchioles for air and no gas exchange occurs at this point. Terminal bronchioles then branch into respiratory or transitional bronchioles, featuring occasional alveoli on their walls. These respiratory bronchioles further divide into alveolar ducts, completely lined with alveoli, collectively forming the acinus. The acinus, comprising respiratory airways, constitutes the functional gas exchange units of the lung [4, 6].

The lungs are enclosed by a double-layered serous membrane, the pleura, which consists of the visceral pleura covering the lung surface and the parietal pleura lining the thoracic cavity [7]. Between these two layers lies the pleural space, a narrow, fluid-filled cavity. The pleural fluid within this space serves multiple physiological functions, acting as a lubricant to reduce friction between the pleural surfaces during the respiratory cycle, and generating surface tension that helps maintain close apposition of the lung surface to the thoracic wall [8, 9]. The negative

intrapleural pressure created by the pleural space is essential for lung expansion during inspiration, ensuring that the lungs follow the movements of the thoracic cage and diaphragm. Additionally, the pleural fluid provides a cushioning effect, protecting delicate lung tissue from mechanical trauma. Any disruption to the pleural space, such as fluid accumulation (pleural effusion) or air entry (pneumothorax), can significantly impair normal respiratory mechanics and gas exchange [9, 10].

Gas exchange occurs at the level of the alveoli, which are tiny, thin-walled sacs optimised for diffusion due to their large surface area and close proximity to the pulmonary capillaries [3]. Each alveolus is surrounded by a dense network of pulmonary capillaries supplied by pulmonary arterioles and drained by venules. Oxygen from the inhaled air diffuses across the alveolar epithelium, basement membrane and capillary endothelium into the blood, where it binds to haemoglobin within red blood cells. Conversely, carbon dioxide, produced as a metabolic by-product in tissues, diffuses from the blood plasma into the alveolar space for elimination during exhalation [3, 11, 12].

The alveolar ducts, which arise from respiratory bronchioles, serve as conduits lined entirely with alveoli, thereby maximising the available surface area for gas exchange. The efficiency of this process is maintained by the minimal thickness of the blood-gas barrier and the constant renewal of alveolar air through ventilation. Importantly, the matching of alveolar ventilation to pulmonary perfusion (ventilation-perfusion coupling) ensures that regions of the lung receiving the most airflow are also the best perfused with blood, thereby optimising the exchange of gases [3, 13, 14]. Furthermore, the elastic properties of the alveoli, together with surfactant secretion by type II alveolar cells, prevent alveolar collapse during expiration and facilitate efficient re-expansion during inspiration [15, 16]. This structural and functional specialisation ensures the continuous maintenance of arterial oxygen levels and the removal of carbon dioxide, both essential for sustaining cellular metabolism and systemic homeostasis [17, 18].

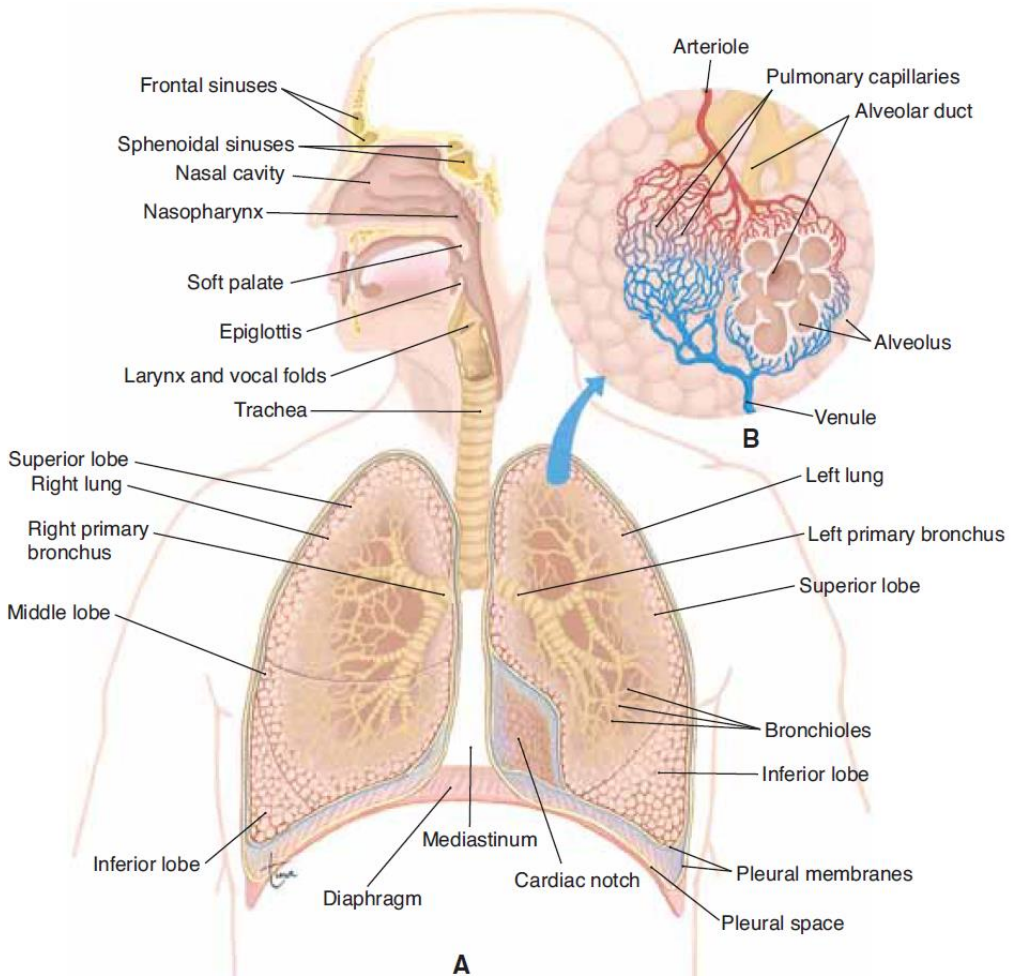

Figure 1.1. Diagram illustrating the human respiratory system. **A)** The upper and lower respiratory tracts as seen from the anterior perspective. **B)** A microscopic depiction showcasing alveoli and pulmonary capillaries. (Figure adapted from Scanlon, V. C., & Sanders, T. (2018). Essentials of anatomy and physiology (8th ed.). F.A. Davis Company [19]).

1.2. Mechanics of pulmonary ventilation

The process of breathing adheres to Boyle's law, which asserts that, at a constant temperature, the pressure of a gas diminishes as its volume expands. There is an inflow of air and a drop in intrathoracic pressure when the volume of the thoracic cavity increases. Relaxation of the inspiratory muscles raises intrathoracic pressure leading to exhalation, which reduces the volume of the thoracic cavity [20].

1.2.1. Muscles responsible for lung expansion and contraction

Two main processes are involved in the expansion and contraction of the lungs: (1) the descent and ascent of the diaphragm (referred to as bucket handle motion), which changes the length of the chest cavity; and (2) the elevation and depression of the ribs, which changes the anteroposterior diameter of the chest [21]. The diaphragm contracts during inhalation to draw the lower lung surfaces downward, essentially driving inspiration during normal breathing. The diaphragm relaxes during expiration, enabling the lungs to compress and release air due to the elastic recoil of the lungs, chest wall and abdominal tissues. In more vigorous breathing, additional force is generated by contraction of the abdominal muscles, pushing abdominal contents against the diaphragm to aid in lung compression. This can be especially important while breathing heavily or exercising, as elastic forces might not be enough to cause quick expiration on their own [22, 23]. The second technique for expanding the lung entails raising the rib cage, moving the ribs (referred to as pump handle motion), and thickening the chest from the anteroposterior to the posterior [24].

1.2.2. Pressures driving the inflow and outflow of air within the lungs

The lung naturally collapses and expels air through the trachea in the absence of any supporting force. Essentially, a thin film of pleural fluid surrounds the lung, allowing for smooth mobility as it "floats" inside the thoracic cavity [25]. An adhesive-like effect is created between the parietal pleural surface of the thoracic cavity and the visceral surface of the lung pleura by the continuous suction of surplus fluid into lymphatic channels [26]. This unique arrangement allows the lungs to adhere to the thoracic wall as if glued, yet they remain well-lubricated and can slide freely during chest expansion and contraction [7]. The pressure in the area between the pleura of the lung and the pleura of the chest wall is known as pleural pressure.

Pleural pressure is often negative, in the range of -5 cm of H_2O at the start of inspiration to -7.5 cm of H_2O during a typical inspiration [27, 28].

The pressure inside the lung alveoli (alveolar pressure) is crucial for breathing, as alveolar pressure drops to around -1 cm of H_2O during inspiration, generating a slight negative pressure gradient that allows passive airflow into the lungs. On the other hand, during expiration, inspired air is expelled from the lungs as alveolar pressure increases to around +1 cm of H_2O. The difference between alveolar pressure and pleural pressure is termed transpulmonary pressure [29-31].

Transpulmonary pressure = Alveolar pressure - Pleural pressure

This pressure gradient represents the elastic forces within the lungs, contributing to their tendency to collapse at each respiratory cycle, known as the recoil pressure. Transpulmonary pressure is crucial in maintaining lung elasticity and preventing complete lung collapse during expiration. The dynamics of pleural and alveolar pressures are crucial aspects of respiratory mechanics [32-34].

1.2.3. Compliance of the lungs

A critical component of respiratory physiology is lung compliance, which measures the amount of lung expansion for every unit rise in transpulmonary pressure [35]. The typical overall compliance of both lungs in a normal adult person is around 200 ml air per cm of H_2O transpulmonary pressure [36]. Lung compliance is not constant throughout the entire range of lung volumes, instead, it varies depending on the volume of the lungs. At the extremes of functional residual capacity (FRC), compliance is lowest, suggesting that both fully expanded and completely deflated lungs have reduced capacity to stretch or distend under a given pressure. In normal breathing without any forced effort, the intrapleural pressure is approximately -8 cm of H_2O at the apex (top) of the lung and -1.5 cm of H_2O at the base [4]. This indicates that the alveoli at the apex are exposed to a greater distending pressure (difference between alveolar pressure and intrapleural pressure) compared to those at the base. At the apex, this pressure difference is 8 cm H_2O, while at the base, it is 1.5 cm H_2O. This means that the alveoli at the top of the lung experience a higher pressure, promoting greater lung expansion and distention compared to those at the bottom [4].

1.3. Airway cell composition and roles

The respiratory airways comprise a highly specialised and heterogeneous population of cells that work in concert to maintain pulmonary function and defence. Various cell types are present in the airways, including epithelial cells, smooth muscle cells, fibroblasts, mast cells, and endothelial cells (Figure 1.2) [37, 38]. The cellular composition varies along the tracheobronchial tree depending on the region-specific physiological demands. Epithelial cells form the first line of defence, providing both a physical barrier and active participation in mucociliary clearance and host immunity. Structural cells such as fibroblasts and smooth muscle cells maintain airway integrity, responsible for extracellular matrix (ECM) production, and regulate bronchomotor tone, while resident and recruited immune cells protect against pathogens and contribute to inflammatory responses [39-43].

1.3.1. Epithelial cells

Human airways are lined with a continuous epithelial layer that varies in shape and cellular composition between the respiratory and conducting zones, extending from the nasal passage to the alveolar sacs [44]. In the proximal regions of the conducting zone, such as the nasal passage, trachea, and bronchi, the airway epithelium takes on a columnar, pseudostratified form [45]. At more distal regions of the conducting zone, the height of the epithelia diminishes, resembling a cuboidal structure in the small airways. The principal cell types within the large airway epithelium include goblet cells, which are responsible for mucus production and secretion, ciliated cells that facilitate mucus movement through coordinated ciliary action, and basal cells that line the basement membrane without contacting the apical surface [46]. In the bronchioles, the cuboidal epithelium comprises secretory club cells (Clara cells), which have fewer ciliated cells compared to more proximal airway segments. Eventually, in the alveolar region, the epithelium is characterised by type I and II alveolar epithelial cells (AT1 and AT2, respectively). AT1 cells are thin, squamous in shape, and extend over nearly 70% of the alveolar surface, making them well-suited for facilitating gas exchange. They are closely associated with the pulmonary capillary endothelium through a shared basement membrane, together forming the air-blood barrier. The tight junctions between adjacent cells help prevent fluid leakage into the alveolar space. In contrast, AT2 cells occupy a smaller proportion of the alveolar surface, around 7%, but they are metabolically

active. These cuboidal cells contain lamellar bodies that store and release pulmonary surfactant, which reduces alveolar surface tension and prevents collapse during respiration [16, 45, 47-49].

The airway epithelium serves as a crucial barrier and passageway, ensuring the movement of air between the external environment and the alveoli [50]. Beyond its structural role, it is a primary line of defence against inhaled pathogens and particulate matter. The coordinated activity of ciliated and secretory cells enables effective mucociliary clearance, while additional defence mechanisms support host protection. Rather than acting in isolation, the epithelial layer operates in close interaction with neighbouring epithelial subtypes, mesenchymal and endothelial cells, as well as the extracellular matrix of the bronchial wall. Dysregulation of epithelial function is a key feature in the development of several major pulmonary diseases, including asthma, chronic obstructive pulmonary disease (COPD), and lung cancer, where local immune and inflammatory mediators further influence epithelial responses [50, 51].

1.3.2. Airway smooth muscle cells

Airway smooth muscle (ASM) forms an integral part of the airway wall, extending throughout the bronchial tree from the trachea down to the terminal bronchioles. It is also present in alveolar ducts within the lung parenchyma. In the trachea, it is confined to the trachealis membrane [52]. Beyond its structural role, ASM is central to airway narrowing in asthma, where bronchoconstriction is driven largely by mediators such as acetylcholine (ACh), histamine, cysteinyl leukotrienes, and prostaglandin D_2 released from mast cells. ASM contraction is primarily governed by intracellular Ca^{2+} dynamics. Activation of G-protein-coupled receptors, such as muscarinic M3 receptors (M3R), by ACh triggers phospholipase C-mediated inositol trisphosphate (IP_3) production, leading to Ca^{2+} release from the sarcoplasmic reticulum (SR) and activation of calmodulin-myosin light-chain kinase (MLCK) complexes [53-56]. Additional Ca^{2+} influx occurs via L-type voltage-gated Ca^{2+} channels and receptor-operated channels, sustaining contraction. Potassium channels, particularly Kv7 channel maintain resting membrane potential [57]. Their dysfunction enhances excitability and hypercontractility of ASM cells, features observed in asthma and COPD [58, 59]. Furthermore, the RhoA/ROCK pathway

mediates Ca^{2+} sensitisation by inhibiting myosin light-chain phosphatase (MLCP), amplifying contractile responses independent of cytosolic Ca^{2+} levels [60, 61].

Asthmatic airways also exhibit an increase in ASM mass, resulting from both hyperplasia and hypertrophy, processes fuelled by epithelial and inflammation-derived growth factors [62]. These changes are particularly prominent in severe asthma, where enhanced proliferative activity of ASM has been observed. Importantly, ASM cells are highly responsive to mitogenic stimuli, including epidermal growth factor, fibroblast growth factor, mast cell proteases (such as tryptase), histamine, leukotriene D_4, and interleukins such as IL-1 and IL-11 [54, 63]. In addition to their contractile properties, ASM cells exhibit a remarkable synthetic capacity, releasing a wide spectrum of cytokines, chemokines, and growth factors such as IL-6, IL-8, IL-11, eotaxin, GM-CSF, and prostaglandins, thereby actively contributing to airway inflammation and remodelling [64, 65]. Experimental studies have demonstrated that muscarinic stimulation of ASM with carbachol induced pro-inflammatory gene expression (IL-6, IL-8, COX-2) and augmented cyclic stretch-induced responses [66]. Similarly, carbachol and methacholine enhanced the release of IL-6 and IL-8 through M3R activation, with methacholine markedly amplifying cigarette smoke extract (CSE) induced IL-8 release. These cytokine responses are regulated through ERK1/2 and NF-κB signalling pathways, aligning with observations in epithelial cells [66, 67]. Some emerging evidence also suggests that ASM cells can adopt a synthetic, extracellular matrix (ECM) producing phenotype, secreting collagens (majorly type I and III) and are responsible for small-airway fibrosis, a common trait observed in COPD patients [68-70]. Collectively, these findings highlight ASM as not only a contractile element but also a dynamic immunomodulatory cell population that significantly influences the pathogenesis of airway diseases.

1.3.3. Lung fibroblasts

Lung fibroblasts are the principal mesenchymal cells responsible for producing, organising, and remodelling the ECM that scaffolds the conducting airways and alveoli [71]. In healthy lungs, they maintain tissue homeostasis by synthesising collagen (e.g., COL1A1, COL3A1), elastin, proteoglycans and matricellular proteins, and also by responding to mechanical stress and paracrine signals from epithelium, smooth muscle, endothelium and immune cells [72, 73].

Based on gene expression and functional characteristics, fibroblasts in the lung are often classified into lipofibroblasts, myofibroblasts, and matrix fibroblasts. Lipofibroblasts, typically localised within the alveolar interstitium, are characterised by lipid droplet content and expression of PLIN2 and PPARG, enabling them to support alveolar type II epithelial cells by storing and transferring neutral lipids for surfactant synthesis. Myofibroblasts, defined by the expression of myogenic proteins such as ACTA2 (α-SMA) and production of elastin matrix, arise predominantly during injury or disease states and are key drivers of pathological fibrosis [74-77]. Matrix fibroblasts, in contrast, represent a more diverse population with high expression of extracellular matrix genes (collagens, fibronectin, periostin) and are enriched around conducting airways and vessels, where they contribute to structural integrity and inflammatory signalling [74, 75]. Spatially, alveolar fibroblasts largely overlap with lipofibroblasts but can also transition towards matrix-producing or myofibroblast phenotypes under stress or injury, while peribronchiolar fibroblasts are typically aligned with the matrix fibroblast category and can serve as a source of myofibroblasts in airway remodelling [78-80].

Upon tissue injury or chronic inflammation, fibroblasts can differentiate into contractile α-SMA-positive myofibroblasts which is a phenotypic switch driven by canonical profibrotic pathways (TGF-β/SMAD and WNT) and reinforced by matrix stiffness and mechanical stress [81, 82]. TGF-β is particularly central cytokine as it promotes fibroblast proliferation, myofibroblast differentiation, and excessive deposition of fibrillar collagens that thicken airway walls and basement-membrane-like zones [81, 83]. In asthma, TGF-β signalling intersects with type-2 cytokine pathways (IL-13, IL-4), linking inflammation to structural change; IL-13 acts directly on structural cells including fibroblasts to enhance ECM production, while TGF-β shapes myofibroblast phenotype and airway hyperresponsiveness (AHR) [77, 84, 85]

In COPD, small-airway fibrosis and loss of alveolar attachments narrow terminal bronchioles and increase airflow resistance. Cigarette smoke and oxidative stress perturb epithelial-mesenchymal signalling and activate fibroblast TGF-β pathways, driving ECM remodelling with increased collagen deposition and elastin disruption. Circulating and airway levels of profibrotic mediators (including TGF-β

and urotensin-II) are elevated in COPD and associate with disease severity, supporting a profibrotic milieu [86-91].

1.3.4. Endothelial cells

The pulmonary endothelium forms a vast and metabolically active interface between the circulation and lung parenchyma, playing essential roles in gas exchange, vascular tone, immune regulation, and tissue repair [92]. Endothelial cells (ECs) are heterogeneous, encompassing pulmonary arterial and venous ECs as well as capillary subsets such as aerocytes (specialised for gas exchange and leukocyte trafficking) and general capillary ECs (involved in barrier and matrix functions). This heterogeneity allows ECs to integrate haemodynamic cues with inflammatory and structural signals in the lung, making them key participants in airway disease pathogenesis [93, 94].

One of the primary functions of lung ECs is to regulate vascular smooth muscle cell (VSMC) tone through the release of vasoactive mediators. Nitric oxide (NO), produced mainly via endothelial nitric oxide synthase (eNOS), is synthesised from L-arginine through a two-step oxidation reaction in which L-arginine is first converted to Nω-hydroxy-L-arginine and subsequently to L-citrulline with the release of NO. This process requires molecular oxygen and NADPH and depends on cofactors including tetrahydrobiopterin (BH_4), flavin adenine dinucleotide (FAD), flavin mononucleotide (FMN) and haem, and is tightly regulated by Ca^{2+}/calmodulin binding following endothelial stimulation (e.g., shear stress or receptor activation). The NO generated diffuses into adjacent VSMCs, where it activates soluble guanylate cyclase (sGC), increasing cyclic GMP (cGMP) levels and activating protein kinase G (PKG). PKG subsequently reduces intracellular Ca^{2+} levels and promotes MLCP activity, leading to decreased myosin light chain phosphorylation and smooth muscle relaxation [95-97]. This mechanism maintains low pulmonary vascular resistance and contributes indirectly to airway calibre, as peribronchial vessels influence local tissue mechanics [92]. In asthma and COPD, eNOS activity is often impaired, while inducible NOS (iNOS) expression is increased, leading to an imbalance between protective NO signalling and oxidative/nitrosative stress. Reduced NO bioavailability diminishes vasodilation and may contribute to pulmonary hypertension in COPD, whereas excessive reactive nitrogen species amplify airway inflammation in both diseases [98-100].

Cholinergic pathways also intersect with endothelial regulation. ACh activates endothelial muscarinic receptors, particularly M3Rs, which stimulate Ca^{2+} influx and NO production. In healthy lungs, this M3R-NO pathway contributes to vasodilation and bronchoprotection [100, 101]. However, in asthma and COPD, altered M3R signalling on ECs and VSMCs favours bronchoconstriction and vascular dysregulation [102, 103]. Overactivation of M3Rs on ASM drives bronchospasm, while impaired endothelial M3R-NO coupling reduces the vasodilatory counterbalance, enhancing AHR. This dual role underscores the importance of endothelial muscarinic pathways in coordinating vascular and airway tone [92, 104].

In COPD, chronic cigarette smoke exposure induces oxidative stress, DNA damage, and apoptosis in ECs [105, 106]. Loss of endothelial integrity contributes to microvascular rarefaction in emphysematous regions, while peribronchiolar ECs undergo pathological activation, secreting TGF-β and endothelin-1 that stimulate fibroblast and VSMC proliferation. This promotes airway wall fibrosis, vascular remodelling, and fixed airflow limitation [92]. Impaired eNOS activity and reduced NO bioavailability further exacerbate pulmonary vascular constriction and increase the risk of pulmonary hypertension [92, 100]. Evidence also suggests that endothelial-to-mesenchymal transition adds to the fibroblast pool in COPD, linking vascular injury directly to airway fibrosis [107].

1.3.5. Immune and inflammatory cells

The lung immune system is rich with leukocytes that coordinate host defence and drive chronic inflammation and remodelling in asthma and COPD. Key effector populations like macrophages, neutrophils, eosinophils, mast cells, dendritic cells (DCs), T and B lymphocytes communicate intensely with structural cells, especially ASM, shaping contractility, growth and ECM deposition [108, 109].

Macrophages: Alveolar and interstitial macrophages integrate environmental stimuli (allergens, smoke, pathogens) and metabolic stress. In chronic airways disease, they adopt disease-associated states that produce TGF-β, IL-6, TNF-α and chemokines (e.g., CCL2), amplifying leukocyte recruitment and fibroblast activation [110, 111]. Oxidative stress and mediator signals from mast cells further prime macrophages. Histamine can directly induce macrophage cytokine release via H1 receptors, adding to a self-reinforcing inflammatory loop.

Macrophage-derived TGF-β promotes ASM synthetic remodelling (ECM production) and hypercontractility indirectly via fibroblast cross-talk [112, 113].

Neutrophils: Prominent in COPD and in steroid-resistant (T2-low) asthma, neutrophils deliver proteases (neutrophil elastase, proteinase-3, cathepsin G) to form neutrophil extracellular traps (NETs) which damage epithelium, thicken the airway wall, and correlate with airflow limitation. Neutrophil elastase also enhances ASM calcium (Ca^{2+}) signalling and contractile responsiveness. Neutrophil-dominant cytokines (IL-17 axis) are also linked with ASM hyperplasia and steroid insensitivity [114, 115].

Eosinophils: Canonical in allergic (T2-high) asthma, eosinophils are recruited by IL-5 and eotaxins. They release cationic proteins (MBP, ECP), lipid mediators and TGF-β that injure epithelium and directly potentiate ASM contraction. Eosinophil-ASM crosstalk enhances ASM proliferation and chemokine secretion (e.g., IL-8), linking inflammation to remodelling and hyperresponsiveness [116, 117].

Mast cells: Mast cells infiltrate ASM bundles in asthma and release histamine, cysteinyl-leukotrienes and prostaglandin D_2 which are potent bronchoconstrictors that acutely raise ASM tone. They also secrete tryptase, PDGF and IL-4/IL-13 that drive ASM growth and phenotype switching. Emerging work highlights bidirectional signalling with nerves and macrophages, and purinergic pathways whereby ATP can trigger mast-cell cysteinyl leukotrienes (cysLT) release that feeds back to contract ASM [118, 119].

Dendritic cells: Airway DCs sample inhaled antigens and migrate to lymph nodes to prime naïve $CD4^+$ T cells. In allergic asthma, epithelial alarmins (TSLP, IL-25, IL-33) condition DCs towards Th2 priming, resulting in IL-4/IL-5/IL-13-dominant responses. Through this axis, DCs indirectly modulate ASM by fostering eosinophilia and IL-13 exposure (which increases ASM contractility and mucus secretion) [120, 121].

T lymphocytes: In classic allergic asthma, Th2 cells dominate the immune landscape, releasing IL-4, IL-5 and IL-13. IL-13 enhances ASM contractility predominantly through Ca^{2+} sensitisation mechanisms involving RhoA/ROCK-mediated inhibition of myosin light chain phosphatase, rather than by upregulating classical contractile genes such as ACTA2, MYH11, or CNN1 [122, 123]. IL-5

sustains eosinophil survival and activity, further potentiating ASM hyperreactivity [124, 125]. In contrast, Th17 cells and their key cytokine IL-17 are closely linked with neutrophilic inflammation, steroid-refractory asthma and COPD. IL-17 promotes ASM proliferation, chemokine release and contributes to corticosteroid insensitivity, features that complicate disease management. Regulatory T cells (Tregs) serve as a counterbalance, moderating both Th2 and Th17-driven inflammation; however, relative deficiency or functional impairment of Tregs has been associated with persistent AHR and structural remodelling [120, 126].

B lymphocytes and IgE: IL-4/IL-13 drive class-switch recombination to IgE, producing plasma cells that maintain mast-cell and basophil activation on re-exposure to allergen. There is growing evidence for lung-resident memory B cells/plasma cells sustaining local IgE, providing a substrate for chronicity. IgE-mediated mast-cell activation strongly influences ASM via histamine and leukotrienes [120, 127].

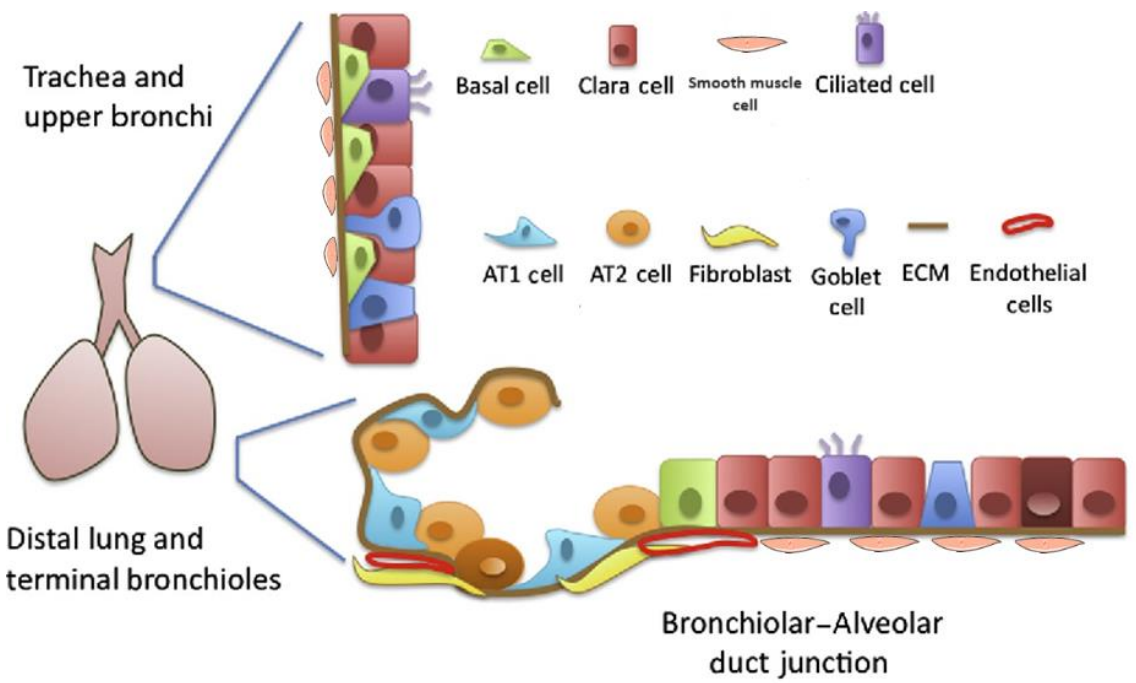

Figure 1.2. The figure illustrates the regional distribution of key cell types along the respiratory tract. In the trachea and upper bronchi, a pseudostratified epithelium contains basal, ciliated, goblet, and club (Clara) cells, supported by underlying smooth muscle. Toward the distal lung and terminal bronchioles, the epithelium becomes simpler, with increased club cells and fewer ciliated cells. At the bronchiolar-alveolar duct junction, a transitional cell population is present. The alveolar region is composed of type I (AT1) cells for gas exchange and type II (AT2) cells for surfactant production, alongside fibroblasts, extracellular matrix, and endothelial cells (Figure adapted from Leeman et al. (2014) [37]).

1.4. Mechanisms underlying bronchoconstriction

Bronchoconstriction represents force generation by ASM encircling intrapulmonary airways. Classically, excitation-contraction coupling begins when bronchoconstrictor agonists such as ACh (via vagal stimulation), histamine (from mast cells) and cysLT activate $G_{q/11}$-coupled receptors (M3R, H1R and $CysLT_1$) on ASM [128, 129]. Activation of $G_{q/11}$ stimulates phospholipase Cβ (PLC_β), which generates IP_3 and diacylglycerol (DAG). IP_3 binds to its receptors on the SR and releases Ca^{2+} into the cytosol. The released Ca^{2+} binds to calmodulin, and this calcium-calmodulin complex activates MLCK, which then phosphorylates the 20 kDa regulatory myosin light chain (MLC), permitting actomyosin cross-bridge cycling and ASM shortening (Figure 1.3). In parallel, DAG together with Ca^{2+} activates protein kinase C (PKC). PKC phosphorylates and activates CPI-17, which inhibits MLCP, reduces dephosphorylation of the regulatory light chain, increases Ca^{2+} sensitivity, and thereby further strengthens contraction (Figure 1.3) [56, 130]. Sustained Ca^{2+} entry mainly occurs through voltage-gated L-type Ca^{2+} channels, store-operated Ca^{2+} entry (STIM1-Orai), and TRP channels. Membrane depolarisation (e.g., by inhibition of K^+ currents such as Kv7 or BK_{Ca} channels) augments this influx and maintains tone.

Apart from G_q GPCR-mediated ASM contraction, studies have also shown that G_i GPCRs can also participate in ASM contraction, although the exact mechanism of action is still unclear. Studies have shown that activation of G_i GPCRs inhibits G_s-stimulated AC, lowering cAMP, thereby reducing an important inhibitory influence on ASM contraction (Figure 1.3) [56, 131]. Activation of G_i also engages pro-contractile pathways. For example, G_i activation stimulates RhoA via Rho-GEFs, which promotes actin polymerisation and Ca^{2+} sensitisation through inhibition of MLCP, which enhances contraction at any given Ca^{2+} level [132, 133]. Beyond these effects, G_i-G_q crosstalk can amplify phosphoinositide signalling. For example, Pfeil et al. (2020) demonstrated that G_i-derived $G_{\beta\gamma}$ subunits can activate PLC_β and mobilise Ca^{2+} in the presence of $G_{\alpha q/11}$, identifying $G_{\alpha q}$ as a ‘master switch’ that enables $G_{i\beta\gamma}$-PLC_β signalling [134]. Fisher et al. (2020) further showed that $G_{\alpha q}$ and $G_{\beta\gamma}$ cooperatively activate $PLC_{\beta 2/3}$, with $G_{\alpha q}$ relieving autoinhibition and $G_{\beta\gamma}$ recruiting PLC_β at the membrane [135]. Consistent with this, Sánchez et al. (2022)

characterised $PLC_{\beta 3}$ as a coincidence detector that integrates inputs from G_q and G_i-coupled receptors to drive phosphatidyl inositol hydrolysis [136].

In parallel, RhoA-ROCK signalling increases force at any given $[Ca^{2+}]_i$ by promoting Ca^{2+} sensitisation. This pathway is engaged downstream of GPCRs not only via G_q/PLC but also critically through $G_{12/13}$ proteins, which activate RhoA via RhoGEF. Activated RhoA (GTP-bound) stimulates Rho-associated coiled-coil containing kinase (ROCK1/2), which phosphorylates MYPT1, the regulatory subunit of MLCP, thereby inhibiting MLCP activity and maintaining MLC20 phosphorylation independently of further increases in intracellular Ca^{2+}. In addition, ROCK can directly phosphorylate MLC20 and inhibit MLCP via CPI-17 phosphorylation, further amplifying contractile responses. Beyond contractility, ROCK regulates F-actin remodelling through LIM kinase (LIMK) mediated inhibition of cofilin, promoting actin polymerisation and strengthening cytoskeletal force transmission. These cytoskeletal effects also facilitate ASM migration, adhesion and phenotypic modulation, processes that contribute to airway remodelling. Importantly, $G_{12/13}$-driven RhoA activation provides a parallel and often dominant pathway for sustained contraction and Ca^{2+} sensitisation, particularly under conditions of chronic agonist stimulation, thereby linking GPCR signalling to both acute bronchospasm and persistent AHR. Collectively, these ROCK-dependent mechanisms represent key drivers of both immediate and long term ASM dysfunction, making the RhoA-ROCK axis an important therapeutic target [60, 61].

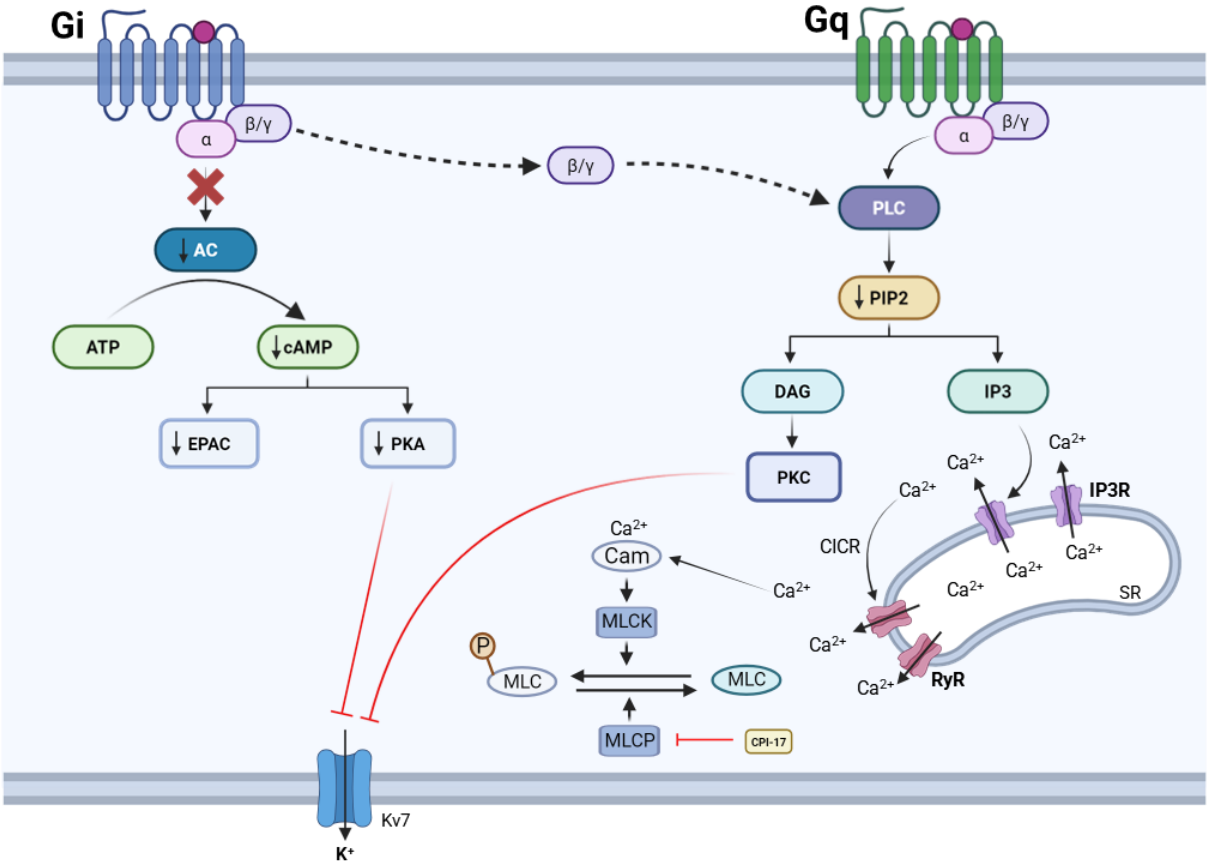

Figure 1.3: G_q and Gi-mediated signalling pathways in ASM contraction. G_q-coupled receptor activation stimulates PLC, leading to PIP_2 hydrolysis into IP_3 and DAG. IP_3 induces Ca^{2+} release from the sarcoplasmic reticulum via IP_3 receptors, amplified by ryanodine receptors, while DAG activates PKC. Increased intracellular Ca^{2+} activates calmodulin and MLCK, promoting myosin light chain (MLC) phosphorylation and contraction. PKC further sustains contraction by inhibiting MLCP. In parallel, G_i-coupled receptors inhibit adenylyl cyclase, reducing cAMP and downstream PKA/EPAC signalling, thereby suppressing relaxation pathways. Together, these mechanisms enhance ASM contraction and bronchoconstriction. Figure created with a licensed version of BioRender.com. AC, adenylyl cyclase; ATP, adenosine triphosphate; cAMP, cyclic adenosine monophosphate; EPAC, exchange protein directly activated by cAMP; PKA, protein kinase A; PLC, phospholipase C; PIP_2, phosphatidylinositol 4,5-bisphosphate; DAG, diacylglycerol; IP_3, inositol 1,4,5-trisphosphate; PKC, protein kinase C; IP_3R, inositol 1,4,5-trisphosphate receptor; RyR, ryanodine receptor; SR, sarcoplasmic reticulum; Ca^{2+}, calcium ion; CaM, calmodulin; MLCK, myosin light chain kinase; MLCP, myosin light chain phosphatase; MLC, myosin light chain; CPI-17, protein kinase C-potentiated inhibitory protein of 17 kDa; Gα, G protein alpha subunit; Gβγ, G protein beta-gamma subunits; CICR, calcium-induced calcium release.

1.5. Lung innervation

The lungs are innervated by two primary sources: the pulmonary plexus, which comprises both parasympathetic and sympathetic nerves, and the phrenic nerve which provides motor innervation to the diaphragm [137]. The network of autonomic neurons and ganglia that makes up the pulmonary plexus is located at the pulmonary hila of each lung and controls blood flow, vascular permeability, submucosal glandular mucus production, and bronchial smooth muscle tone.

Parasympathetic nerves represent the predominant innervation of ASM in human airways, while sympathetic nerves are relatively sparse. The parasympathetic innervation results in increased gland secretion, pulmonary vessel dilatation, and bronchoconstriction [138-140]. Conversely, sympathetic innervation induces bronchial dilation and constriction of the pulmonary vessels [141]. Non-adrenergic, non-cholinergic (NANC) nerves induce smooth muscle relaxation through the release of NO and vasoactive intestinal peptide (VIP) or contraction via the release of neurokinins and substance P. Since human ASM lacks adrenergic nerves, NANC nerves are the predominant neural inhibitory pathway responsible for inducing smooth muscle relaxation. [142, 143].

1.5.1. Cholinergic innervation of the Lungs

1.5.1.1. Muscarinic Receptors

Parasympathetic nerves induce bronchoconstriction by releasing ACh that activates muscarinic receptors on ASM cells. Mammalian airways contain M1R, M2R, and M3R subtypes [144, 145]. M1Rs are located in peripheral airways, bronchial fibroblasts and bronchial epithelial cells in humans [146-148]. M2Rs are expressed in human airway epithelial cells, fibroblasts, smooth muscle cells and neurons [146, 147, 149-151] while M3R expression has been detected in ASM of humans and mice, as well as in human fibroblasts and epithelial cells [146, 147, 152]. M2Rs are the predominant muscarinic receptor subtype in ASM, with an M2R:M3R expression ratio of 4:1 in bovine trachea, equine and porcine bronchi [153]. Notably, expression of M1R, M4R, and M5Rs was not identified in human ASM [154]. M2Rs are coupled to G_i proteins, whereas M3Rs couple to G_q proteins [155]. Although M2Rs outnumber their M3R counterparts, it is the M3Rs that are thought to mediate the bronchoconstrictor effects of neurally released ACh [156]. However, it is now recognised that M2R also play a significant role in the contraction of ASM [153].

1.5.1.1.1. Postjunctional M2 receptor signalling pathways

M2Rs couple to $G_{i/o}$ proteins that inhibit adenylate cyclase and reduce cAMP levels [55, 157, 158]. The $G_{i/o}$ protein family contains a range of α-subunits including $G_{\alpha i1}$-$G_{\alpha i3}$ [159]. All members of the $G_{i/o}$ family contain a cysteine residue close to the C-terminus of their α-subunit which becomes covalently attached to an ADP-ribose

moiety in pertussis toxin (PTX) that prevents receptor activation of the $G_{i/o}$ proteins [160]. Therefore, PTX is recognised as a valuable tool for the investigation of $G_{i/o}$ signalling pathways, and sensitivity of cholinergic contractions to PTX may imply involvement of M2Rs. Kume et al. (1995) [161] and Hirschmann et al. (1999) [162] showed that PTX reduced the amplitude of contractions of ASM evoked by cholinergic agonists, consistent with a role for M2Rs in these responses. Unno et al. (2005) noted that PTX could inhibit contractions of intestinal smooth muscle by the cholinergic agonist carbachol (CCh), but only when low concentrations of the agonist were employed (70% reduction at 0.1 μM and no reduction at 10 μM CCh) [163]. This indicated that M2R/$G_{i/o}$ signalling was only involved in responses evoked by relatively low concentrations of ACh, whereas M3R/$G_{q/11}$ signalling prevailed at higher agonist concentrations. Semenov et al. (2011) reported that the M2R antagonist AFDX-116 inhibited contractions of murine trachea induced by sub-micromolar concentrations of CCh, but not those evoked by higher concentrations, perhaps suggesting that a similar pattern exists in the airways [164]. Further, indirect evidence in support of a role for M2Rs in cholinergic contractions of ASM came from studies which demonstrated that muscarinic agonists evoked robust contractions of ASM taken from M3R knock-out (KO) mice. These responses were not attributed to compensatory upregulation of M2Rs, as M2R mRNA expression was not elevated in whole lung preparations or tracheal muscle from M3R KO mice [165, 166]; however, it should be noted that transcript levels do not necessarily reflect protein expression or functional receptor abundance. More definitive evidence in support of a role for M2Rs in ASM contraction came from Stuckmann et al. (2003) who showed that KO of both M2Rs and M3Rs was required to abolish CCh-evoked contractions of tracheal smooth muscle [145].

A recent study from our laboratory further examined the contribution of postjunctional M2Rs to cholinergic contractions of ASM by investigating whether their involvement was related to the stimulus parameters used to evoke the contractions [153]. It was found that responses to EFS at 2 Hz were affected by the stimulus interval. A reduction in the stimulus interval from 100 to 10 s greatly augmented the amplitude of contractions (Figure 1.4A). This effect was absent in ASM taken from M2R KO mice (Figure 1.4B) and was reversed by application of the M2R antagonists methoctramine and AFDX-116 (Figure 1.4C, D), demonstrating

that it was mediated by M2Rs. It should also be noted that, although the augmented responses to 2 Hz EFS at 10 s intervals were mediated by activation of M2Rs, the entire response was abolished by a blockade of M3Rs. This shows that M3R activation was still a prerequisite for these neurogenic contractions and suggests that activation of postjunctional M2Rs sensitises the M3R response. In contrast to the responses to 2 Hz stimulation, contractions evoked by EFS at 20 Hz were unaffected by a reduction in the stimulus interval from 100 to 10 s. Also, unlike the case for 2 Hz EFS, where methoctramine blocked a proportion of the response (Figure 1.4C and D), responses to 20 Hz stimulation were slightly potentiated by methoctramine. This was consistent with the blockade of prejunctional autoinhibitory M2Rs, which suppress the output of ACh from cholinergic nerves.

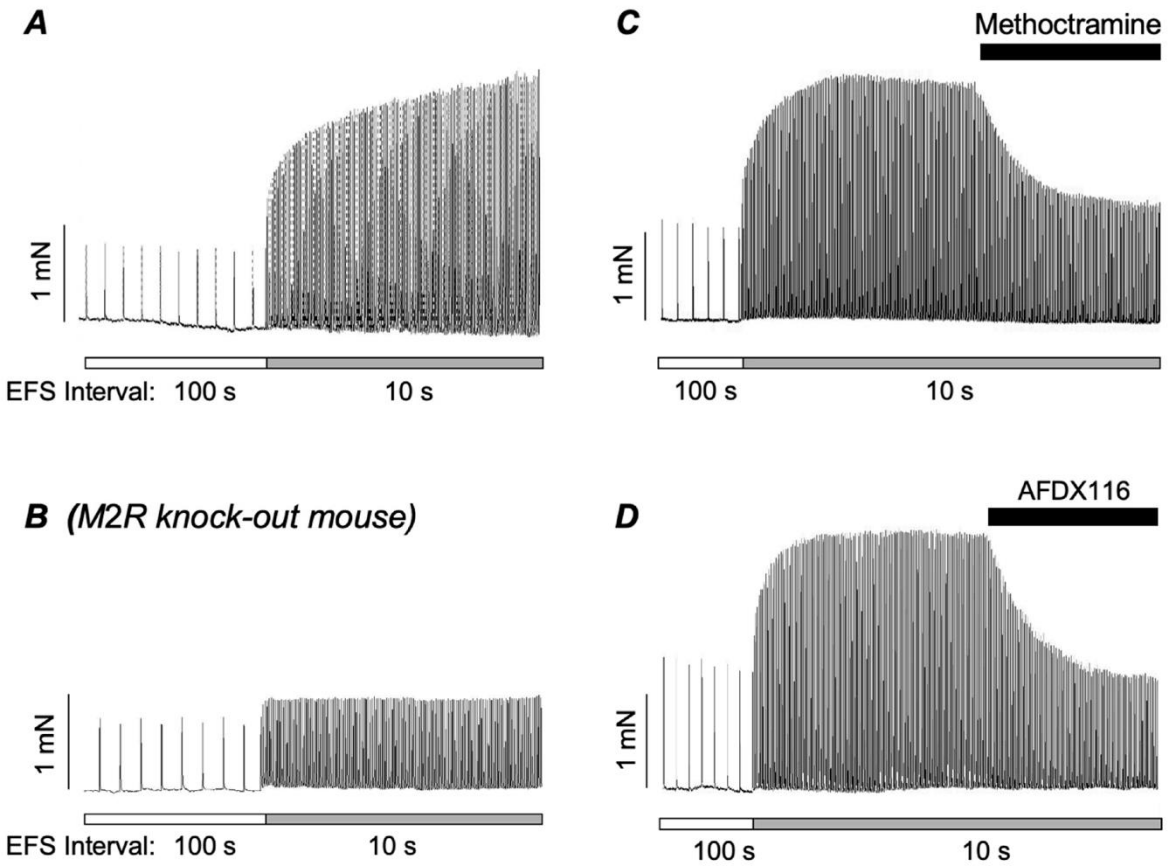

Figure 1.4. (A) Representative trace showing contractions of murine bronchial rings evoked by EFS at 100 and 10 s intervals. Reducing the stimulus interval to 10 s enhanced contraction amplitude. **(B)** Representative trace showing the effect of reducing the stimulus interval from 100 to 10 s on a bronchial ring taken from a M2R KO mouse. **(C)** Effect of the M2R antagonists, methoctramine and **(D)** AFDX116 on contractions of bronchial rings from wild-type mice evoked at 10 s intervals. (Figure adapted from Alkawadri et al. (2022) [153]).

Overall, these data indicate that cholinergic contractions of ASM rely on activation of M3Rs, but they also highlight a prominent role for postjunctional M2Rs in responses evoked by low stimulus frequencies and intervals. These observations accord with previous studies which indicated that involvement of postjunctional M2Rs in cholinergic contractions of ASM was restricted to responses involving low concentrations of ACh [163, 164]. This may explain why the contribution of postjunctional M2Rs has been underestimated in studies that employ higher-frequency stimulation or higher concentrations of cholinergic agonists to evoke contractions of ASM.

1.5.1.1.2. Prejunctional M2 receptors

M2Rs are also present on parasympathetic nerve terminals which innervate the lungs [167]. Fryer and Maclagan (1984) found that the activation of these receptors using muscarinic agonists inhibited vagally mediated bronchoconstriction by up to 80% in guinea pigs [156, 167]. Therefore, prejunctional M2Rs are thought to act as autoinhibitory receptors that suppress further release of ACh.

Several respiratory diseases are associated with dysfunction of prejunctional M2Rs. In a landmark study by Fryer and Jacoby (1991), it was shown that guinea pigs inoculated intranasally with parainfluenza type 3 virus exhibited impaired M2R function. In these animals, pilocarpine failed to inhibit vagally induced bronchoconstriction, and gallamine did not enhance vagally induced bronchoconstriction to the same extent as observed in uninfected controls (Figure 1.5). These findings indicated that prejunctional M2R-mediated inhibition of ACh release from parasympathetic nerves in the lungs was diminished in animals infected with the parainfluenza virus. Loss of this inhibitory mechanism likely led to increased release of ACh from parasympathetic nerves, promoting AHR [168]. Fryer and Wills-Karp (1991) reported that pilocarpine also failed to inhibit vagally induced bronchoconstriction in guinea pigs that were sensitised and challenged with ovalbumin to induce AHR. Additionally, gallamine did not enhance vagally-induced bronchoconstriction to the same extent as observed in the control group [169]. Furthermore, Larsen et al. (1994) found that repeated allergen exposure in IgE-immune mice led to a disruption in M2R function, resulting in the loss of their ability to regulate ACh release. This dysfunction caused increased release of ACh from

cholinergic nerves in immune mice, whereas non-immune mice retained normal M2R function [170]. Schultheis et al. (1994) reported that acute ozone exposure in guinea pigs also caused loss of M2R function on pulmonary parasympathetic nerves, leading to increased ACh release and exaggerated bronchoconstrictor responses to vagal stimulation [171]. They speculated that ozone exposure led to accumulation of reactive oxygen species (ROS) resulting from lipid peroxidation of pulmonary cell membranes. ROS trigger rapid release of cytokines including IL-1β, IL-6, IL-33, TNF-α, and TSLP to promote neutrophil infiltration and activation. Once activated, neutrophils in the airway mucosa release additional ROS, proteases, and cytokines, which can directly damage M2Rs (Figure 1.5) [172-174]. Gambone et al. (1994) showed that cyclophosphamide prevented ozone-induced loss of prejunctional M2R function by acting as an immunosuppressive agent and reducing neutrophil levels [175, 176].

The role of prejunctional M2R dysfunction in human asthma remains unclear. Earlier *in vivo* studies suggested that prior muscarinic stimulation protects against histamine-induced bronchoconstriction through activation of inhibitory prejunctional M2R. However, this interpretation did not account for the abundant post-junctional M2Rs now known to participate in airway smooth muscle contraction [177]. In contrast, research by Okayama et al. (1994) showed that pilocarpine at threshold doses (at which M2Rs are activated) significantly inhibited propranolol-induced bronchoconstriction, indicating some retained prejunctional M2R function in stable asthmatic airways [178].

Eosinophils are key drivers of asthma exacerbations through IL-5, GM-CSF, CCR3-directed chemokines, and interactions with mast cells and neutrophils [179, 180]. Antigen-induced, vagally mediated AHR has been linked to loss of neuronal M2R function. Jacoby et al. (1993) showed that eosinophil granule proteins, such as major basic protein (MBP), eosinophil peroxidase (EPO), eosinophil cationic protein (ECP) and eosinophil-derived neurotoxin (EDN) bind allosterically to negatively charged, sialylated M2Rs, inhibiting their function and promoting excess ACh release (Figure 1.5) [150, 181]. This antagonism is reversible: anionic poly-L-glutamate and heparin displace MBP and reduce vagally-induced bronchoconstriction in ovalbumin-challenged guinea pigs, with no effect in controls [182]. Preventing eosinophil influx preserves M2R function, anti-IL-5 (TRFK-5)

blocks eosinophil migration and maintains pilocarpine-responsive M2R; anti-VLA-4 (HP1/2) yields similar protection; and anti-MBP prevents MBP-mediated antagonism and antigen-induced AHR [183-185].

Neuronal M2R dysfunction during viral infection is not solely eosinophil driven. Parainfluenza neuraminidase removes sialic acids, selectively lowering agonist affinity at M2R and enhancing vagally mediated bronchoconstriction [181, 186]. Moreover, viral infection and IFN-γ reduce M2R mRNA and receptor function, increasing ACh release and thereby amplifying bronchoconstriction during viral airway disease [187].

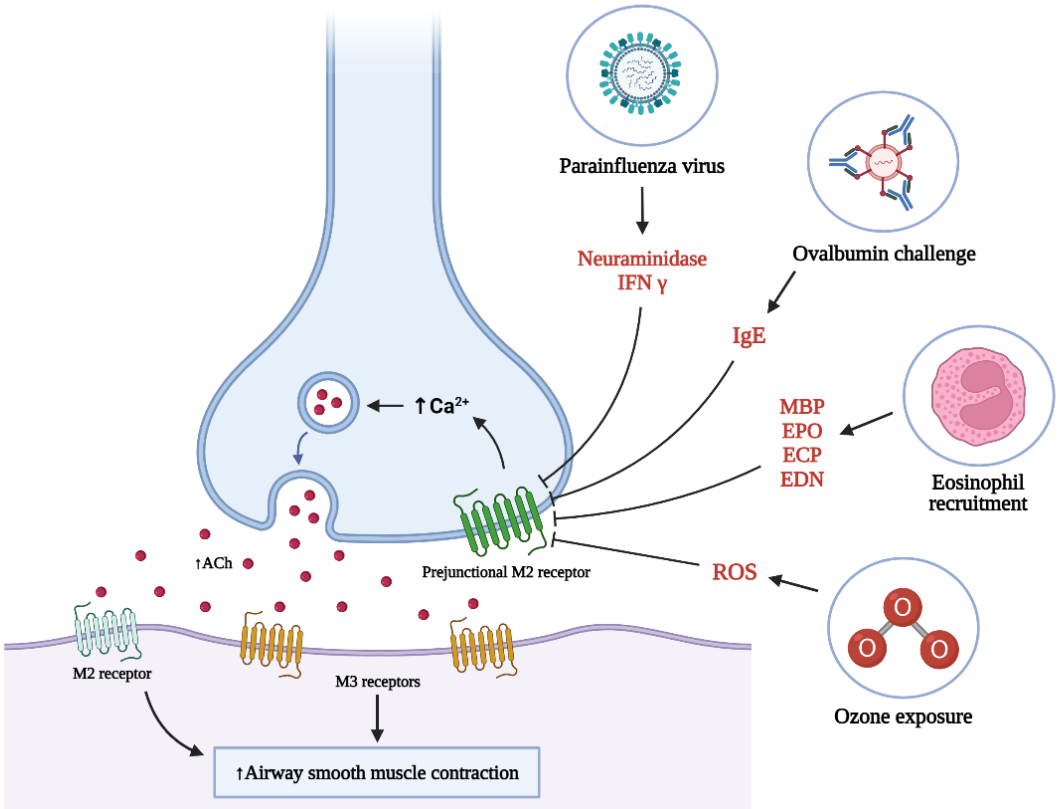

Figure 1.5: Dysfunction of prejunctional M2R in AHR. Prejunctional M2Rs normally act as inhibitory autoreceptors that limit ACh release from parasympathetic nerves. Loss or dysfunction of M2R signalling leads to excessive ACh release, resulting in enhanced activation of postjunctional M3R on ASM and increased contraction. Multiple inflammatory and environmental factors contribute to M2R impairment, including viral infections (e.g. parainfluenza virus via neuraminidase and IFN-γ), allergen exposure (ovalbumin-induced IgE responses), eosinophil-derived cationic proteins (MBP, EPO, ECP, EDN) and oxidative stress from ozone exposure (ROS generation). Together, these mechanisms disrupt M2R function, amplifying cholinergic signalling and promoting exaggerated bronchoconstriction characteristic of AHR. Figure created with a licensed version of BioRender.com. ACh, acetylcholine; IFN-γ, interferon gamma; IgE, immunoglobulin E; MBP, major basic protein; EPO, eosinophil peroxidase; ECP, eosinophil cationic protein; EDN, eosinophil-derived neurotoxin; ROS, reactive oxygen species.

1.5.1.1.3. M3 receptors

M3Rs couple to $G_{q/11}$, activating PLC_{β}, generating IP_3 and DAG. IP_3 engages IP_3 receptors (IP_3R) on the SR to release Ca^{2+} and then further Ca^{2+} release via RyR2 due to a local Ca^{2+}-induced Ca^{2+} release (CICR) process. Ca^{2+} binds with calmodulin to form Ca^{2+}-calmodulin complex which further activates MLCK, which phosphorylates MLC_{20} and initiates actomyosin cross-bridge cycling. This pathway is the primary driver of cholinergic bronchoconstriction [188, 189]. Beyond this mechanism, GPCR-driven receptor-operated Ca^{2+} entry (ROCE) contributes to M3R responses. The TRPC family is a prime candidate. TRPC3/6/7 can be DAG-activated downstream of the G_q-PLC pathway, whereas TRPC1/4/5 typically form heteromers engaged by PLC pathways. In airways, TRPC1/3/6 expression is reported and becomes functionally upregulated in disease or growth-factor conditions [190-193]. Thus, M3R activation can recruit TRPC currents, depolarise the membrane and facilitate voltage-dependent Ca^{2+} entry. Apart from Ca^{2+} mobilisation, M3R also activates RhoA/ROCK, which phosphorylates MYPT1 and inhibits MLCP, increasing Ca^{2+} sensitivity of contraction. These sensitisation routes are key amplifiers of cholinergic bronchoconstriction and are heightened in asthma and COPD [194].

Henrot et al. (2022) reported that approximately one-third of fibrocytes isolated from the blood of COPD patients express functional M3R, which on activation, induces cellular contraction [152]. Gosens et al. (2009) reported that CSE enhanced methacholine-dependent secretion of IL-8 and that these effects were inhibited by the M3R antagonists DAU5884 or 4-DAMP, but not the M2R-selective antagonist, gallamine [195]. M3R knockout (KO) mice were shown to have diminished goblet cell metaplasia in response to OVA challenge, indicating that M3Rs may exert a significant influence on allergen-induced airway remodelling [196].

1.5.1.2. Nicotinic Receptors

Nicotinic acetylcholine receptors (nAChRs) are pentameric ligand-gated cation channels assembled from α (α2-α10) and β (β2-β4) subunits. In the respiratory tract, they occur on neurons (parasympathetic ganglia, sensory nerves) and non-neuronal cells (ASM, epithelium, endothelium, and immune cells) [197]. Khalfaoui et al. (2023) demonstrated that α7 nAChRs are functionally expressed on

human ASM, with greater α7 abundance in asthmatic tissue. Activation of α7 raised intracellular Ca^{2+} and augmented contractility, indicating a direct role for α7 nAChRs in bronchoconstriction in asthma [198]. Borkar et al. (2024) further emphasised α7-dependent nicotinic effects on airway cells as a key mechanistic axis by which nicotine exposure (smoking or vaping) may worsen airway disease [199]. nAChRs on epithelium regulate mucus programmes and ion transport. Gundavarapu et al. (2012) showed that α7 nAChR signalling is critical for mucous cell hyperplasia and MUC5AC upregulation [200]. In parallel, Maouche et al. (2013) found α7 nAChR-CFTR coupling in airway epithelium, linking nicotinic signalling to ion transport and smoking-related chronic lung disease mechanisms [201].

1.5.2. Adrenergic sympathetic nerves

The sympathetic nervous system has a less prominent role in the human airways compared to the parasympathetic nervous system and is notably concentrated near submucosal glands and bronchial arteries. Its primary neurotransmitters include noradrenaline and neuropeptide Y (NPY) [202]. ASM appears to lack innervation by sympathetic nerves, but they express adrenergic receptors and are activated by circulating catecholamines [203, 204]. β-adrenergic receptors, which induce bronchorelaxation, are widely distributed in the human lung. Human ASM exclusively express β_2 adrenergic receptors, with their abundance escalating towards the peripheral airways [205].

Activation of β_2 receptors induces activation of the alpha subunit of G_s proteins, which separates and reattaches to AC, activating the enzyme to catalyse the conversion of ATP into cyclic adenosine monophosphate (cAMP). cAMP releases the protein kinase catalytic subunit (PKA) that phosphorylates different proteins, such as phospholamban (PLB), involved in the relaxation of smooth muscles in the airways [206-210]. In addition, cAMP activates exchange protein directly activated by cAMP (EPAC) which also induces ASM relaxation by decreasing MLC phosphorylation due to inhibition of RhoA/ROCK signalling [211, 212]. Chen et al. (2019) found that EPAC provides a protective function against airway inflammation and remodelling in murine models of asthma [213].

A recent study by Alkawadri et al. (2022) demonstrated that M2R-dependent ASM contractions were directly inhibited by β-adrenoceptor activation (Figure 1.6)

[214]. β_1-adrenergic receptor activation suppressed M2R-dependent contraction, and KO of M2Rs reduced the efficacy of β-adrenergic receptor agonists against cholinergic contractions, implicating post-junctional M2R signalling as a determinant of β-agonist responsiveness [214].

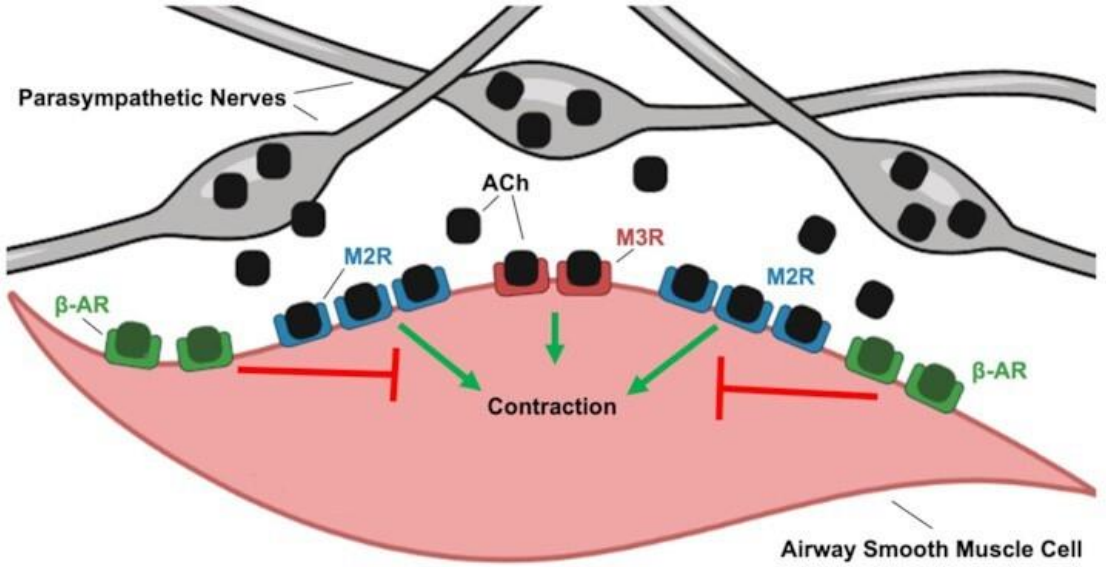

Figure 1.6: Model depicting M2R-dependent contractions of ASM are inhibited by activation of β-adrenoceptors. Parasympathetic nerve stimulation releases ACh, which activates postjunctional M3R on ASM to induce contraction. M2R on ASM further contribute to contractile responses by enhancing excitability and limiting relaxation pathways. In contrast, activation of β-adrenoceptors opposes contraction by promoting bronchodilatory signalling, thereby inhibiting M2R and M3R-mediated effects. The balance between cholinergic contraction and β-adrenergic relaxation determines overall ASM tone. (Figure adapted from Alkawadri et al. (2022) [214]).

1.6. Ion channels and receptors involved in ASM contraction

ASM cells express a plethora of ion channels which regulate ASM excitability. The role of these channels will be discussed below.

1.6.1. L-Type Ca^{2+} Channels

LTCC serve as the predominant pathway for Ca^{2+} entry in ASM [215-217]. LTCC are activated by numerous signalling pathways. For example, activation of G_qPCRs leads to the formation of IP_3 and DAG, and DAG further activates PKC which can activate LTCC [218]. LTCC exhibit Ca^{2+}-dependent inactivation (CDI), a feedback process which results in the inactivation of the channels when the concentration of intracellular Ca^{2+} rises. CDI of LTCC are essential for preventing excessive Ca^{2+} entry, helping to maintain cellular homeostasis and regulate various physiological processes [219-221].

It is widely accepted that ACh-induced contractions of ASM rely on Ca^{2+} release from intracellular stores via IP_3 receptors and ryanodine receptors (RyRs) [222-225]. However, the role of Ca^{2+} entry via LTCC in these responses is controversial as there is a discrepancy in the reported contribution of LTCC to contractions of ASM induced by cholinergic stimuli [226-228]. For example, the cholinergic agonist CCh was reported to induce sustained Ca^{2+} entry via LTCC in bovine ASM [229], but ACh-induced contractions of guinea-pig trachea were unaffected by blockade of LTCC with nifedipine [230]. Flores-Soto et al. (2013) observed that cholinergic contractions of murine and guinea pig airways were also unaffected by nifedipine [231]. Similarly, Ahmed et al. (1985) found that contractions induced by ACh and histamine in guinea pig trachea were resistant to nifedipine [232]. Studies on canine trachea showed that the effect of the LTCC inhibitor verapamil on ACh-induced contractions of canine trachea was dependent upon the concentration of ACh used to evoke the contraction. Verapamil inhibited contractions evoked by low concentrations (<1 μM) of ACh but did not affect contractions induced by higher ACh concentrations [233]. Similarly, Byron et al. (2013) found that low concentrations of agonist appear to act predominantly via activation of LTCCs, while higher concentrations act predominantly via IP_3-mediated Ca^{2+} release from the SR [234]. This also fits with the observation that contractions induced by low concentrations of cholinergic agonists were inhibited by membrane hyperpolarisation, while those evoked by high concentrations were entirely resistant to this intervention [235]. It is noteworthy that in ileum strips from M3R KO mice, nicardipine abolished contractions initiated by CCh, whereas no inhibition was observed in M2R KO mice. This suggests that LTCC may be involved in M2R-mediated contractions, but not those brought about by M3R activation [236].

1.6.2. Non-selective cation channels

Non-selective cation channels (NSCC) facilitate the transit of cations, including Na^+, K^+, and Ca^{2+}. Transient Receptor Potential (TRP) channels are a superfamily of 31 cation channels [237, 238], categorised into 10 families based on structural similarity: TRPC (canonical), TRPM (melastatin), TRPA (ankyrin), TRPP (polycystin), TRPN (no mechanoreceptor potential C), TRPML (mucolipin), TRPQ (Quartet), TRPY (yeast), TRPV (vanilloid) and TRPS (soromelastatin) [239]. Within ASM, the three most prominent and well-studied subfamilies are TRPC, TRPV, and

TRPM. These channels play a role in facilitating Ca^{2+} influx, thereby regulating both contraction and proliferation [227].

The TRPC family comprises seven members which are subdivided into four subtypes: TRPC1, TRPC2, TRPC4/5, and TRPC3/6/7. Recent evidence indicates the prevalence of mRNA encoding TRPC1, TRPC3, TRPC4, TRPC5, and TRPC6 in human ASM cells [240, 241], with TRPC2 mRNA showing enrichment in pig ASM cells [242]. White et al. (2006) observed a substantial rise in both TRPC3 mRNA and protein expression in human ASM cells treated with TNF-α compared to untreated controls. Additionally, it was shown that inhibition of TRPC3 reduced the ACh-induced elevation of intracellular Ca^{2+} in TNF-α treated human ASM cells [240]. Xiao et al. (2010) demonstrated a three-fold upregulation in the protein expression of TRPC3 in a murine model of asthma challenged with OVA when compared to controls. Conversely, no change in TRPC1 protein expression was observed [191]. In gastrointestinal smooth muscle, stimulation of M2Rs by ACh leads to activation of TRPC4 channels, resulting in the generation of cation currents (mICAT). This process induces cell depolarisation, serving as a crucial trigger for stimulation of voltage-dependent Ca^{2+} channels [243, 244].

The TRPV subfamily comprises six homologous members, each with distinct functions. TRPV1-TRPV4 are nonselective cation channels believed to be involved in nociception, whereas TRPV5 and TRPV6 play a role in maintaining epithelial Ca^{2+} homeostasis [245]. Jia et al. (2004) demonstrated that TRPV2 and TRPV4 acted as osmolarity sensors in human airways [246]. TRPV1 channel agonists elicit bronchoconstriction in both humans and animal models [247, 248] and research indicates that activation of TRPV4 channels may directly lead to constriction of ASM [249]. Bonvini et al. (2013) demonstrated that a selective TRPV4 channel activator induced contraction of both human and guinea pig ASM. Moreover, in anaesthetised guinea pigs with severed vagal nerves, the TRPV4 activator triggered bronchoconstriction. These findings suggest an important role for TRPV4 channels in bronchoconstriction observed in asthma [250].

The TRPM subfamily encompasses eight members (TRPM1-TRPM8) [251] and there is evidence that both TRPM4 and TRPM5 control membrane depolarisation and are involved in cellular proliferation, temperature sensing,

vascular development, and inflammation [252, 253]. Earley (2013) showed that TRPM4 channels are present in rat ASM [254], however little is known about the distribution and functional role of TRPM channels in ASM.

1.6.3. Ano1 Ca^{2+}-Activated Cl^- Channels

Ano1 is a member of the anoctamin (ANO1-ANO10) family of paralogous proteins. TMEM16A encodes Ano1 Ca^{2+}-activated Cl^- channels (CACC) [255] and is widely expressed in ASM and epithelial cells and is upregulated in inflammatory airway diseases such as COPD and asthma [256, 257]. Furthermore, AHR has also been linked to dysregulation of Ano1 function [255, 258]. Danielsson et al. (2019) showed that the transcriptional expression of Ano1 was approximately eight times higher in human ASM than in the epithelium [259]. Immunostaining of the Ano1 protein in ASM indicated that Ano1 was upregulated in ASM cells from OVA-sensitised mice by 48%, in comparison to control animals [260]. Furthermore, Ano1 currents were enhanced by the cytokines IL-4 and IL-13, which are highly elevated in asthma [256]. Cabrita et al. (2019) found that the expression of Ano1 and Ano6 plays a significant role in the regulation of mucus secretion in the airways. When both genes were knocked down, MUC5AC production was severely impaired [261].

In smooth muscle cells, intracellular Cl^- concentration (~55 mM) is substantially higher than would be predicted by passive distribution when compared to extracellular levels (~135 mM), unlike skeletal muscle where intracellular Cl^- is low (~4 mM) and closely follows passive Donnan equilibrium. This elevated intracellular Cl^- in smooth muscle is maintained by active transport mechanisms, including Na^+-K^+-Cl^- cotransport and Cl^-/HCO_3^- exchange, as well as an additional Cl^- influx pathway (historically termed “Pump III”), which sustains Cl^- accumulation even when the major transporters are inhibited. As a result, the Cl^- equilibrium potential (E_{Cl}) is more positive than the resting membrane potential (E_m), creating a favourable electrochemical gradient for Cl^- efflux under resting conditions [262-264]. Upon activation of CACCs such as Ano1, Cl^- exits the cell, leading to membrane depolarisation and subsequent activation of voltage-dependent pathways. Although several Cl^- channels are expressed in smooth muscle, including bestrophins, ClC3 channels and CFTR channels, Ano1 is considered the functional channel mediating

Ca^{2+}-dependent Cl^- efflux in ASM, thereby contributing to excitation-contraction coupling [262-264].

Wang et al. (2018) showed that genetic KO of Ano1 greatly attenuated contractile responses to histamine and the thromboxane agonist, U46619. In contrast, responses induced by maximal concentrations of methacholine were unaffected in Ano1 KO mice. However, responses induced by lower concentrations of methacholine were 50% smaller than those in wild-type mice [265]. Several studies concluded that Ano1 channels are important for excitation coupling of responses to cholinergic agonists in ASM, even at higher concentrations [256, 259, 266]. However, these studies relied, at least in part, on the Ano1 blocker benzbromarone, the specificity of which has since been questioned [267]. Dwivedi et al. (2023) found that benzbromarone inhibited CCh-induced contractions over the concentration range of 0.1-10 μM. Worryingly, however, it had a markedly greater inhibitory effect than nifedipine and a further inhibitory effect in tissues that had already been exposed to nifedipine. These data indicated that benzbromarone had one or more off-target effects beyond blocking the membrane depolarisation responsible for activating LTCCs. On the other hand, the selective Ano1 blocker, Ani9 had no effects on CCh-evoked contractions when used at a concentration range of 0.1-10 μM, although it abolished phasic contractions induced by 5-HT [267].

1.6.4. Potassium channels

Potassium channels are classified into four primary types based on their structure and function: voltage-gated potassium channels (K_v), Ca^{2+}-activated potassium channels (K_{Ca}), ATP-sensitive potassium channels (K_{ATP}), and inward rectifier potassium channels (K_{IR}) [268]. The K_{Ca} channels are further divided into three types: small conductance (SKCa, 4-14 pS), intermediate conductance (IK_{Ca}, 32-40 pS), and large conductance (BK_{Ca} or Maxi K, 200-300 pS) [269].

1.6.4.1. BK_{Ca} channels

The name "big conductance" reflects the high permeability of BK_{Ca} channels to potassium ions [270]. These channels are widely expressed in epithelial cells, endothelial cells, smooth muscle cells and in motor and sensory neurones [271-

274]. They have been found in abundance in ASM cells of murine, canine, bovine, swine, and human airways where they are believed to regulate tone [275-278]. BK_{Ca} channels depend on both Ca^{2+} and voltage for activation. Their activation in smooth muscle cells is triggered by spontaneous Ca^{2+} release from the peripheral SR, contributing to the regulation of cellular excitability and membrane potential [269, 279]. Activation of G_s proteins that lead to the formation of cAMP also activates BK_{Ca} channels to cause vasodilation in VSMC [280]. Barman et al. (2003) found that activation of PKC hindered cAMP-induced activation of BK_{Ca} channels in pulmonary arterial smooth muscle [281]. Modulation of BK_{Ca} channels in ASM contributes to bronchoconstriction, plasma extravasation and cough [282]. Recent research has determined that inflammation upregulates BK_{Ca} channel expression which further potentiates Ca^{2+} signalling in ASM [283-285]; however, increased expression does not necessarily equate to potentiated Ca^{2+} signalling, as BK_{Ca} channels are Ca^{2+}-activated K^+ channels that typically act as a negative feedback mechanism to limit membrane depolarisation and Ca^{2+} influx. Thus, their functional impact depends on factors such as channel coupling to Ca^{2+} sources, subcellular localisation and regulatory signalling pathways rather than expression levels alone. Zhou et al. (2018) found that $G_{\beta\gamma}$ dimers released from activated M2Rs inhibited BK_{Ca} channel activity via direct effects on the BK_{Ca} channel α-subunit and via activation of PKCs via the PLC_{β} pathway [286]. However, although cholinergic agonists were able to inhibit BK_{Ca} via M2Rs, another study suggested that this mechanism plays only a minor role in mediating the contractions of ASM induced by M2Rs [164]. Activation of BK_{Ca} channels has been identified as a factor that suppresses airway inflammation and improves symptoms associated with asthma [287].

1.6.4.2. Kv7 channels

Kv7 channels are voltage-gated K^+ channels which serve as crucial determinants of membrane potential (E_m) as they activate at relatively negative potentials, compared to other K^+ channels and play a crucial role in controlling smooth muscle contractility [288]. Activation of these channels results in hyperpolarisation and relaxation of smooth muscle cells by reducing the activity of voltage-gated Ca^{2+} channels and diminishing Ca^{2+} influx [288]. The Kv7 family comprises five recognised members (Kv7.1-Kv7.5) encoded by distinct genes (KCNQ1-5) [289]. In lung tissues, Kv7 channels are expressed in pulmonary artery

smooth muscle cells, ASM cells and airway epithelial cells [290]. Notably, qRT-PCR of human tracheal muscle showed that Kv7.1 expression is highest in human trachea, followed by Kv7.4 and Kv7.5 [291]. Evseev et al. (2013) found that Kv7.1 was the predominant Kv7 subtype expressed in mouse airway tissues, followed by Kv7.4, with Kv7.5 showing weak expression. In rat trachea, Kv7.1 expression was also highest, but Kv7.5 mRNA levels exceeded those of Kv7.4, and low levels of Kv7.3 were additionally detected, which were largely absent in mice. Similarly, Guinea pig ASM cell also express Kv7 channels with relative abundance order of Kv7.2 > Kv7.5 > Kv7.4 > Kv7.3 > Kv7.1 [292].

Cholinergic agonists have long been known to suppress Kv7 channel activity, most prominently through inhibition of the neuronal M current, a non-inactivating, subthreshold K^+ current mediated predominantly by Kv7.2-Kv7.5 channels. Activation of muscarinic receptors, particularly M1R in neurons, leads to a reduction in M current, resulting in membrane depolarisation and enhanced cellular excitability [293, 294]. Several mechanisms may underlie cholinergic suppression of Kv7 currents. Firstly, all K_V7 subtypes bind to phosphatidylinositol 4,5-bisphosphate (PIP_2), which facilitates channel opening; hence, PIP_2 depletion closes the channel [295]. Zhang et al. (2003) found that in excised inside-out patches from cells expressing Kv7 channels, bath application of PIP_2 diC8 (an exogenous analogue of PIP_2) restored rundown and robustly activated the channels, demonstrating direct PIP_2 dependence [296]. Similarly, Li et al. (2005) found that in CHO cells expressing Kv7.2-Kv7.4, inside-out patch recordings showed that PIP_2 diC8 increased open probability well above cell-attached levels, confirming direct activation by PIP_2 [297]. Therefore, activation of M3Rs could, via activation of PLC, inhibit Kv7 channels with resultant depolarisation. It has also been shown that cAMP, working via both PKA and EPAC, increased Kv7 channel open probability [298, 299]. Hence, a reduction in cAMP levels via activation of $G_{i/o}$ could provide a possible link between M2R stimulation and inhibition of Kv7 channels.

1.6.4.2.1. Kv7 channel structure

The structure of Kv7 channels resembles that of other Kv channels, with each functional channel forming homo or heterotetramers of six transmembrane (S1-S6) domains (Figure 1.7) [298]. The S1-S4 transmembrane domains have regions that are responsible for sensing the voltage difference across the membrane, with S4

possessing many charged residues, which are essential for voltage-sensing. The S5 and S6 domains, along with the pore loop region, form the ion conduction pathway through which the ions pass when the channels are in an activated and open state [300, 301]. In the tetrameric arrangement, the S6 domain forms the inner lining of the pore. Both the C and N termini are cytosolic in this channel. The C-terminal of Kv7 channels is quite large and is involved in tetramerisation of the channels [300, 301]. It also has special regions called A-D helices, which act as docking stations for calmodulin (CaM) and other regulatory proteins to bind. Calmodulin binding is essential for the channel to fold correctly and reach the cell surface. Depending on Ca^{2+} levels, CaM can also change how easily the channel opens [302]. The N-terminal is shorter than the C-terminal but plays an important role in the control of channel gating and phosphorylation. For example, in Kv7.5, the N-terminus contains a key PKA phosphorylation site (Serine 53) which causes a conformation change that makes the PIP_2 binding site more susceptible to bind to PIP_2 [299, 303, 304]. PIP_2 is essential for Kv7 channel opening, and its binding sites are spread across several key regions of the protein. These include the intracellular S2-S3 linker and S4-S5 linker, which connect the voltage-sensing parts of the channel to the pore, as well as the proximal end of the S6 helix, which lines the inner pore (Figure 1.7) [305-307]. In addition, clusters of positively charged residues in the proximal C-terminal helices (A/B domain) help anchor PIP_2. Together, these sites form a binding pocket where PIP_2 stabilises the channel in its open state by linking voltage sensor movement to pore opening. When PIP_2 is depleted, for example by muscarinic receptor activation and PLC-mediated hydrolysis, these stabilising interactions are lost, causing the channel to close. Several kinases fine tune the channel, for example, PKA usually enhances Kv7 currents by phosphorylating specific serine residues (e.g., N-terminal Serine 53 in Kv7.5), which makes the channel open more easily [308, 309]. PKC often inhibits Kv7 activity via phosphorylation sites in the C-terminal (Serine 541 in Kv7.2) and promotes muscarinic suppression of Kv7 currents [310, 311]. In contrast, PKG (protein kinase G), activated by the NO-cGMP pathway, increases Kv7 currents in vascular smooth muscle, leading to relaxation, although the exact residues it phosphorylates are less clearly known [312, 313].

Formation of Kv7 heterotetramers is restricted to certain combinations. The most well-characterised heteromer is Kv7.2/Kv7.3, which accounts for functional M-type currents in many neurons [314, 315]. In vascular smooth muscle cells, Kv7.4 and Kv7.5 are often co-expressed, and dominant negative experiments suggest that native currents frequently depend on heteromeric Kv7.4/Kv7.5 assemblies rather than pure homomers [316, 317]. Chadha et al. (2014) further reported that Kv7.4/Kv7.5 heteromers largely underlie intrinsic myogenic responses and vasodilation in arteries, reinforcing their physiological relevance in vascular tone control [317]. Oliveras et al. (2014) demonstrated that Kv7.1 and Kv7.5 can also form functional heterotetramers with distinct electrophysiological and pharmacological properties in vascular smooth muscle cells [318]. Heteromerisation can also occur with Kv7.2/Kv7.5 or Kv7.3/Kv7.5 in certain tissues, expanding the diversity of channel properties [319]. Other combinations (e.g. Kv7.4 with Kv7.2 or Kv7.3) are more restricted, likely due to structural compatibility or trafficking constraints. Structural studies suggest that the C-terminal A-domains of Kv7 subunits modulate promiscuous assembly and may restrict certain heteromeric partnerships [320]. Functionally, heteromerisation often yields channels with intermediate gating and conductance properties, and can magnify current densities compared to some homomers, particularly in Kv7.2/Kv7.3 assemblies [321].

1.6.4.2.2. KCNE subunits

The KCNE family (also called MiRPs) consists of small single-transmembrane “β-subunits” that do not form ion channels by themselves but associate with Kv7 α-subunits to modulate their plasmalemmal expression, biophysical properties and pharmacology (Figure 1.7) [322-324]. Co-expression of KCNE1 with Kv7.1 markedly alters channel behaviour. It increases Kv7.1 current density, induces a positive shift in the voltage activation threshold, and slows both activation and deactivation kinetics [325, 326]. Mechanistic studies demonstrated that KCNE1 stabilises the open conformation of the Kv7.1 pore by modifying interactions between the pore helix, the selectivity filter, and the S5/S6 domain [327]. Beyond Kv7.1, Roura-Ferrer et al. (2009) found that KCNE1 has also been shown to increase Kv7.5 currents in HEK293 cells [328] and Abbott (2015) discovered that KCNE1 mildly augments Kv7.4 currents when co-expressed in *Xenopus* oocytes [329].

KCNE2 was also found to alter the gating mechanism of Kv7.1 channels [330] and the Kv7.1/KCNE2 complex was found to play an essential role in establishing the resting membrane potential in parietal cells of the gastric glands [331]. Later, Lundby et al. (2009) found that KCNE2 makes the Kv7.1 channels constitutively open [326]. The effects of KCNE3 vary among different isoforms of Kv7 channels. In mammalian cells, co-expression with Kv7.1 produces little change in the current-voltage (I-V) relationship [332]. However, KCNE3 strongly suppresses Kv7.5 currents in HEK293 cells and markedly inhibits Kv7.4 activity in Xenopus oocytes [328, 329]. KCNE4 is predominantly inhibitory to Kv7.1, suppressing current amplitude at physiologically relevant voltages in both mammalian cells and *Xenopus* oocytes [333]. Interestingly, in stably transfected HEK293 cells, KCNE4 increased Kv7.4 current amplitude and produced a negative shift in the $V_{1/2}$ of activation [334]. In native tissue, proximity ligation assays demonstrated that KCNE4 co-localises with Kv7.4 and Kv7.5 in freshly isolated mesenteric smooth muscle cells, supporting a role for KCNE4 in regulating cell-surface expression and Kv7.4 function [335].

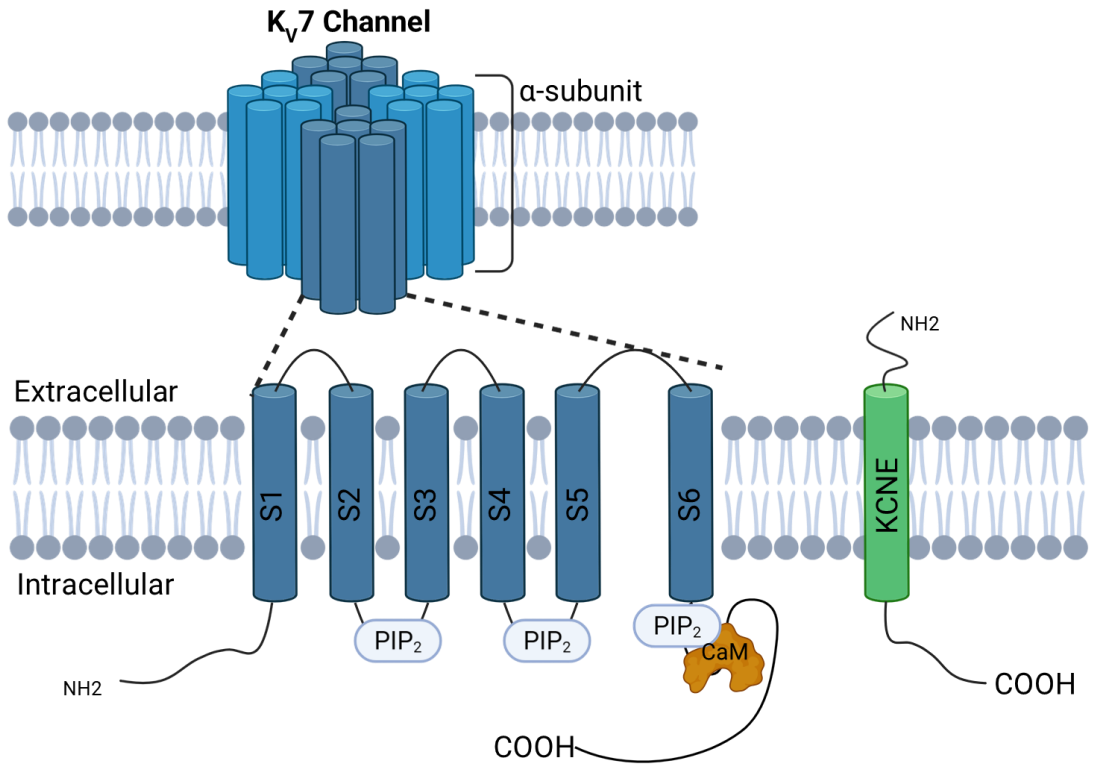

Figure 1.7. Schematic representation of the Kv7 channel α-subunit topology, illustrating the six transmembrane segments (S1-S6) embedded within the lipid bilayer. The upper panel shows a top-down view of the tetrameric assembly, while the lower panel depicts a single α-subunit monomer with its voltage-sensing domain (S1-S4) and pore-forming domain (S5-S6). Key regulatory interactions are highlighted, including intracellular PIP_2 binding sites, constitutively associated calmodulin (CaM), and the single-pass accessory KCNE β-subunit, all of which collectively modulate channel gating, kinetics and membrane trafficking. Figure created with a licensed version of BioRender.com.

Finally, KCNE5 produces a marked depolarising shift in Kv7.1 activation, such that Kv7.1/KCNE5 channels activate only at voltages >+40 mV, leaving them effectively closed under physiological conditions [336, 337]. KCNE5 was also reported to inhibit Kv7.4 currents by about 65% in CHO cells, although no significant effects were observed in *Xenopus* oocytes [334, 336]. Co-expression of Kv7.5 with KCNE4 or KCNE5, in either oocytes or mammalian cells, produced no major functional changes [328].

1.6.5. Intracellular Ca^{2+} stores

Intracellular Ca^{2+} is stored in organelles, including the SR [338]. Within ASM cells, release of intracellular Ca^{2+} from stores is a crucial process which is facilitated by two types of Ca^{2+} release channels residing on the SR: RyRs and IP_3Rs. These channels play a pivotal role in orchestrating the controlled release of Ca^{2+}, influencing various cellular functions in ASM cells [339].

1.6.5.1. IP_3 receptors (IP_3Rs)

IP_3Rs form a family of tetrameric Ca^{2+} release channels situated on the SR membrane in nearly all mammalian cell types, including smooth muscle cells [340]. Stimulation of ASM by histamine, methacholine or carbachol stimulates PLC, resulting in the generation of IP_3 and release of Ca^{2+} from the SR via IP_3Rs [341]. Mammalian smooth muscle cells express three different isoforms of IP_3R, namely IP_3R1, IP_3R2, and IP_3R3 [342]. IP_3R activation produces a broad range of Ca^{2+} signals, including puffs, waves, ripples, sparks, and global $[Ca^{2+}]_i$ [340]. Expression studies revealed that activation of M2Rs can also stimulate PLC which initiates the breakdown of PIP_2 into IP_3 and DAG [343]. Asthma is linked to increased intracellular IP_3, heightened IP_3R signalling and enhanced contractility in ASM cells. This association contributes to AHR and remodelling. In Fisher rats, utilised as an asthma animal model, there is a reduction in both the expression and activity of IP3,5-phosphatase, resulting in elevated levels of $[IP_3]_i$ and heightened IP_3R-mediated Ca^{2+} release in ASM cells [340, 344].

1.6.5.2. Ryanodine receptors (RyRs)

RyRs are intracellular Ca^{2+} release channels located on the SR membrane in various types of smooth muscle cells [345]. While RyRs and IP_3Rs possess a similar architectural framework, RyRs have developed additional domains within their

cytosolic region. Due to their substantial size, RyRs can be regulated by a multitude of proteins and small molecules, influencing the opening and closing of the channels [346]. RyRs exist in three isoforms (RyR 1-3) and are named after the plant alkaloid ryanodine [347, 348]. Hyvelin et al. (2000) found that human bronchial smooth muscle cells only express the RyR3 isoform [349], while all the RyR isoforms are expressed in rat and mice ASM cells with the expression of RyR1 being elevated in cases of chronic asthma [350, 351]. These channels have been implicated in the amplification of Ca^{2+} transients triggered by opening of LTCC or IP_3Rs in smooth muscle cells [345]. Additionally, RyRs appear to play a role in regulating BK channel activity [345]. Du et al. (2005) demonstrated that both RyR1 and RyR3 are expressed in mouse ASM and are involved in mediating bronchoconstriction induced by the muscarinic receptor agonist, CCh. When RyR isoforms were inhibited using ryanodine at concentrations greater than 200 μM, the contractile responses of mouse bronchial rings and Ca^{2+} responses of ASM cells to various concentrations of CCh (ranging from 50 nM to over 3 μM) were attenuated. Conversely, inhibiting only RyR1 and RyR3 with dantrolene (25 μM) attenuated the responses induced by high CCh concentrations (>500 nM) but not by low concentrations [352].

1.6.5.3. SERCA

The Sarcoplasmic/Endoplasmic Reticulum Ca^{2+}-ATPase (SERCA) pump has three primary isoforms that are expressed in smooth muscle; SERCA2b is the most prevalent (91%), whereas SERCA2a (6%) and SERCA3 (3%) are present in lower quantities [353]. Maintenance of intracellular free Ca^{2+} levels within a physiological range relies on SERCA-mediated Ca^{2+} uptake into stores. Furthermore, sequestration of Ca^{2+} by SERCA facilitates relaxation of smooth, cardiac and skeletal muscles [354]. Janssen et al. (1999) demonstrated that Ca^{2+} entry through LTCC in canine tracheal myocytes is strongly buffered by SERCA pumps located on the superficial sarcoplasmic reticulum, which lies in close proximity to the plasma membrane [355]. This arrangement allows the superficial SR to rapidly sequester incoming Ca^{2+} before it can diffuse to the contractile apparatus, a process described as the superficial buffer barrier (SBB) hypothesis [356-358]. In vascular smooth muscle, inhibition of this barrier has been proposed to enhance agonist-induced contraction by permitting greater Ca^{2+} access to the myofilaments following opening

of voltage-gated Ca^{2+} channels [355]. However, whether the SBB mechanism contributes to force generation in airway smooth muscle remains unclear. Mahn et al. (2009) demonstrated that ASM cells from individuals with asthma displayed reduced levels of SERCA2 expression, and this reduction was found to be associated with the severity of the disease. When healthy ASM cells were subjected to siRNA-induced knockdown of SERCA2, they exhibited characteristics similar to those observed in asthmatic ASM cells, such as delayed recovery from an increase in $[Ca^{2+}]_i$, increased cellular motility, proliferation and secretion [359]. Clark et al. (2010) provided findings supporting the idea of two distinct functionally separated SR Ca^{2+} stores within pulmonary arterial smooth muscle cells. One of these stores was positioned in proximity to the plasma membrane, likely regulated by SERCA2b, and releasing Ca^{2+} via RyR1, to facilitate pulmonary artery dilation. In contrast, the second store was centrally located, served by SERCA2a, and released Ca^{2+} via RyR3. This release may trigger recruitment of RyR2 through Ca^{2+}-induced Ca^{2+} release, initiating a propagating global Ca^{2+} wave and subsequent pulmonary artery constriction [360].

1.6.5.4. Calcium Release Activated Calcium (CRAC) channels

CRAC channels serve as a pivotal pathway for Ca^{2+} signalling within cells. Their activation is triggered by depletion of Ca^{2+} from the endoplasmic reticulum (ER) / SR by a phenomenon referred to as Store-Operated Ca^{2+} Entry (SOCE) [361]. It is now known that the $[Ca^{2+}]_{SR}$ sensor STIM1 dynamically reorganises its spatial structure into aggregate clusters in response to a decrease in Ca^{2+} concentration in the ER. These aggregate clusters interact with Orai channels in the plasmalemma to enable CRAC [362]. STIM1 and Orai1 could be important targets for ASM remodelling in asthma, as decreased expression of these proteins resulted in considerable inhibition of chemotactic migration and smooth muscle cell proliferation [363-365]. In addition, expression of STIM1 and Orai1 proteins was increased in smooth muscle cells from tracheal and bronchial tissue derived from OVA-challenged mice with asthma.

1.7. Obstructive Airway Diseases

Obstructive airway diseases such as asthma and COPD are characterised by reduced airflow during exhalation. Key indicators including forced expiratory volume

in the first second (FEV1), FEV1/FVC ratio and forced expiratory flow between 25% to 75% of FVC (FEF25-75) fall below expected levels [366]. Forced vital capacity (FVC) refers to the total volume of air that can be forcibly exhaled from the lungs after a maximal inspiration and reflects lung function. Changes in the contractile properties and mass of ASM can result in airway inflammation, hyperresponsiveness, and remodelling, which are major characteristics of COPD and asthma [367].

1.7.1. Asthma

Asthma is an obstructive airway disease characterised by impaired relaxation and enhanced bronchoconstriction in response to relatively little provocation, which is denoted as airway hyperresponsiveness (AHR) (Figure 1.4) [368]. Thus, in response to low-level stimuli, the contractile response of ASM in asthma causes severe bronchoconstriction and airflow blockade [54, 368, 369]. Substantial loss of heat and water through respiration during exercise in temperate or cold conditions can also induce bronchoconstriction. This is likely facilitated by increased activity of cholinergic nerves [370-373] or release of inflammatory mediators from mast cells in response to exposure to a hyperosmolar environment [368]. Understanding the cellular processes that underlie excitation-contraction coupling of ASM is crucial to better understand the disease.

In normal lung function, muscarinic receptors regulate ASM tone, mucus production, vasodilation and inflammation. However, in conditions like asthma and COPD, cholinergic pathways exacerbate bronchoconstriction and mucus secretion, leading to airflow restriction [374]. Under physiological conditions, muscarinic receptor activation maintains airway tone primarily through M3R-mediated Ca^{2+} mobilisation and myosin phosphorylation. In asthma, however, this pathway becomes hyperresponsive, leading to exaggerated ASM contraction. Enhanced G_q-coupled M3R signalling augments IP_3-dependent Ca^{2+} release and DAG-driven PKC activation, which sustains myosin light-chain phosphorylation via CPI-17 mediated inhibition of MLCP. Collectively, these changes amplify cholinergic bronchoconstriction and contribute to airway hyperreactivity [375, 376].

Enhanced proliferation and secretion of pro-inflammatory chemokines result in ASM remodelling that is often regulated by $[Ca^{2+}]_i$. Release of these mediators is

significantly influenced by Ca^{2+} signalling. For example, it was found that IL-13 caused secretion of eotaxin-1 from ASM following the knockdown of SERCA, which recruited eosinophils and perpetuated airway inflammation [377]. Furthermore, M3Rs on ASM play a crucial role in airway remodelling by promoting smooth muscle proliferation and migration. In addition, ASM from asthmatic individuals shows heightened responsiveness to cholinergic stimulation, indicating that M3R activation can drive pathological changes in muscle mass and structure [378]. M3R activation also contributes to altered ASM mechanobiology including changes in the stiffness, ECM coupling and force-transmission of ASM have been linked to enhanced muscarinic responsiveness, implicating M3Rs in the shift of ASM phenotype in asthma [54, 378]. Beyond the local effects on muscle, cholinergic stimulation through M3Rs can also modulate vagal reflex sensitivity, thereby amplifying parasympathetic tone and contributing to the excessive airway narrowing characteristic of AHR [379].

1.7.2. COPD

COPD encompasses a range of conditions characterised by airflow obstruction and respiratory difficulties, including emphysema and chronic bronchitis (figure 1.8) [380]. Like asthma, COPD patients have a thickened ASM layer surrounding the airways [381]. However, in COPD, the smooth muscle layer also experiences a rise in ECM, which makes it more difficult for air to pass through the airways and causes irreversible breathing problems [382]. The size of the ASM cell or the expression of the contractile proteins like alpha-actin, smooth muscle myosin heavy-chain isoforms, myosin light-chain kinase, and the phosphorylated form of the regulatory light chain of myosin does not increase, according to bronchoscopy biopsies, in contrast to individuals with severe chronic asthma [383, 384]. The stiffness of the airway wall is determined by its passive and active components. While the active component results from smooth muscle contraction, the passive component is based on the physical characteristics of the tissues (such as smooth muscle and ECM) in the airway wall. The distensibility or flexibility of the airway wall is decreased in COPD, making it less able to expand while breathing. This is especially true for those who have emphysema [382, 385, 386]. In the lungs of persons with COPD, a process known as airway remodelling takes place where the structure of the airways alters in response to chronic inflammation and other

variables. The remodelling process can result in a variety of modifications to the airways, including thickening of the smooth muscle layer and airway walls. However, it has been noted that the ASM thickening is similar to COPD as in asthma [387]. The main reason behind this may be because the airflow restriction in COPD is not only due to ASM changes, but several variables, such as inflammation, airway constriction brought on by the creation of mucus and emphysema [387, 388]. Furthermore, in asthma, ASM thickening is more prominent in the larger airways, whereas in COPD, it is more pronounced in the small airways [389, 390]. However, similar to asthma, patients with COPD also exhibit reduced SERCA activity [391]. Nguyen et al. (2005) found that severe COPD elicited marked decreases in SERCA1 isoform and no change in SERCA2 isoform content was seen in airway skeletal muscles [392].

Due to heightened cholinergic activity in COPD, long-acting muscarinic antagonists (LAMA) are utilised to primarily target M3 receptors (M3R). These receptors play key roles in bronchoconstriction, mucus secretion, and inflammation, contributing to COPD pathophysiology [393, 394]. The 2022 report from the Global Initiative for Chronic Obstructive Lung Disease (GOLD) suggests starting pharmacological therapy with either a long-acting muscarinic antagonists (LAMA) or a long-acting β_2-agonist (LABA) for most patients [395]. As prolonged usage of LABA may eventually result in diminished effectiveness and receptor desensitisation and most LAMAs do not show signs of intolerance, LAMAs are the mainstay therapeutic agents for the control of COPD exacerbations [396]. For those experiencing more severe symptoms, regardless of their exacerbation history, dual bronchodilator therapy (LABA/LAMA) is recommended. In Europe, three LAMAs- tiotropium bromide, glycopyrronium bromide, and aclidinium bromide have been approved for the treatment of COPD [394].

1.7.3. Are M2R involved in Obstructive Airway Diseases?

Asthma and COPD are associated with increased activity of parasympathetic cholinergic nerves and increased hyperresponsiveness to ACh agonists [397-400]. However, despite the upregulation of cholinergic activity in asthma, this does not appear to be associated with a change in M3R functionality. For example, Whicker et al. (1990) showed that antigen challenge in guinea pig ASM led to increased sensitivity to CCh, but this was not associated with a change in the binding of a

radiolabelled muscarinic receptor ligand [401]. Similarly, Haddad et al. (1996) showed that there was no significant difference in the affinity or the density of muscarinic receptors in peripheral lung samples taken from asthmatics compared with non-asthmatics [402]. In addition, single-nucleotide polymorphisms in the promoter region of the human M3R gene did not appear to be associated with asthma as there was no difference in the recorded frequency of SNPs among asthmatic patients and healthy control subjects [403]. Therefore, although ASM in asthmatic patients is hyperresponsive to ACh, this enhanced responsiveness is unlikely to result from increased M3R expression or receptor affinity, but rather from downstream signalling alterations or impaired regulatory mechanisms that amplify cholinergic responses.

It is well established that asthma and COPD are associated with dysfunction in prejunctional M2Rs; however, there is also some indication that postjunctional M2Rs may also play a role in the pathogenesis of these conditions. The primary lines of evidence in this regard are the sensitivity of heightened cholinergic responses of ASM to PTX and the increased expression of $G_{i/0}$ proteins that couple to M2Rs in experimental models of asthma. For example, Hakonarson et al. (1995) showed that rabbit tracheal smooth muscle that was passively sensitised with serum from atopic asthmatics had enhanced contractile responses to ACh that were attenuated by PTX. Furthermore, $G_{i\alpha}$ subunit expression was increased in tissues treated with serum from atopic asthmatics [404]. Similarly, Chiba et al. (2001) demonstrated that augmented responses to ACh in antigen-treated ASM of rats were reduced by PTX and that $G_{i\alpha3}$ protein levels were greatly enhanced [405]. The inflammatory mediators, IL-1β and TNF-α, play important roles in the pathogenesis of the airway inflammatory response in asthma [406-409]. Hakonarson et al. (1996) showed that IL-1β and, to a lesser extent, TNF-α attenuated β-AR-mediated relaxations of ASM that were precontracted with ACh. It was suggested that the effects of IL-1β were due to activation of an M2R-signalling pathway as methoctramine potentiated isoproterenol-induced relaxations of tissues treated with IL-1β, but not controls. This study also found that the expression of $G_{i\alpha2}$ and $G_{i\alpha3}$ subunits was enhanced in ASM treated with IL-1β [410]. Therefore, it is possible that postjunctional M2Rs may not be directly upregulated in airway disease, but that M2R-dependent signalling pathways could be enhanced as a result of increased $G_{i\alpha}$ subunit expression and enhanced $G_{i\alpha}$/M2R coupling.

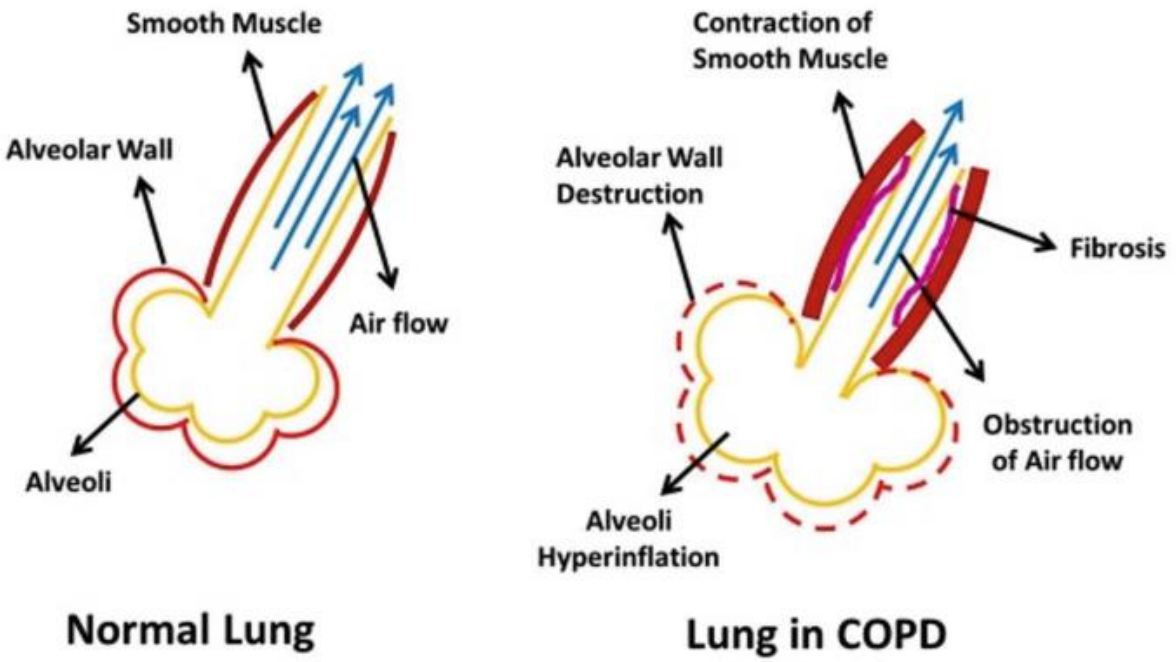

Figure 1.8: Diagram Comparative schematic illustrating the structural and functional differences between a normal lung and a lung affected by COPD. In the normal lung, intact alveolar walls, compliant smooth muscle and unobstructed airways permit unrestricted airflow. In COPD, a combination of pathological changes, including alveolar wall destruction, alveolar hyperinflation, smooth muscle contraction and airway fibrosis, collectively result in significant obstruction of airflow, reflecting the hallmark progressive airflow limitation characteristic of the disease *(*Figure adapted from Bhatt et al. (2021) [411]).

1.8. Project aims and objectives

The contractile effects of ACh are mediated by activation of muscarinic receptors on ASM cells. ASM express both M2Rs and M3Rs, although the M2Rs outnumber the M3Rs by a ratio of 4:1 in most species. Despite this, it is widely considered that it is the M3Rs that mediate the contractile effects of ACh on ASM. Instead, the M2Rs were thought to be redundant, apart from being able to offset relaxations induced by activation of β-adrenergic receptors. However, there is now growing evidence that postjunctional M2Rs have a pivotal role in sensitising ASM to stimulation of M3Rs [153]. Furthermore, it has also been shown that β-adrenergic receptor-mediated inhibition of ACh-induced contraction of ASM is brought about by inhibition of M2R-dependent responses. Therefore, M2Rs have an important role in ASM contractions induced by cholinergic stimulation, but little is known about the mechanisms that underlie their effects.

The overarching aim of this study was to elucidate the mechanisms underlying M2R-dependent contractions of ASM.

Chapter 2

Materials and Methods

2.1. Tissue preparation

Male and female wild-type (WT) C57BL/6 mice (aged between 9-14 weeks old) were humanely euthanised by intraperitoneal injection of phenobarbitone sodium (100 mg/kg), in accordance with EU Directive 2010/63/EU and with the approval of Dundalk Institute of Technology Animal Ethics Committee. Environmental conditions within the animal facility were maintained using a closed-circuit system with temperature ranging between 18-20°C and 50% humidity.

The airways were removed and pinned on a Sylgard base petri dish containing Krebs solution. The bronchial tree was exposed by sharp dissection under a dissection microscope to remove surrounding blood vessels, fats, and lung tissue. The left and right primary bronchi were cut into two pieces to form four bronchial rings of approximately 2-3 mm in length.

2.2. Transgenic mice

M2 muscarinic receptor knockout (M2R KO) mice were obtained from The Jackson Laboratory. The M2R knockout allele was originally generated by Jürgen Wess through targeted disruption of the CHRM2 gene on chromosome 6. The colony was backcrossed onto a C57BL/6 background for at least ten generations. Heterozygous mice were intercrossed to generate wild-type, heterozygous, and homozygous littermates. Genotypes were confirmed using standard PCR-based methods from ear tissue samples. Murine bronchi isolated from M2R KO mice were used for the experiments described in Chapter 3 (Figure 3.4B).

2.3. Isometric tension recording

Bronchial rings were mounted in water-jacketed organ baths using two ‘S’ shaped hooks, perfused with warmed Krebs solution (37°C) bubbled with 95% O_2 and 5% CO_2 to maintain a pH of 7.4. Tissues were placed between two platinum electrodes (5 mm length, 2.5 mm apart; Fig. 2.1) for electric field stimulation (EFS). A resting tension of 5 mN was applied and rings were allowed to equilibrate for 1 hour. Isometric tension was recorded using a multi-channel Myobath system, and data acquired using Labscribe v4 software (World Precision Instruments). EFS was used to excite transmural nerves via a MultiStim system-D330 stimulator (Digitimer Ltd, England), which delivered trains of pulses (pulse amplitude 20 V, nominal; pulse

width 0.3 ms; 1 s duration) at a frequency of 2 Hz, at intervals of 10 or 100 s. Mean contraction amplitude was measured by averaging the peak contraction amplitude of ten EFS-induced contractions during each parameter, before and during drug addition (when they had their maximal effect). In addition, the contraction area (area under the curve, AUC) was quantified using LabScribe by integrating the force-time trace. Cursor 1 was positioned at the baseline at the beginning of the response, and cursor 2 was initially placed at the end of the drug effect to obtain the total AUC. Cursor 2 was then shifted leftwards to define a specific time window (e.g. the final 10 min of the response), and the corresponding AUC was recorded. The AUC for the defined period was subsequently calculated by subtracting the smaller area from the total area, thereby isolating the contractile response over the selected time interval. All the experiments were carried out in the presence of the non-selective cyclooxygenase (COX) inhibitor, indomethacin (10 μM) to prevent the release of endogenous prostaglandins by COX 1 and 2.

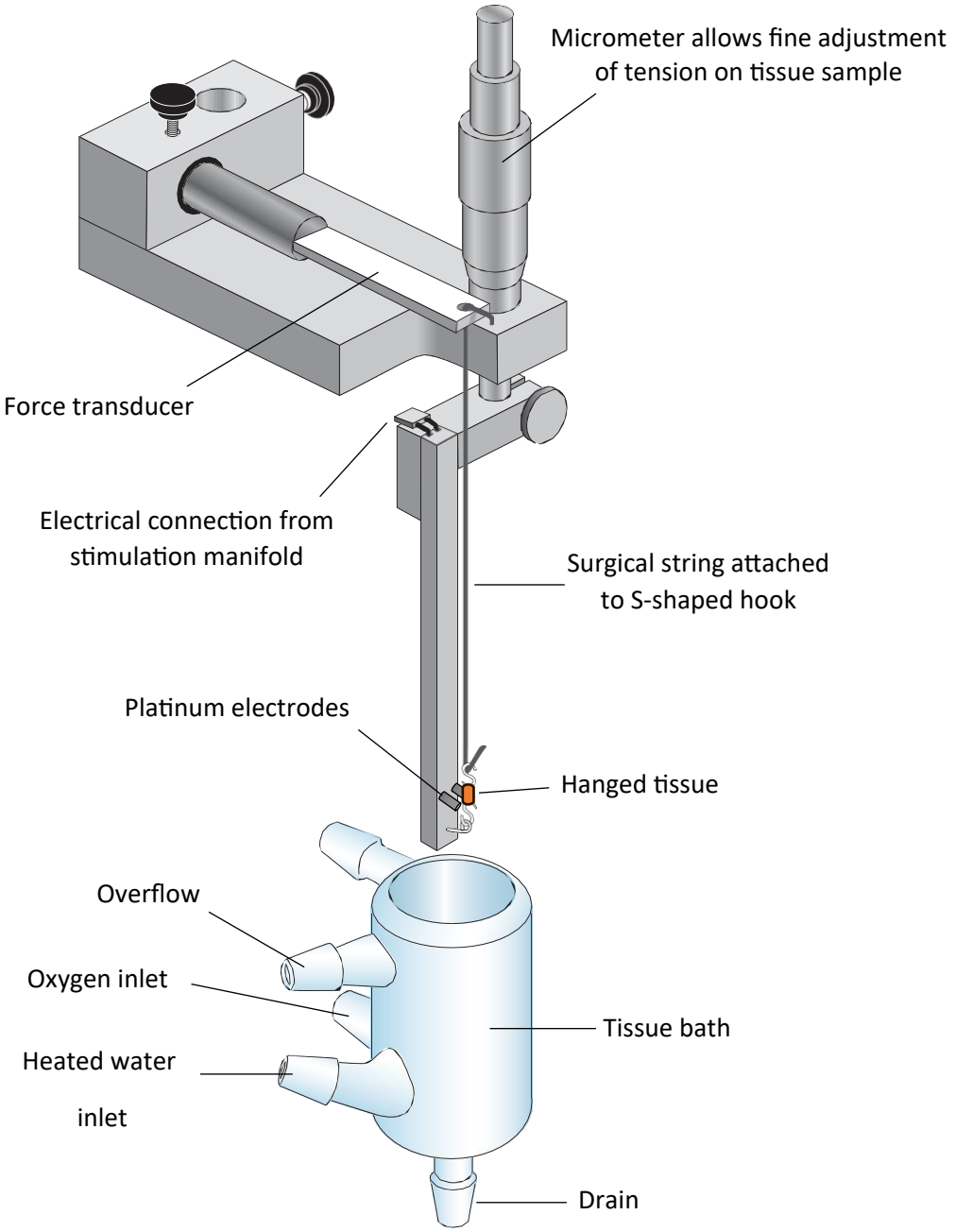

Figure 2.1 Illustration of the isometric tension setup and the Myobath system. Bronchial rings (2-3 mm) were mounted between two “S” shaped hooks and connected to the tension transducer. The tissue was submerged in Krebs solution within the organ bath. A stable temperature (37°C) was maintained by the water jacket surrounding the organ bath.

2.4. Cell dispersion and Immunocytochemistry

Murine ASM cells were isolated from primary bronchi which were chopped into smaller pieces for cell dispersal. Tissue pieces were incubated in a collagenase/papain mixture consisting of a primary dispersal medium of 1 mg/ml papain (Sigma-Aldrich), 1 mg/ml bovine serum albumin (Sigma-Aldrich) and 1 mg/ml dithioerythritol (Sigma-Aldrich) for ~30 minutes at 37°C without any agitation. The suspension was washed thoroughly with Ca^{2+}-free dissection solution prior to being subjected to incubation in a second enzyme mixture, comprising 1 mg/ml collagenase (Sigma-Aldrich type II) and 1 mg/ml bovine serum albumin (Sigma-Aldrich) for approximately 5 minutes at 37°C. Digested tissues were further washed with Ca^{2+}-free dissection solution and rested on ice for 10 minutes. ASM cells were released by gentle trituration using glass pipettes of gradually decreasing diameters. Isolated cells were preserved in a Ca^{2+}-free dissection solution, with the addition of Ca^{2+} to achieve a concentration of 100 µM, and stored at 4°C.

Coverslips (22x22 mm, #1.5, VWR) were prepared by treatment with poly-L lysine (Sigma Aldrich) for 30 minutes, followed by multiple washes with double-distilled water. After coverslips were left to completely air-dry, they were placed in a six-well plate. A volume of 150-200 µl of suspension containing isolated ASM cells was pipetted onto each coverslip and allowed to settle for 45 minutes on ice. Cells were fixed in 2 ml of 2% paraformaldehyde (PFA, Sigma Aldrich) made up in phosphate buffered saline solution (PBS, Gibco) for 13 minutes at room temperature. Cells were washed three times with PBS for 5 minutes and permeabilised with 0.1% Triton X-100 (Sigma Aldrich) for 10 minutes at 4°C. Three x 5-minute washes with PBS were performed prior to the blocking step, which required blocking the cells with 50% SEA Block (Thermofischer) for 2 hours at 4°C. Antibody incubation solution (20% SEA Block, 0.05% Triton X and 1% BSA) was prepared and mixed with the primary antibodies (Rabbit polyclonal anti-SERCA2/ATP2A2 antibody (27311-1-AP, Proteintech), 1:200 dilution; Rabbit polyclonal anti-KCNQ1 antibody (A2174, ABclonal), 1:200 dilution; Rabbit polyclonal anti-KCNQ4 antibody (APC-164, Alomone Labs), 1:200 dilution; Rabbit polyclonal anti-KCNQ5 antibody (PA1-941, Thermo Fisher Scientific), 1:200 dilution; and mouse monoclonal smooth muscle actin (M0851, Agilent), 1:100 dilution. A volume of 50 µl of the primary antibody solution was pipetted onto the antibody tray and

coverslips were carefully placed using forceps. Antibody trays were transferred to a glass mega-dish and the antibodies were left to incubate overnight at 4°C. Coverslips were removed from the antibody trays and placed in the six-well plate, where the primary antibody was removed by three x 5-minute washes with 20% SEA Block. Secondary antibody solution (Alexa Fluor 488, 1:1000 dilution (Invitrogen), Alexa Fluor 555, 1:1000 (Life Technologies) in PBS) was pipetted onto the antibody trays and the coverslips were carefully placed using forceps. Cells were incubated in secondary antibodies for 2 hours in the dark at room temperature. Coverslips were placed back in the six-well plates and the cells were washed with ice-cold PBS for 5 minutes (x 4). A drop of a mounting medium (VectaShield, Vector Laboratories) was added to slides (0.8-1 mm, VWR) labelled with the respective antibodies and the coverslips were carefully placed on the slides and sealed using nail varnish. Control coverslips were simultaneously prepared by omitting the primary antibody incubation step (secondary antibody only). Control dishes were imaged using the same experimental parameters for each image to ensure no positive immunoreactivity occurred. Immunofluorescence of isolated ASM cells was imaged with an Olympus IX31 microscope (Olympus Life Science) using an oil-immersed 60x objective lens (for Figure 6.1A) and with Axioskop 2 LSM 510 Meta confocal microscope (Zeiss, Germany; for Figure 4.5C). Using a laser, excitation wavelengths of 488 and 561 nm were used to visualise immunoreactivity in cells. Images were analysed using ImageJ (version 1.48, National Institute of Health, MD, USA) software.

2.5. Validation of antibodies

Mouse monoclonal smooth muscle actin (M0851) from Agilent was validated by the manufacturer, showing prominent staining in colonic smooth muscle cells but not in epithelia. We also showed that it positively stained isolated airway smooth muscle cells, but not HEK293 cells or colonic epithelial cells [412]. Rabbit polyclonal anti-SERCA2/ATP2A2 (27311-1-AP, Proteintech), anti-KCNQ1 (A2174, ABclonal), anti-KCNQ4 (APC-164, Alomone labs) and anti-KCNQ5 (PA1-941, Thermo Fisher Scientific) were validated by the manufacturer (validation data present on their websites).

2.6. Molecular biology

2.6.1. mRNA extraction

Bronchi from three wild-type mice (identical age and sex) were pooled to create a single RNA sample in order to generate sufficient RNA for PCR analysis. Tissues were stored in Trizol at -80°C. Total RNA from the tissue samples was extracted using the TRIZOL method (Invitrogen). Tissue pieces were flash frozen in liquid nitrogen and homogenised using a chilled pestle and mortar. Homogenised tissues were transferred into a micro-centrifuge tube free of ribonuclease (RNase) containing 1 ml of Trizol. The mixture was incubated at room temperature for 5 minutes. Further homogenisation was accomplished by passing the tissue through an 18-gauge needle and then a 21-gauge needle. After adding chloroform to the tissue homogenate in Trizol, the mixture was centrifuged for 15 minutes at 4°C (13,000 rpm). RNA was retained in the top aqueous phase, while proteins accumulated in the heavier organic phase and interphase at the bottom of the micro-centrifuge tube. The aqueous phase was then carefully transferred to a clean RNase-free vial. RNA precipitation occurred by introducing isopropanol (500 µl) and centrifuging at 4°C for 10 minutes, yielding a pellet. This resulting pellet underwent a washing step with 75% ethanol (1 ml) and was then allowed to air-dry. The pellet was resuspended in TE buffer (30 µl) and stored at -80°C. The RNA concentration was assessed using a Nanodrop 2000 spectrophotometer (Thermo Scientific).

2.6.2. cDNA synthesis

Complementary DNA (cDNA) refers to double-stranded DNA synthesised from single-stranded RNA; a process catalysed by the enzyme reverse transcriptase. RNA extracted from primary bronchi tissues underwent cDNA synthesis using SuperScript-II RNase-H reverse transcriptase from Invitrogen. The reverse transcription utilised random hexamers (200 µg/µl) to reverse transcribe (5-10 µl / 1 ng- 5 µg) of total RNA, conducted in a TECHNE thermal cycler. The reaction began heating at 65°C for five minutes, followed by a brief ice chill (2 minutes) and addition of first-strand buffer and 0.1 M dithiothreitol (DTT). The mixture was vortexed and allowed to incubate at 25°C for 2 minutes. Following this, SuperScript-II RT (200 units) was introduced, and the resulting mixture underwent incubation at 25°C for an additional 10 minutes. Initial activation of SuperScript-II occurred at 42°C

for 50 minutes, followed by an inactivation step at 70°C for 15 minutes. The obtained cDNA was subsequently stored at -20°C.

2.6.3. Primer design

Primers for SERCA isoforms, KCNQ subtypes and KCNE subunits were used to perform qPCR. SERCA2a and b primers were designed as described previously by Fransen et al. (2020) [413]. SERCA3 a, b, c and KCNE5 were designed in-house using NCBI primer design and Benchling software. KCNQ1-5 primers were designed as described previously by Mercer et al. (2025) [414]. KCNE1-4 primers were adapted from studies by Pluteanu et al. (2020) and Roepke et al. (2011), [415, 416]. Primer sequences are detailed in Table 2.1. The length of each primer varied between 16 to 24 bp and the predicted amplicon size ranged from 85 to 274 bp. The melting temperature for each primer was between 49-57°C and the guanine-cytosine (GC) content ranged between 40-65%. Primers were designed to encompass exon-exon boundaries whenever feasible. Primers were synthesised by Invitrogen and were stored at -20°C.

Primer specificity was initially verified in silico using BLAST analysis to ensure target selectivity. For primer efficiency, 10 µM primer stocks were used and brain cDNA was serially diluted to 1:10, 1:30, 1:100 and 1:300. qPCR was then performed for each dilution, and a standard curve was generated by plotting cDNA dilution on the x-axis against Ct values on the y-axis. The slope of the standard curve was recorded, and primer efficiency was calculated using the formula: Efficiency (%) = $(10^{(-1/slope)} - 1) \times 100$. Primer specificity was also assessed by examination of melt curves to confirm the presence of a single amplification product. Only primers exhibiting efficiencies within the acceptable range of 90-110% were used for further experiments.

Primer name	Genbank ID	Sequence	Size (bp)	Amplicon size (bp)
SERCA2A FWD	NM_009722.3	CACTTCTTGATCCTCTACGTGGAA	24	168
SERCA2A REV	NM_009722.3	CTCCAGTATTGCGGGTTGTTC	21	

SERCA2B FWD	NM_001110140.3	CACTTCTTGATCCTCTACGTGGAA	24	178
SERCA2B REV	NM_001110140.3	CAGGCTGCACACACTCTTTACC	22	
SERCA3A FWD	NM_001163336.1	GTGGTGCTTCAGATGTCTCTGC	22	85
SERCA3A REV	NM_001163336.1	CCTTTTTTTCATCCATGTGATTCC	24	
SERCA3B FWD	NM_016745.3	GTGGTGCTTCAGATGTCTCTGC	22	158
SERCA3B REV	NM_016745.3	CCTTTTTTTCCGGTGTGGTATGG	23	
SERCA3C FWD	NM_001163337.1	GTGGTGCTTCAGATGTCTCTGC	22	166
SERCA3C REV	NM_001163337.1	TTTTCCAAGAAGCCAACCCGG	21	
KCNQ1 FWD	NM_008434.2	AGCACACCCCATTTCTTGAG	20	274
KCNQ1 REV	NM_008434.2	ACTGATCCAGCCTTCTCTGT	20	
KCNQ2 FWD	NM_010611.3	CGGCAGAATTCAGAAGAAGCA	21	211
KCNQ2 REV	NM_010611.3	CCGAGTACTGTTCGATGACG	20	
KCNQ3 FWD	NM_152923.2	CCAGCAGTCTCCAAGGAATG	20	204
KCNQ3 REV	NM_152923.2	GCCCCCTTAGTTGGGTAGTA	20	
KCNQ4 FWD	NM_001081142.2	CGATCACACTGACGACCATT	20	216
KCNQ4 REV	NM_001081142.2	ACGCAGCCTGGATGAGATTA	20	
KCNQ5 FWD	NM_001160139.1	TCTTGGCTCAGGTTTTGCAT	20	193
KCNQ5 REV	NM_001160139.1	CTTCTGATTGGTAGGGCTGC	20	
KCNE1 FWD	NM_008424.4	ATGAGCCTGCCCAATTCCAC	20	108
KCNE1 REV	NM_008424.4	GAGCTGAGACTTACGAGCCA	20	

KCNE2 FWD	NM_134110.3	CACATTAGCCAATTTGACCCAGA	23	175
KCNE2 REV	NM_134110.3	GAACATGCCGATCATCACCAT	21	
KCNE3 FWD	NM_001190869.1	GGCTCTGAACACAACCCTTC	20	205
KCNE3 REV	NM_001190869.1	TTTGTCCACTTTGCGTGAAC	20	
KCNE4 FWD	NM_021342.2	CTTTGCTCGATGGAAGGGGAC	21	126
KCNE4 REV	NM_021342.2	GCTGTCGTTGAGAGGCGTC	19	
KCNE5 FWD	NM_021487.1	GCTGCAAACCCTCTTGAACC	20	156
KCNE5 REV	NM_021487.1	TAAGCGTCGTTACCCTTGGC	20	
B-ACTIN FWD	NM_007393.3	CTAGGCACCAGGGTGTG	17	205
B-ACTIN REV	NM_007393.3	GTGAGCAGCACAGGGT	16	

Table 2.1 List of primer sequence (5'-3') and amplicon size used in this study

2.6.4. Real-time quantitative polymerase chain reaction (qPCR)

PCR is a method used to amplify cDNA fragments for the identification of target genes of interest (GOI). In the presence of the target GOI within the cDNA sequence, PCR facilitates the exponential amplification of the designated DNA sequence, generating millions of copies of the specific DNA fragments. qPCR was employed to assess the relative transcriptional expression of selected genes of interest in murine bronchial tissue. qPCR was performed using a QUANTICA real-time PCR system (TECHNE) using SYBR Green PCR Master Mix (Applied Biosystems) which contains the necessary components needed to complete PCR (such as DNA polymerase, deoxynucleotide triphosphates (dNTPs) and a buffer solution). The cycling conditions were as follows: an initial 5-minute denaturation at 95°C was followed by 40 cycles of: denaturation at 95°C for 30 s, annealing at 52-56°C for 1 minute and extension at 72°C for 45 s. Tissue samples were analysed in

triplicate with cDNA obtained from nine different mice. β-Actin was used as an endogenous standard to determine the transcriptional expression levels of SERCA2a, 2b, 3a-c, KCNQ1-5 and KCNE1-5 in murine ASM. The expression levels of the mRNA, relative to β-actin, were calculated using $2^{-\Delta Ct}$ analyses.

In addition, non-template controls (NTC) were included for all primer sets. After real-time qPCR, a dissociation curve (70-90°C) was obtained. Subsequent analysis of the individual melting curves allowed us to verify the specificity of primer sets.

A typical qPCR reaction mix consisted of the following:

Reagents	**Volume (µl)**
SYBR Green	12.5
PCR grade water	8.5
Sense primer	1
Anti-sense primer	1
Template cDNA	2

Table 2.2 A typical qPCR reaction mix

2.7. Cell culture

Human embryonic kidney (HEK293) cells are widely employed as host systems for the heterologous expression of recombinant ion channel proteins, enabling detailed investigation of their structural, biophysical, and pharmacological properties [417, 418]. HEK293 cells are particularly well-suited for membrane protein expression due to their efficient post-translational modification machinery, which ensures proper protein folding and biological activity. Compared to CHO cells, HEK293 cells exhibit higher transfection efficiency, accurate translation, and superior protein processing, resulting in elevated recombinant protein yields [419]. Their favourable characteristics, including uniform morphology, rapid proliferation rate, ease of maintenance, and the capacity to express transgenic receptor proteins and ion channels with high fidelity have established HEK293 cells as the preferred heterologous system for electrophysiological studies [420, 421].

HEK293 cells were maintained in a mixed medium of Dulbecco's Modified Eagle Medium (DMEM) and Minimum Essential Medium (MEM) supplemented with 10% foetal bovine serum (FBS) and 1% penicillin-streptomycin. Cultures were incubated at 37°C in a humidified atmosphere containing 5% CO_2. Subculturing was performed by rinsing confluent cultures with sterile 1× PBS followed by enzymatic detachment using 0.05% Trypsin-EDTA (Gibco, Thermo Fisher Scientific) for 2-3 minutes.

Initially, HEK293 cells were cultured in 100 mm culture dishes. A confluent 100 mm dish typically contains approximately 8-10 × 10^6 cells [422]. After trypsinisation, the cell suspension was resuspended in 9 ml of fresh growth medium. Cells were then seeded into 35 mm dishes containing 2 ml of growth medium per dish, at a density of 1 × 10^5 cells per dish. After 18-24 hours of seeding, each 35 mm dish contained 40-50% of cell density (4 x 10^5). At this stage, the dishes were transfected with the desired plasmids.

For cryopreservation, detached HEK293 cells were mixed with an equal volume of growth medium containing 10% dimethyl sulfoxide (DMSO) to achieve gradual freezing. The mixture was cooled slowly at -80°C for approximately 30 minutes before being transferred to liquid nitrogen for long-term storage.

For revival, frozen vials were rapidly thawed in a 37°C water bath and immediately transferred to a 15 ml Falcon tube containing 5 ml of pre-warmed growth medium. The suspension was centrifuged at 2,000 rpm for 3 minutes to remove residual DMSO, and the resulting cell pellet was resuspended in 5 ml of fresh growth medium. The cells were then plated into a T25 flask and maintained under standard culture conditions for expansion.

2.8. Transfection

HEK293 cells were transfected with the plasmid cDNA for human Kv7.1, Kv7.4 or Kv7.5, with and without M2R plasmid cDNA. The Kv7 plasmids were kindly supplied as gifts from Prof. Søren Peter Olesen, University of Copenhagen, Denmark, while the mouse M2R plasmid (pRP[Exp]-Neo-CAG>mChrm2) was designed and synthesised by VectorBuilder. The day before transfection, cells were plated in 35 mm dishes at 30-40% density.

Plasmid construct (Kv7 and M2R) complexes were diluted in 100 µl serum-free media. In another tube, lipofectamine reagent (0.3 µl for 100 ng DNA) was diluted in 100 µl serum-free media. These two solutions were mixed together and incubated for 30 minutes at room temperature. Cells were replaced with serum and antibiotic-free media before transfection. Following 20 minutes of incubation at room temperature, the 200 µl transfection mixture was added to the dish, drop by drop. After a further 3 hours, the transfection was stopped by replacing the media in each dish with fresh growth media.

Transfection efficiency was monitored by co-transfection with a fluorescent reporter plasmid (e.g. GFP) and the proportion of fluorescent cells was assessed using fluorescence microscopy 24-48 hours post-transfection. In addition, successful expression of Kv7 and/or M2R constructs was functionally confirmed by patch-clamp electrophysiology through the presence of characteristic Kv7 currents and their modulation by pharmacological agents.

2.9. Electrophysiology

In this study, all electrophysiology experiments were carried out at room temperature using the whole-cell patch clamp technique as described previously [423]. The voltage clamp method was employed throughout to permit the cell voltage across the membrane to be controlled and the resultant currents from voltage steps to be measured.

To carry out voltage clamp recording on HEK293 cells in this study, a glass pipette containing a chlorided silver wire electrode was filled with whole-cell K^+ pipette solution. A similar silver electrode was present in the bath which acted as an earth electrode. The pipette was then steered towards the surface of the HEK293 cell under study and an attempt was made to form a gigaseal between the cell membrane and the glass pipette. To help promote gigaseal formation, gentle suction was applied after the tip of the pipette touched the surface of the HEK293 cell. Typically, these gigaseals had an electrical resistance of more than 10 gigaohms (GΩ), prior to breaking into the cell. The formation of such a high resistance seal not only isolates the membrane patch from the external solution and thus allows the experimenter to record ionic currents across the cell membrane, but it also ensures that background noise is reduced. Strong suction was also used to rupture the cell

membrane after generating a gigaseal in this configuration, thus allowing the pipette to have direct contact with the cytoplasm, permitting the flow of currents across the cell membrane to be recorded.

The electrode and pipette were electrically continuous and connected to the negative input (-) of the patch-clamp amplifier, while the command potential (V_{com}), representing the experimenter's applied voltage, was connected to the positive input (+). A feedback resistor between the amplifier's output and negative input enabled real-time comparison of the pipette potential (V_p) with V_{com}. Whenever a difference occurred between these two potentials, a compensatory current was automatically injected into the cell through the feedback circuit to maintain $V_p = V_{com}$. This compensatory current reflects the net ionic flux across the cell membrane and forms the basis of current recordings in whole-cell patch-clamp experiments.

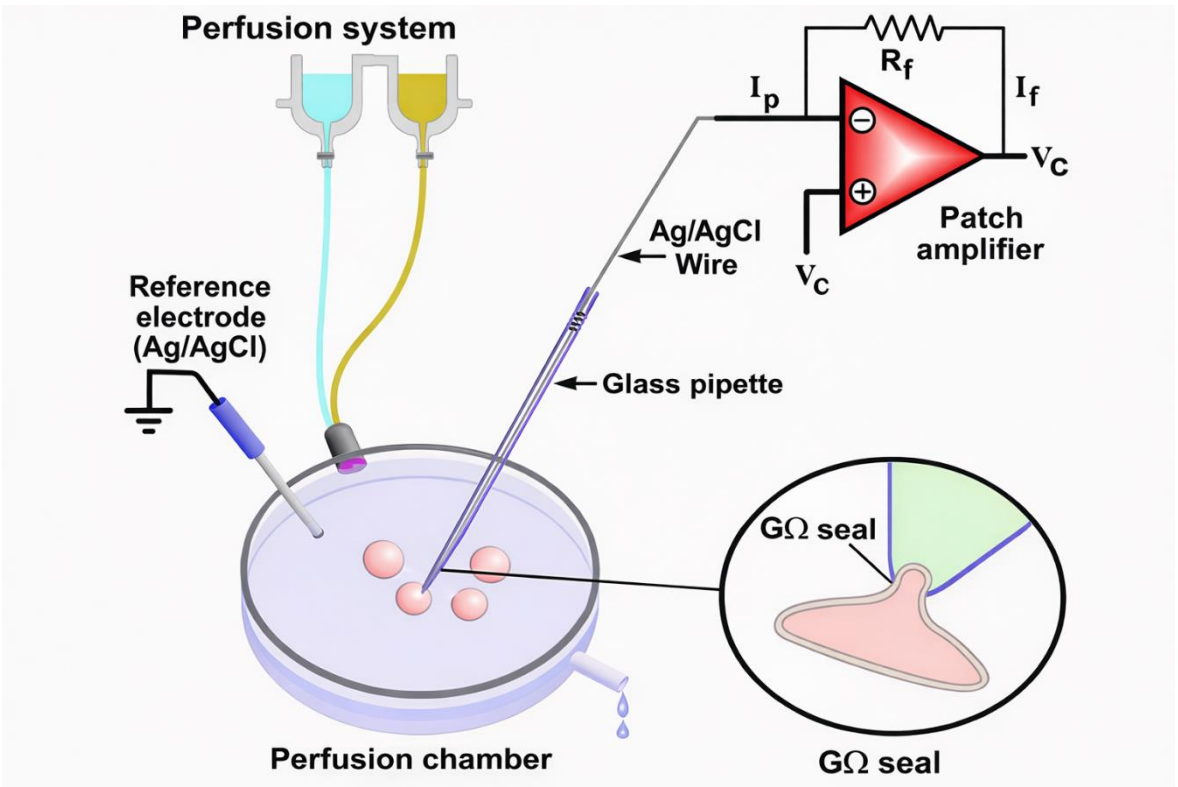

Figure 2.2. Diagrammatic representation of the whole-cell patch clamp electrophysiology setup, illustrating the key components required for recording ionic currents from isolated cells. A glass pipette, connected via an Ag/AgCl wire to a patch amplifier (incorporating a feedback resistor, R_f), is positioned onto a cell within a perfusion chamber, where continuous solution exchange is facilitated by a dual-channel perfusion system. A grounded Ag/AgCl reference electrode maintains a stable electrical reference in the bath solution, while the inset depicts the critical gigaohm (GΩ) seal formed between the pipette tip and the cell membrane which is a prerequisite for high-resolution, low-noise current recordings under precise voltage-clamp conditions.

Throughout the experiment, the bath chamber was continuously perfused with Hanks' balanced salt solution. Drugs were applied using a custom-designed, gravity-fed drug perfusion system. Multiple 20 ml syringes containing test solutions were mounted above the bath, each connected via fine-bore tubing to a central 1 ml manifold syringe. The individual tubes terminated within this manifold and were sealed in place using silicone adhesive, which was allowed to cure overnight before use. A glass pipette (200-300 μm in diameter) was connected to the manifold via silicone tubing and positioned approximately 300 μm from the recorded cell, allowing rapid and localised delivery of test solutions or pharmacological agents. Switching between control and drug-containing solutions was achieved with an approximate dead-space time of five seconds, ensuring precise temporal control of drug application.

2.9.1. Patch clamp recordings

Whole-cell patch-clamp recordings were performed on single HEK293 cells transiently expressing human Kv7.1, Kv7.4, or Kv7.5 channels, with or without co-expression of M2R, 24-48 hours post-transfection. During recordings, cells were continuously superfused with Hanks' balanced salt solution, using the gravity-fed drug delivery system. All experiments were conducted at room temperature (~22-24 °C). Patch pipettes were fabricated from thin-walled borosilicate glass capillaries (1.5 mm OD × 1.17 mm ID; Clark Medical Instruments) using a Sutter P-97 micropipette puller, yielding tip diameters of approximately 1-1.5 μm and resistances of ~2.5 MΩ when filled with the appropriate internal solution. Voltage-clamp protocols were delivered via an Axopatch 200B amplifier (Axon Instruments), and signals were digitised using a Digidata 1550B AD/DA converter (Axon Instruments). Data acquisition and analysis were performed using pCLAMP software (Clampex and Clampfit 10). Currents were sampled at 10 kHz and filtered at 2 kHz.

Leak currents were manually subtracted offline. Electrical interference at 50 Hz was minimised using a HumBug noise eliminator (Quest Scientific) placed between the amplifier and digitiser. Series resistance was not routinely compensated; however, associated voltage errors were estimated to be less than 15 mV and thus unlikely to significantly affect data interpretation.

2.9.2. Current, voltage and resistance

The electrical activity of a cell arises from the movement of charged ions such as Na^+, Ca^{2+}, K^+, and Cl^- across the plasma membrane. Because the lipid bilayer is impermeable to ions, their movement occurs through specific ion channels embedded in the membrane.

Current (I) represents the movement of ions across the membrane and is driven by the electrochemical gradient, often referred to as the driving force. Voltage (V, measured in millivolts, mV) is the electrical potential difference that provides the energy required to move these ions, while resistance (R, measured in ohms, Ω) describes the opposition to ion flow. The relationship between these three parameters is described by Ohm's law:

$$\mathbf{V=IR}$$

Rearranging the equation gives:

$$\mathbf{I=V/R}$$

This indicates that the current is directly proportional to voltage and inversely proportional to resistance.

An example of this relationship is when a constant voltage step of 5 mV was applied to the patch pipette before it contacted the cell, a current of approximately 2.0 nA was recorded, indicating low resistance. As the pipette touched the cell surface, resistance increased, resulting in a marked decrease in current. When gentle suction was applied to form a high-resistance seal (gigaseal) between the pipette and the cell membrane, current flow dropped further, reflecting the increased resistance at the pipette tip.

Using Ohm's law, the pipette resistance before seal formation can be calculated as:

$$R = (5 \times 10^{-3})\ V / (2.0 \times 10^{-9})\ A$$
$$= 2.5\ M\Omega$$

After the gigaseal was formed, the same voltage pulse produced a current of less than 5 pA, corresponding to a seal resistance exceeding 1 GΩ. This illustrates how an increase in resistance drastically reduces current flow at a constant voltage.

2.9.3. Series resistance

During whole-cell patch-clamp recordings, a series circuit is established that includes the pipette resistance (R_p), access resistance (R_a), and membrane resistance (R_m). The combined resistance of Rp and Ra is referred to as the series resistance (R_s). High series resistance can introduce significant voltage errors, particularly when recording large currents [424].

Rs is typically determined by applying a hyperpolarising voltage protocol consisting of successive 10 mV step increments from a holding potential of -80 mV and analysing the resulting passive current transients. The time constant (τ) of the capacitive current decay is used to calculate Rs as described by:

$$\tau = R_s \times C_m \quad \text{or} \quad R_s = \frac{\tau}{C_m}$$

Membrane capacitance (C_m) is calculated using the formula below, where Q_c is the total charge transferred during the capacitive transient and ΔV_m is the applied change in membrane voltage:

$$C_m = \frac{Q_c}{\Delta V_m}$$

In the present study, the mean series resistance recorded from HEK293 cells was approximately 4 MΩ (Ra ≈ 1.5 MΩ; Rp ≈ 2.5 MΩ). This resulted in an estimated uncompensated voltage error of ~10 mV, as series resistance compensation could not be applied. To minimise voltage errors, cells exhibiting current amplitudes greater than 4 nA at +50 mV under control conditions were excluded from analysis.

2.10. Data analysis

All the experiments were carried out in the whole-cell configuration [425]. Cells were routinely held at -80 mV and stepped from -100 mV to +50 mV for 1 s in 10 mV increments, with a 10 s interval between steps. Activation curves were constructed from the tail currents generated by repolarisation back to -120 mV following the depolarisation voltage steps. The expressed summary data were in mean ± SEM. G-V relationships were fitted with the Boltzmann equation below:

$$\frac{\mathrm{G}}{\mathrm{G_{max}}} = \frac{1}{1 + \exp\left[\frac{\mathrm{V_{1/2}} - \mathrm{V}_m}{\mathrm{Slope}}\right]}$$

where G was the conductance at test potential, G_{max} was the maximal conductance, $V_{1/2}$ was the membrane potential at which there was half maximal activation and V_m was the membrane potential. G was calculated as follows: $G = I/(V_m - E_k)$, where E_k is the calculated Nernst potential for K^+ and I is the current recorded.

2.11. Statistical analysis

Experimental series were obtained from four or more animals; n refers to the number of tissue strips studied and N to the number of animals. The minimum N number used was 4 and the minimum experimental run (n) conducted was 3 for molecular biology (pooled samples) and 6 for all other experiments. Data were analysed using GraphPad Prism 9 software. Summary data are presented as mean ± standard error of mean (SEM). Statistical comparisons were performed on original (non-normalised) data using either Student's paired t-test or, if three experimental groups were compared, one-way ANOVA followed by Bonferroni post hoc test. Data sets were considered statistically significant when $p<0.05$ (*$p<0.05$, **$p<0.01$, ***$p<0.001$, and ***$p<0.0001$).

2.12. Solutions and drugs

Concentrations within parentheses are mM, unless stated otherwise.

2.12.1. Solutions

Krebs solution

120 mM NaCl, 5.9 mM KCl, 25 mM $NaHCO_3$, 1.2 mM $NaH_2PO_4 \cdot 2H_2O$, 5.5 mM glucose, 1.2 mM $MgCl_2$, and 2.5 mM $CaCl_2$. pH was adjusted to 7.4 by bubbling the solution with 95% O_2–5% CO_2.

Ca^{2+}-free dissection solution

80 mM monosodium glutamate, 55 mM NaCl, 6 mM KCl, 10 mM glucose, 2 mM $MgCl_2.6H_2O$ and 10 mM HEPES. pH was adjusted to 7.3 using NaOH and HCl.

Hanks' Solution

125 mM NaCl, 5.4 mM KCl, 10 mM Glucose, 2.9 mM Sucrose, 4.2 mM $NaHCO_3$, 0.4 mM KH_2PO_4, 0.3 mM NaH_2PO_4, 0.5 mM $MgCl_2 \cdot 6H_2O$, 1.8 mM $CaCl_2 \cdot 2H_2O$, 0.4 mM $MgSO_4$, 10 mM HEPES; pH adjusted to 7.4 with NaOH.

Potassium whole-cell patch pipette solution

133 mM KCl, 1.0 mM $MgCl_2 \cdot 6H_2O$, 0.5 mM EGTA, 10 mM HEPES, 1.0 mM Na_2ATP, 0.1 mM NaGTP, 2.5 mM Na_2-phosphocreatine; pH adjusted to 7.2 with KOH. In some experiments (mentioned in the chapter), PIP_2 diC8 (200 μM) was also included in the pipette solution.

2.12.2. Drugs

Drugs were prepared in stock solutions using either distilled water, ethanol, or DMSO, following the manufacturer's guidelines, and stored at the recommended temperature (Table 2.2). Serial dilutions of the stock solutions were conducted daily when lower concentrations were required.

Drugs	Mechanism of Action	Supplier
Carbachol	Non-selective muscarinic receptor agonist	Sigma Aldrich
Indomethacin	Cyclooxygenase (COX) inhibitor	Abcam
4-DAMP	Selective M3R antagonist	Tocris
Methoctramine	Selective M2R antagonist	Sigma Aldrich
Nifedipine	L-type Ca^{2+} channel blocker	Tocris
FPL64176	L-type Ca^{2+} channel activator	Tocris
Verapamil	L-type Ca^{2+} channel blocker	Ascent scientific
GSK7975A	ORAI (CRAC) channel inhibitor	Sigma Aldrich
Pyr3	TRPC3 channel inhibitor	Tocris
HC070	TRPC4/5 channel inhibitor	MedChem Express
HC067047	TRPV4 channel antagonist	MedChem Express
Iberiotoxin	BK_{Ca} channel blocker	Smartox Biotechnology
Thapsigargin	SERCA inhibitor	Tocris
Ani9	Ano1 (CaCC) channel inhibitor	Tocris
CaCCinh-A01	Ano1 (CaCC) channel inhibitor	MedChem Express
XE991	Kv7 channel blocker	Tocris
Retigabine	Kv7 channel activator	Tocris
Tetrodotoxin citrate	Voltage-gated Na^+ channel blocker	Alomone labs

Atropine	Non-selective muscarinic receptor antagonist	Sigma Aldrich
Compound X	BK_{Ca} channel activator	Manufactured In-house
Zinc pyrithione	Kv7.1/7.2/7.4/7.5 channel activator	Sigma Aldrich
ML213	Kv7.2/7.4/7.5 channel activator	Tocris
ICA069673	Kv7.2/7.3/7.4 channel activator	MedChem Express
ML277	Kv7.1 channel activator	MedChem Express
Chromanol 293B	Kv7.1 channel blocker	MedChem Express
6MB-cAMP	PKA activator (cAMP analogue)	Biolog Life Science Institute
PIP_2 diC8	Membrane-permeable PIP_2 analogue	Echelon Biosciences

Table 2.2. List of drugs used in the study along with their mechanism of action and suppliers.

Chapter 3

Contribution of Ca^{2+} influx and Ca^{2+} release pathways to M2 muscarinic receptor-dependent contractions of murine airway smooth muscle

3.1. Introduction

Contraction of ASM is regulated by the release of ACh from parasympathetic nerves [156]. ASM contains both M2R and M3R; however, while the M2Rs outnumber their M3R counterparts by a ratio of 4:1 in the airways of most species, it is the M3Rs that are thought to mediate the bronchoconstrictor effects of ACh [153, 426, 427]. Nevertheless, recent studies from our lab by Alkawadri et al. (2022) showed that activation of M2Rs in mouse ASM augmented cholinergic nerve-induced contractions of ASM which were initiated by activation of M3Rs [153]. These effects were observed when the stimulus interval was reduced from 100 to 10 seconds, but only at a low (2 Hz) stimulus frequency. When a higher stimulus frequency (20 Hz) was employed, no increase in contraction amplitude was observed upon the reduction in stimulus interval. Therefore, it is apparent that activation of postjunctional M2Rs can make a significant contribution to ASM contraction induced by cholinergic nerves, under specific conditions. However, the cellular mechanisms that underpin the effects of M2R-dependent contractions of ASM have not been elucidated. Ca^{2+} is the principal mediator of smooth muscle contraction, as elevations in intracellular Ca^{2+} activate calmodulin and myosin light chain kinase, driving actin-myosin cross-bridge cycling [339, 428]. Hence, identifying how Ca^{2+} entry and release are regulated downstream of M2R activation is essential in understanding ASM contractility. In the present study, we investigated the contribution of distinct Ca^{2+} influx pathways, including L-type voltage-gated Ca^{2+} channels and non-selective cation channels, as well as intracellular Ca^{2+} release from stores to M2R-dependent contractions of murine ASM.

3.2. Results

3.2.1. Contribution of Ca^{2+} influx via L-type Ca^{2+} channels to M2R dependent contractions of ASM

Experiments were performed to investigate the contribution of LTCC to M2R-mediated contractions of ASM evoked by EFS (2 Hz). Data shown in Figure 3.1 compares the effect of nifedipine (1 μM) on contractions of ASM evoked by EFS at 100 s intervals, which does not involve activation of M2Rs, versus those at 10 s intervals, which does involve M2R activation. Figure 3.1A is a representative tension recording showing that application of nifedipine (1 μM), an LTCC blocker, had no effect on the amplitude of contractions of ASM induced by EFS at 100 s intervals. In contrast, Figure 3.1B shows that a decrease in the stimulus intervals, from 100 to 10 s, increased the amplitude of EFS-induced contractions of ASM and that this effect was reversed by nifedipine. Summary data for these experiments are shown in Figures 3.1C and D, respectively. The reduction in stimulus interval resulted in an increase in mean contraction amplitude from 0.79 ± 0.09 to 1.6 ± 0.13 mN ($p<0.0001$, n=9) and addition of nifedipine (1 μM) reduced mean contraction amplitude to 0.83 ± 0.1 mN ($p<0.0001$, n=9) (Figure 3.1D). There was no statistical difference between the mean amplitude of contractions at 100 s intervals under control conditions versus those in the presence of nifedipine at 10 s intervals. Similar results were achieved with a different LTCC blocker, verapamil which also reversed the enhancement of contractions induced by a reduction in stimulus intervals to 10 s (Figure 3.2A). Verapamil decreased mean contraction amplitude from 1.8 ± 0.25 to 0.32 ± 0.05 mN ($p<0.0001$, n=6) (Fig. 3.2B).

The idea that M2R-dependent contractions of ASM involved Ca^{2+} influx via LTCC was examined further by comparing the effects of nifedipine and FPL64176 (an LTCC activator) on CCh-evoked contractions of ASM that were performed in the presence of 4-DAMP to inhibit M3Rs. Addition of 4-DAMP converted sustained contractions induced by CCh into a series of oscillatory contractions. Figure 3.3A is a representative isometric tension recording showing that nifedipine abolished 4-DAMP-resistant contractions of ASM induced by 300 nM CCh. Addition of nifedipine reduced mean contraction area from 1907 ± 190 to 59 ± 71 mN.s ($p<0.0001$, n=10, Figure 3.3C). In contrast, FPL64176 (300 nM) augmented the 4-DAMP-resistant contractions (Figure 3.3B). Mean contraction area increased from 880.1 ± 204.9 to

2566 ± 407.3 mN in FPL64176 ($p<0.05$, n=6, Figure 3.3D). These data suggest that M2R-dependent contractions of ASM rely on Ca^{2+} influx via LTCC.

To rule out the possibility that the inhibitory effects of nifedipine involved an action on nerves, these experiments were repeated in the presence of the voltage-gated Na^+ channel (Na_V) blocker, tetrodotoxin (TTX, 1 μM). Figures 3.4A and B show that TTX did not affect the oscillatory contractions of ASM induced by CCh or the inhibitory effects of nifedipine on these responses. Experiments were also performed on tissues taken from M2R KO mice to confirm that the CCh-induced contractions that remained in the presence of the M3R antagonist 4-DAMP were mediated by M2Rs. In this case, blockade of M3Rs with 4-DAMP did not result in any oscillatory contractions (Figure 3.4B) and the mean contraction area was reduced from 3355 ± 288.2 mN.s before, to -36.5 ± 76.5 mN.s during 4-DAMP treatment ($p<0.0001$, n = 8; Figure 3.4D).

3.2.2. Contribution of Ca^{2+} release from intracellular stores to M2R dependent contractions of ASM

Figure 3.5A shows the effect of GSK7975A, an inhibitor of Ca^{2+} release-activated Ca^{2+} channels [429], on EFS-evoked contractions of ASM. Inhibition of SOCE would be expected to deplete intracellular Ca^{2+} stores. We reasoned that if EFS-evoked contraction of ASM relied on Ca^{2+} release from stores, then depletion of these stores with GSK7975A should inhibit these responses. The data in Figure 3.5A shows that GSK7975A (10 μM) did not inhibit contractions of ASM induced by EFS at 10 s intervals. However, subsequent addition of nifedipine abolished the enhanced contractions. Summary data in Figure 3.5C shows that GSK7975A had little effect on mean contraction amplitude (1.76 ± 0.21 mN under control conditions versus 1.73 ± 0.2 mN in GSK7975A, ns, n=7), whereas nifedipine (1 μM) reduced the mean contraction amplitude to 0.21 ± 0.05 mN ($p<0.001$, n=7). Conversely, in another set of experiments when nifedipine was added first, before GSK7975A (Figure 3.5B), we found that GSK7975A had an additional inhibitory effect to nifedipine on EFS-evoked contractions. Summary data in Figure 3.5D shows that nifedipine decreased the mean contraction amplitude from 2.04 ± 0.36 to 0.7 ± 0.15 mN ($p<0.05$, n=6) and addition of GSK7975A further reduced contraction amplitude to 0.18 ± 0.03 mN ($p<0.05$, n=6).

3.2.3. Effect of Transient Receptor Potential (TRP) channel blockers on M2R-mediated contractions evoked by EFS

Experiments were performed to elucidate the mechanisms by which activation of M2Rs could depolarise cells sufficiently to activate LTCC. M2Rs are coupled to pertussis toxin-sensitive G_i proteins [430, 431] and ACh has been shown to activate pertussis toxin-sensitive cation currents in tracheal smooth muscle cells [432]. Therefore, it was possible that the stimulatory effects of M2R activation observed in the present study could be mediated by activation of a non-selective cation current. ASM expresses several members of the TRP family, including TRPC3 [191, 240, 433], TRPC4/5 [242, 434] and TRPV4 [246], which encode non-selective cation channels and are involved in cholinergic responses in smooth muscle [435]. However, data shown in Figure 3.6 indicate that blockers of these channels did not inhibit EFS-induced contractions of murine ASM, indicating that they were unlikely to account for the contractile effects of M2R stimulation in murine ASM. Figures 3.6A and B show that Pyr3 (10 μM), a pyrazole compound that inhibits TRPC3 and TRPC6 channels [436, 437] had a little effect on the amplitude of EFS-evoked contractions induced by 2 Hz EFS at 10 s intervals. In 7 experiments, mean contraction amplitude was 2 ± 0.33 mN before and 1.84 ± 0.33 mN in Pyr3 (ns, n=7). Similarly, HC070, a highly potent TRPC4/5 channel blocker showed small reduction on EFS-evoked contractions (Figures 3.6C and D). In 6 experiments, the mean contraction amplitude was 2.42 ± 0.47 mN before and 2.21 ± 0.46 mN (1 μM, ns, n=6) in HC070. Finally, HC067047, which inhibits TRPV4 channels, also failed to significantly reduce the amplitude of EFS responses in murine ASM. Mean contraction amplitude was 2.74 ± 0.57 mN before, compared to 2.67 ± 0.57 mN in HC067047 (1 μM, Figures 3.6E and F, ns, n=6).

The effects of the TRP channel blockers on M2R-dependent contractions of ASM were tested further by examining their effects on contractions induced by CCh in the presence of 4-DAMP. Figure 3.7A and B show representative traces and summary data for the effect of Pyr3 (10 μM) on M2R-mediated oscillatory contractions. Pyr3 had no significant effect on the oscillatory activity; however, subsequent addition of nifedipine (1 μM) completely abolished the response. Addition of carbachol (300 nM) to the tissues elevated the mean contraction area to 3816 ± 584.4 mN.s and addition of 4-DAMP reduced the mean contraction area to

1583 ± 203.1 mN.s ($p<0.05$, n=6). Mean area slightly increased to 1931 ± 189.1 mN.s in Pyr3 (ns, n=6) whereas nifedipine reduced it to 40.86 ± 88.63 mN.s ($p<0.001$, n=6; Figure 3.9B). Similarly, application of HC-070 (1 μM; Figure 3.7C and D) and HC-067047 (1 μM; Figure 3.7E and F) failed to suppress the oscillatory contractions, which were again abolished upon nifedipine treatment. These findings indicate that TRPC3, TRPC4/5 and TRPV4 channels do not make a major contribution to M2R-mediated ASM contractions.

We also assessed whether the effects of Pyr3 on ASM contraction could be unmasked when SOCE was inhibited by GSK7975A, since Ca^{2+} release from the sarcoplasmic reticulum can induce CDI of TRP channels and potentially limit their activity [438-441]. However, the combination of Pyr3 and GSK7975A did not cause a significant reduction in the amplitude of ASM contractions evoked by EFS at 10 s intervals. The representative isometric tension recordings shown in Figures 3.8A and B illustrate the impact of applying GSK7975A followed by Pyr3, and the reverse order (Pyr3 followed by GSK7975A), respectively, in murine bronchial rings. Summary data in Figure 3.8C demonstrate that addition of 10 μM GSK7975A reduced the mean contraction amplitude from 1.30 ± 0.11 mN to 1.23 ± 0.10 mN (ns, n = 7). Subsequent application of Pyr3 (10 μM) produced a further small decrease to 1.05 ± 0.09 mN (ns, n = 7). Similarly, when Pyr3 was applied first (Figure 3.8D), contraction amplitude decreased modestly from 2.21 ± 0.31 mN to 2.05 ± 0.30 mN (ns, n = 6), with further addition of GSK7975A reducing the amplitude to 1.90 ± 0.30 mN (ns, n = 6). These results indicate that neither Pyr3 nor GSK7975A, alone or in combination, significantly affected the amplitude of EFS-induced ASM contractions, suggesting that TRP channels and SOCE make only a limited contribution to ASM contractions under these conditions.

3.2.4. Role of postjunctional M2Rs in neostigmine potentiated ASM responses

To further investigate the mechanism underlying cholinergic contractions of ASM, we examined the effects of the reversible acetylcholinesterase (AChE) inhibitor, neostigmine which prolongs the lifetime of ACh in the synaptic cleft by preventing its enzymatic degradation. We applied cumulative concentrations of neostigmine (1 nM-1 μM) during EFS-evoked contractions at 100 s intervals (Figure 3.9A). Neostigmine produced a concentration-dependent increase in the amplitude

of nerve-evoked contractions and on basal tone. The largest enhancement of nerve-evoked responses was observed at 100 nM. At 1 μM neostigmine, no further increase in contraction amplitude was observed but the mean contraction amplitude was significantly higher than that of the control. Mean contraction amplitude increased from 1.12 ± 0.12 mN in control to 2.13 ± 0.3 mN ($p<0.05$, n=6) in 1 μM neostigmine (Figure 3.9B). A marked elevation in overall mean contraction area was observed at 1 μM neostigmine (as compared to control) from 32.29 ± 4.3 to 3272 ± 307.7 mN.s ($p<0.01$, n=6; Figure 3.9C). Based on these observations, 1 μM neostigmine was selected for subsequent experiments as is the case in other studies where it was employed to elicit smooth muscle contraction [442, 443].

Next, we examined the specific contribution of M2R and M3Rs to neostigmine-mediated contractions of ASM. Application of 1 μM neostigmine during EFS-evoked responses at 100 s intervals increased basal tone and the amplitude of EFS responses. The overall contraction area increased from 37.44 ± 9.3 mN.s to 4723 ± 634.1 mN.s in neostigmine ($p<0.01$, n=6; Figure 3.10A and B). Subsequent addition of methoctramine (100 nM) reduced contraction area to 2592 ± 352.7 mN.s ($p<0.05$, n=6), however, the EFS responses remained intact. Addition of 4-DAMP diminished the remaining contractions and reduced mean contraction area to 80.35 ± 50.2 mN.s ($p<0.01$, n=6). Experiments were then performed to isolate the M2R-dependent component of the neostigmine response by blocking M3Rs with 4-DAMP. Application of 1 μM neostigmine produced a sustained tonic contraction, as shown in the representative isometric tension recording (Figure 3.11A). Subsequent addition of 4-DAMP (300 nM) induced oscillatory contractions, similar to the effects of 4-DAMP on CCh responses. Further addition of methoctramine in the presence of 4-DAMP abolished the oscillatory component, confirming involvement of M2Rs in these responses. Summary data presented in Figure 3.11C demonstrate that 4-DAMP reduced the mean contraction area induced by neostigmine from 7972 ± 525.5 to 2928 ± 546.5 mN.s ($p<0.0001$, n=6). Further addition of methoctramine reduced the mean contraction area to 86.1 ± 51.6 mN.s ($p<0.01$, n=6). Finally, to examine if the M2R-dependent component of the neostigmine response was mediated by Ca^{2+} influx via LTCC, we examined the effect of nifedipine. In the presence of neostigmine and 4-DAMP, addition of nifedipine abolished the M2R-mediated oscillations and reduced mean contraction area from 2189 ± 222.3 mN.s

to 105.7 ± 83.35 mN.s ($p<0.01$, n=6, Figure 3.11B and D), confirming involvement of Ca^{2+} influx through LTCC in these responses.

3.3. Discussion

The results in this chapter demonstrate that M2R-mediated contractions of ASM primarily depend on Ca^{2+} influx through LTCC, rather than Ca^{2+} release from intracellular stores or TRP channel-mediated cation entry. The data also indicate that post-junctional M2Rs contribute significantly to the enhanced cholinergic responses induced by neostigmine, further supporting a role for M2R-LTCC coupling in sustaining airway contractility.

It is widely accepted that ACh-induced contractions of ASM rely on Ca^{2+} release from intracellular stores via IP_3R and RyRs [444]. ASM also possess LTCC; however, their contribution to cholinergic contractions of ASM is disputed [226]. Many studies advocate an important role for LTCCs in cholinergic contractions of ASM (comprehensively reviewed in Byron et al., 2014) [234], but results from early clinical trials with Ca^{2+} channel blockers (CCBs) for treating asthma were relatively disappointing compared to their therapeutic efficacy in hypertension and angina [445, 446]. M3Rs are coupled, via $G_{q/11}$, to PLC that generates production of IP_3, which, in turn, causes SR Ca^{2+}-release. Therefore, it is easy to see how cholinergic contractions of ASM could occur independently of LTCCs. This led some researchers to conclude that pharmaco-mechanical coupling is the predominant mechanism responsible for mediating cholinergic contractions of ASM and that electromechanical coupling is only of minor importance. One possible explanation for these disparate findings is to take into account the protocols used extensively in pharmacological experiments. A careful reading of the literature revealed that CCBs are much more effective at reducing responses to submaximal, physiological concentrations of cholinergic agonists than responses elicited by maximal, pharmacological concentrations [233, 234, 267]. Hence, as discussed by Byron et al. (2014), low concentrations of agonist appear to act predominantly via activation of LTCCs, while higher concentrations act predominantly via IP_3-mediated Ca^{2+} release from the SR [234]. This also fits with the observation that contractions induced by low concentrations of cholinergic agonists can be inhibited by membrane

hyperpolarisation, while those evoked by high concentrations are entirely resistant to this intervention [235].

Our findings align with previous work by Alkawadri et al. (2022), which demonstrated that postjunctional M2Rs make a greater contribution to cholinergic nerve-induced bronchoconstriction than previously appreciated. Using low-frequency EFS (2 Hz), they showed that M2R activation sensitises ASM to M3R stimulation, effectively doubling the force of M3R-dependent contractions. Importantly, they reported that reducing the stimulus interval from 100 s to 10 s potentiated nerve-evoked contractions, an effect abolished by M2R antagonists (methoctramine and AFDX116) and absent in M2R knockout mice. In contrast, the M3R antagonist 4-DAMP abolished the entire EFS-evoked contraction. These findings indicate that while M3Rs are essential for initiating cholinergic contraction, M2Rs play a critical modulatory role by amplifying M3R-dependent responses [153].

Consistent with this framework, we found that nifedipine, an LTCC blocker, had no effect on EFS responses evoked at 100 s intervals, indicating that these M3R-dependent responses did not involve Ca^{2+} influx via LTCCs (Figure 3.1A). In contrast, nifedipine completely reversed the increase in contraction amplitude induced by reducing the stimulus interval to 10 s (Figure 3.1B). As the enhancement in contraction amplitude is mediated by activation of M2Rs [153], it is apparent that M2R-dependent potentiation of cholinergic contractions of ASM relies on Ca^{2+} influx via LTCC. This idea was supported by the finding that verapamil, another LTCC inhibitor, also inhibited contractions of ASM evoked at 10 s intervals. Furthermore, CCh-evoked contractions that remained in the presence of the M3R antagonist, 4-DAMP were abolished by nifedipine (Figure 3.3A and C) and enhanced by the LTCC opener FPL64176 (300 nM; Figure 3.3B and D). Taken together, these results support the idea that M2R-mediated contractions rely on Ca^{2+} influx through LTCCs, while these channels contribute only a little to M3R-dependent responses.

The contribution of M2Rs to cholinergic contractions of ASM is heavily dependent upon the stimulus protocol used to evoke the response [153]. Hence, the contribution of M2Rs to cholinergic contractions of ASM has been underestimated in studies that use high-frequency EFS or high concentrations of agonist to induce contractions. Since the M2R responses are mediated by LTCC, we believe that this

may also contribute to the disparity in the effects of LTCC blockade in previous studies. A feature of LTCC is that they can become inactivated by high levels of $[Ca^{2+}]_i$ [447]. This phenomenon of CDI of LTCC provides a feedback mechanism to prevent Ca^{2+} overload and therefore pathways that activate LTCC are negated under these conditions. Unno et al. (2005) suggested that the relative lack of involvement of M2Rs in contractions of ileal smooth muscle induced by high frequency EFS was due to inactivation of LTCC following Ca^{2+} release from intracellular stores following M3R activation [236, 448]. The present study demonstrates that M2R-dependent contractions of ASM are mediated by Ca^{2+} influx via LTCC, therefore it is possible that these responses could also be susceptible to inhibition by Ca^{2+} released from stores following M3R stimulation. If so, this may explain why LTCC blockers exert greater inhibitory effects on cholinergic contractions of ASM when intracellular Ca^{2+} stores have been depleted as observed in experiments using GSK7975A (Figure 3.5A) [449]. It may also explain why the contribution of M2Rs to ACh-induced bronchoconstriction is more prominent in tissues lacking functional M3Rs compared to wild-type controls [145].

ASM cells express a wide range of TRP channels, including TRPA1, TRPC, and TRPV isoforms [241, 246, 450] and these channels have been implicated in cholinergic responses resulting in aggravated bronchoconstriction in asthma and COPD. For example, TRPV4 channels are widely expressed in human ASM and have been found to increase ASM contraction [246, 249]. Nassini et al. (2012) reported that stimulation of TRPA1 channels with CSE led to the release of IL-8 from cultured human ASM cells [451] and Zhang et al. (2018) found that TRPC3 expression was upregulated in asthmatic mouse ASM cells and increased the Ca^{2+} concentration and cell viability of asthmatic mouse ASM cells [452]. Moreover, Belvisi et al. (1992) showed that activation of TRPV1 channels contracted isolated guinea pig tracheal smooth muscle [453]. However, we found that Pyr3 (TRPC3/6 antagonist), HC-070 (TRPC4/5 antagonist) and HC-067047 (TRPV4 antagonist) had little effects on M2R-mediated contractions of ASM (Figure 3.6). Therefore, although the M2R responses involve activation of voltage-dependent Ca^{2+} channels, these effects do not appear to involve activation of TRP channels. Our results contrast to those of Xiao et al. (2010) which advocated an important role for TRPC3 channels in cholinergic contractions of mouse ASM cells [191]. Precise reasons for

this difference are unclear, but it may be due to the effects of cell culture as they studied the effects of TRPC1 and TRPC3 in ASM cells after 72 hours of culture, whereas we used fresh bronchial rings in isometric tension studies. The lack of effect of Pyr3 on contractions evoked by EFS at 10 s intervals could also be attributed to the possibility that TRPC3 channels are involved in the M3R, but not M2R-dependent responses, as TRPC3 channels are activated by cytosolic DAG and PKC [454, 455], which are formed following M3R activation [188].

The contribution of M2Rs to cholinergic contractions of ASM was investigated using neostigmine which acts as a reversible AChE inhibitor that prolongs the lifetime of ACh in the synaptic cleft by preventing its enzymatic degradation. Neostigmine (1 μM) elicited two main responses: an increase in basal tone and an increase in the amplitude of nerve-evoked responses. We found that its effects on basal tone were reversed by methoctramine, whereas effects on the EFS responses were abolished by 4-DAMP. One explanation for these results is that M3Rs represent the primary target for ACh released from cholinergic nerves, whereas M2Rs are located extrajunctionally, but may be activated by overspill of ACh from nerve-muscle junctions that may occur when the stimulus interval was reduced or when AChE was inhibited. Therefore, postjunctional M2Rs may contribute to ASM contractions evoked by ACh release from non-neuronal sources such as airway epithelial cells, endothelial cells, and immune/inflammatory cells like macrophages, lymphocytes and mast cells [456-459]. The M2R-component of the neostigmine response was also inhibited by nifedipine, further supporting the idea that M2R-dependent contractions of ASM rely on Ca^{2+} influx via LTCC.

In conclusion, the findings from the current study indicate that the enhancement of cholinergic nerve mediated contractions in ASM through M2R activation is dependent on Ca^{2+} influx via LTCC and does not involve significant contributions from intracellular Ca^{2+} store release or TRP channel activation. We also found that neostigmine-induced enhancement of ASM tone is primarily mediated by postjunctional M2Rs, highlighting their potential role in modulating cholinergic airway tone and as a therapeutic target in asthma.

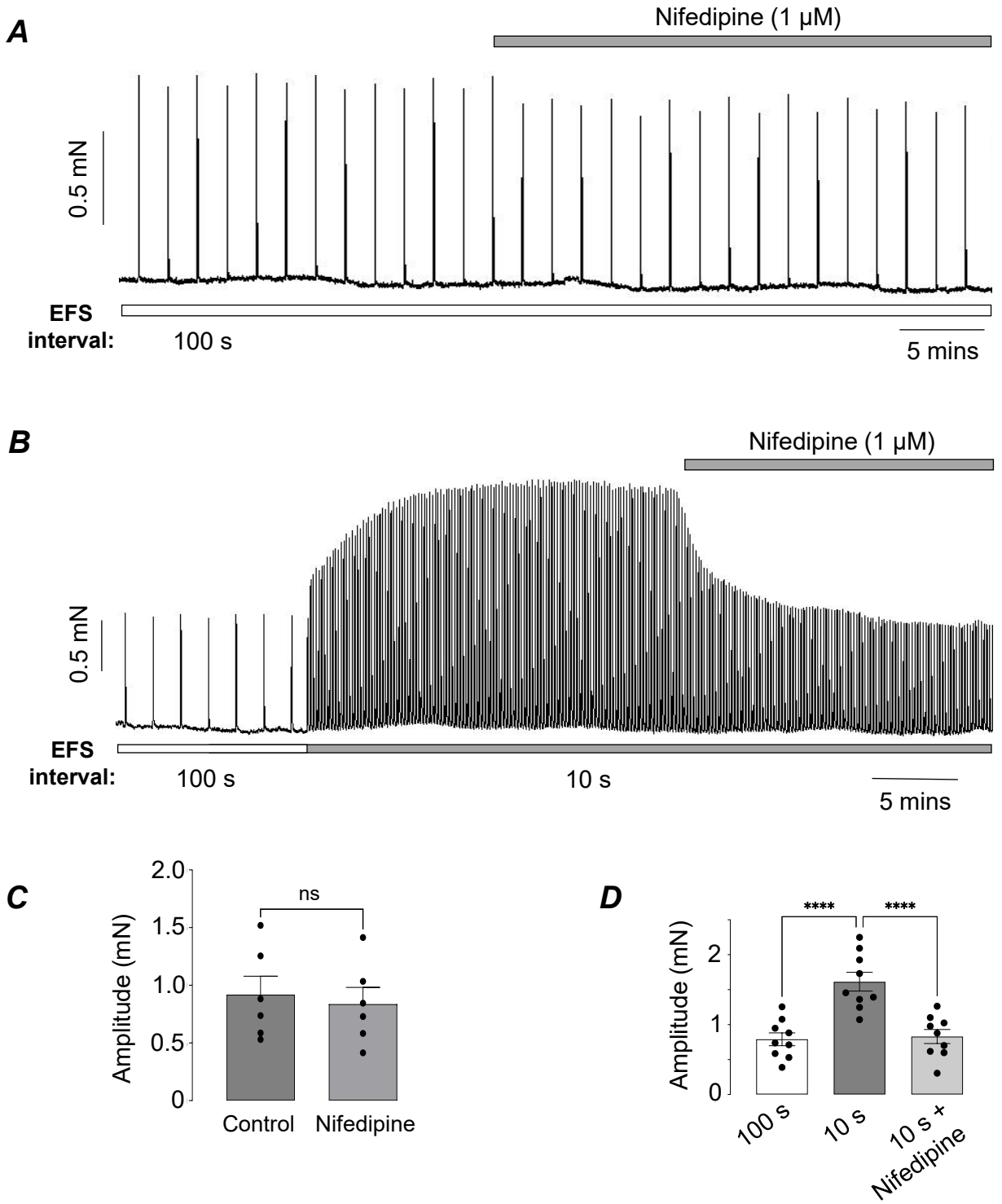

Figure 3.1. Effect of LTCC inhibitor, nifedipine on EFS-evoked contractions of ASM. **(A)** Representative isometric tension recording showing the effects of nifedipine (1 μM) on EFS-evoked contractions at 100 s interval. **(B)** Nifedipine (1 μM) reversed the M2R-mediated increase in contraction amplitude induced by reducing the EFS interval to 10 s. **(C)** Summary bar chart showing that nifedipine had no effect on contractions evoked by EFS at 100 s intervals (ns, non-significant, n=6, N=6, paired t-test). **(D)** Summary bar chart showing the effect of nifedipine on contractions of ASM evoked at 10 s intervals (****p<0.0001, n=9, N=6, one-way ANOVA).

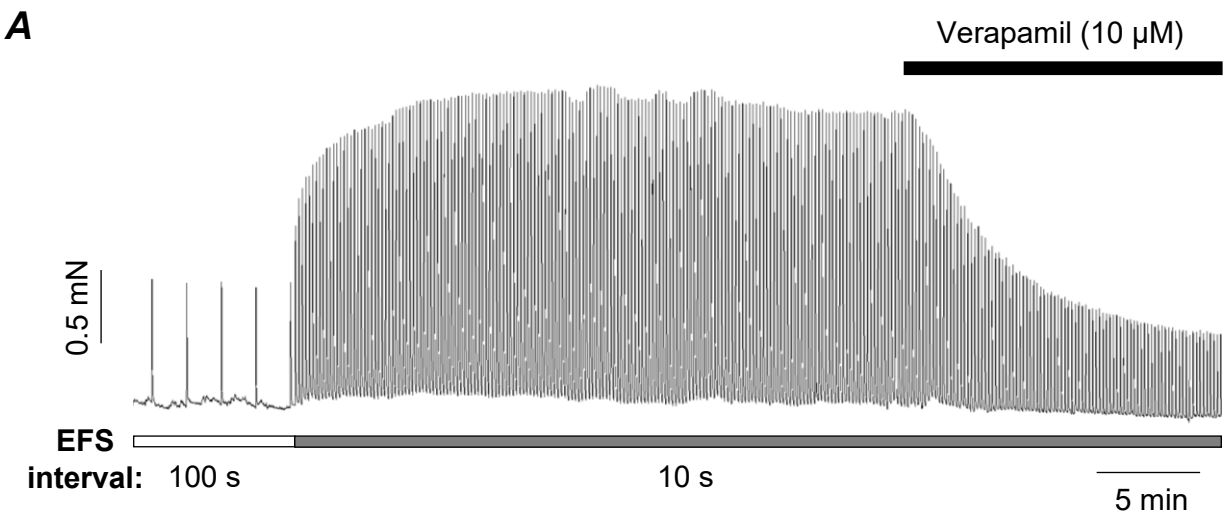

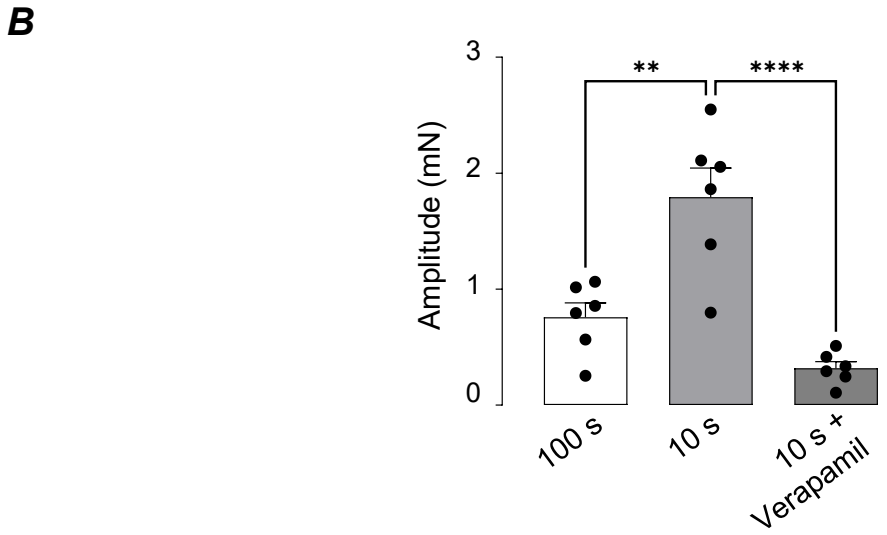

Figure 3.2. Effect of LTCC inhibitor, verapamil on EFS-evoked contractions.
(A) Representative isometric tension recording showing the effects of 10 μM verapamil on EFS evoked contractions at 10 s intervals. Verapamil blocked the M2R-mediated increase in contraction amplitude **(B)** Summary bar chart showing the effect of verapamil on EFS-evoked contractions at 10 s intervals (**p<0.01, ****p<0.0001, n=6, N=4, one-way ANOVA).

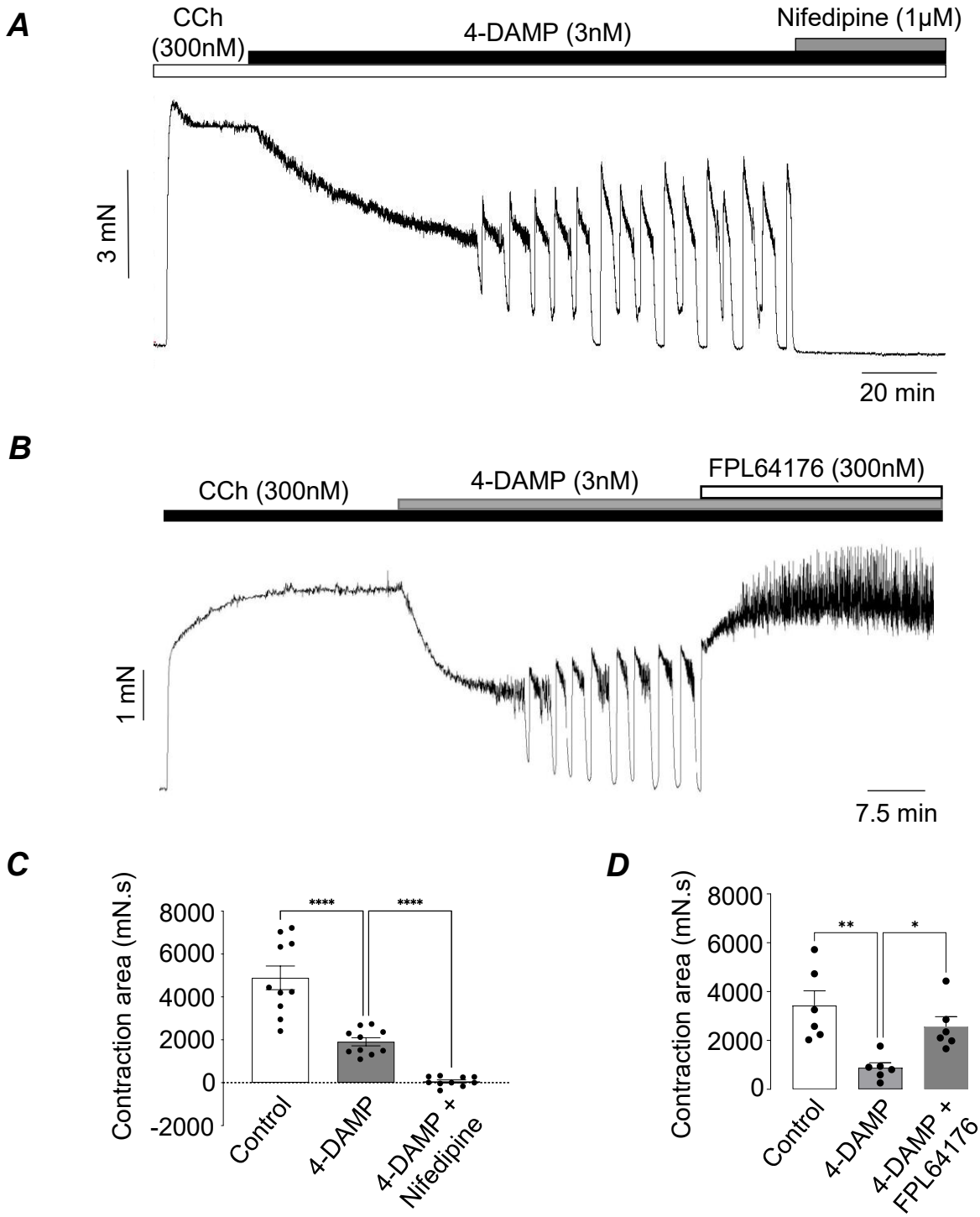

Figure 3.3. Effects of the nifedipine and LTCC activator, FPL64176 on CCh-evoked contractions of murine bronchial rings in the presence of 4-DAMP. (A) Representative isometric tension recording showing the effects of 4-DAMP (3 nM) and nifedipine (1 μM) on ASM contractions induced by CCh (300 nM). 4-DAMP reduced contraction amplitude and converted the sustained CCh response into a series of oscillatory contractions. The 4-DAMP-resistant activity was abolished by nifedipine. **(B)** shows that 300 nM FPL64176 converted the M2R-mediated oscillatory contractions to a sustained tonic contraction with rapid phasic contractions superimposed. **(C)** Summary bar chart plotting CCh contraction amplitude (measured by area under the curve) before and during the presence of 4-DAMP and 4-DAMP + nifedipine (****p<0.0001, n=10, N=6, one-way ANOVA). **(D)** Summary bar chart plotting CCh contraction amplitude (measured by area under the curve) before and during the presence of 4-DAMP and 4-DAMP + FPL64176 (*p<0.05, **p<0.01, n=6, N=5, one-way ANOVA).

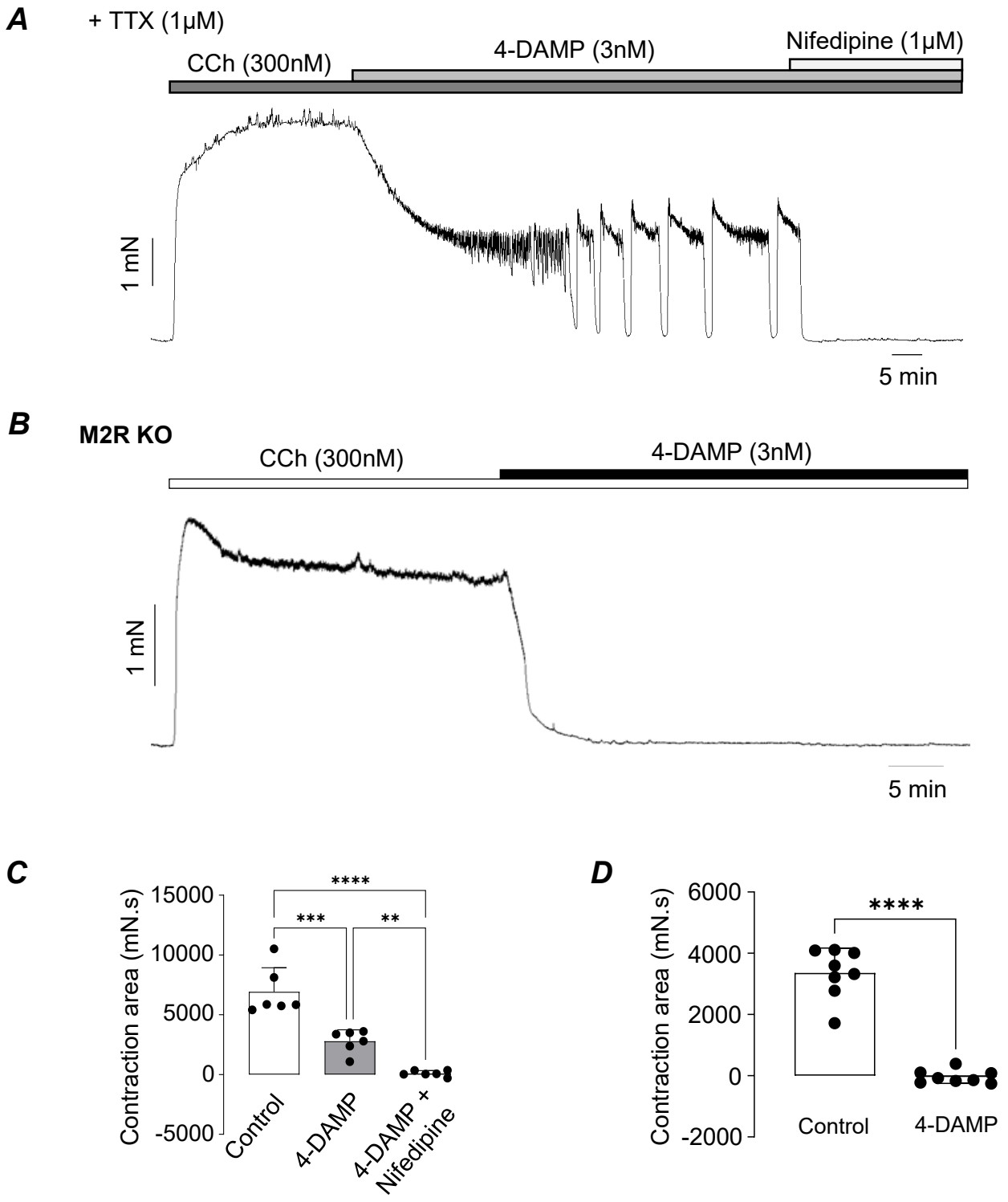

Figure 3.4. Effects of nifedipine and 4-DAMP on CCh-evoked contractions of murine bronchial rings. (A) Representative isometric tension recording showing effect of TTX on CCh (300 nM)-induced contractions in the presence of 4-DAMP (3 nM). Subsequent addition of nifedipine (1 μM) abolished the 4-DAMP-resistant oscillations. TTX (1 μM) was added into bath before start of the experiment. **(B)** Representative trace from M2R KO bronchial tissue showing that addition of 4-DAMP in the presence of CCh (300 nM) failed to evoke oscillatory contractions, confirming the dependence on postjunctional M2Rs. **(C)** Summary bar chart plotting CCh contraction amplitude (measured by area under the curve) before and during the presence of 4-DAMP and 4-DAMP + nifedipine (**p<0.01, ***p<0.001, ****p<0.0001, n=6, N=6, one-way ANOVA). **(D)** Summary data showing the reduction in mean contraction area following 4-DAMP addition in M2R knockout tissues (****p<0.0001, n=8, N=6, paired t-test).

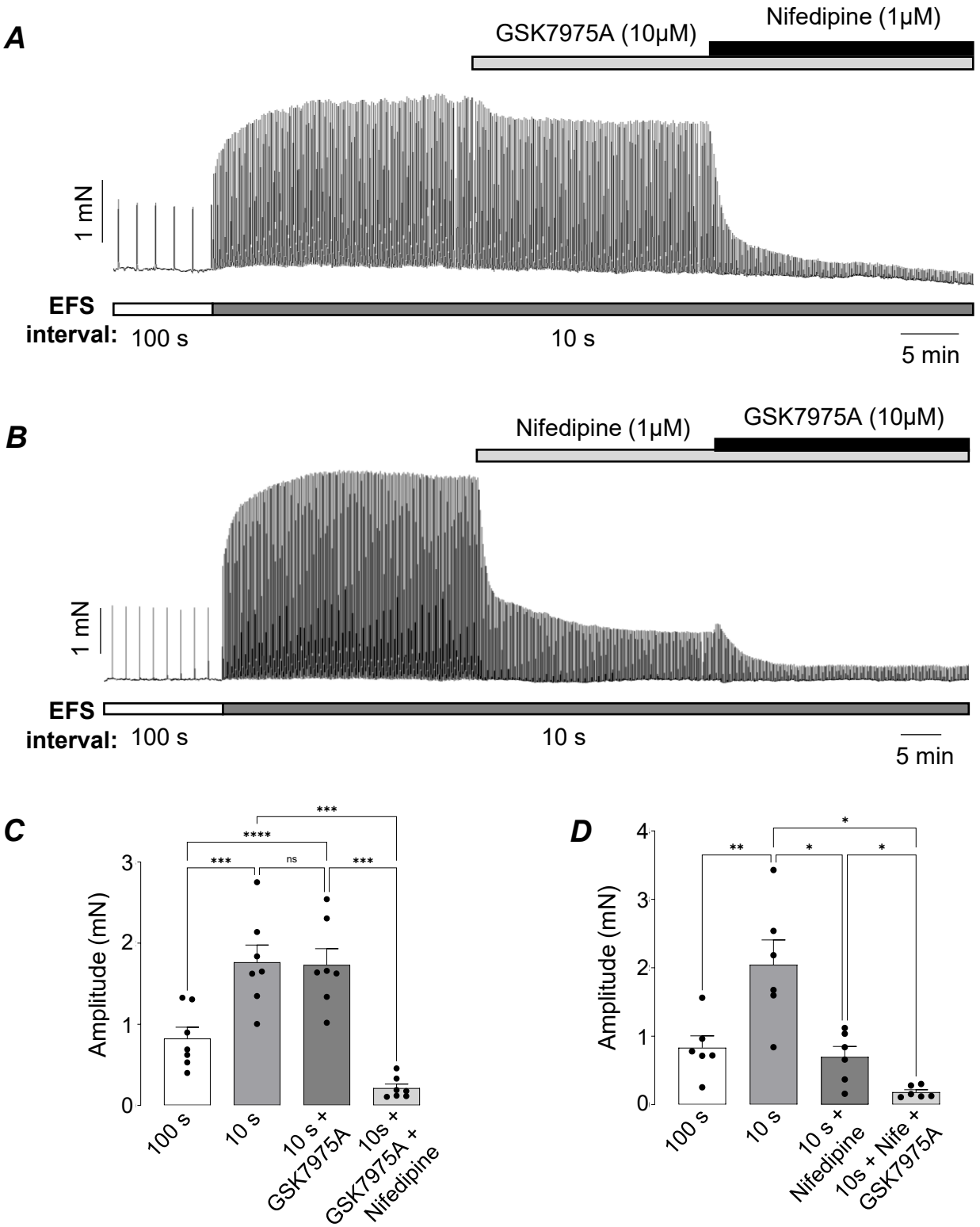

Figure 3.5. Effect of CRAC Channel Inhibitor, GSK7975A and nifedipine on EFS-evoked contractions of ASM at 10 s intervals. (A) Representative isometric tension recording showing the effects of GSK7975A (10 μM) on contractions of ASM evoked by EFS at 10 s intervals. Non-significant change in contraction amplitude was observed with GSK7975A, but addition of nifedipine (1 μM) significantly reduced the effects. **(B)** GSK7975A induced an additional inhibitory effect on EFS-evoked contractions of ASM when applied in the presence of nifedipine. **(C)** Summary bar chart showing the effect of nifedipine and GSK7975A on EFS-evoked contractions at 10 s intervals (***p<0.001, ****p<0.0001, n=7, N=5, one-way ANOVA). **(D)** Summary bar chart depicting the effect of nifedipine and GSK7975A on EFS 10 s contractions (*p<0.05, **p<0.01, n=6, N=5, one-way ANOVA).

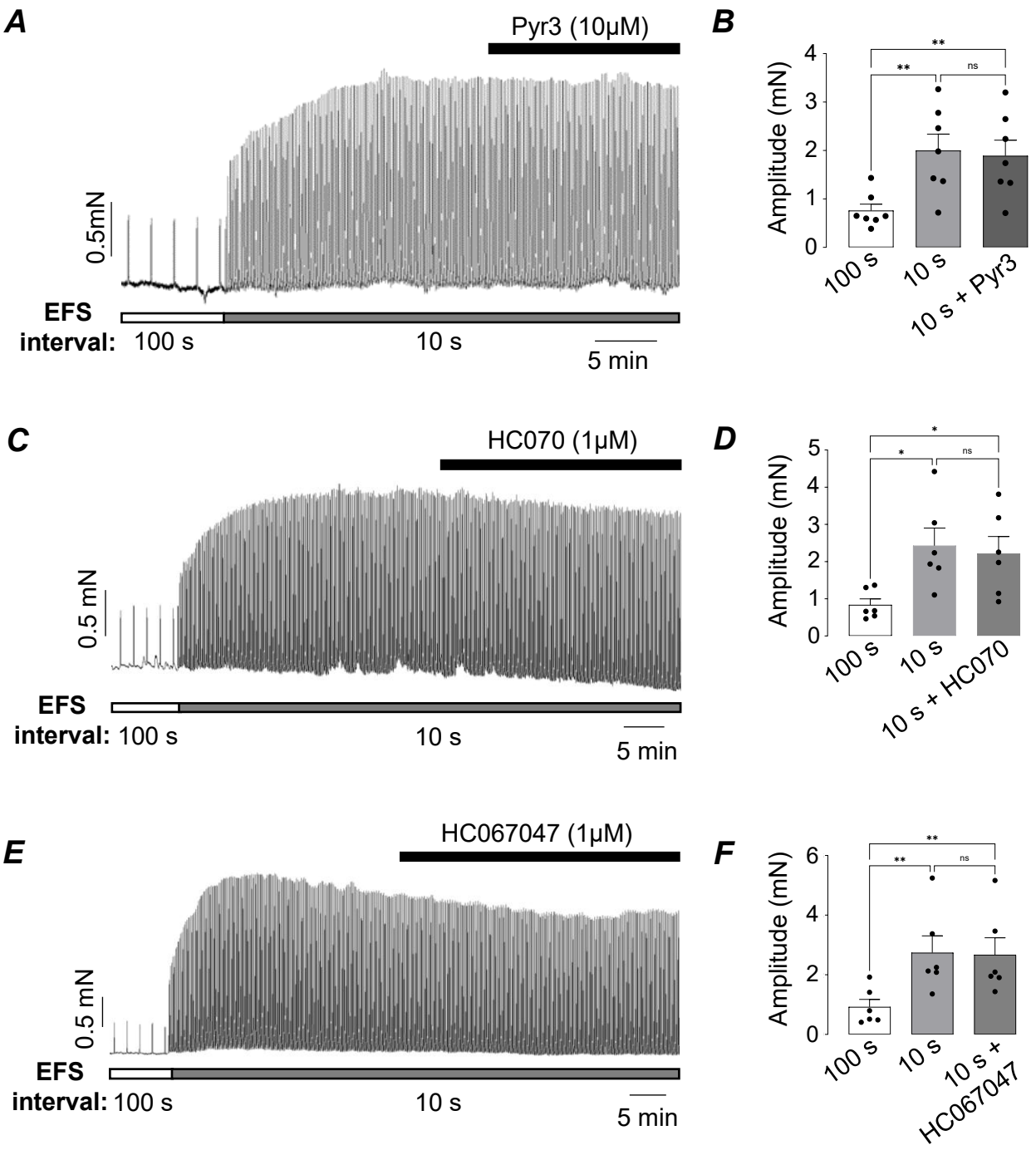

Figure 3.6. Effect of different TRP channel inhibitors on EFS-evoked contractions at 10 s intervals. (A) Representative isometric tension recording showing that 10 μM Pyr3, had no effect on EFS-evoked contractions of mice bronchial rings at 10 s intervals. **(B)** Summary bar graph of the effect of Pyr3 on mean contraction amplitude (ns, non significant, **p<0.01, n=7, N=5, one-way ANOVA). **(C)** trace showing that 1 μM HC070 (TRPC4/5 inhibitor) did not inhibit EFS-evoked contractions at 10 s interval. **(D)** Summary bar graph showing the effect of HC070 on mean contraction amplitude (ns, non-significant, *p<0.05, n=6, N=4, one-way ANOVA). **(E)** shows that HC067047 (1 μM) did not inhibit EFS contractions evoked at 10 s intervals. **(F)** Summary bar graph showing the effect of HC067047 on EFS-evoked contractions at 10 s intervals (ns, non-significant, **p<0.01, n=6, N=5, one-way ANOVA).

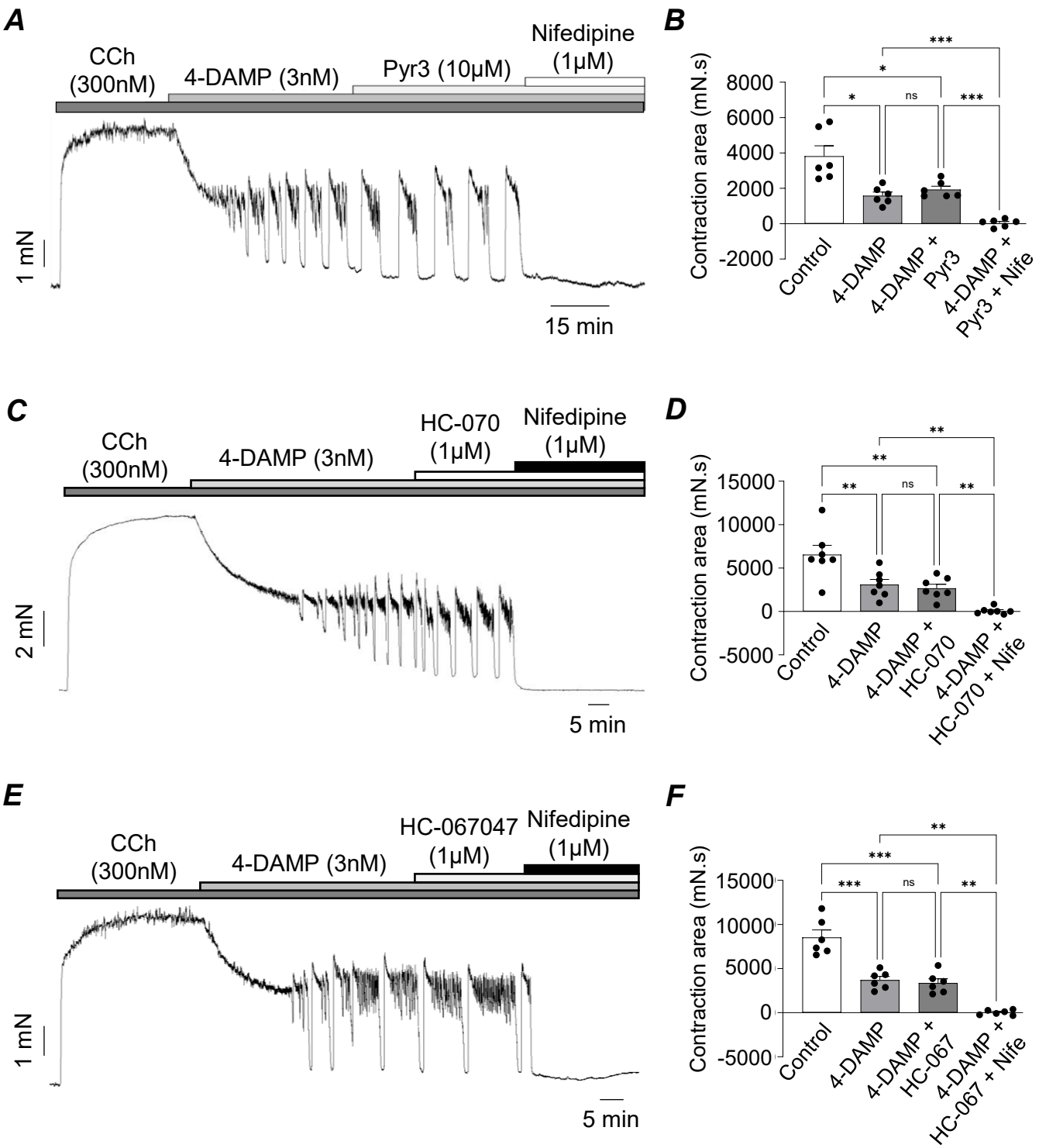

Figure 3.7. Effect of TRP channel inhibitors on M2R-dependent contractions of murine bronchial rings induced by CCh in the presence of 4-DAMP. (A) Representative isometric tension recording showing that M2R-dependent contractions of murine bronchial rings induced by CCh (300 nM) in the presence of 4-DAMP (3 nM) were unaffected by the Pyr3 (10 μM) but abolished by nifedipine (1 μM). **(C)** HC-070 (1 μM) similarly failed to inhibit 4-DAMP-resistant contractions, whereas further addition of nifedipine abolished these responses. **(E)** HC-067047 (1 μM) also had no significant effect on M2R-mediated contractions but the effects were inhibited by nifedipine. **(B, D and F)** Summary bar graphs showing mean contraction area (mN.s) for each condition (ns, non-significant, *p<0.05, **p < 0.01, ***p < 0.001; one-way ANOVA).

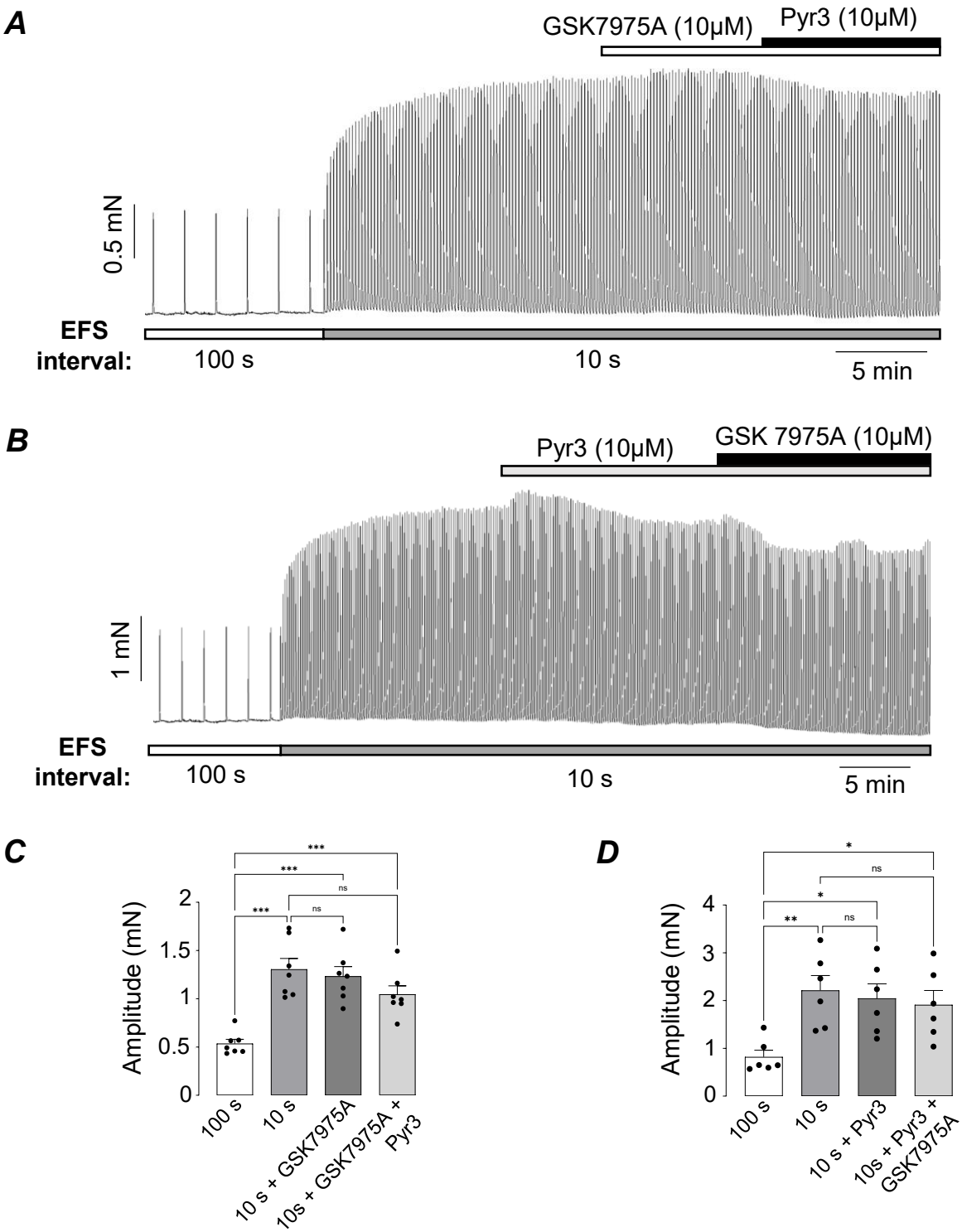

Figure 3.8. Effect of GSK7975A and Pyr3 on EFS mediated contractions at 10 s intervals. (A) and (B) Representative isometric tension recordings showing the effect of 10 μM GSK7975A and 10 μM Pyr3 on EFS-evoked contractions of mice bronchial rings at 10 s intervals. Addition of both the drugs did not abolish the M2R mediated contractions **(C)** and **(D)** Summary bar graphs showing the effect of GSK7975A and Pyr3 (n=7, N=5) and Pyr3 and GSK7975A (n=6, N=6) on mean contraction amplitude, respectively (ns, non-significant, *p<0.05, **p<0.01, ****p<0.0001, one-way ANOVA).

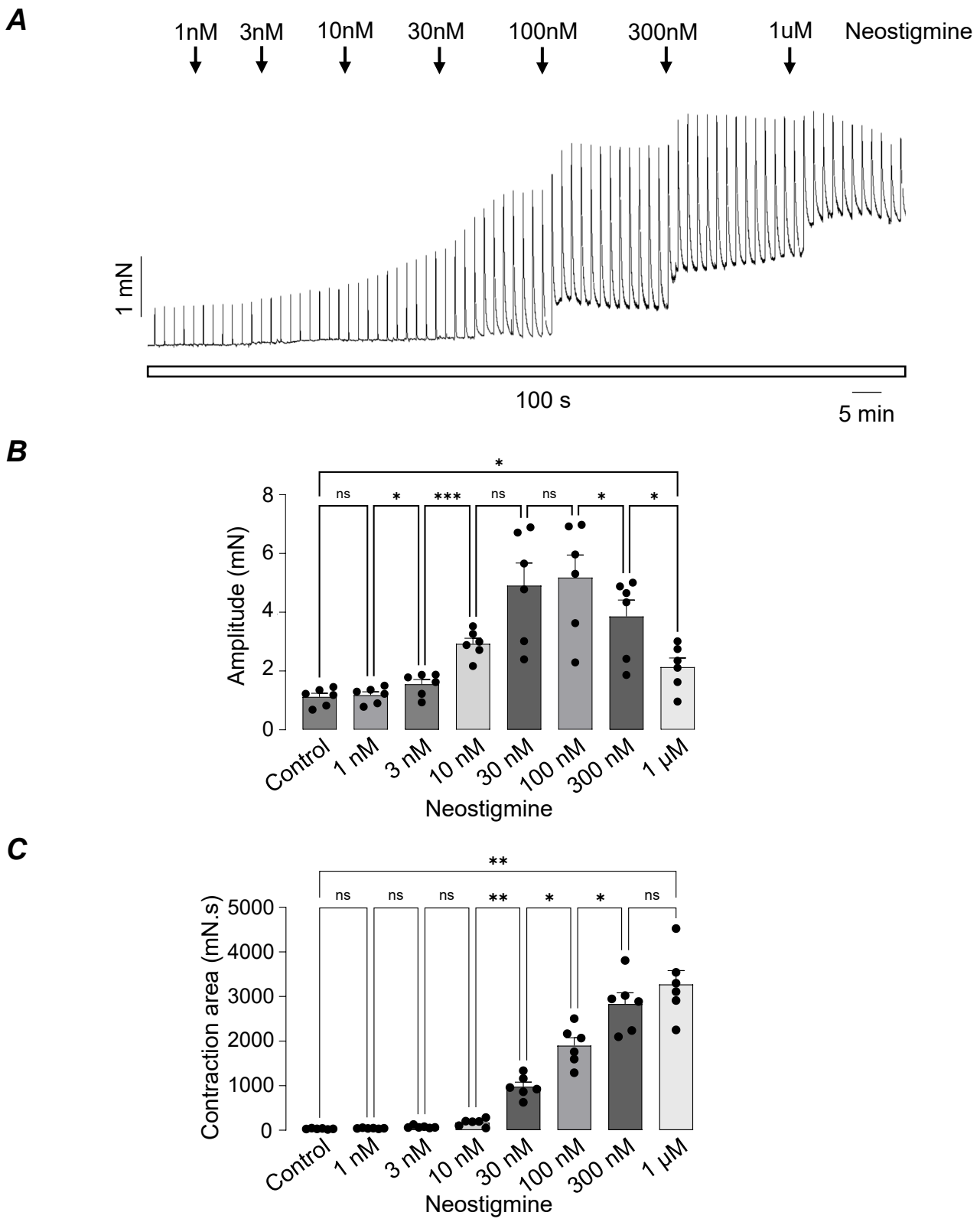

Figure 3.9. Concentration-dependent effects of neostigmine on EFS-evoked contractions. (A) Representative isometric tension recording showing the cumulative concentration-response effect of neostigmine (1 nM-1 µM) on EFS-evoked contractions of ASM at 100 s intervals. Neostigmine progressively enhanced contraction amplitude and induced a tonic rise in baseline tension at higher concentrations. **(B)** Summary bar graph showing mean contraction amplitude at each neostigmine concentration compared with control values (ns, not significant, *p<0.05, ***p<0.001; n=6, N=3; one-way ANOVA). **(C)** Summary bar graph showing changes in total contraction area (mN.s) with increasing concentrations of neostigmine (ns, not significant; *p<0.05, **p<0.01; n=6, N=3; one-way ANOVA). Maximal enhancement of contraction amplitude occurred at 100 nM neostigmine, while tonic activity increased markedly at 1 µM.

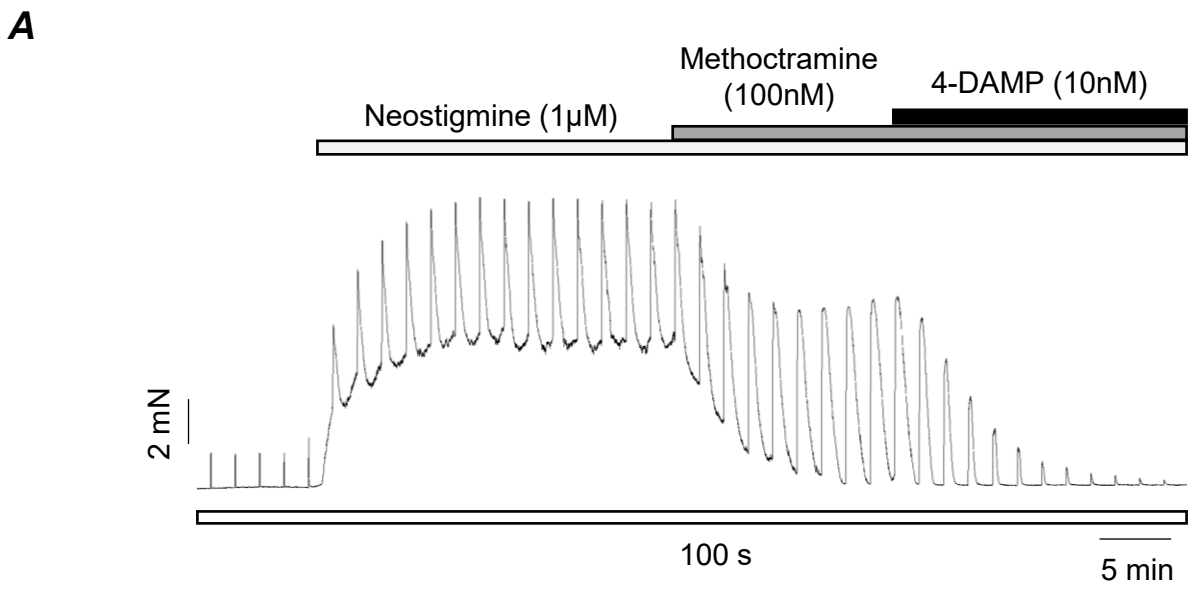

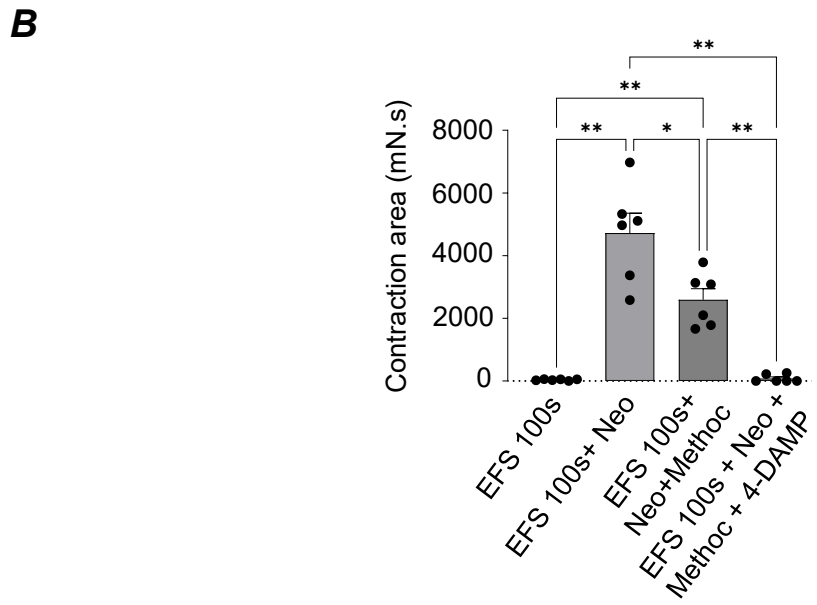

Figure 3.10. Effect of methoctramine and 4-DAMP on neostigmine-induced enhancement of EFS-evoked contractions in murine bronchial rings. (A) Representative isometric tension recording showing the effect of neostigmine (1 µM) on EFS-evoked contractions applied at 100 s intervals. Neostigmine increased both the tonic component and EFS-induced contraction amplitude. Subsequent addition of methoctramine (100 nM) abolished the tonic response, while 4-DAMP (10 nM) abolished the nerve-evoked contraction amplitude. **(B)** Summary bar graph showing mean contraction area (mN.s) under control conditions (EFS at 100 s intervals), after neostigmine addition and during methoctramine and 4-DAMP treatment (*p<0.05, **p<0.01, ***p<0.001; n=6, N=5; one-way ANOVA).

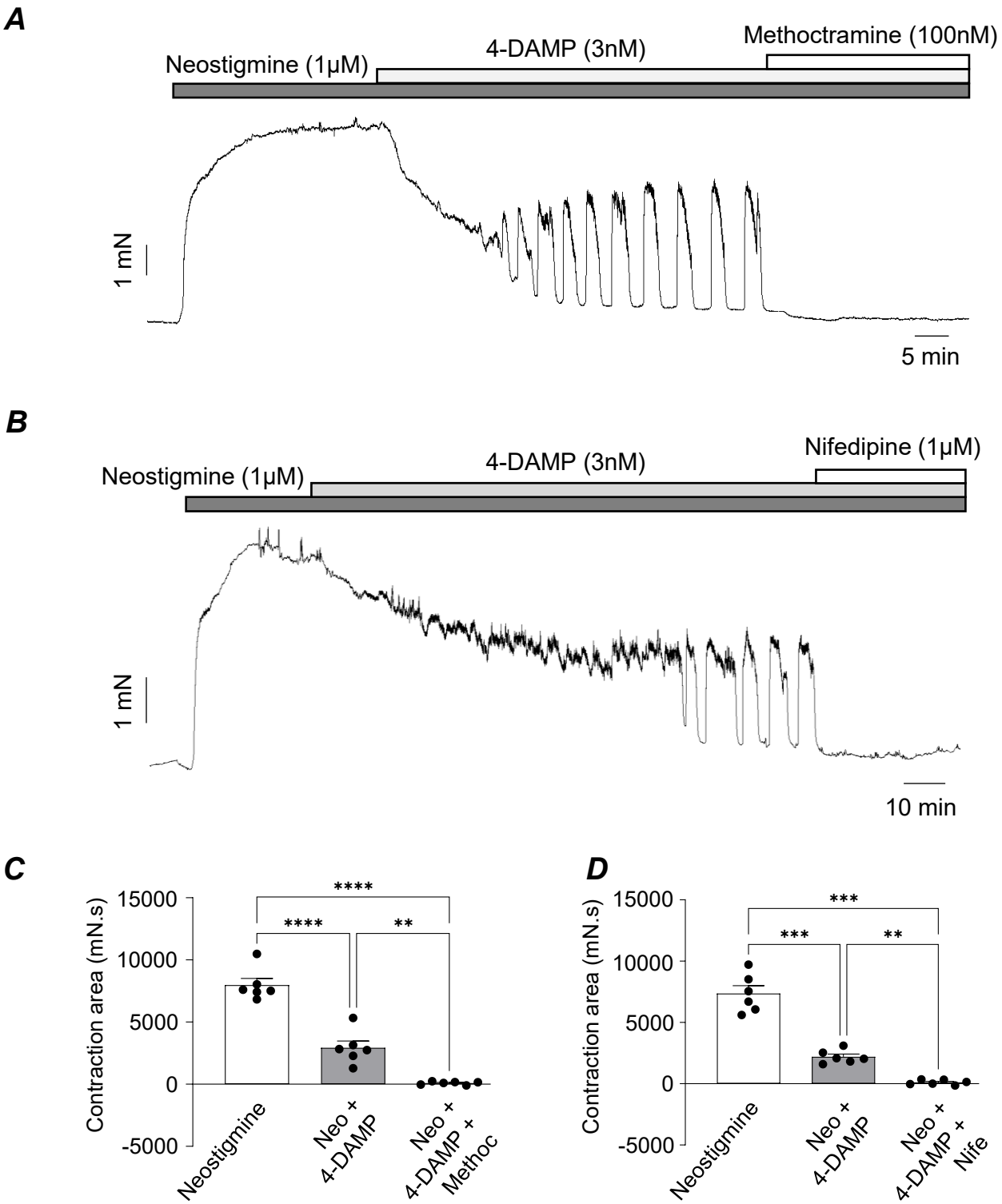

Figure 3.11. Effect of methoctramine and nifedipine on neostigmine and 4-DAMP-mediated oscillatory contractions of murine bronchial rings. (A) Representative isometric tension trace showing the effect of methoctramine and 4-DAMP on neostigmine-induced contractions of ASM. Subsequent addition of the 4-DAMP (3 nM) converted the sustained neostigmine-induced contraction into oscillatory activity. The selective M2R antagonist methoctramine (100 nM) abolished these oscillations. **(B)** Representative trace showing that addition of nifedipine (1 μM) inhibited the 4-DAMP-resistant M2R oscillatory contractions. **(C and D)** Summary bar graphs showing mean contraction area (mN.s) for neostigmine alone and following 4-DAMP and either methoctramine **(C)** or nifedipine **(D)** treatment (**p<0.01, ***p<0.001, ****p<0.0001; n = 6, N = 5; one-way ANOVA).

Chapter 4

Contribution of potassium channels to M2R-dependent contractions of murine ASM

4.1. Introduction

Data in chapter 3 showed that M2R-mediated contractions of ASM relied on Ca^{2+} influx through LTCC. However, the mechanisms that coupled stimulation of M2Rs to activation of LTCC were not resolved. K^+ channels act as regulators of membrane potential and therefore have the capacity to influence smooth muscle contraction by affecting the activity of voltage-dependent Ca^{2+} channels (VDCC). Opening of K^+ channels in ASM cells, at physiological membrane potentials, exerts a hyperpolarising influence on membrane potential and opposes Ca^{2+} entry via VDCC, whereas closure of K^+ channels promotes membrane depolarisation and bronchoconstriction [234]. ASM cells possess an array of K^+ channels including BK_{Ca} channels [460] and members of the Kv7 family of voltage-gated K^+ channels [58, 234, 292]. Zhou et al. (2008) demonstrated that the activation of M2R in murine ASM resulted in the suppression of BK_{Ca} channels [286]. Kv7 channels underlie the neuronal M-current, so named because it is inhibited by activation of muscarinic receptors [461, 462] and Brueggemann et al. (2012) revealed that stimulation of muscarinic receptors in ASM cells decreased Kv7 current amplitude [286, 292]. As M2R-dependent contractions of ASM are mediated by activation of LTCC, it is possible that this involves inhibition of Kv7 channels or BK_{Ca} channels. However, although cholinergic agonists can suppress ASM Kv7 currents [292, 463, 464], the muscarinic receptor subtype underlying this effect was not investigated and M2R-mediated inhibition of Kv7 channels has not been reported previously. The purpose of the present study was to investigate the involvement of BK_{Ca} and Kv7 channels in M2R-dependent potentiation of cholinergic nerve-mediated contractions of murine ASM.

4.2. Results

4.2.1. Effect of BK_{Ca} channel modulators on EFS-evoked contractions of ASM

Zhou et al. (2008) showed that activation of M2Rs in murine ASM led to inhibition of BK_{Ca} channels [286]. Therefore, we investigated if activation of BK_{Ca} channels could reverse the M2R-dependent potentiation of cholinergic nerve-evoked contractions of ASM. Figure 4.1A is a representative tension recording showing that application of the BK_{Ca} channel opener, compound X reduced the M2R-mediated enhancement of contraction amplitude induced by reducing the stimulus interval from 100 to 10 s intervals. The summary data in Figure 4.1C show that the reduction in stimulus interval to 10 s resulted in an increase in mean contraction amplitude from 1.7 ± 0.17 mN to 4.2 ± 0.3 mN ($p<0.001$, n=6), and subsequent addition of compound X (3 μM) reduced mean contraction amplitude to 2.2 ± 0.3 mN ($p<0.01$, n=6). Conversely, we reasoned that if the enhanced contractions induced by the reduction in stimulus interval from 100 to 10 s resulted from inhibition of BK_{Ca} channels, then application of the BK_{Ca} channel inhibitor, iberiotoxin should exert similar stimulatory effects as those induced by the interval change. However, the data shown in Figure 4.1B demonstrated that iberiotoxin (300 nM) only induced a small increase in amplitude of contractions evoked at 100 s intervals. Mean contraction amplitude was 1.16 ± 0.2 mN before, compared to 1.55 ± 0.2 mN (ns, n=7) in iberiotoxin (Figure 4.1D). In contrast, the reduction in stimulus interval to 10 s (under control conditions) increased mean contraction amplitude to 2.21 ± 0.4 mN ($p<0.05$, n=7). Therefore, it seems unlikely that inhibition of BK_{Ca} channels in ASM cells was responsible for the increase in contraction amplitude brought about by the switch from 100 to 10 s stimulus intervals.

ASM cells express Kv7 channels and activation of muscarinic receptors reduced Kv7 current amplitude in guinea-pig and rat ASM cells [292, 464]. Furthermore, contractions of rat airways induced by the cholinergic agonist methacholine were inhibited by three structurally unrelated Kv7 channel activators [463]. It is also known that inhibition of PKA reduces the activation of Kv7 channels [298, 465]. We hypothesised that M2R activation may inhibit Kv7 channels leading to activation of LTCC and ASM contraction. Data in Figure 4.2A and B show that application of the Kv7 channel blocker, XE991 (10 μM) increased mean amplitude

of contractions induced by EFS at 100 s intervals from 1.4 ± 0.2 mN to 2.5 ± 0.3 mN ($p<0.01$, n=8). Subsequent addition of nifedipine reduced contraction amplitude to 1.2 ± 0.2 mN ($p<0.001$; Figure 4.2B). Therefore, inhibition of Kv7 channels mimicked the effect of M2R stimulation by increasing contraction amplitude, albeit to a lesser extent than that induced by a reduction in stimulus interval to 10 s.

Next, we investigated the effect of XE991 on EFS-induced contractions when the stimulation interval was already reduced to 10 s. As shown in Figure 4.3A and B, application of XE991 (10 μM) during EFS-evoked contractions at 10 s intervals produced no significant change in contraction amplitude. The representative trace and summary data (Figure 4.3A and B) confirm that XE991 did not further enhance the amplitude of contractions evoked at 10 s intervals when M2R were already activated ($p>0.05$, n=7).

4.2.2. Combined effect of XE991 and iberiotoxin on EFS-evoked contractions of ASM

A series of experiments was carried out to examine the combined effect of XE991 and iberiotoxin on EFS-evoked contractions of ASM at 100 s intervals. As displayed in Figure 4.4A, XE991 (10 μM) increased the amplitude of EFS-evoked contractions. Addition of 300 nM iberiotoxin, in the continued presence of XE991, induced a dramatic increase in basal tone and in the amplitude of EFS responses. Data in Figure 4.4B shows that 10 μM XE991 increased mean contraction amplitude from 0.85 ± 0.21 to 1.31 ± 0.25 mN ($p<0.05$, n=6) and addition of iberiotoxin further elevated mean contraction amplitude to 2.25 ± 0.37 mN ($p<0.05$, n=6). Application of nifedipine abolished the stimulatory effects of XE991 & Iberiotoxin, reducing mean contraction amplitude to 0.82 ± 0.16 mN ($p<0.05$, n=6), suggesting that these effects were reliant on activation of LTCC.

Next, we checked if the excitatory effects of XE991 & iberiotoxin, on basal tone and EFS responses, were mediated by an effect on nerves. Figure 4.4C shows that addition of the neurotoxin tetrodotoxin (100 nM) abolished all EFS responses, but that the increase in basal contractile activity was little affected. Application of tetrodotoxin reduced mean EFS-evoked contraction amplitude from 2.36 ± 0.39 to 0.3 ± 0.09 mN ($p<0.001$, n=6, Figure 4.4D). Figure 4.4E shows that EFS responses in the presence of XE991 & Iberiotoxin were also inhibited by addition of the

muscarinic receptor antagonist, atropine. However, atropine did not affect tone. The data in Figure 4.4F shows that addition of atropine (1 μM) reduced the mean EFS-induced contraction amplitude from 1.36 ± 0.19 to 0.3 ± 0.06 mN ($p<0.01$, n=6).

4.2.3. Examination of the expression of Kv7 and KCNE subtypes in airway smooth muscle cells

There are five members of the Kv7 channel family (Kv7.1-Kv7.5), each encoded by a single KCNQ gene (KCNQ1-KCNQ5). All five subtypes have previously been detected at the transcriptional level in guinea-pig, mouse, and human ASM, with Kv7.4 (KCNQ4) and Kv7.5 (KCNQ5) representing the most abundant isoforms. To characterise their expression in murine airways, we examined the transcriptional profile of KCNQ1-5 in mouse bronchial tissues using real-time qPCR. As shown in Figure 4.5A, detectable expression of KCNQ1, KCNQ4, and KCNQ5 was observed, whereas KCNQ3 showed minimal expression and KCNQ2 was undetectable. Protein expression of Kv7.1, Kv7.4 and Kv7.5 was confirmed using immunocytochemistry in isolated ASM cells (Figure 4.5C). The identity of ASM cells was verified by positive staining with anti-α-smooth muscle actin, a specific marker for smooth muscle cells. KCNE subunits associate with Kv7 α-subunits to alter their plasmalemmal expression, biophysical properties and pharmacology [322-324]. We determined the transcriptional expression of KCNE subunits in mice bronchial tissues. Figure 4.5B shows that KCNE3 expression was the highest in mice bronchi, followed by KCNE4 and KCNE1.

4.2.4. The Kv7 channel activator, zinc pyrithione activates Kv7.1, 7.4 and 7.5 channels

Since Kv7.1, Kv7.4, and Kv7.5 subtypes are predominantly expressed in ASM cells, we sought to investigate the effect of opening of these channels using the Kv7 channel activator, zinc pyrithione which is reported to selectively activate Kv7.1, Kv7.2, Kv7.4 and Kv7.5, with no effect on Kv7.3 [466]. We examined the effects of zinc pyrithione on Kv7.1, Kv7.4, and Kv7.5 currents recorded from HEK293 cells expressing each subtype using patch clamp electrophysiology.

Whole-cell currents were recorded using the voltage protocol illustrated in the inset of Figure 4.6. Cells were held at -80 mV and then stepped through a series of test potentials ranging from -100 mV to +50 mV. Tail currents were subsequently

recorded during a step to -120 mV. Figures 4.6A and B display representative families of currents from HEK293 cells transfected with Kv7.4, recorded under control conditions and following application of zinc pyrithione (10 μM). Summary activation (G/G_{max}) curves, derived from tail currents, revealed that zinc pyrithione increased the mean G_{max} of Kv7.1 currents by 61.6% ($p<0.05$, n=7), accompanied by a negative shift in the $V_{1/2}$ of activation from -29.9 ± 1.5 mV (control) to <-50 mV in the presence of zinc pyrithione (Figure 4.6C). Additionally, the deactivation time constant increased from 83.4 ± 8.1 msec in control to 241.9 ± 40.07 msec in zinc pyrithione (Figure 4.6D). Similarly, zinc pyrithione significantly increased the mean G_{max} of Kv7.4 currents from 1.0 to 2.17 ± 0.35 ($p<0.05$, n=7; Figure 4.7C) and prolonged the deactivation time constant from 30.6 ± 4.6 msec to 108.2 ± 11.7 msec ($p<0.001$, n=7; Figure 4.7D). Likewise, the G_{max} of Kv7.5 currents increased from 0.97 ± 0.01 to 2.26 ± 0.24 ($p<0.01$, n = 6; Figure 4.8C) and the time constant of deactivation increased from 52.2 ± 3.7 to 118.8 ± 11.3 msec ($p<0.01$, n=6; Figure 4.8D). It was also evident that zinc pyrithione negatively shifted the activation $V_{1/2}$ of Kv7.4 and Kv7.5 currents (<-70mV and <-134mV, respectively); however, it was not possible to determine the precise $V_{1/2}$ of activation of Kv7.4 and Kv7.5 in the presence of zinc pyrithione as these data were not well fit with a Boltzmann equation.

4.2.5. Effect of zinc pyrithione on M2R-mediated ASM contractions

Since the Kv7 channel blocker XE991 was able to partially replicate the effects of M2R activation on cholinergic nerve-induced contractions of ASM, we reasoned that stimulation of M2Rs may induce contraction via inhibition of Kv7 channels. This idea was investigated by examining the effects of zinc pyrithione on M2R-dependent contractions of ASM, induced by reducing the stimulus interval to 10 s and by applying CCh, or neostigmine, in the presence of the M3R antagonist, 4-DAMP. The representative trace in Figure 4.9A shows that zinc pyrithione (3 μM) did not inhibit EFS contractions elicited at 100 s intervals (which do not involve M2Rs). The data in Figure 4.9C shows that the mean contraction amplitude was 1.62 ± 0.16 mN under control conditions compared to 1.7 ± 0.2 mN in the presence of zinc pyrithione (ns, n=6). In contrast, zinc pyrithione reversed the M2R-mediated enhancement in the contraction amplitude evoked by EFS at 10 s intervals (Figure 4.9B). The summary data in Figure 4.9D show that the mean contraction amplitude

during EFS at 10 s intervals decreased significantly from 2.08 ± 0.5 mN under control conditions to 0.65 ± 0.20 mN in the presence of zinc pyrithione ($p<0.05$, n=7).

Data in Figure 4.10A show that zinc pyrithione had little effect on contractions evoked by CCh alone. However, when it was applied following the addition of 4-DAMP, it abolished the 4-DAMP-resistant contractions. In six preparations, zinc pyrithione markedly reduced mean contraction area recorded in the presence of 4-DAMP from 2641 ± 443.9 to 188.8 ± 142.1 mN.s ($p<0.01$, n=6). Furthermore, zinc pyrithione also abolished 4-DAMP-resistant contractions evoked by neostigmine ($p<0.001$, n=6; Figure 4.11A and B).

4.2.6. Zinc pyrithione can activate Kv7 and BK_{Ca} channels

Although most studies describe zinc pyrithione as a selective activator of Kv7 channels, Eid and Gurney (2018) reported that zinc pyrithione also activated BK_{Ca} channels in rat pulmonary artery smooth muscle cells [467]. To determine whether a similar mechanism operates in ASM, we investigated the effect of zinc pyrithione in the presence of XE991. As shown in Figure 4.12A, addition of zinc pyrithione gradually reduced the amplitude of contractions evoked by EFS (10 s intervals) in the presence of XE991. Mean contraction amplitude was reduced from 3.8 ± 0.8 to 0.76 ± 0.3 mN; $p<0.05$, n=6, Figure 4.12C). These data suggest that zinc pyrithione can inhibit cholinergic-nerve contractions of ASM, even when Kv7 channels are blocked. To evaluate whether BK_{Ca} channels were involved in this effect, we examined the effects of zinc pyrithione in the presence of the BK_{Ca} channel blocker, iberiotoxin. As illustrated in Figure 4.12B and D, zinc pyrithione again caused a gradual decrease in contraction amplitude over time ($p<0.01$, n=7), indicating that its relaxant effects persisted even when the BK_{Ca} channels were inhibited. The effects of zinc pyrithione were investigated further by examining its effects on tissues that were treated with both XE991 and iberiotoxin. As shown in Figure 4.13A and B, zinc pyrithione did not affect contractions when it was applied in the presence of both XE991 and iberiotoxin. Application of iberiotoxin alone increased mean contraction area from 1185 ± 90.07 to 2590 ± 340.1 mN.s ($p<0.05$, n=7) and addition of XE991 further enhanced mean contraction area to 3382 ± 265.7 mN.s ($p<0.05$, n=7). Addition of zinc pyrithione did not significantly reduce mean contraction area under these conditions (3166 ± 310.2 mN.s, ns, n=7). Similarly, when the order of drug application was reversed (XE991 applied first, followed by iberiotoxin; Figure

4.14A), both blockers again produced a marked increase in contraction area and addition of zinc pyrithione failed to reduce the contractile response. These findings suggest that zinc pyrithione exerts its inhibitory effects on cholinergic contractions of ASM via effects on both Kv7 and BK_{Ca} channels.

4.2.7. Effect of M2R activation on Kv7 channel activity

The experiments above suggest that M2R-dependent contractions of ASM may involve inhibition of Kv7 channels. Previous studies demonstrated that M1R activation inhibits Kv7.2/7.3 (M-current) channels when co-transfected in tsA-201 cells [468] therefore, we examined whether M2R activation produced a similar inhibitory effect on Kv7.1, Kv7.4, and Kv7.5 currents. HEK293 cells were co-transfected with plasmids encoding M2Rs and individual Kv7 subtypes, and whole-cell patch-clamp recordings were performed to assess whole cell currents before and after M2R stimulation with CCh (10 μM).

Figures 4.15, 4.16 and 4.17 are representative current traces recorded from HEK293 cells co-expressing M2Rs with either Kv7.1, Kv7.4, or Kv7.5 channels, respectively. Families of currents were recorded under control conditions and in the presence of CCh. G/G_{max} activation curves constructed from these currents demonstrated that CCh significantly reduced the mean G_{max} of Kv7.1 currents by 54% ($p<0.001$, n=8). However, the activation $V_{1/2}$ was similar under both conditions (-23.6 ± 0.95 mV under control vs. -25.7 ± 6.2 mV in CCh; $p>0.5$; Figure 4.15C). Similarly, for Kv7.4, CCh caused a 53% reduction in G_{max} ($p<0.0001$, n=8), with no significant change in $V_{1/2}$ of activation (-21.0 ± 1.1 mV before vs. -26.6 ± 3.5 mV in CCh; ns; Figure 4.16C). Figure 4.17C shows that CCh reduced the mean G_{max} of Kv7.5 currents in HEK293 cells co-expressing M2Rs and Kv7.5 by 63% ($p<0.0001$, n=8) and positively shifted the $V_{1/2}$ of activation (from -41.7 ± 0.9 mV in control conditions to -34.3 ± 3.4 mV in CCh, ns, n=8). Collectively, these data demonstrate that M2R activation reduces the maximal conductance (G_{max}) of Kv7.1, Kv7.4, and Kv7.5 currents, and positively shifts the voltage-dependence of activation of Kv7.5 (although this did not reach statistical significance), but not Kv7.1 or Kv7.4 currents.

4.3. Discussion

In this chapter, we assessed the contribution of Kv7 and BK_{Ca} channels to M2R-dependent contractions of ASM. We found that M2R-dependent enhancement of cholinergic nerve-induced contractions of ASM was mimicked by blockade of Kv7 channels with XE991, but not BK_{Ca} channels with iberiotoxin. However, XE991 had little effect on contractions that were already enhanced by reducing the EFS interval to 10 s intervals. Mouse ASM expressed Kv7.1, 7.4 and 7.5 channels and patch clamp experiments showed that zinc pyrithione enhanced Kv7.1, 7.4 and 7.5 currents recorded from HEK293 cells. Zinc pyrithione inhibited M2R-dependent contractions of ASM. These effects were absent in tissues treated with XE991 and iberiotoxin, but not individual application of either blocker, suggesting that zinc pyrithione can activate both Kv7 and BK_{Ca} channels, but that activation of either channel is able to compensate for the inhibitory effects induced by blockade of the other. Finally, we showed, for the first time, that activation of M2Rs in HEK293 with CCh reduced the activity of Kv7.1, 7.4 and 7.5 currents.

There is evidence that M2R activation is associated with closure of BK_{Ca} channels. Zhou et al. (2008) demonstrated that $G_{\beta\gamma}$ dimers from M2Rs inhibit BK_{Ca} channel activity through two mechanisms. Firstly, they directly interact with the BK_{Ca} channel α subunits or an associated protein, reducing the open probability of the channel. Secondly, they activate PKC via the PLC_{β} pathway, further contributing to inhibition of channel activity [286]. In addition, Semenov et al. (2011) demonstrated that the β1-subunit of the BK_{Ca} channel substantially restrains M2R-mediated ASM contraction. Mechanistically, β1-subunit-containing BK_{Ca} channels normally oppose M2R-mediated depolarisation as they help maintain a more negative resting membrane potential, preventing activation of LTCCs. Without the β1-subunit, the resting potential is shifted toward depolarisation, thereby augmenting M2R-driven Ca^{2+} influx via LTCCs and enhancing ASM contraction. This indicates that BK_{Ca} β1-subunits play a key modulatory role in M2R signalling [164]. Further, studies by Suzuki et al. (2013) found a direct coupling phenomenon between LTCC and BK_{Ca} channels in VSMC [469]. We found that opening BK_{Ca} channels with compound X inhibited M2R-dependent contractions of ASM, similar to effects previously reported on histamine-induced responses by Bradley et al. (2018) [275]. However, blocking BK_{Ca} channels with iberiotoxin only slightly elevated the amplitude of contractions

evoked by EFS at 100 s intervals. Therefore, it appears that inhibition of BK_{Ca} channels does not recapitulate the effects of M2R activation on cholinergic-nerve evoked contractions, but that opening of these channels can suppress M2R responses. These data suggest M2R-dependent inhibition of BK_{Ca} channels is not the primary mechanism by which M2Rs functionally couple to LTCC. It was noteworthy that blockade of BK_{Ca} channels with iberiotoxin exerted greater effects when Kv7 channels were blocked with XE991 and when M2Rs were activated by the reduction in stimulus interval. Therefore, it is possible that the effects of closure of BK_{Ca} channels were compensated for by activation of Kv7 channels. Similar findings were reported in rabbit urethral smooth muscle cells, whereby the effects of Kv2 channel activation were only revealed when BK_{Ca} channels were blocked [470]. A similar interaction between these channels was described by Zavaritskaya et al. (2020), who showed in rat arteries that the relaxant effect of a BK_{Ca} channel opener (GoSlo-SR compounds) was only fully inhibited when both BK_{Ca} and Kv7 channels were blocked, implying functional interplay between the two channel types [423]. It was also notable that, in addition to increasing the amplitude of EFS-evoked contractions, that co-application of XE991 and iberiotoxin led to a rise in the basal contractile activity. This effect was reversed by nifedipine suggesting that both channels could have a role in the regulation of ASM contractility by regulating membrane potential and Ca^{2+} influx via LTCC.

Previous qPCR studies on cDNA obtained from rat trachea showed that KCNQ1 was the most abundantly expressed KCNQ subtype, closely followed by KCNQ5 and KCNQ4, with low expression of KCNQ3 and no detectable KCNQ2 [464]. In human trachealis muscle, KCNQ1 expression predominates, with modest levels of KCNQ4 and KCNQ5, while KCNQ2 and KCNQ3 transcripts are absent [292]. In mouse bronchial tissues, we found that KCNQ5 showed the highest expression, followed by KCNQ4 and KCNQ1. These three subtypes were also abundantly expressed in ASM cells. This expression profile is consistent with previous reports demonstrating that KCNQ4 and KCNQ5 are the predominant Kv7 subtypes in smooth muscle cells [471, 472]. Brueggemann et al. (2018) also reported the highest mRNA expression of KCNQ5 in cultured human ASM cells using qRT-PCR [299]. We also examined the expression of KCNE subunits in ASM, which are known to modulate both the expression and biophysical properties of Kv7

channels. In our study, KCNE3 was the most abundantly expressed subunit among the KCNE family members. Previous studies reported that, in mammalian cells, co-expression of KCNE3 with Kv7.1 produces minimal alterations in the I-V relationship [332]. In contrast, KCNE3 markedly suppresses Kv7.5 currents in HEK293 cells and strongly inhibits Kv7.4 channel activity in *Xenopus* oocytes [328, 329]. These findings suggest that, in ASM, the presence of KCNE3 may contribute to a partially inhibited state of Kv7.4 and Kv7.5 channels under basal conditions. Consequently, activation of M2Rs could further suppress these already restrained Kv7 subtypes, leading to enhanced membrane depolarisation and contractile responses.

Our expression data showed that Kv7.1, Kv7.4, and Kv7.5 were the predominant subtypes in ASM. To investigate if opening of these channels could affect M2R-dependent contractions of ASM, we investigated the effects of zinc pyrithione as it has been shown to activate these channels. This was confirmed by our patch clamp experiments which showed that zinc pyrithione increased the amplitude and negatively shifted the voltage-dependence of activation of Kv7.1, Kv7.4, and Kv7.5 currents recorded from HEK293 cells. A distinctive feature of Kv7 channels is their dependence on PIP_2 for maintaining the open state. Thus, agents that deplete PIP_2 generally suppress channel activity [473]. Several Kv7 activators, such as retigabine, require sufficient intracellular PIP_2 levels to exert their effects [474, 475]; however, zinc pyrithione activates Kv7.1, Kv7.4, and Kv7.5 channels independent of PIP_2 availability. Since M3R activation triggers PIP_2 hydrolysis through the G_q/PLC pathway, we opted to use zinc pyrithione instead of drugs like retigabine which selectively activate Kv7.2-Kv7.5 but not Kv7.1. Our experiments showed that zinc pyrithione did not affect EFS-evoked contractions at 100 s intervals or on CCh-induced responses in the absence of 4-DAMP, which do not involve activation of M2Rs. However, it was effective in inhibiting responses evoked by EFS at 10 s intervals and it abolished 4-DAMP-resistant contractions induced by CCh or neostigmine. Therefore, zinc pyrithione was effective at inhibiting M2R-dependent contractions of ASM. However, the effects of zinc pyrithione were not reversed by selective blockade of either Kv7 channels with XE991 or BK_{Ca} channels with iberiotoxin but were absent in tissues treated with both blockers. This suggests that zinc pyrithione can modulate both Kv7 and BK_{Ca} currents (as reported by Eid & Gurney (2018) [467] and that blockade of both channels was required to suppress its effects on EFS-evoked contractions of ASM.

Zinc pyrithione did not affect EFS-evoked contractions at 100 s intervals or on CCh-induced responses in the absence of 4-DAMP. This is likely due to the fact that such contractions are primarily mediated by M3R activation (PLC activation leading to IP_3-mediated Ca^{2+} release and RhoA/ROCK/PKC-dependent Ca^{2+} sensitisation), processes that render force generation relatively membrane potential-insensitive [476, 477]. Under these conditions, even though zinc pyrithione can open Kv7 and BK_{Ca} channels, the dominant M3R-driven Ca^{2+} sensitisation and PKC-mediated inhibition of BK_{Ca} channels prevent membrane hyperpolarisation from translating into a reduction in force. It is also important to note that zinc pyrithione is not a selective Kv7 channel opener. As demonstrated by Betrie et al. (2021), zinc pyrithione acts as a zinc ionophore and exerts multiple off-target effects, including activation of TRPA1-dependent sensory pathways, modulation of endothelial prostanoid signalling, and inhibition of LTCC [478]. These additional mechanisms can independently influence smooth muscle tone and Ca^{2+} handling, complicating the interpretation of its pharmacological effects. In contrast, M2R-mediated contractions depend more on membrane potential-regulated Ca^{2+} entry via LTCC and involve minimal Ca^{2+} sensitisation [412]. Consequently, zinc pyrithione, by opening Kv7 (and BK_{Ca}) channels, promotes membrane hyperpolarisation, reduces Ca^{2+} influx and thereby diminishes contractile force, although contributions from its off-target actions cannot be excluded.

Several studies have indicated that activation of muscarinic receptors can affect Kv7 channel activity in heterologous expression systems. For example, Shapiro et al. (2000) co-expressed the M1R with Kv7.2/7.3 channels in tsA-201 cells (a HEK293-derived line) and demonstrated that activation of M1Rs with oxotremorine-M suppressed Kv7 currents [468]. Similarly, Kosenko et al. (2012) used CHO-hM1 cells, which stably express the human M1R, and transiently transfected them with wild-type or mutant Kv7.2 channels to investigate muscarinic receptor-mediated inhibition of M-currents [479]. Beyond Kv7 channels, Zhou et al. (2008) utilised HEK293 cells stably expressing M2Rs and transiently co-transfected them with the BK_{Ca} channel α-subunit and studied the behaviour of the BK_{Ca} channel upon M2R activation [286]. However, M2R-dependent modulation of Kv7 channels has not been previously reported in either native tissues or heterologous expression systems. To address this gap, we examined whether M2R activation could inhibit

Kv7 channel activity by co-expressing M2Rs with either Kv7.1, Kv7.4, or Kv7.5 in HEK293 cells. Application of CCh to these co-transfected cells led to a pronounced reduction in the current amplitude of Kv7 currents, without significantly altering the $V_{1/2}$ of activation of Kv7 channels (Figure 4.15B, 4.16B and 4.17B). This indicates that M2R activation could decrease the number or open probability of functional Kv7.1, Kv7.4 and Kv7.5 channels, rather than altering their voltage-sensitivity of gating.

These findings provide the first direct evidence that M2R activation inhibits Kv7 channel activity when co-expressed in a heterologous system and may play a role in coupling stimulation of M2Rs to activation of LTCC to induce contraction of ASM. Our next objective was to investigate the mechanisms by which activation of M2Rs could lead to inhibition of Kv7 channels.

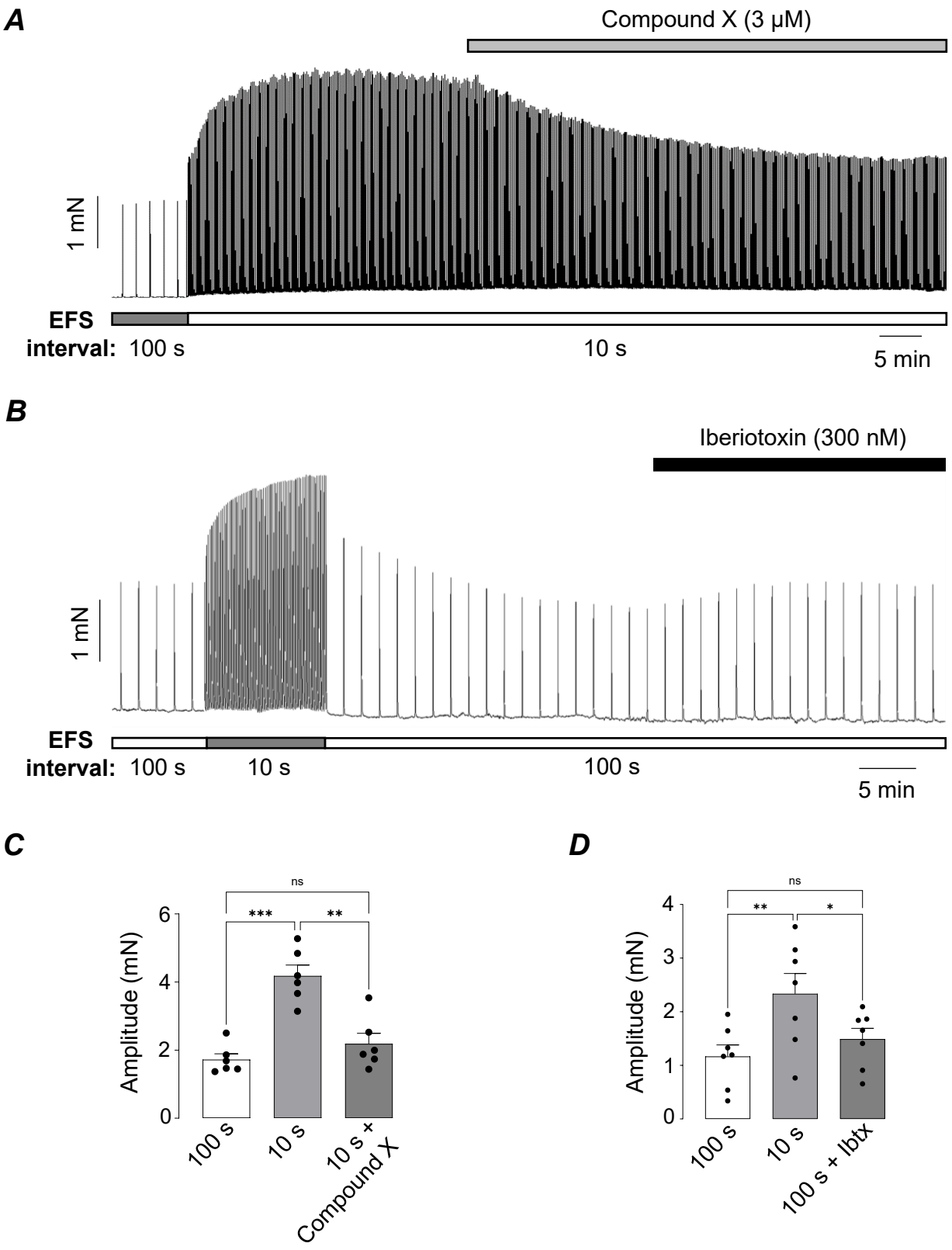

Figure 4.1. Effect of BK_{Ca} channel activator, compound X and blocker, iberiotoxin on EFS-evoked contractions of ASM. (A) Representative isometric tension trace showing that Compound X (3 μM) attenuated the M2R-mediated enhancement of EFS-evoked contractions at 10 s stimulation intervals. **(B)** Representative trace illustrating that iberiotoxin (300 nM) failed to augment EFS-evoked contraction amplitude significantly at 100 s intervals. **(C)** Summary bar chart showing the effect of compound X on EFS contractions at 10 s intervals (ns, non-significant, **p<0.01, ***p<0.001, n=6, N=4, one-way ANOVA). **(D)** Summary bar chart depicting the response of iberiotoxin on EFS contractions at 100 s interval (ns, non-significant, *p<0.05, **p<0.01, n=6, N=5, one-way ANOVA).

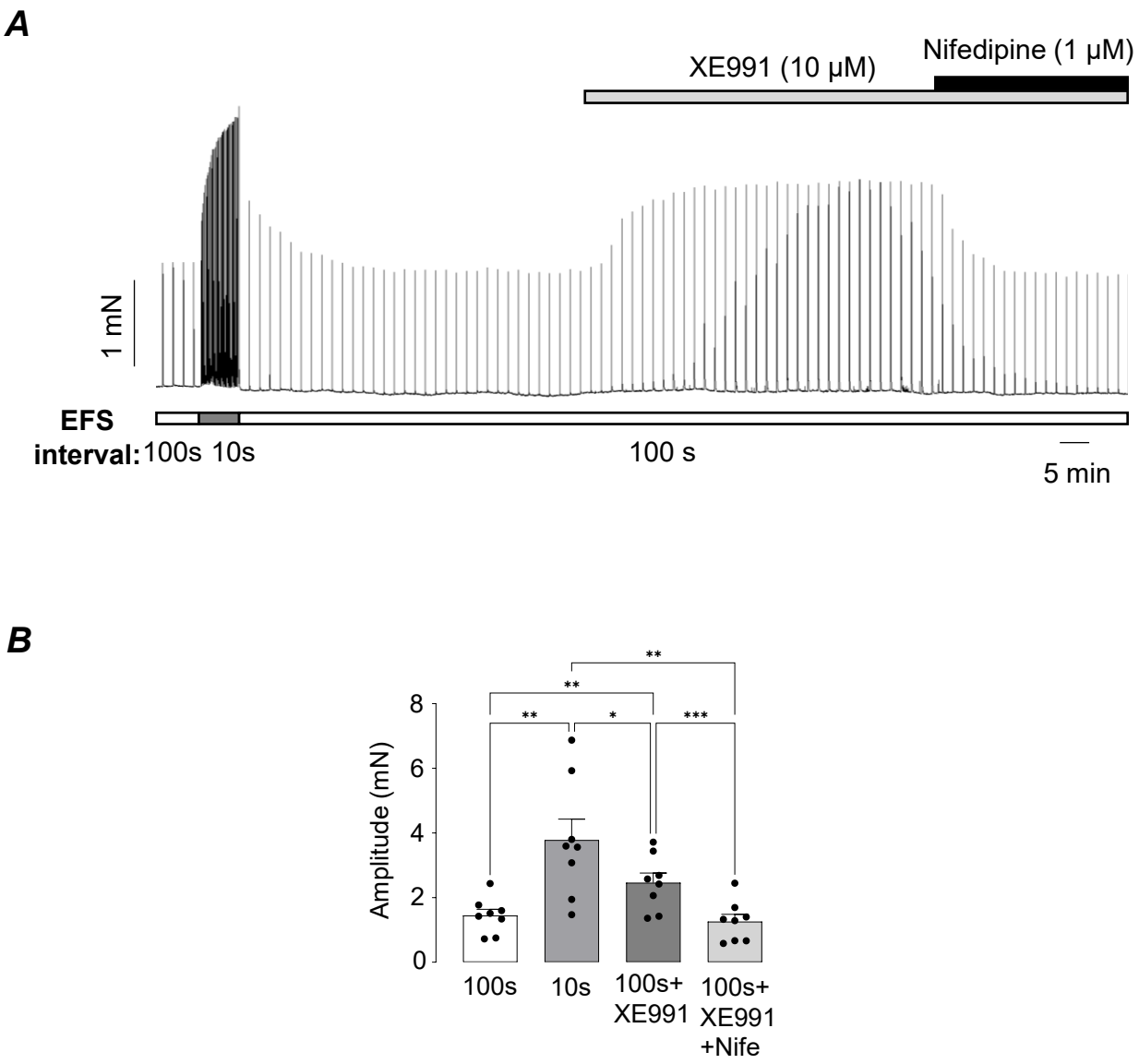

Figure 4.2. Effect of Kv7 channel inhibitor, XE991 on EFS-evoked contractions of ASM. (A) Representative isometric tension recording showing the effects of XE991 (10 μM) on EFS-evoked contractions at 100 s intervals. **(B)** Summary bar chart showing that XE991 enhanced the mean amplitude of contractions evoked by EFS at 100 s intervals and this effect was reversed by nifedipine (*p<0.05, **p<0.01, ***p<0.001, n=8, N=6, one-way ANOVA).

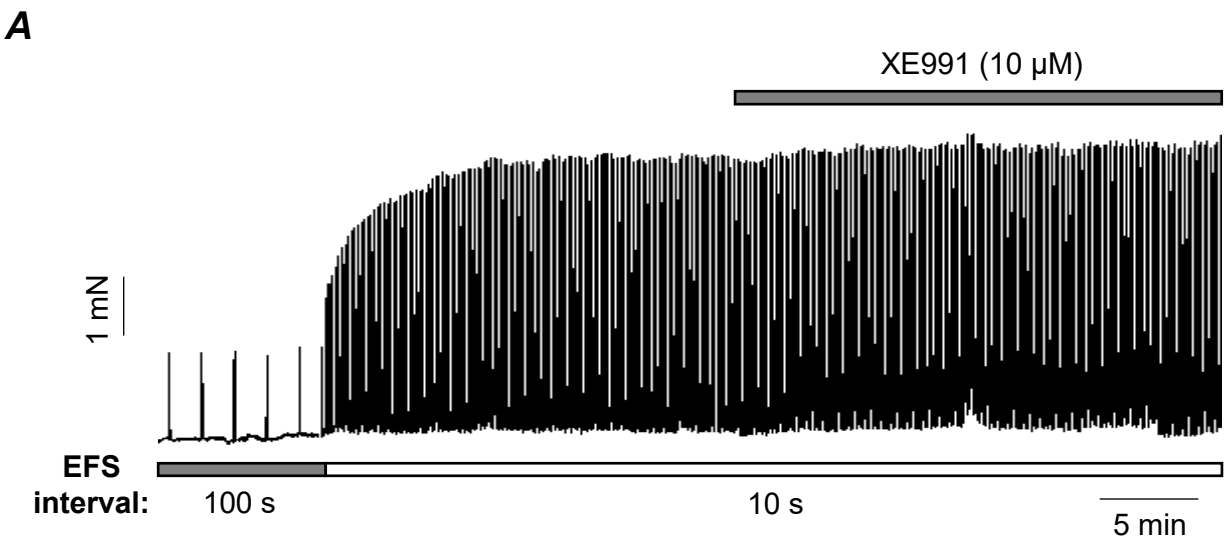

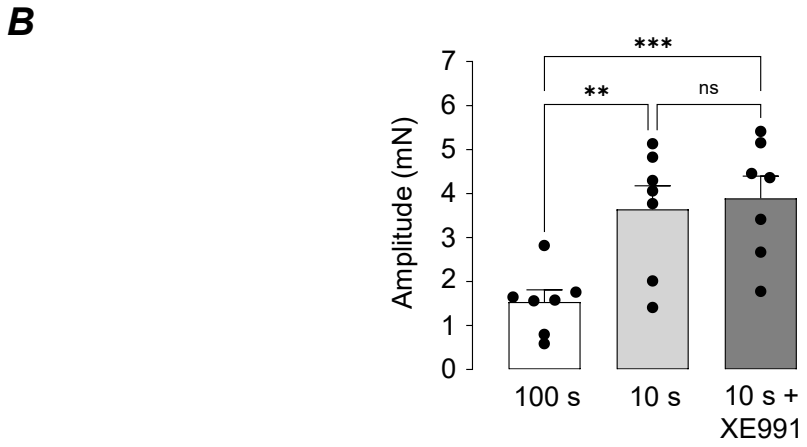

Figure 4.3. Effect of XE991 on EFS-evoked contractions of ASM.
(A) Representative trace showing that XE991 (10 μM) applied during EFS-evoked contractions at 10 s intervals produced no significant additional effect on contraction amplitude. **(B)** Summary bar graphs showing the effect of XE991 on EFS-evoked contractions at 10 s intervals (ns, non-significant, **p<0.01, ***p<0.001; n=7, N=5; one-way ANOVA).

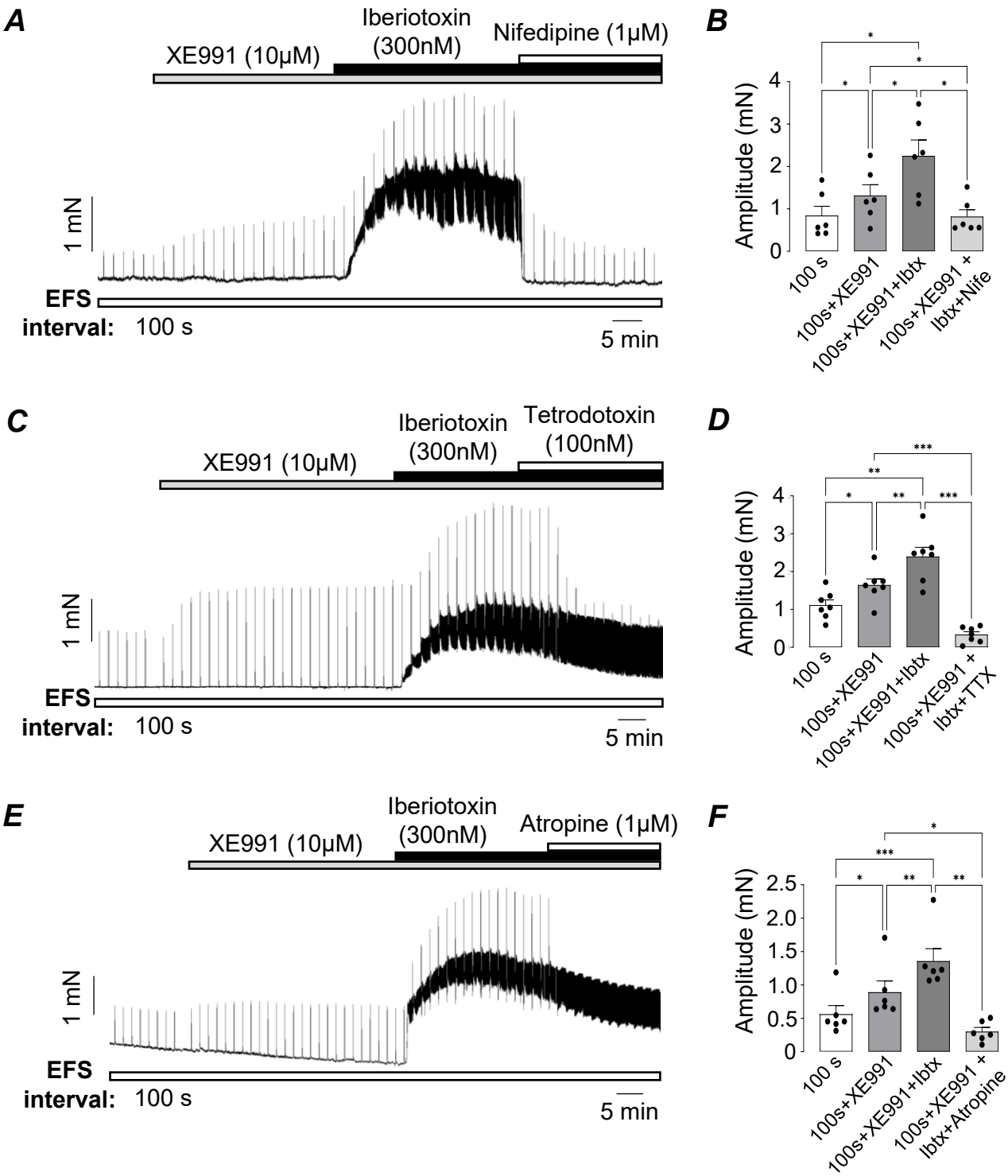

Figure 4.4. Effects of XE991 and iberiotoxin on EFS-evoked contractions of ASM.
(A) and **(B)** Representative trace and summary bar chart showing effects of nifedipine (1 μM) on contractions of ASM evoked by EFS at 100 s intervals that were augmented by co-addition of 10 μM XE991 and 300 nM iberiotoxin (n=6, N=5, *p<0.05, one-way ANOVA). **(C)** and **(D)** Representative trace and summary bar chart showing effects of tetrodotoxin (100 nM) on contractions of ASM evoked by EFS at 100 s intervals that were augmented by co-addition of XE991 and iberiotoxin (n=6, N=5, *p<0.05, **p<0.01, ***p<0.001, one-way ANOVA). **(E)** and **(F)** Representative trace and summary bar chart showing effects of atropine (1 μM) on contractions of ASM evoked by EFS at 100 s intervals that were augmented by co-addition of XE991 and iberiotoxin (n=6, N=4, *p<0.05, **p<0.01, ***p<0.001, one-way ANOVA).

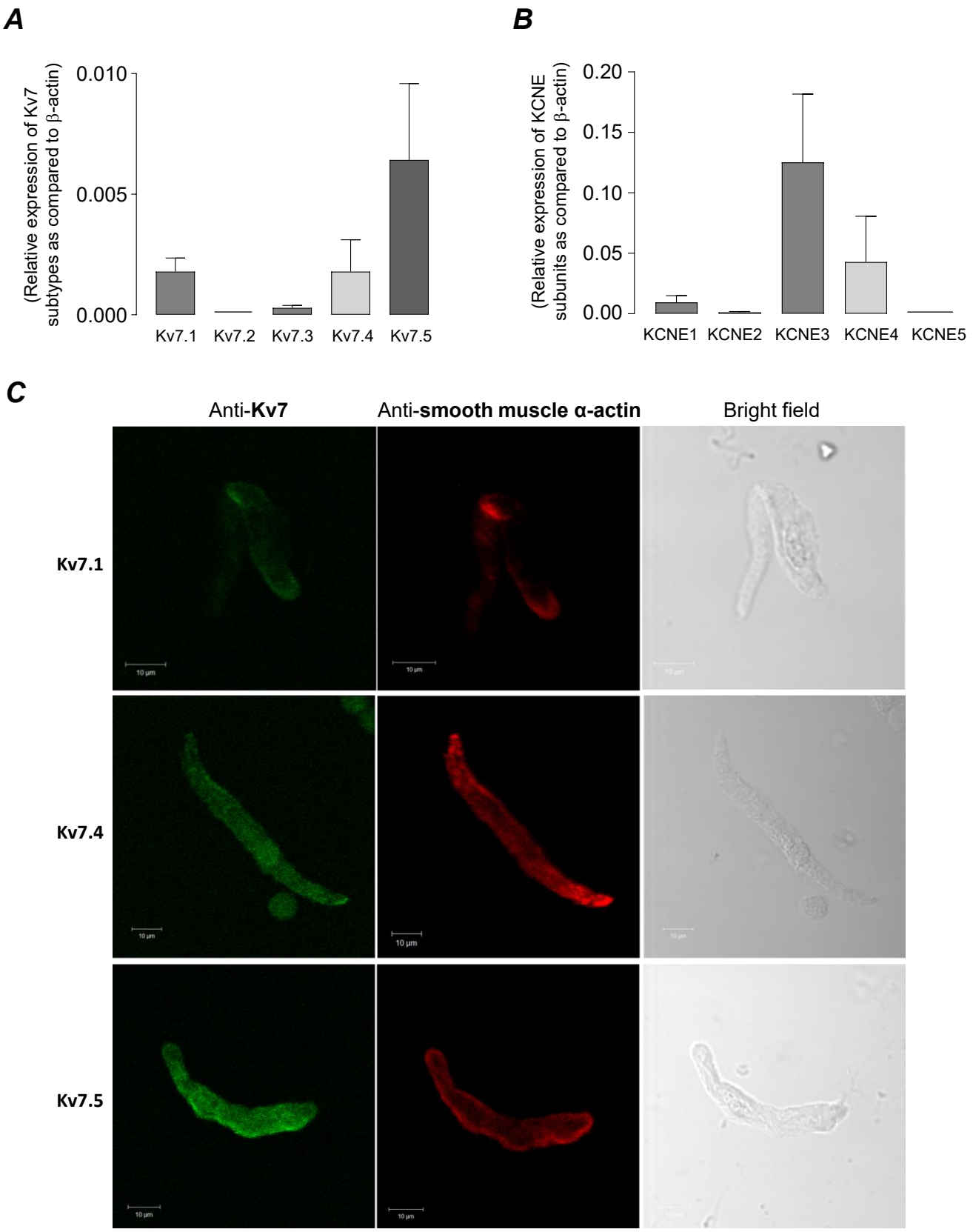

Figure 4.5. Expression analysis of Kv7 subtypes and KCNE subunits in mice bronchi tissue and ASM cells. (A) Summary bar chart showing relative expression of kv7 subtypes from murine bronchial tissues using real-time quantitative PCR, relative to β-actin (n=5, N=15). **(B)** Results from quantitative PCR experiments showing expression of KCNE subunits in murine bronchial tissues, relative to β-actin (n=4, N=12). **C)** Immunocytochemistry experiments showing immunofluorescence of freshly isolated airway smooth muscle cells stained with antibodies against Kv7.1, Kv7.4 and Kv7.5.

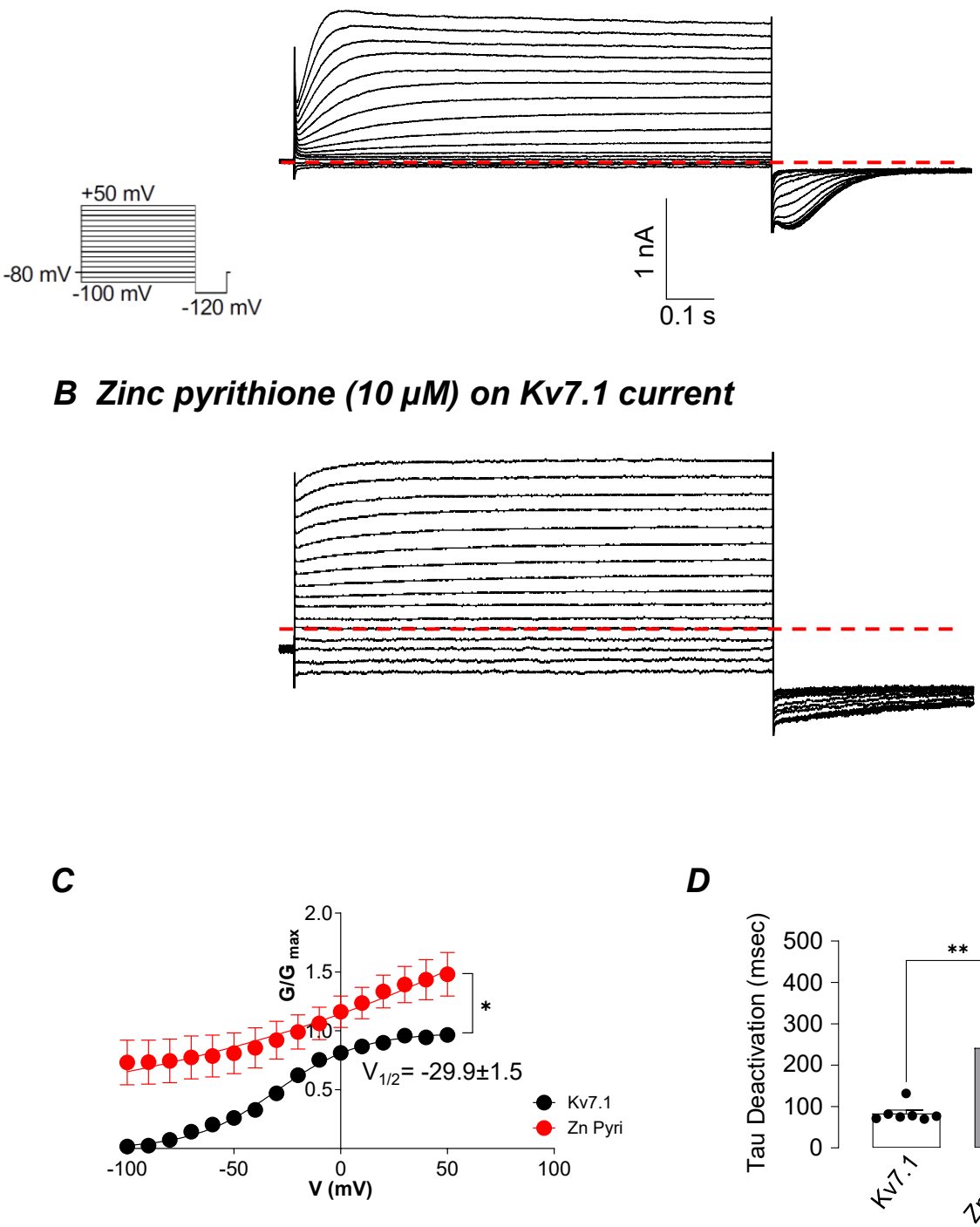

Figure 4.6. Effects of Kv7 channel activator, zinc pyrithione on Kv7.1 currents.
(A) Typical families of currents obtained from wildtype Kv7.1 channels expressed in HEK293 cells. Voltage clamp protocol is illustrated in the inset. Dotted lines represent the zero current levels. (**B)** Effect of zinc pyrithione (10 μM) on currents from the same cell. **(C)** Summary activation curves obtained by measuring tail currents in seven cells before (black circles) and during (red circles) application of zinc pyrithione (n=7). The curves were fit with the Boltzmann equation. **(D)** Summary graph showing the increase in the deactivation time constant (τ) following zinc pyrithione treatment (**p<0.01, n=7, paired t-test).

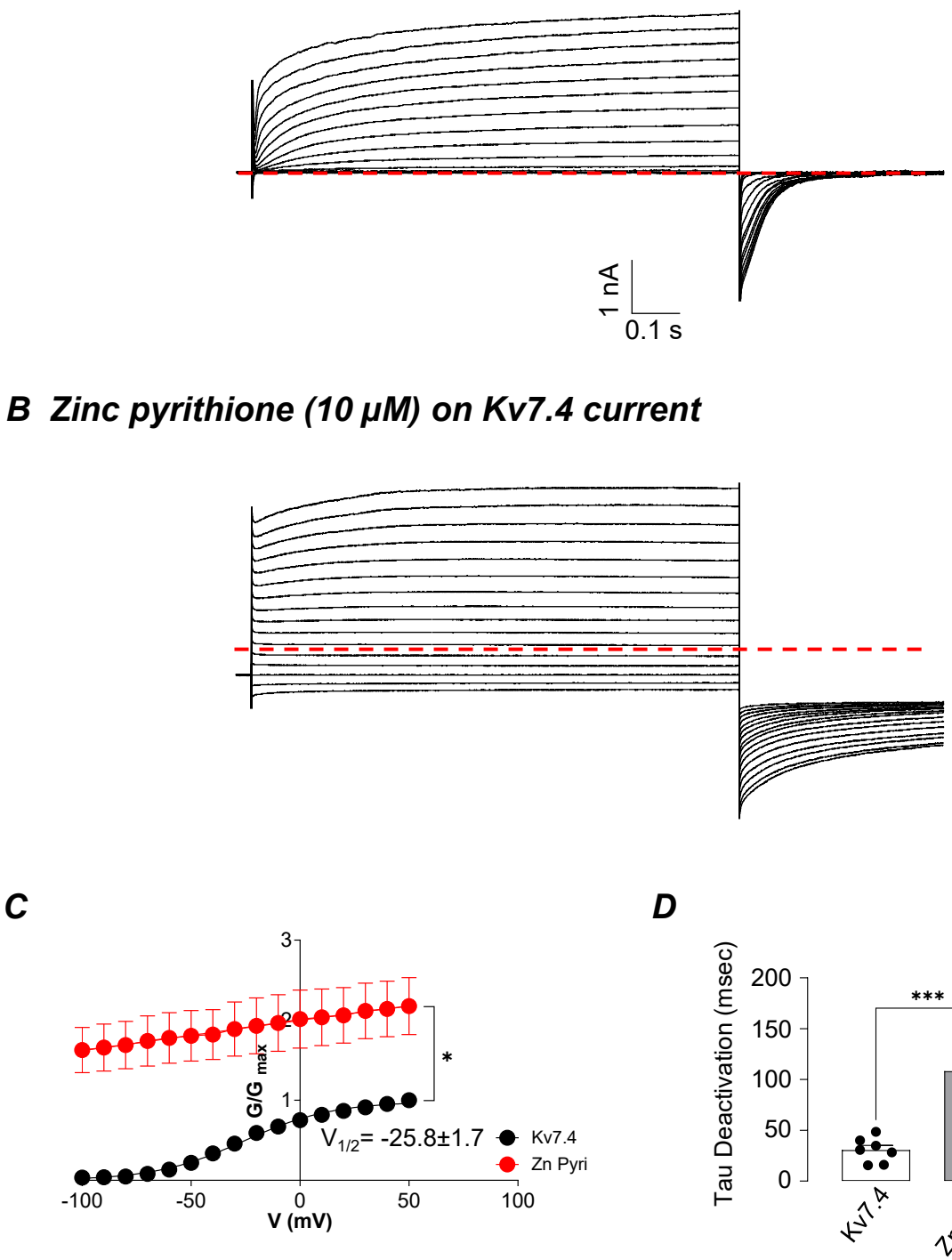

Figure 4.7. Effects of zinc pyrithione on Kv7.4 currents.
(A) Typical families of currents obtained from wildtype Kv7.4 channels expressed in HEK293 cells. Dotted lines represent the zero current levels. (**B)** Effect of zinc pyrithione (10 µM) on currents from the same cell. **(C)** Summary activation curves obtained by measuring tail currents in seven cells before (black circles) and during (red circles) application of zinc pyrithione (n=7). The curves were fit with the Boltzmann equation. **(D)** Summary graph showing the increase in the deactivation time constant (τ) following zinc pyrithione treatment (***p<0.001, n=7, paired t-test).

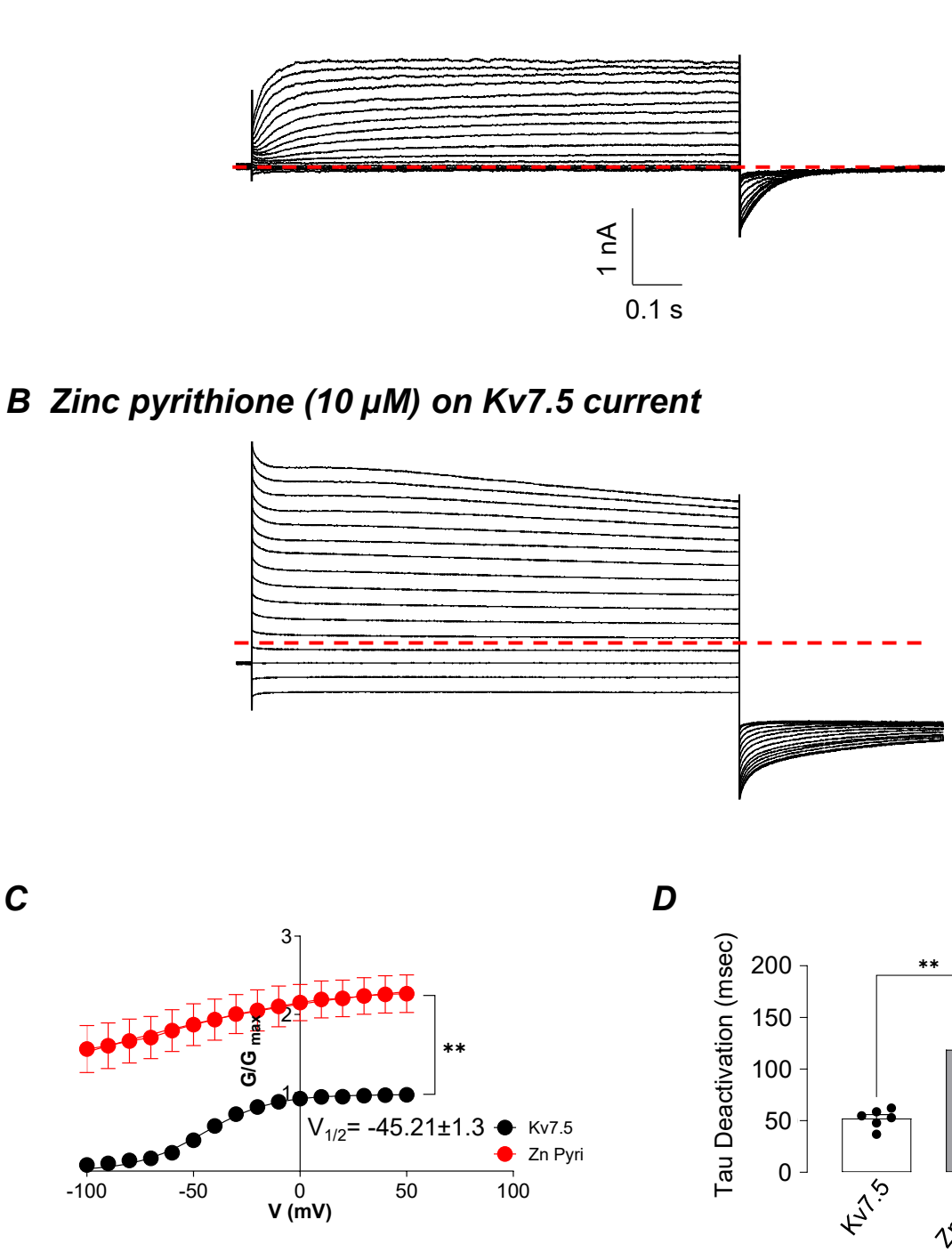

Figure 4.8. Effects of zinc pyrithione on Kv7.5 currents.
(A) Typical families of currents obtained from wildtype Kv7.5 channels expressed in HEK293 cells. Dotted lines represent the zero current levels. (**B)** Effect of zinc pyrithione (10 µM) on currents from the same cell. **(C)** Summary activation curves obtained by measuring tail currents in six cells before (black circles) and during (red circles) application of zinc pyrithione (n=6). The curves were fit with the Boltzmann equation. **(D)** Summary graph showing the increase in the deactivation time constant (τ) following zinc pyrithione treatment (**p<0.01, n=6, paired t-test).

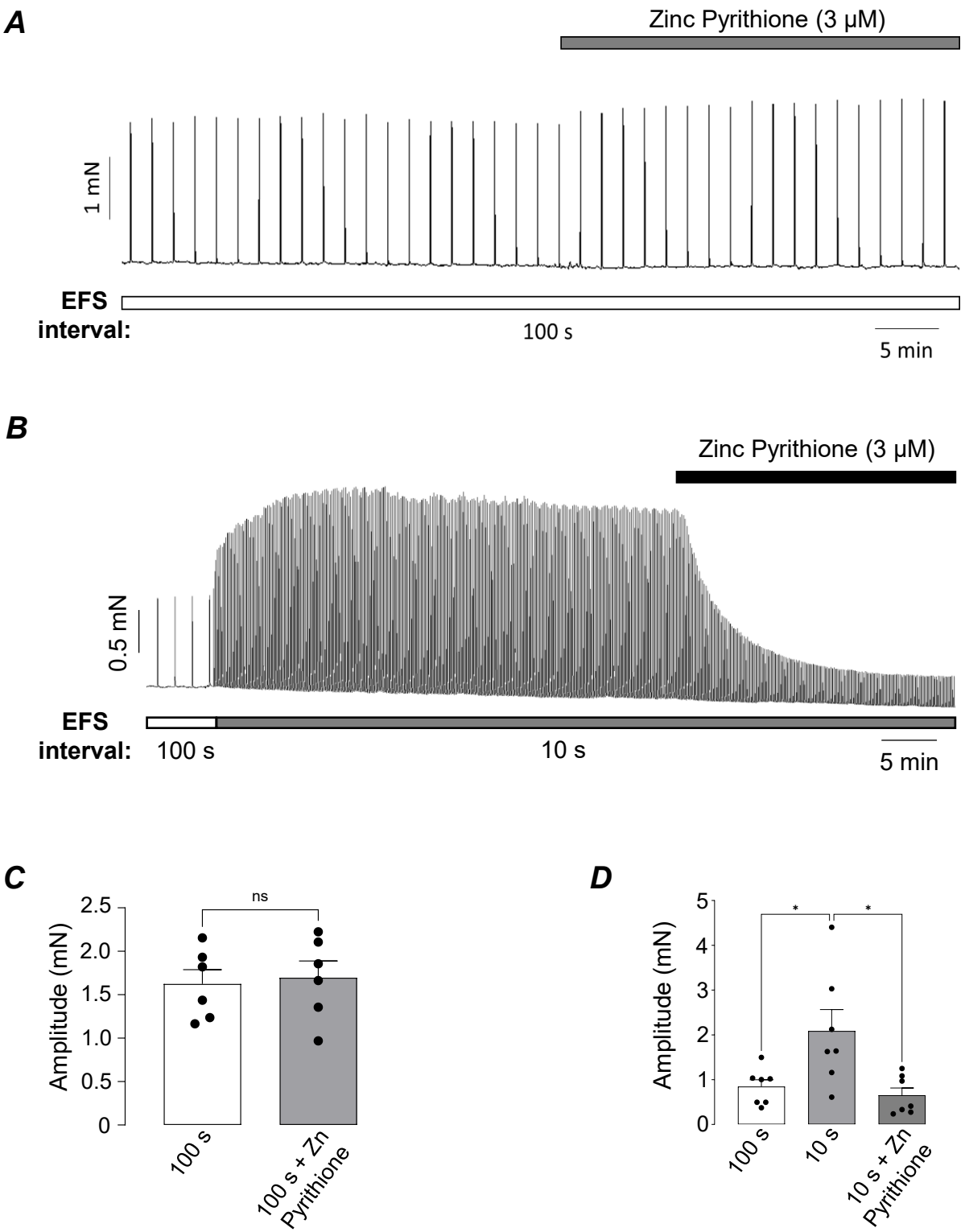

Figure 4.9. Effect of zinc pyrithione on EFS-evoked contractions of ASM.
(A) Representative isometric tension recording showing the effects of zinc pyrithione (3 μM) on EFS-evoked contractions at 100 s intervals. **(B)** Representative trace showing that zinc pyrithione reversed the M2R-mediated increase in contraction amplitude on EFS contractions induced by reducing the stimulus interval from 100 s to 10 s. **(C)** Summary bar chart showing the effect of zinc pyrithione on EFS 100 s contractions (ns, non-significant, n=6, N=4, paired t-test). **(D)** Summary bar chart showing the effect of zinc pyrithione on mean contraction amplitude evoked by EFS at 10 s intervals (*p<0.05, n=7, N=4, one-way ANOVA).

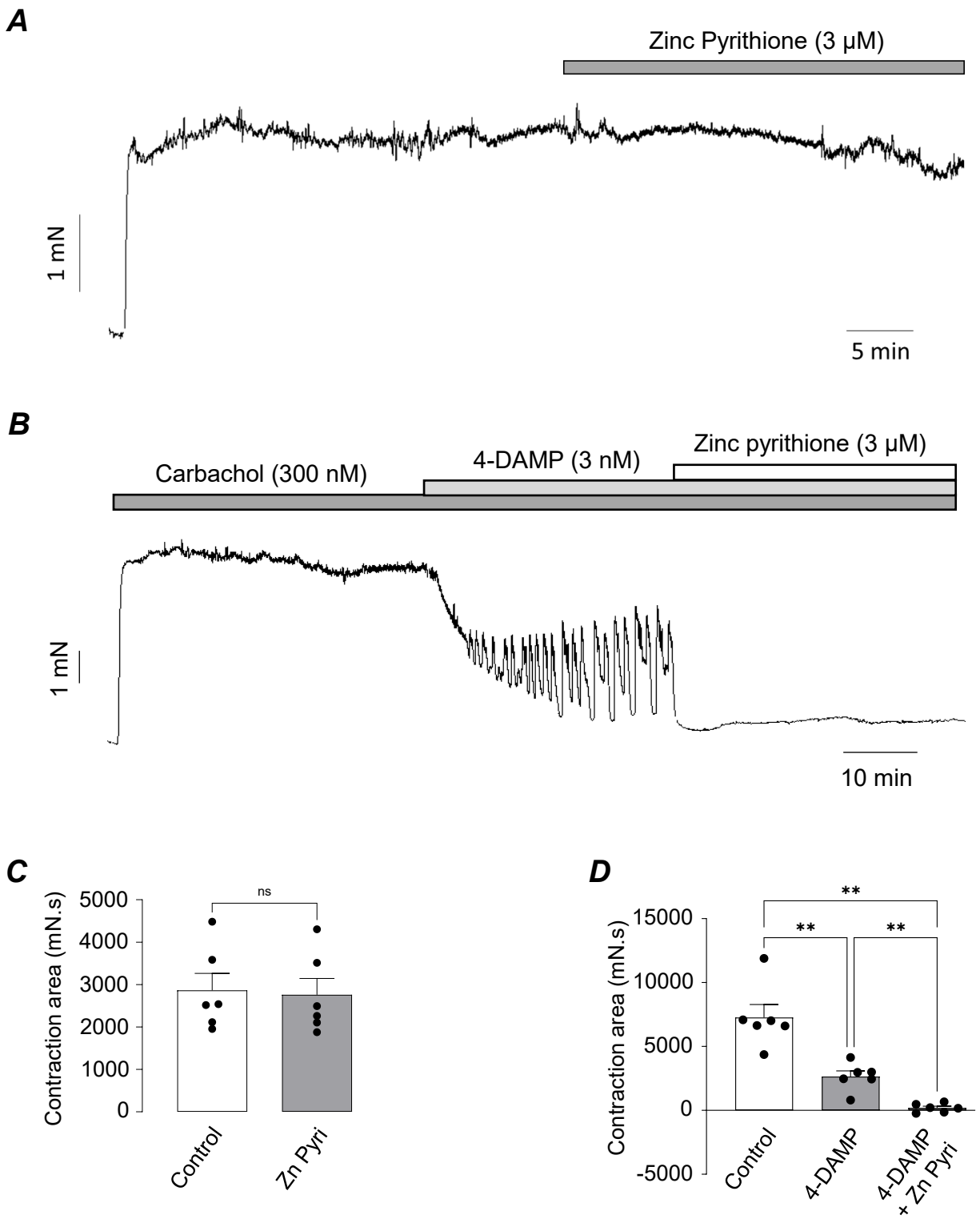

Figure 4.10. Effect of zinc pyrithione on carbachol induced contractions of ASM. **(A)** and **(B)** Representative traces showing the effect of zinc pyrithione (3 μM) on contractions of ASM induced by CCh in the absence and presence of 4-DAMP, respectively **(C)** Summary bar chart showing that zinc pyrithione had no significant effect on CCh-mediated contractions (ns, non-significant, n=6, N=6, paired t-test). **(D)** Summary bar chart showing mean contraction area evoked by CCh in the presence of 4-DAMP and 4-DAMP plus zinc pyrithione (**p<0.01, n=6, N=5, one-way ANOVA).

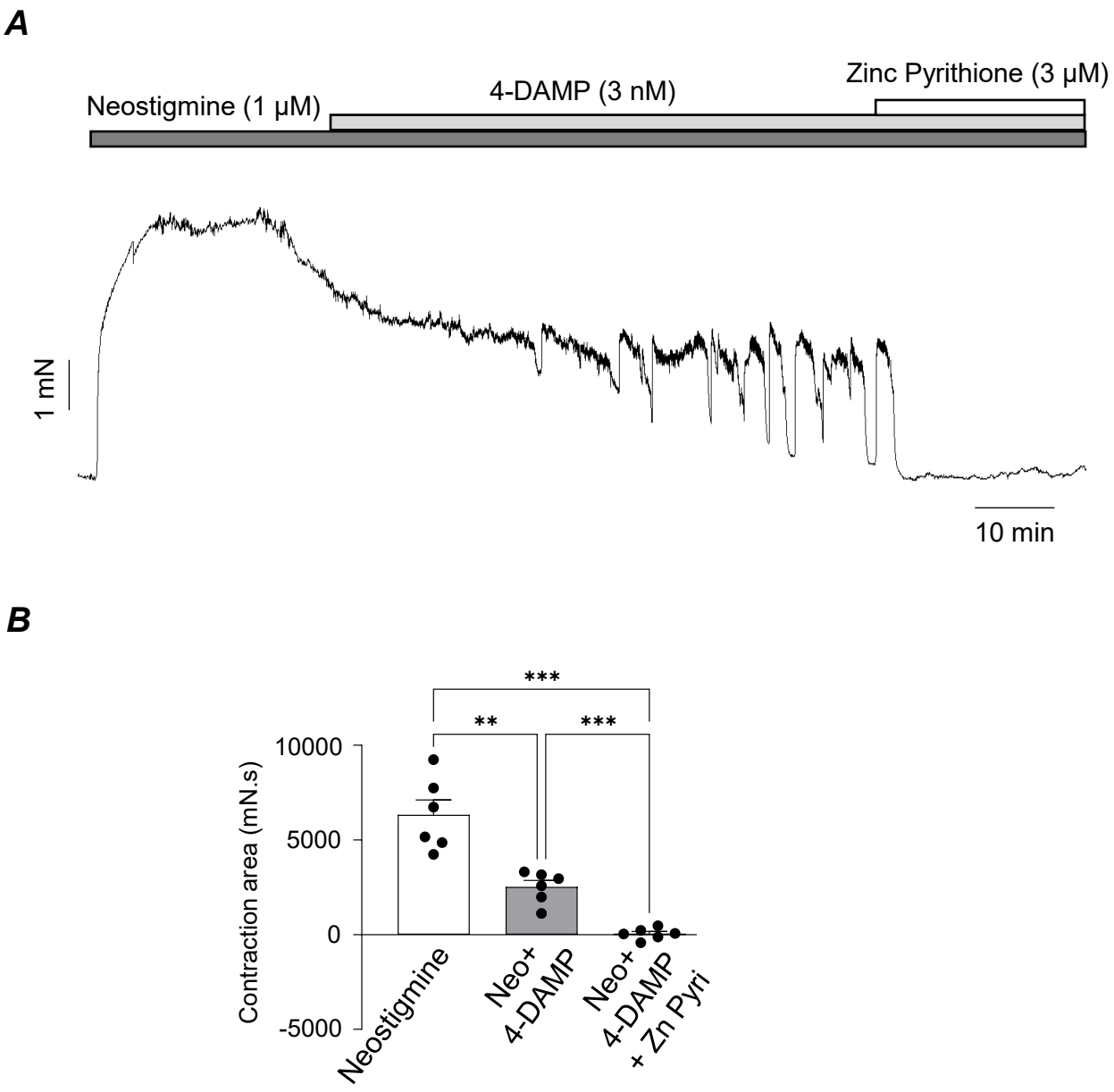

Figure 4.11. Effect of zinc pyrithione on neostigmine-evoked contractions of ASM. **(A)** Representative isometric tension recording showing the effects of zinc pyrithione (3 μM) on contractions of ASM evoked by neostigmine in the presence of 4-DAMP. **(B)** Summary bar chart showing that zinc pyrithione (3 μM) significantly reduced the mean contraction area of neostigmine-evoked contractions that remained in the presence of 4-DAMP (**p<0.01, ***p<0.001, n=6, N=4, one-way ANOVA).

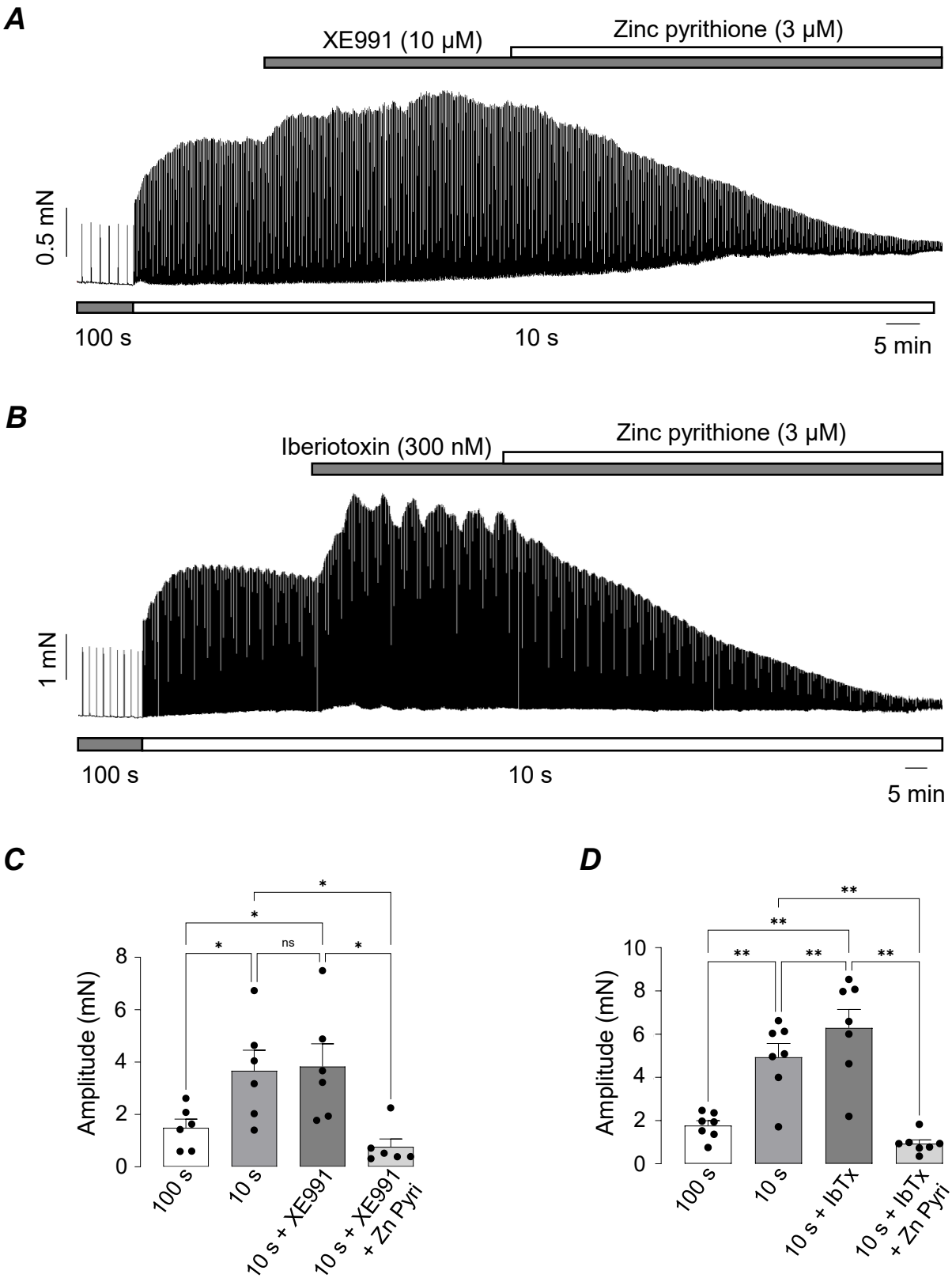

Figure 4.12. Effect of zinc pyrithione on EFS-evoked contractions of ASM in the presence of XE991 and iberiotoxin. (A) Representative isometric tension trace showing that zinc pyrithione (3 μM) reduced contraction amplitude even in the presence of the Kv7 channel blocker, XE991 (10 μM) during EFS-evoked contractions at 10 s intervals. **(B)** Representative isometric tension trace showing that zinc pyrithione (3 μM) reduced contraction amplitude even in the presence of BK_{Ca} channel blocker, iberiotoxin (300 nM) during EFS-evoked contractions at 10 s intervals. **(C)** Summary bar graph showing the effect of XE991 and zinc pyrithione on EFS-evoked contractions at 10 s intervals (ns, non-significant, *p<0.05; n=6, N=5, one-way ANOVA). **(D)** Summary bar graph showing the effect of iberiotoxin and zinc pyrithione on EFS-evoked contractions at 10 s intervals (**p<0.01; n=7, N=6, one-way ANOVA).

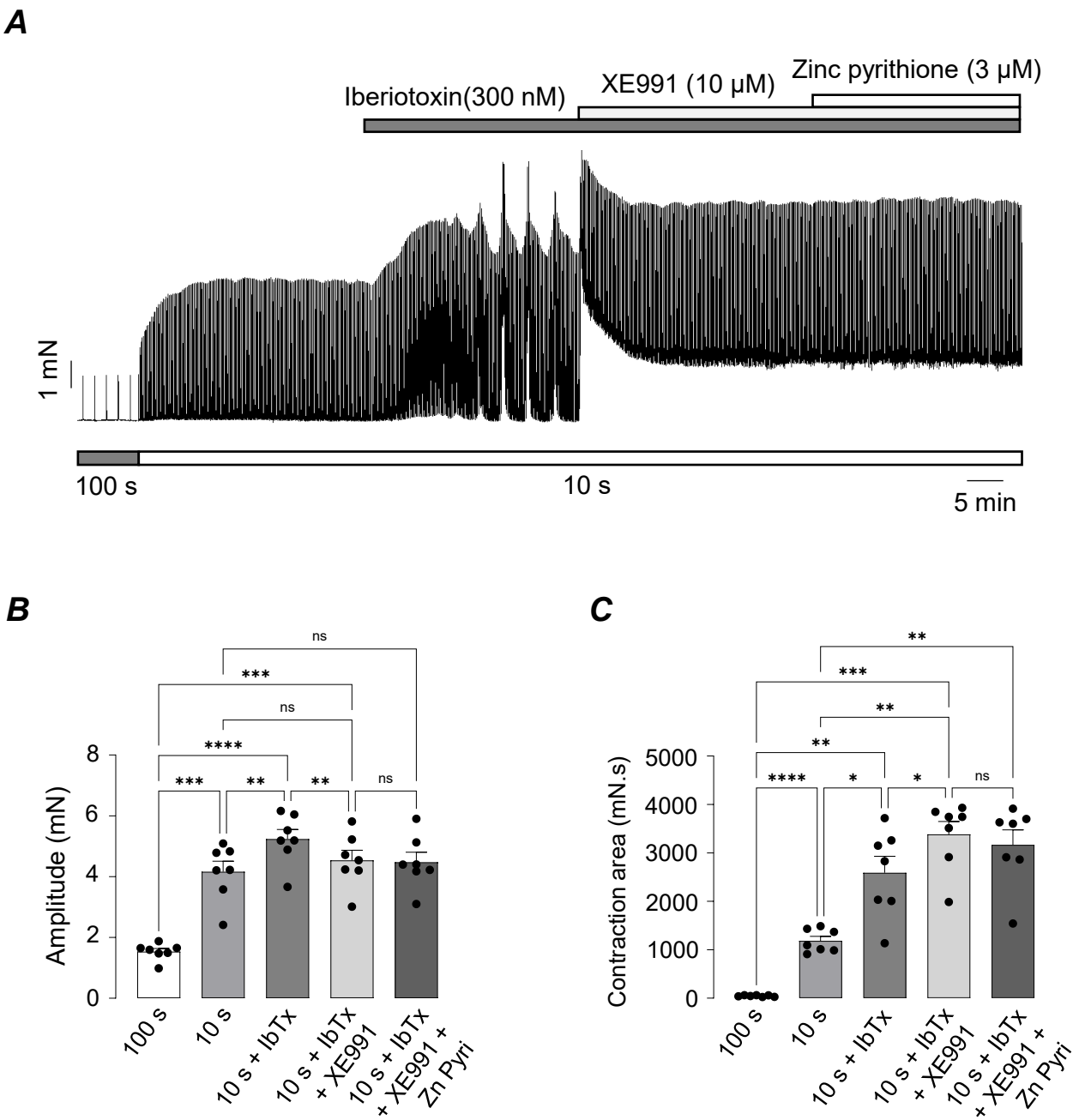

Figure 4.13. Effect of zinc pyrithione on EFS-evoked contractions of ASM evoked at 10 s intervals in the presence of iberiotoxin and XE991. (A) Representative isometric tension trace showing that zinc pyrithione (3 μM) had no significant effect when added in the presence of iberiotoxin (300 nM) and XE991 (10 μM) during EFS-evoked contractions at 10 s intervals. **(B)** Summary bar graph showing the effect of zinc pyrithione on mean contraction amplitude when added in the presence of iberiotoxin and XE991 at EFS 10 s response (ns, non-significant, **p<0.01, ***p<0.001, ****p<0.0001; n=7, N=5, one-way ANOVA). **(C)** Summary bar graph showing the effect of zinc pyrithione on mean contraction area when added to the EFS-mediated contractions at 10 s intervals in the presence of iberiotoxin and XE991 (ns, non-significant, *p<0.05, **p<0.01, ***p<0.001, ****p<0.0001; n=7, N=5, one-way ANOVA).

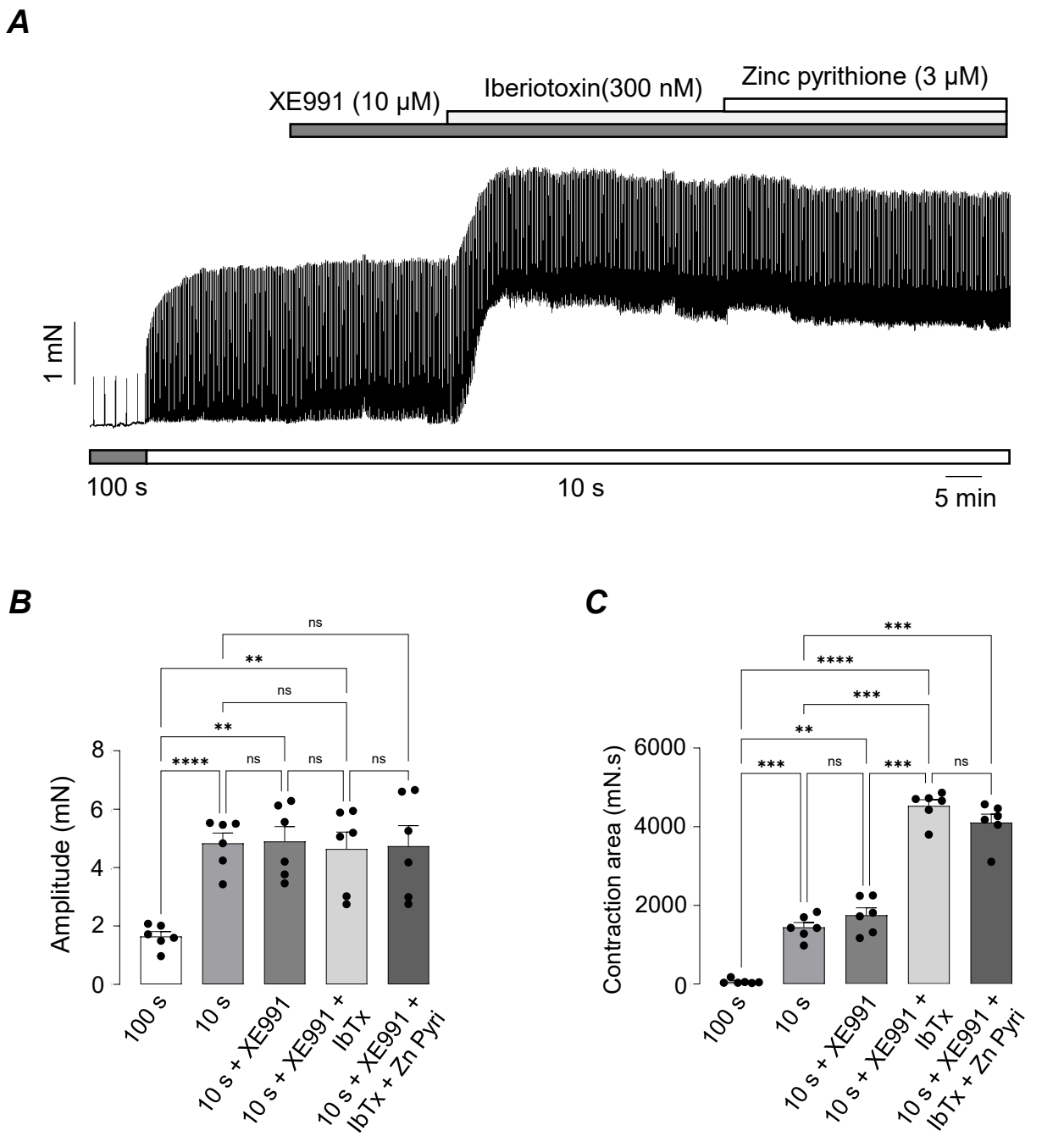

Figure 4.14. Effect of zinc pyrithione on EFS-evoked contractions of ASM evoked at 10 s intervals in the presence of XE991 and iberiotoxin. (A) Representative isometric tension trace showing that zinc pyrithione (3 μM) had no significant effect when added in the presence of XE991 (10 μM) and iberiotoxin (300 nM) during EFS-evoked contractions at 10 s intervals. **(B)** Summary bar graph showing the effect of zinc pyrithione on mean contraction amplitude when added to the EFS-mediated contractions at 10 s intervals in the presence of XE991 and iberiotoxin (ns, non-significant, **p<0.01, ****p<0.0001; n=6, N=4, one-way ANOVA). **(C)** Summary bar graph showing the effect of zinc pyrithione on mean contraction area when added to the EFS-mediated contractions at 10 s intervals in the presence of XE991 and iberiotoxin (ns, non-significant, **p<0.01, ***p<0.001, ****p<0.0001; n=6, N=4, one-way ANOVA).

A M2R and Kv7.1 control

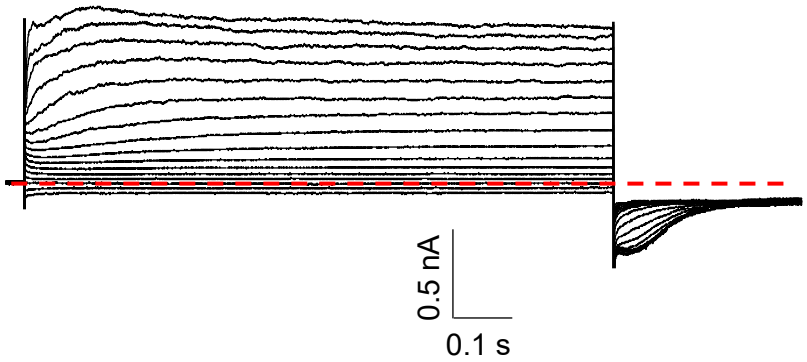

B Carbachol (10 μM) on M2R and Kv7.1 current

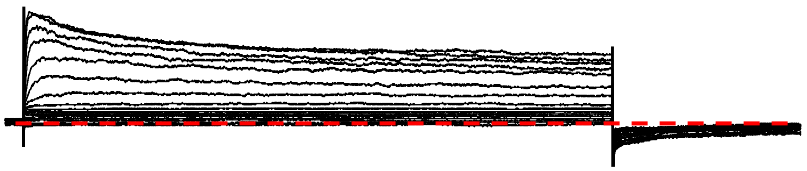

C

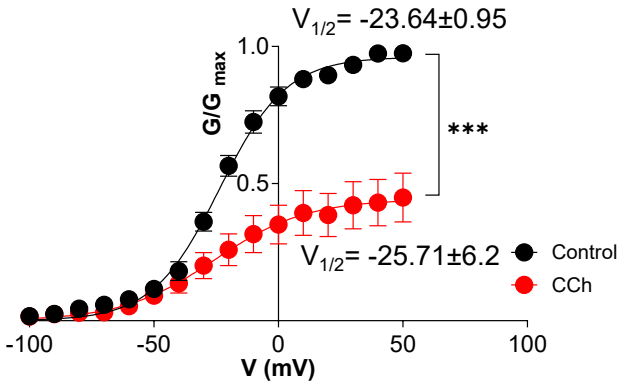

Figure 4.15. Effects of carbachol (10 μM) on M2R and Kv7.1 currents.
(A) Families of currents, recorded from HEK293 cells co-expressing M2R with Kv7.1. Dotted lines represent the zero current levels. (**B)** Families of currents, recorded in the presence of carbachol (10 μM) from the same HEK293 cells co-expressing M2R with Kv7.1 **(C)** Summary activation curves obtained by measuring tail currents before (black circles) and during (red circles) application of carbachol (n=8). The curves were fit with the Boltzmann equation.

A M2R and Kv7.4 control

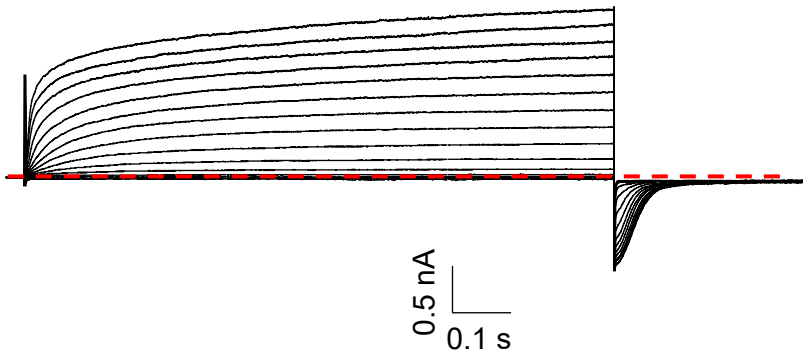

B Carbachol (10 µM) on M2R and Kv7.4 current

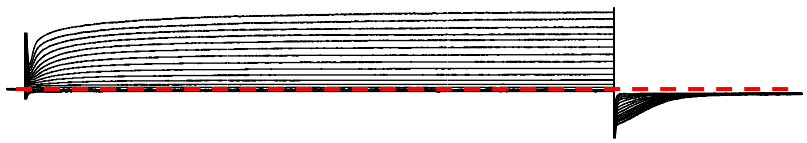

C

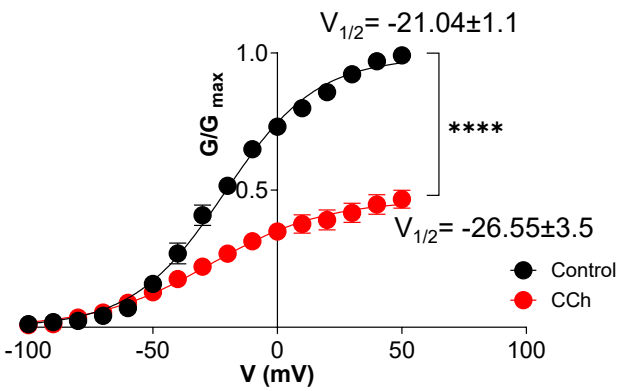

Figure 4.16. Effects of carbachol (10 µM) on M2R and Kv7.4 currents.
(A) Families of currents, recorded from HEK293 cells co-expressing M2R with Kv7.4. Dotted lines represent the zero current levels. (**B)** Families of currents, recorded in the presence of carbachol (10 µM) from the same HEK293 cells co-expressing M2R with Kv7.4 **(C)** Summary activation curves obtained by measuring tail currents before (black circles) and during (red circles) application of carbachol (n=8). The curves were fit with the Boltzmann equation.

A M2R and Kv7.5 control

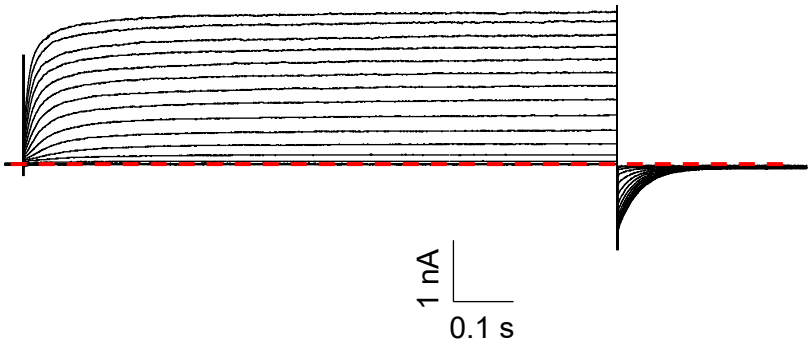

B Carbachol (10 µM) on M2R and Kv7.5 current

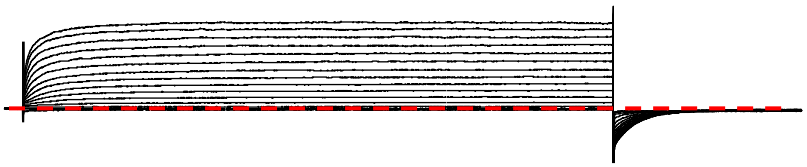

C

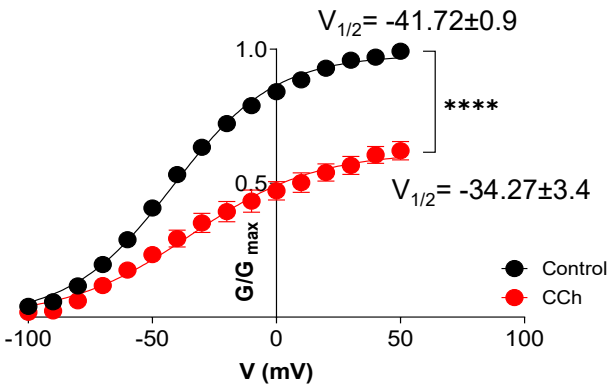

Figure 4.17. Effects of carbachol (10 µM) on M2R and Kv7.5 currents.
(A) Families of currents, recorded from HEK293 cells co-expressing M2R with Kv7.5. Dotted lines represent the zero current levels. (**B)** Families of currents, recorded in the presence of carbachol (10 µM) from the same HEK293 cells co-expressing M2R with Kv7.5 **(C)** Summary activation curves obtained by measuring tail currents before (black circles) and during (red circles) application of carbachol (n=8). The curves were fit with the Boltzmann equation.

Chapter 5

Contribution of Kv7 subtypes to M2R-mediated contractions of ASM

5.1. Introduction

The data presented in chapter 4 indicated that M2R-mediated contractions of ASM may involve inhibition of Kv7 channels, leading to enhanced Ca^{2+} influx via LTCC. However, the contribution of individual Kv7 subtypes to these responses was not established, nor were the intracellular signalling mechanisms which could link activation of M2Rs to inhibition of Kv7 channels. Kv7 channels account for the neuronal M-current, so named because it is inhibited by activation of muscarinic receptors (Brown & Adams, 1980 and Constanti & Brown, 1981). Suppression of Kv7 currents in neurones by M1R or M3R activation is primarily driven by depletion of membrane PIP_2, following activation of PLC by $G_{q/11}$ α subunits [480-482]. PIP_2 is an essential cofactor for Kv7 channel opening and its depletion leads to Kv7 current inhibition and increased neuronal excitability. Kv7 channels are also directly modulated by G-protein βγ subunits and PKC-dependent phosphorylation events [468, 483]. Unlike M1R or M3Rs, M2Rs primarily couple to $G_{i/o}$ proteins, which inhibit adenylyl cyclase and reduce intracellular cAMP and PKA activity [484, 485]. Activation of M2Rs, therefore, has the potential to alter Kv7 channel gating by shifting the phosphorylation balance or by promoting PIP_2 hydrolysis through βγ subunit-mediated PLC activation [486, 487]. However, whether such mechanisms operate in ASM following M2R activation has not been elucidated.

Given that M2R-mediated enhancement of cholinergic contractions of ASM depends on LTCC activation, and that Kv7 inhibition promotes depolarisation and Ca^{2+} influx, it is plausible that M2R activation suppresses Kv7 activity. The purpose of this chapter was to: 1) investigate the contribution of different Kv7 subtypes expressed in ASM (Kv7.1, Kv7.4 & Kv7.5) to M2R-dependent contractions, and 2) elucidate the cellular mechanisms underlying M2R-mediated inhibition of Kv7 channels in ASM. To achieve this, a combination of pharmacological approaches was employed to examine the contribution of G-protein subunits, PKA inhibition and PIP_2 depletion in the regulation of Kv7 activity following M2R stimulation. Understanding this mechanistic link will provide new insights into muscarinic receptor regulation of ASM excitability and may identify potential therapeutic targets for AHR in obstructive lung diseases.

5.2. Results

5.2.1. Contribution of Kv7.1 channels in M2R-mediated contractions of ASM

Data in Chapter 4 reported that Kv7.1, Kv7.4 and Kv7.5 were expressed in ASM and that activation of M2Rs inhibited Kv7.1, Kv7.4 and Kv7.5 currents when co-expressed with each of these subtypes in HEK293 cells. We targeted these three Kv7 subtypes to examine their involvement in M2R-mediated contractions of ASM. Experiments were first performed to examine the involvement of Kv7.1 channels in M2R-mediated ASM contractions. The selective Kv7.1 channel blocker, chromanol 293B (30 μM), was applied during EFS-induced contractions delivered at 100 s intervals. In contrast to the effects of the non-selective Kv7 blocker XE991 (Figure 4.2), application of chromanol 293B did not enhance the amplitude of ASM contractions evoked by EFS at 100 s intervals (Figure 5.1A and B). Mean contraction amplitude induced by EFS at 100s intervals was 1.8 ± 0.2 mN, compared to 1.9 ± 0.3 mN in chromanol 293B (ns, n = 6). To further test the role of Kv7.1 channels, we examined the effect of the Kv7.1 activator ML277 (10 μM) on ASM during EFS stimulation at 10 s intervals, to induce M2R-dependent potentiation of the responses. Figure 5.2A shows that addition of ML277 failed to reduce contraction amplitude. Mean contraction amplitude was 3.97 ± 0.3 mN under control conditions (at EFS 10 s intervals), compared to 3.9 ± 0.3 mN in the presence of ML277 (ns, n = 6; Figure 5.2C). M2R-dependent contractions of ASM evoked by carbachol, in the presence of the M3R antagonist 4-DAMP, were also unaffected by ML277 (Figure 5.2B and D). These findings indicate that blocking Kv7.1 channels did not enhance contractions of ASM and that activation of Kv7.1 channels did not reduce the amplitude of M2R-dependent contractions of ASM, suggesting that Kv7.1 channels were unlikely to have a major role in M2R-mediated contractions of ASM.

5.2.2. Effect of the Kv7.4 channel activator, ICA069673 on M2R-mediated ASM contractions

Brueggemann et al. (2014) reported that ICA069673 robustly activated Kv7.4 channels but was significantly less effective on homomeric Kv7.5 channels [471]. We investigated the effects of ICA069673 on Kv7.4 and Kv7.5 currents recorded from HEK293 cells. Currents were evoked using the voltage protocol illustrated in the inset of Figure 5.3. Application of ICA069673 (30 μM) markedly enhanced Kv7.4 current amplitude, produced a negative shift in the voltage-dependence of

activation, and slowed current deactivation. Representative families of currents, recorded under control conditions and during ICA069673 application, are shown in Figures 5.3A and B, respectively. The corresponding activation curves (Figure 5.3C) demonstrate that ICA069673 shifted the $V_{1/2}$ of activation from -33.8 ± 1.5 mV to -79.3 ± 3.7 mV ($p<0.01$, n=7). Furthermore, the mean tau of deactivation of Kv7.4 tail currents recorded at -120 mV increased from 18.3 ± 2.6 msec (control) to 91.7 ± 9.1 msec in the presence of ICA069673 ($p<0.001$, n=7; Figure 5.3D). In contrast, ICA069673 had minimal effects on Kv7.5 currents (Figure 5.4A and B). The summary activation curves in Figure 5.4C show only a slight shift in the $V_{1/2}$ of activation from -45.4 ± 0.9 mV to -47.1 ± 4.3 mV (ns, n=6). Similarly, the mean tau of deactivation showed no notable alteration, changing from 59.7 ± 13.1 msec under control conditions to 63.7 ± 11.4 msec in the presence of ICA069673 (ns, n=6; Figure 5.4D). These results confirm that ICA069673 enhanced Kv7.4 channel activity with little effect on Kv7.5, indicating that it is a useful pharmacological probe to examine the contribution of Kv7.4 channels to M2R-mediated ASM contraction. The experiments summarised in Figure 5.5 demonstrate that ICA069673 could also reverse the inhibitory effects of carbachol on Kv7.4 currents recorded from HEK293 cells co-expressing M2Rs and Kv7.4, as established in Figure 4.16. Summary activation (G/G_{max}) curves showed that CCh reduced the G_{max} of Kv7.4 currents at +50 mV from 1.0 ± 0 to 0.61 ± 0.07 ($p<0.01$, n=7) and subsequent addition of ICA069673 increased the G_{max} to 0.9 ± 0.07 ($p>0.05$, n=7; Figure 5.5B).

Next, we examined the effects of ICA069673 on M2R-dependent potentiation of EFS-evoked contractions of ASM. Figure 5.6A is a representative trace which shows that ICA069673 (30 μM) partially reversed the stimulatory effects induced by reduction in stimulus interval from 100 to 10 s. The summary data in Figure 5.6C indicate that reducing the stimulus interval to 10 s increased the mean contraction amplitude from 1.4 ± 0.1 to 3.8 ± 0.2 mN ($p<0.0001$, n=7) and that subsequent addition of ICA069673 reduced mean contraction amplitude to 2.3 ± 0.2 mN ($p<0.001$, n=7). The effect of ICA069673 on M2R-dependent contractions of ASM was further investigated by examining their effects on 4-DAMP-resistant contractions induced by CCh. The data shown in Figure 5.6B demonstrate that the phasic contractions which remained in the presence of 4-DAMP (3 nM) were abolished by ICA069673. The mean contraction area was reduced from 2703 ±

248.8 to 262.5 ± 84.3 mN.s ($p<0.001$, n=6) in the presence of ICA069673 (Figure 5.6D). These data suggest that opening of Kv7.4 channels can inhibit M2R-dependent contractions of ASM.

5.2.3. *Effect of the Kv7.4 and Kv7.5 channel activator, ML213 on M2R-mediated ASM contractions*

In addition to ICA069673, Brueggemann *et al.* (2014) reported that another Kv7 channel activator, ML213 markedly increased the maximum conductance of both Kv7.4 and Kv7.5 channels. We examined the effects of ML213 on Kv7.4 and Kv7.5 currents recorded from transfected HEK293 cells using whole-cell patch-clamp recordings. As shown in Figures 5.7A and B, ML213 (5 μM) enhanced Kv7.4 current amplitude, produced a negative shift in voltage-dependence of activation, and prolonged current deactivation. Summary activation curves (Figure 5.7C) indicate that ML213 increased the mean G_{max} of Kv7.4 currents from 1.0 to 1.6 ± 0.08 ($p<0.001$, n=6) and shifted the $V_{1/2}$ to more negative potentials. The mean tau of deactivation measured from tail currents increased from 17.15 ± 1.4 msec (in control) to 43.0 ± 4.6 msec in the presence of ML213 ($p<0.01$, n=6; Figure 5.7D). ML213 produced even greater effects on Kv7.5 currents (Figure 5.8A and B). The activation curves in Figure 5.8C demonstrate that ML213 shifted the $V_{1/2}$ of activation from -46.6 ± 2.3 mV to -84.5 ± 7.3 mV ($p<0.05$, n=6) and increased G_{max} from 0.98 ± 0.01 to 2.6 ± 0.3 ($p<0.01$, n=6). The mean tau of deactivation at -120 mV increased from 46.2 ± 3.3 msec to 100 ± 9.8 msec ($p<0.001$, n=6; Figure 5.8D).

The experiments summarised in Figures 5.9 and 5.10 demonstrate that ML213 also reversed the inhibitory effects of M2R activation (via CCh) on Kv7.4 and Kv7.5 currents, respectively. In Kv7.4 and M2R-expressing cells, addition of CCh (10 μM) reduced G_{max} from 1.0 to 0.61 ± 0.04 ($p<0.001$, n=6), while subsequent addition of 5 μM ML213 restored G_{max} to 1.04 ± 0.1 ($p<0.01$, n=6; Figure 5.9B). A similar trend was observed in M2R and Kv7.5 co-expressing cells (Figure 5.10B), where CCh reduced G_{max} from 0.96 ± 0.02 to 0.49 ± 0.09 ($p<0.01$, n=6), and ML213 subsequently increased it to 1.9 ± 0.2 ($p<0.01$, n=6). These findings demonstrate that ML213 reversed the M2R-mediated inhibition of Kv7.4 and Kv7.5 channels.

We next examined whether ML213 could attenuate M2R-dependent potentiation of EFS-evoked ASM contractions. Representative traces (Figures 5.11A and C) show that 5 μM ML213 abolished the M2R-mediated enhancement in contraction amplitude, reducing the mean contraction amplitude from 3.3 ± 0.3 mN to 0.98 ± 0.2 mN ($p<0.01$, n=6). ML213 also decreased mean contraction area evoked by CCh, in the presence of 4-DAMP, from 3050 ± 37 to 225.1 ± 121.2 mN.s ($p<0.001$, n=7; Figure 5.11B and D).

The experiments above show that ML213 had greater effects than ICA069673, indicating that activation of both Kv7.4 and Kv7.5 channels had greater effects than activation of Kv7.4 alone. This was examined further by examining if ML213 induced additional inhibitory effects when applied to tissues already pretreated with ICA069673. Figure 5.12A shows that the addition of ML213, in the presence of ICA069673, further suppressed EFS-evoked contractions of ASM. Summary data (Figure 5.12B) show that ICA069673 reduced mean contraction amplitude from 3.8 ± 0.2 mN to 2.3 ± 0.2 mN ($p<0.01$, n=7) and that subsequent ML213 application further decreased it to 1.05 ± 0.05 mN ($p<0.0001$, n=7). These results indicate that pharmacological activation of Kv7.4 and Kv7.5 channels reversed M2R-dependent inhibition of Kv7.4 and Kv7.5 currents in HEK293 cells and inhibited M2R-dependent contractions of ASM. Kv7.4 and Kv7.5 are known to co-assemble to form heterotetramers, therefore we examined whether activation of M2Rs was able to reduce the amplitude of currents recorded from HEK293 cells co-expressing M2Rs with both Kv7.4 and Kv7.5. Data shown in Figure 5.13 shows that CCh reduced the mean G_{max} of Kv7.4/7.5 currents by 41.5% ($p<0.001$, n=7).

Control experiments were performed to confirm that the inhibitory effects of CCh on Kv7.4 and Kv7.5 currents were mediated by activation of M2Rs (Figures 5.14 and 5.15). When CCh was applied to HEK293 cells expressing Kv7.4, without M2Rs, it did not reduce the amplitude or affect the voltage-dependence of activation of the Kv7.4 currents (Figures 5.14A and B). The summary activation curves (Figure 5.14C) show that the mean G_{max} shifted from 1.0 to 0.96 ± 0.03 (ns, n=7) in the presence of CCh. CCh was similarly ineffective on HEK293 cells only expressing Kv7.5 (Figures 5.15A-C). These findings confirm that CCh does not directly modulate Kv7.4 or Kv7.5 channels and that the inhibitory effects observed previously in co-expressing cells were specifically mediated via M2R activation.

5.2.4. Role of the adenylate cyclase-cyclic AMP pathway in M2R-mediated inhibition of Kv7 channels

M2Rs couple to G_i α subunits which inhibit adenylate cyclase and suppress cAMP/PKA signalling pathways [158]. Mani et al. (2016) reported that activation of the cAMP/PKA signalling pathway enhanced Kv7.5, but not Kv7.4 currents [465] and Brueggemann et al. (2018) demonstrated that Kv7.5 currents recorded from cultured human ASM cells were augmented by activation of the cAMP/PKA pathway [299]. Therefore, we investigated the effects of the PKA activator 6MB-cAMP (300 μM) on Kv7.4 and Kv7.5 currents recorded from HEK293 cells. As shown in Figure 5.16A and B, Kv7.4 currents were not enhanced by 6MB-cAMP. In 6 cells, the G_{max} of Kv7.4 currents recorded at +50 mV was reduced by 6MB-cAMP, from 0.99 ± 0.001 to 0.7 ± 0.06 ($p<0.0.01$, n=6, Figure 5.15C). In contrast, 6MB-cAMP enhanced the amplitude of Kv7.5 currents across the voltage range and negatively shifted the $V_{1/2}$ of activation from -42.8 ± 1.5 to -54.7 ± 4.4 mV ($p<0.001$, n=6, Figures 5.17). The summary activation curves illustrated in Figure 5.17C show that the G_{max} increased from 0.98 ± 0.02 in control to 1.35 ± 0.1 in the presence of 6MB-cAMP ($p<0.05$, n=6) and the tau of deactivation increased from 56.3 ± 3.7 msec in control to 81.3 ± 10.8 msec in the presence of 6MB-cAMP ($p<0.05$, n=6; Figure 5.17D).

We then investigated if M2R-dependent contractions of ASM were inhibited by activation of PKA. Figure 5.18A shows a representative isometric tension recording demonstrating that 6MB-cAMP (100 μM) reversed the M2R-dependent augmentation of cholinergic nerve-evoked contractions of ASM elicited by a reduction in stimulus interval from 100 to 10 s. Summary data in Figure 5.18C demonstrate that 6MB-cAMP reduced the mean amplitude of EFS-evoked contractions of ASM at 10 s intervals from 4.4 ± 0.3 to 1.7 ± 0.2 mN ($p<0.0001$, n=6). To further examine regulation of M2R responses by the cAMP/PKA pathway, we tested forskolin (1 μM), a direct activator of adenylate cyclase. Figure 5.18B shows that forskolin abolished the M2R-mediated enhancement of contraction amplitude when the EFS interval was reduced to 10 s. The summary data (Figure 5.18D) indicate that forskolin reduced mean contraction amplitude from 4.1 ± 0.4 to 1.6 ± 0.2 mN ($p<0.001$, n=6). Similarly, Alkawadri (2022) also showed that 6MB-cAMP (100 μM) and forskolin (1 μM) abolished the M2R-dependent phasic contractions induced by CCh in the presence of 4-DAMP [488]. These results support the idea

that M2R-mediated suppression of cAMP/PKA signalling could contribute to the inhibition of Kv7.5 channels in ASM.

5.2.5. *Role of PIP_2 depletion in M2R-mediated inhibition of Kv7 channels*

PIP_2 is a membrane phospholipid which couples the voltage-sensing domains (VSDs) and pore domains (PDs) of Kv7 channels to open the channels [306, 489, 490]. Depletion of PIP_2 is known to suppress Kv7 currents [491, 492] and Brueggemann et al. (2020) showed that Kv7.4 channels have a higher resting affinity for PIP_2 than Kv7.5 [493]. Therefore, we hypothesised that the inhibitory effects of M2R activation on Kv7.4 could be related to depletion of PIP_2. To test this idea, we compared the effect of CCh on HEK293 cells co-expressing M2Rs and Kv7.4 channels using patch pipettes that contained the PIP_2 analogue, PIP_2 diC8. Figures 5.19A and B show families of Kv7.4 currents recorded from a cell dialysed with 200 μM PIP_2 diC8, before and in the presence of CCh, respectively. Inclusion of PIP_2 diC8 in the pipette caused a leftward shift in the activation $V_{1/2}$ of Kv7.4 currents and greatly reduced the inhibitory effects of CCh, compared to cells that were not dialysed with PIP_2 diC8. The summary GV curves in Figure 5.19C indicate that, in 6 cells, CCh (10 μM) only reduced the G_{max} at +50 mV by 16%, compared to 53% in cells not dialysed with PIP_2 diC8 (Figure 4.16). The $V_{1/2}$ of activation was -32.1 ± 1.8 mV before addition of CCh compared to -35.3 ± 3.5 mV in its presence ($p>0.05$, n=6). In contrast, the inhibitory effects of CCh on Kv7.5 were unaffected by addition of PIP_2 diC8 in the pipette solution (Figure 5.20). Addition of CCh reduced the mean G_{max} of Kv7.5 currents at +50 mV by 46.5% from 0.92 ± 0.03 mV to 0.43 ± 0.07 mV ($p<0.01$, n=6; Figure 5.20C). These data suggest that the inhibitory effects of CCh on Kv7.4, but not Kv7.5, are related to depletion of PIP_2. Collectively, these findings indicate that PIP_2 depletion contributes to M2R-mediated inhibition of Kv7.4, but not Kv7.5 channels, suggesting that the two subtypes differ in their PIP_2 dependence and regulatory mechanisms during M2R activation.

5.3. Discussion

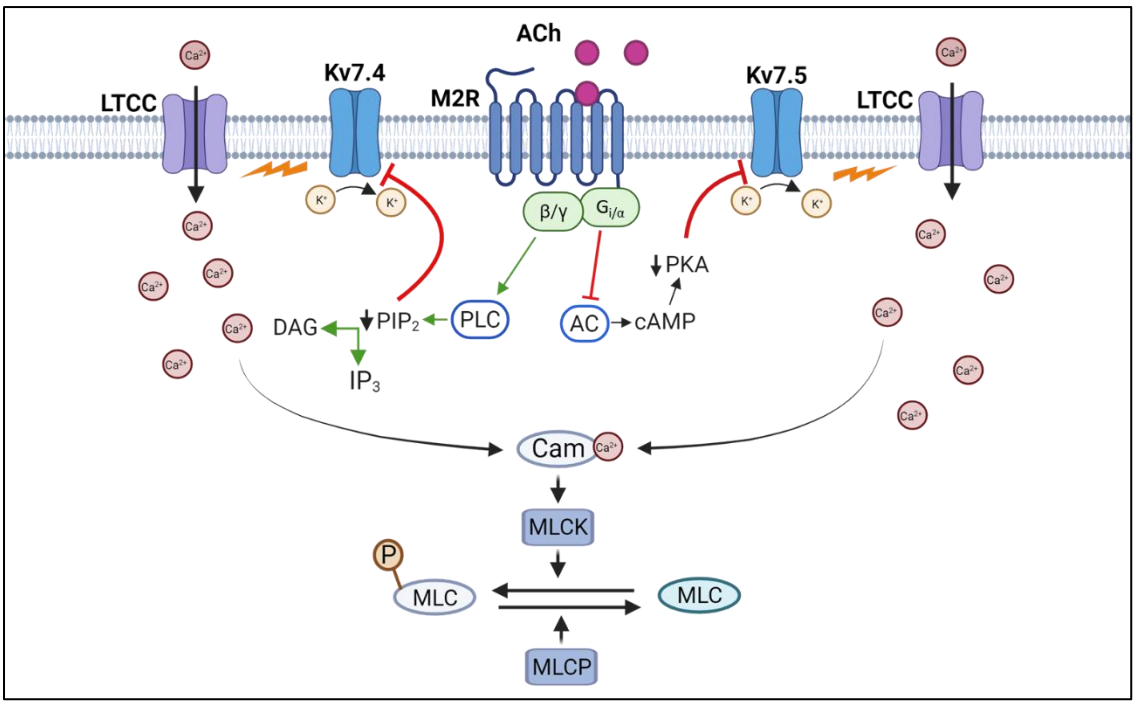

Figure 5.21. Schematic model showing cellular pathways by which activation of M2R leads to contraction of ASM. Binding of ACh to postjunctional M2R induces activation of Giα subunits, which leads to inhibition of Kv7.5 channels via a reduction in PKA levels. Activation of Gβγ subunits leads to inhibition of Kv7.4 channels via stimulation of PLC and depletion of PIP_2. Inhibition of Kv7.4 and Kv7.5 leads to membrane depolarisation and activation of LTCC. Figure created with a licensed version of BioRender.com. ACh, acetylcholine; ASM, airway smooth muscle; Cam, calmodulin; DAG, diacylglycerol; LTCC, L-type Ca2+ channel; MLC, myosin light chain; MLCK, myosin light chain kinase; MLCP, myosin light chain phosphatase; PIP2, phosphatidylinositol 4,5-bisphosphate; PLC, phospholipase C.

The purpose of the experiments performed in Chapter 5 was 1) to investigate the contribution of Kv7.1. Kv7.4 and Kv7.5 channels to M2R-mediated contraction of ASM and 2) to examine the cellular mechanisms responsible for the inhibitory effects of M2R activation on Kv7 currents. We found that activators of Kv7.4 and Kv7.5 channels inhibited M2R-dependent contractions of ASM. In contrast, modulation of Kv7.1 failed to affect ASM contractility. The PKA activator 6MB-cAMP enhanced Kv7.5, but not Kv7.4 currents, and inhibited M2R-dependent contractions of ASM. The inhibitory effects of CCh on Kv7.4 currents were greatly reduced in cells dialysed with PIP_2 diC8, suggesting that M2R-induced inhibition of Kv7.4 currents was related to depletion of PIP_2. In contrast, the inhibitory effects of M2Rs on Kv7.5 were preserved in cells dialysed with PIP_2 diC8. These data suggest that

contractions of ASM induced by activation of M2Rs involve inhibition of Kv7.4 and Kv7.5 channels by pathways that involve depletion of PIP_2 and reduced activation of PKA, respectively (Figure 5.21).

In the previous chapter, we observed that application of CCh to HEK293 cells expressing Kv7.1 and M2Rs led to a reduction in the amplitude of Kv7.1 currents. However, in the present chapter, we found that cholinergic contractions of bronchial rings were unaffected by the Kv7.1 modulators chromanol 293B and ML277, suggesting that Kv7.1 channels are of little functional importance with regard to cholinergic contractions of ASM. This accords with the conclusions of other investigators who reported that Kv7.1 channels were not involved in ASM contraction [494, 495]. Chadha et al. (2012) found that chromanol 293B had little or no contractile effect in vascular smooth muscle, implying that Kv7.1 channels contribute little to the basal Kv7-mediated current in those vessels [495]. Moreover, a review by Haick and Byron (2016) noted that while Kv7.1 is transcriptionally expressed in smooth muscle, there is no convincing electrophysiological or pharmacological evidence that it contributes to smooth muscle membrane potential or contraction [494]. Reasons for this disparity between expression and functional role are unclear but could be related to modulation by KCNE3 and KCNE4 subunits (subunits which showed high mRNA expression in bronchial tissues; Figure 4.5B). High KCNE3 expression may render Kv7.1 channels constitutively open and voltage-independent, while KCNE4 suppresses channel activation by stabilising the closed state. The presence of these subunits could lead to Kv7.1 channels that are either continuously open or non-functional, resulting in little contribution to membrane potential regulation.

ML213 is marketed as a selective activator of Kv7.2 and Kv7.4 channels [496]; however, Brueggemann et al. (2014) found that it can activate homomeric Kv7.4 and Kv7.5 channels, as well as heteromeric Kv7.4/Kv7.5 channels [471]. In contrast, ICA069673 is thought to be a selective opener of Kv7.2 and Kv7.3 channels [497], but Brueggemann et al. (2014) showed that it can also activate Kv7.4 channels [471]. We found that ICA069673 enhanced Kv7.4 currents, but not Kv7.5, whereas ML213 enhanced both Kv7.4 and Kv7.5 currents. As Kv7.2 and Kv7.3 were minimally expressed in ASM, we employed ML213 and ICA069673 as pharmacological tools to investigate the effects of activating Kv7.4 and Kv7.5

channels on M2R-mediated contractions of ASM. We found that M2R-dependent contractions of ASM, evoked by EFS or exogenous application of CCh, were inhibited by both ICA069673 and ML213. However, ML213 had greater effects than ICA069673 and produced additional inhibitory effects when applied in the presence of ICA069673. While this could suggest an additional contribution of Kv7.5 channels, an alternative interpretation should be considered. At the concentration used (30 μM), ICA069673 is reported to produce substantial activation of Kv7.4 channels (Brueggemann et al., 2014) and therefore would be expected to engage the majority of the available Kv7.4 channel population [471]. However, our data indicate that ICA069673 did not produce maximal activation, as evidenced by a relatively modest increase in G_{max} despite a pronounced negative shift in $V_{1/2}$. In contrast, subsequent application of ML213 resulted in a further significant increase in G_{max} along with an additional negative shift in $V_{1/2}$, suggesting that ML213 is capable of recruiting additional channel activity beyond that achieved with ICA069673 alone. In this context, the additional inhibition observed upon ML213 application may reflect further activation of Kv7.4 channels and/or recruitment of Kv7.4/Kv7.5 heteromeric channels, rather than selective engagement of Kv7.5 alone. Consistent with this, we found that CCh reduced the mean G_{max} of Kv7.4/Kv7.5 heteromeric currents when co-expressed with M2Rs in HEK293 cells (Figure 5.13), demonstrating that M2R activation functionally suppresses heteromeric Kv7 channel activity. This supports the view that the observed effects are likely mediated, at least in part, through modulation of Kv7.4/Kv7.5 heteromeric channel complexes.

Importantly, the experimental design, in which ICA069673 was applied prior to ML213, was based on its relatively greater reported selectivity towards Kv7.4, allowing an initial assessment of Kv7.4-mediated effects before introducing a broader Kv7 activator. While reversing the order of application (ML213 followed by ICA069673) could provide further insight into the extent of channel recruitment and maximal activation, the current findings already support the conclusion that Kv7 channel activation exerts a strong inhibitory influence on M2R-mediated ASM contraction. Nevertheless, such experiments would be valuable in future studies to more precisely delineate the relative contributions and pharmacological behaviour of Kv7 channel subtypes in native tissue.

Bruggemann et al. (2018) reported that Kv7.5 channels were the prominent Kv7 subtype in cultured human ASM cells [299]. Kv7.5 currents recorded from these cells were enhanced by activation of the cAMP/PKA pathway, similar to effects demonstrated on cloned Kv7.5, but not Kv7.4 channels [465]. As M2Rs are coupled to G_i proteins that reduce adenylate cyclase activity and cytosolic cAMP levels [158], it is possible that activation of M2Rs could reduce Kv7.5 activity via inhibition of the cAMP/PKA pathway. We found that the PKA activator 6MB-cAMP enhanced the amplitude and negatively shifted the voltage-dependence of activation of Kv7.5 currents in HEK293 cells and inhibited M2R-dependent contractions of ASM. In contrast, 6MB-cAMP did not affect the voltage-dependence of activation of Kv7.4 currents and caused a slight reduction in current amplitude rather than an increase. This suggests that the inhibitory effects of 6MB-cAMP on M2R-dependent contractions of ASM are more likely to be mediated by activation of Kv7.5 than Kv7.4 channels. However, M2R responses in ASM were also reduced by selective activation of Kv7.4 with ICA069673, and ICA069673 was also able to reverse the inhibitory effect of CCh on Kv7.4 currents in HEK293 cells, suggesting that Kv7.4 channels also have an important regulatory role in ASM excitability.

Kv7 channel activity in neurones is reduced by activation of M1R and M3Rs via activation of PKC, increased intracellular Ca^{2+} levels and depletion of PIP_2, which stabilises the open state of Kv7 channels [297, 492, 498-500]. Addition of PIP_2 has also been shown to restore Kv7.2/Kv7.3 channel activity, co-expressed with M1Rs in human tsA-201 cells [480, 501]. In the present study, we found that the inhibitory effects of CCh on Kv7.4 currents were diminished in cells dialysed with PIP_2 diC8. In contrast, dialysis of PIP_2 diC8 did not reduce the inhibitory effects of M2R activation on Kv7.5. Therefore, it is possible that M2R-dependent contractions of ASM involve inhibition of Kv7.4 channels via a pathway that involves PIP_2 depletion. While G_i α subunits are not thought to activate PLC, it is recognised that $G_{\beta\gamma}$ subunits (from $G_i\alpha$-$G_{\beta\gamma}$ heterotrimers) can activate PLC_β isoenzymes to deplete PIP_2 [502-508]. A recent study by Pfeil et al. (2020) demonstrated that activation of PLC_β by G βγ subunits required priming by G_q α subunits [134]. If this is the case in ASM, it could explain why cholinergic contractions of ASM can be potentiated by activation of postjunctional M2Rs, but are fundamentally reliant on activation of M3Rs [153]. It is also worth noting that the net effect of M2R signalling on Kv7.4 activity by the $G_{\beta\gamma}$

subunits would be dependent on a balance between the stimulatory effects of $G_{\beta\gamma}$ subunits on Kv7.4 channels [509] and inhibitory effects induced via activation of PLC_{β} and depletion of PIP_2.

In summary, this study demonstrated, for the first time, that activation of M2Rs in HEK293 cells suppressed Kv7.4 and Kv7.5 currents. The Kv7 channel openers ICA069673 and ML213 reversed the inhibitory effects of M2R activation on Kv7 currents and inhibited M2R-dependent contractions of ASM. While Kv7.4 is well established to form functional homomeric channels, the existence of Kv7.5 as a homomer in native systems is less certain, with increasing evidence suggesting that Kv7.5 preferentially contributes to heteromeric channel assemblies, particularly with Kv7.4. Therefore, it is likely that the functional effects observed in this study arise, at least in part, from modulation of Kv7.4/Kv7.5 heteromeric channels rather than purely homomeric Kv7.5 populations. In this context, the greater inhibitory effect observed with ML213 and its additional effect in the presence of ICA069673 may reflect a synergistic enhancement of activity across heteromeric channel complexes. Mechanistically, these effects were mediated by signalling pathways involving PIP_2 depletion and inhibition of cAMP/PKA signalling.

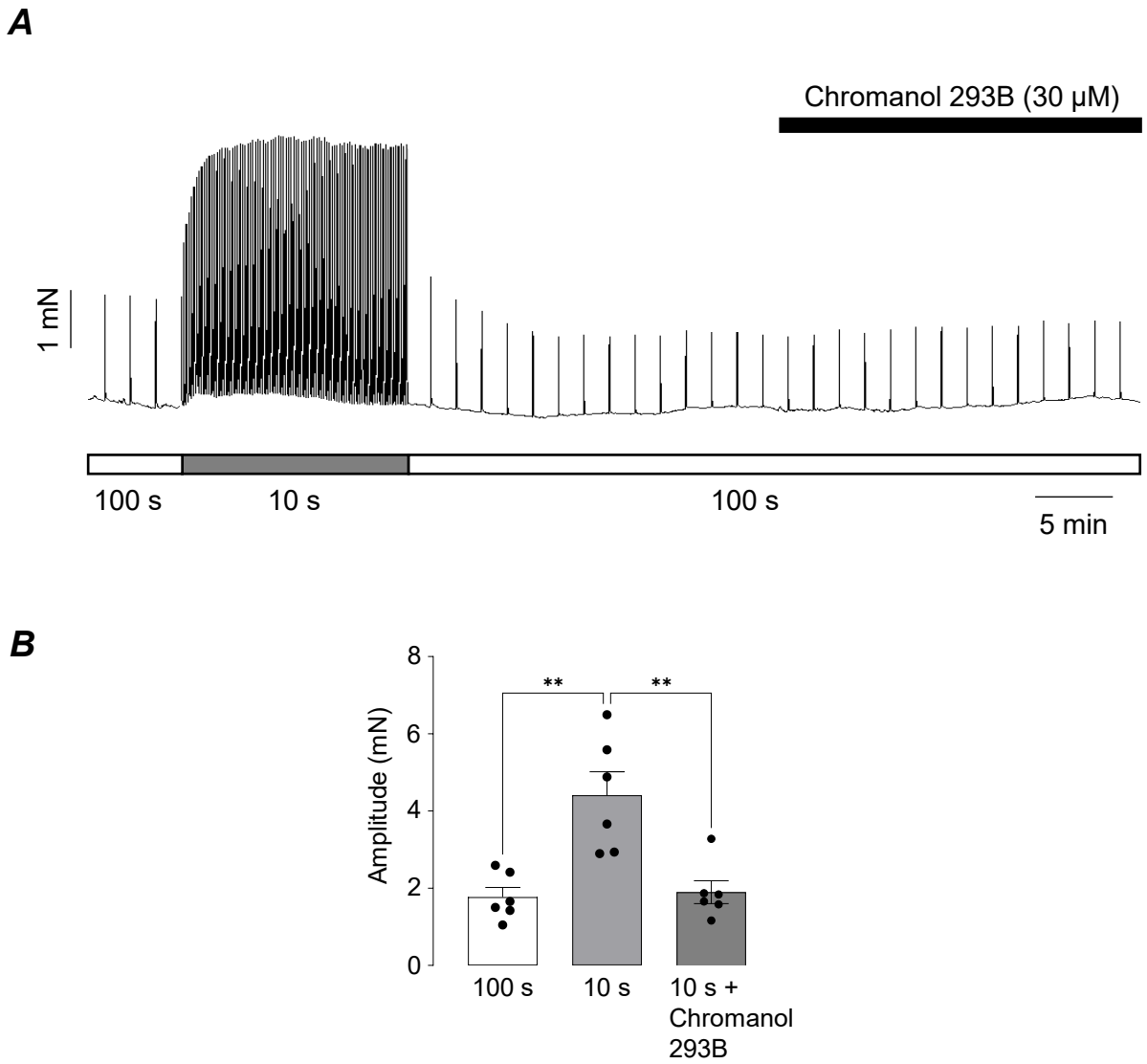

Figure 5.1. Effect of Kv7.1 channel inhibitor, chromanol 293B on EFS-evoked contractions of ASM. (A) Representative isometric tension trace showing that chromanol 293B (30 μM) had no effects on EFS-evoked contractions at 100 s stimulation intervals. **(B)** Summary bar chart showing the effect of chromanol 293B on EFS contractions at 100 s intervals (**p<0.01, n=6, N=4, one-way ANOVA).

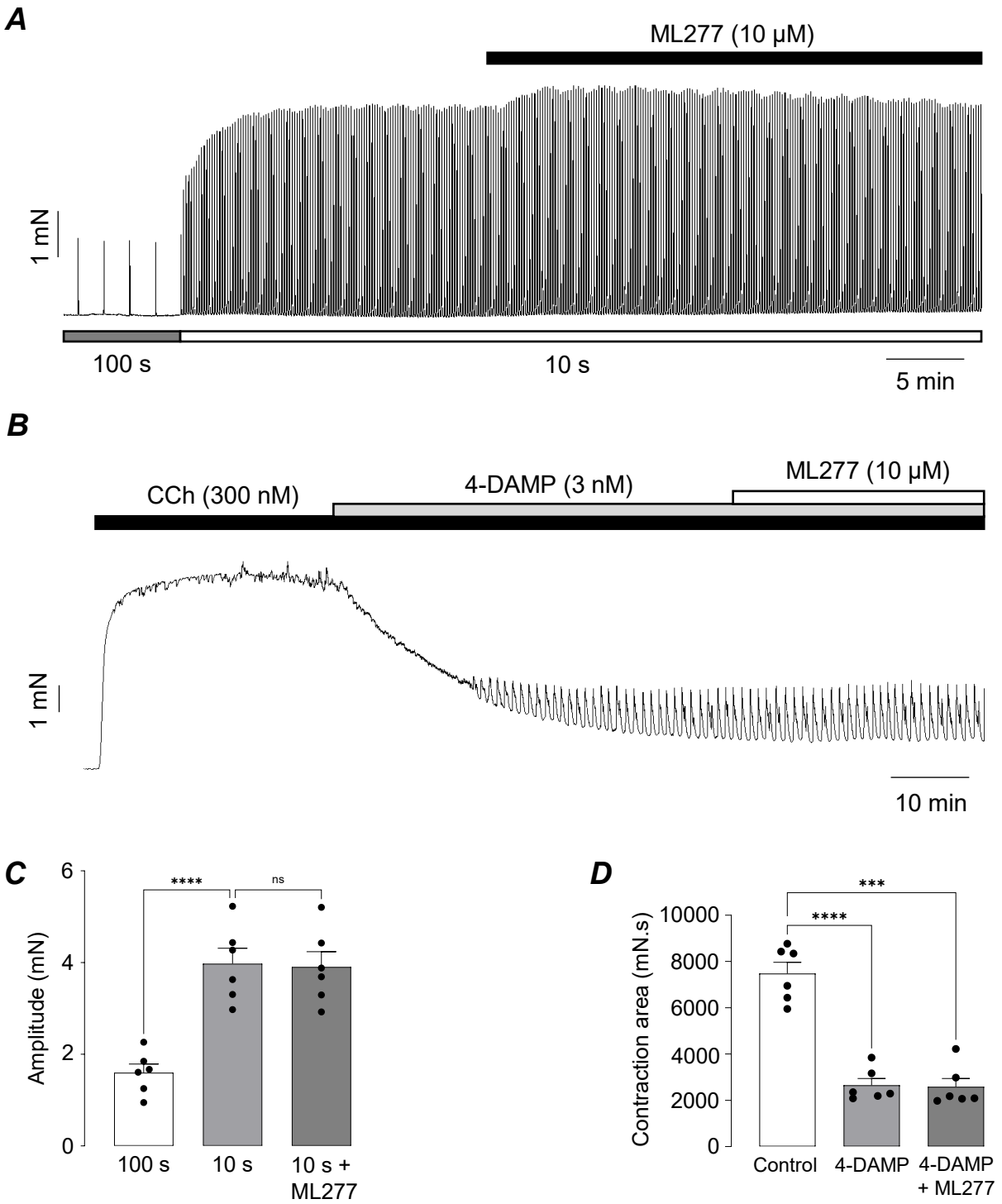

Figure 5.2. Effect of Kv7.1 channel activator, ML277 on EFS and CCh-evoked contractions of ASM. (A) Representative isometric tension trace showing that ML277 (10 μM) did not affect the M2R-mediated enhancement of EFS-evoked contractions at 10 s stimulation intervals. **(B)** Representative trace illustrating that ML277 (10 μM) failed to abolish M2R contractions evoked by CCh that remained in 4-DAMP. **(C)** Summary bar chart showing the effect of ML277 on EFS contractions evoked at 10 s intervals (ns, non-significant, ****p<0.0001, n=6, N=4, one-way ANOVA). **(D)** Summary bar chart showing the response of ML277 on contractions evoked by CCh that remained in 4-DAMP (***p<0.001, ****p<0.0001, n=6, N=4, one-way ANOVA).

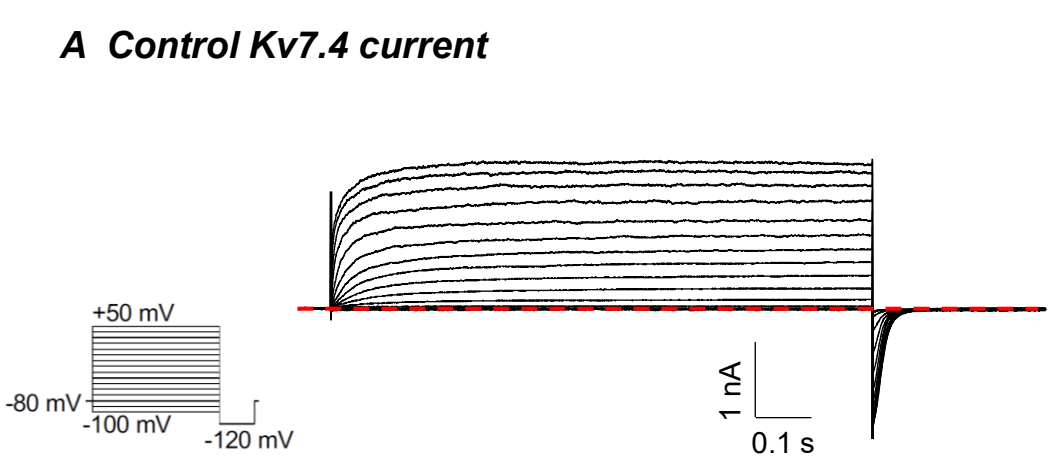

Figure 5.3. Effects of Kv7.4 channel activator, ICA069673 on Kv7.4 currents recorded from HEK293 cells transfected with Kv7.4. (A) Typical families of currents obtained from wildtype Kv7.4 channels expressed in HEK293 cells. Voltage clamp protocol is illustrated in the inset. Red dotted lines represent the zero current levels. (**B)** Effect of ICA069673 (30 µM) on currents from the same cell. **(C)** Summary activation curves obtained by measuring tail currents in seven cells before (black circles) and during (red circles) application of ICA069673 (n=7). The curves were fit with the Boltzmann equation. **(D)** Summary graph showing the increase in the deactivation time constant (τ) following ICA069673 treatment (***p<0.001, n=7, paired t-test).

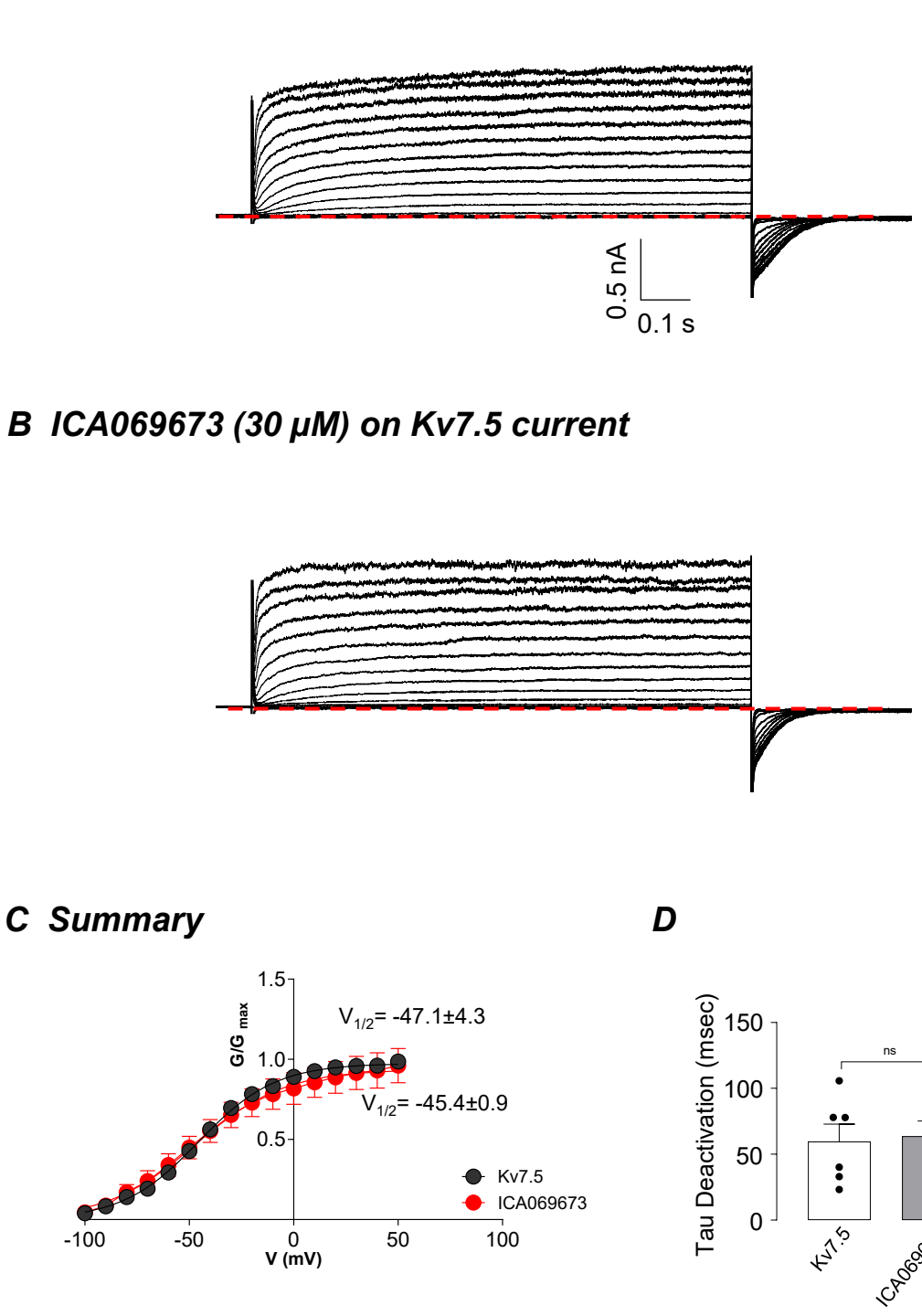

Figure 5.4. Effects of ICA069673 on Kv7.5 currents recorded from HEK293 cells transfected with Kv7.5. (A) Typical families of currents obtained from wildtype Kv7.5 channels expressed in HEK293 cells. (**B)** Effect of ICA069673 (30 µM) on currents from the same cell. **(C)** Summary activation curves obtained by measuring tail currents before (black circles) and during (red circles) application of ICA069673 (n=6). The curves were fit with the Boltzmann equation. **(D)** Summary graph showing the increase in the tau of deactivation (τ) following ICA069673 treatment (ns, non-significant, n=6, paired t-test).

A M2R and Kv7.4 control

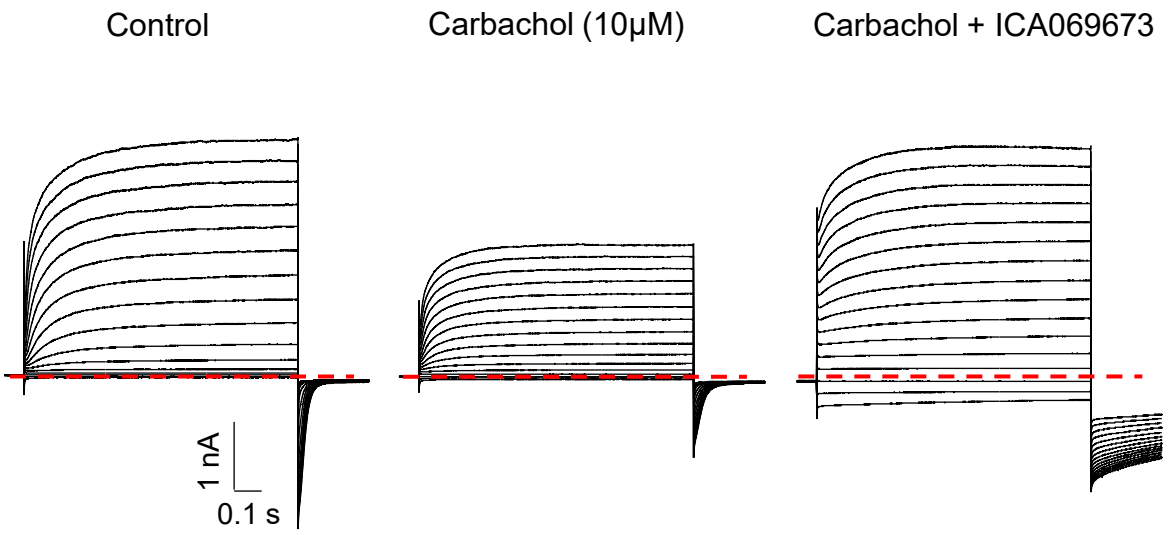

B Summary

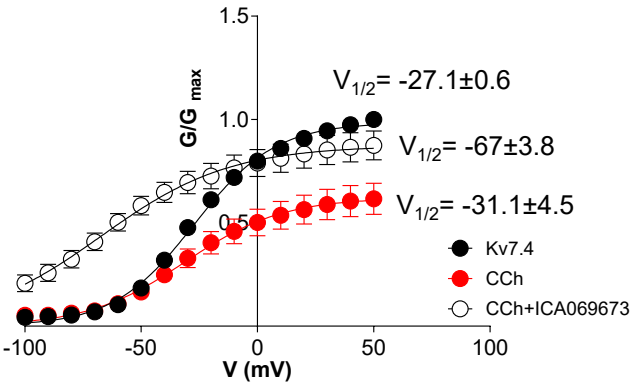

Figure 5.5. Effects of ICA069673 on M2R and Kv7.4 currents in the presence of carbachol (A) Representative families of Kv7.4 currents recorded from HEK293 cells before, in the presence CCh and CCh + ICA069673 (**B)** Summary activation curves obtained by measuring tail currents before (black circles) and during application of CCh (red circles) and ICA069673 (open circles; n=7). The curves were fit with the Boltzmann equation.

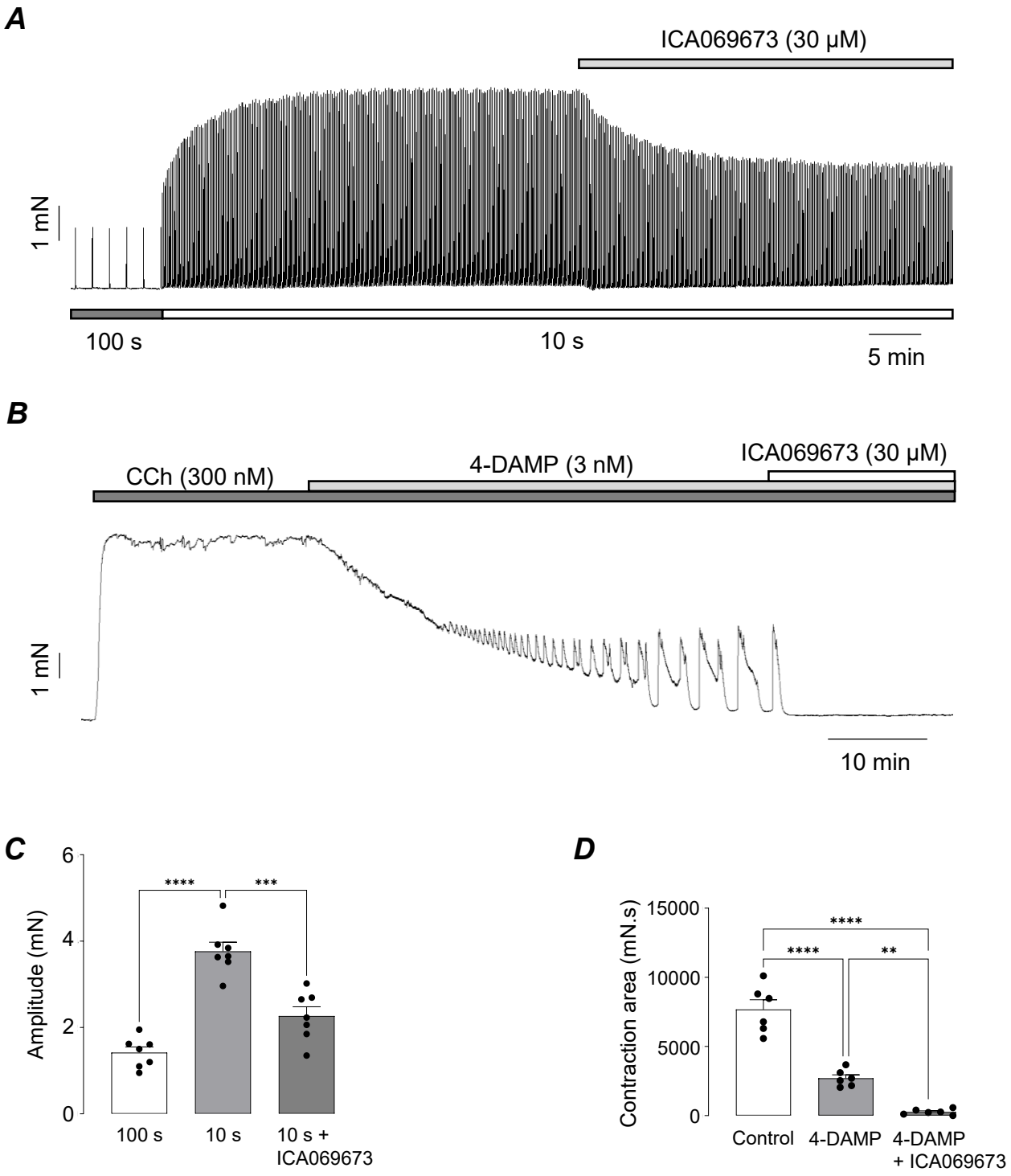

Figure 5.6. Effect of ICA069673 on EFS and CCh evoked M2R contractions of ASM. **(A)** Representative isometric tension trace showing that ICA069673 (30 µM) attenuated the M2R-mediated enhancement of EFS-evoked contractions at 10 s stimulation intervals. **(B)** Representative trace illustrating that ICA069673 (30 µM) abolished CCh-evoked contractions that remained in the presence of 4-DAMP. **(C)** Summary bar chart showing the effect of ICA069673 on EFS contractions at 10s intervals (***p<0.001, ****p<0.0001, n=7, N=4, one-way ANOVA). **(D)** Summary bar chart depicting the response of ICA069673 on M2R response evoked by CCh and 4-DAMP (**p<0.01, ****p<0.0001, n=6, N=5, one-way ANOVA).

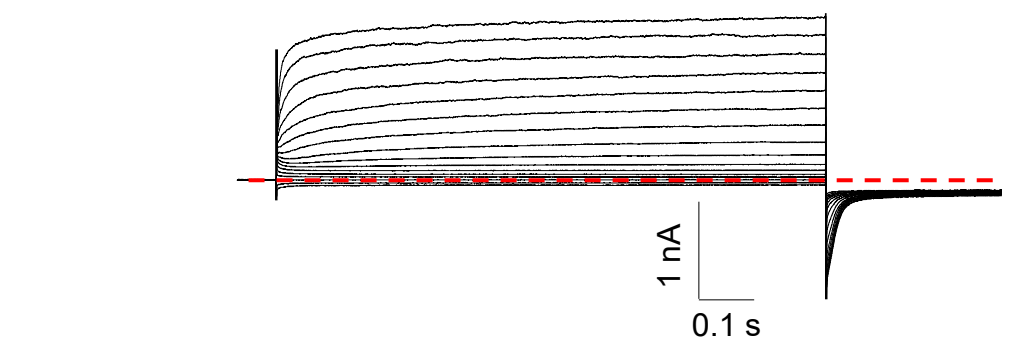

Figure 5.7. Effects of Kv7.4 and Kv7.5 channel activator, ML213 on Kv7.4 currents recorded from HEK293 cells transfected with Kv7.4. (A) Typical families of currents obtained from wildtype Kv7.4 channels expressed in HEK293 cells. (**B)** Effect of ML213 (5 µM) on currents from the same cell. **(C)** Summary activation curves obtained by measuring tail currents before (black circles) and during (red circles) application of ML213 (n=6). The curves were fit with the Boltzmann equation. **(D)** Summary graph showing the increase in the tau of deactivation following ML213 treatment (**p<0.01, n=6, paired t-test).

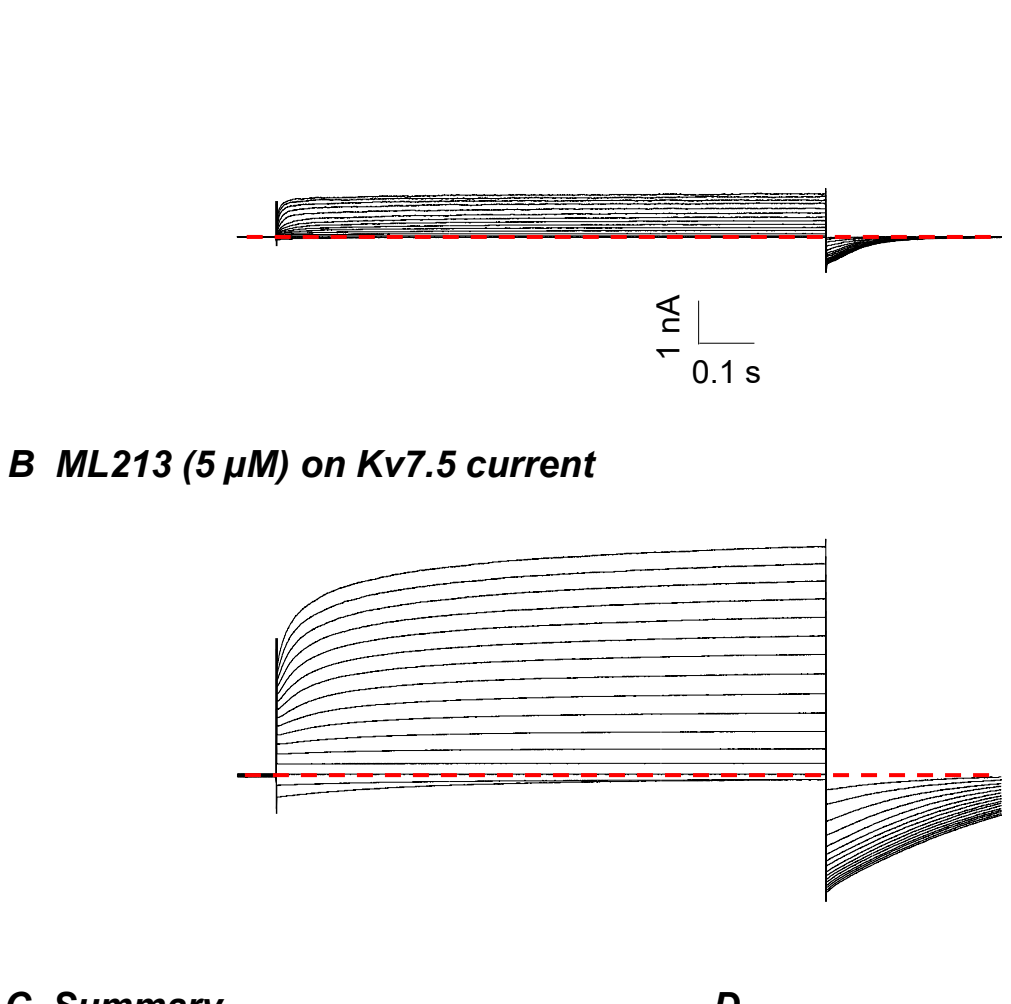

Figure 5.8. Effects of ML213 on Kv7.5 currents recorded from HEK293 cells transfected with Kv7.5. (A) Typical families of currents obtained from wildtype Kv7.5 channels expressed in HEK293 cells. (**B)** Effect of ML213 (5 µM) on currents from the same cell. **(C)** Summary activation curves obtained by measuring tail currents before (black circles) and during (red circles) application of ML213 (n=6). The curves were fit with the Boltzmann equation. **(D)** Summary graph showing the increase in the tau of deactivation following ML213 treatment (***p<0.001, n=6, paired t-test).

A M2R and Kv7.4 control

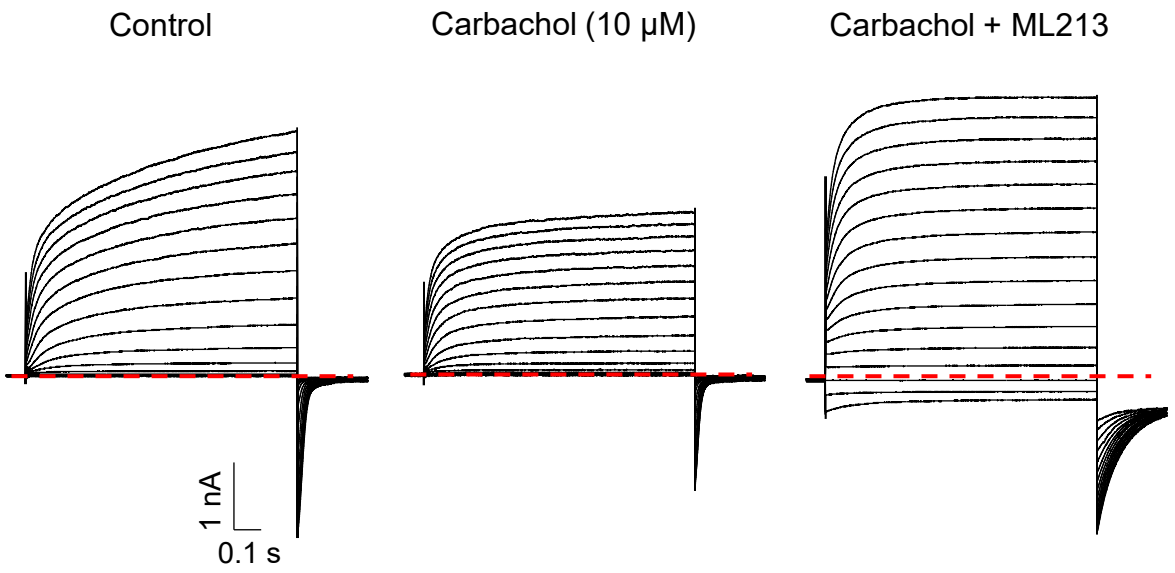

B ML213 (5 µM) on Kv7.4 current

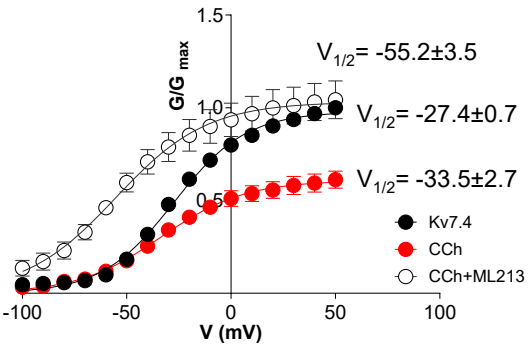

Figure 5.9. Effects of ML213 on M2R and Kv7.4 currents in the presence of carbachol **(A)** Representative families of currents recorded from HEK293 cells expressing M2R and Kv7.4 before and during the presence of CCh and CCh and ML213. CCh application reduced the current amplitude with ML213 (5 µM) reversed the effect of CCh. (**B)** Summary activation curves obtained by measuring tail currents before (black circles) and during application of CCh (red circles) and ML213 (open circles; n=6). The curves were fit with the Boltzmann equation.

A M2R and Kv7.5 control

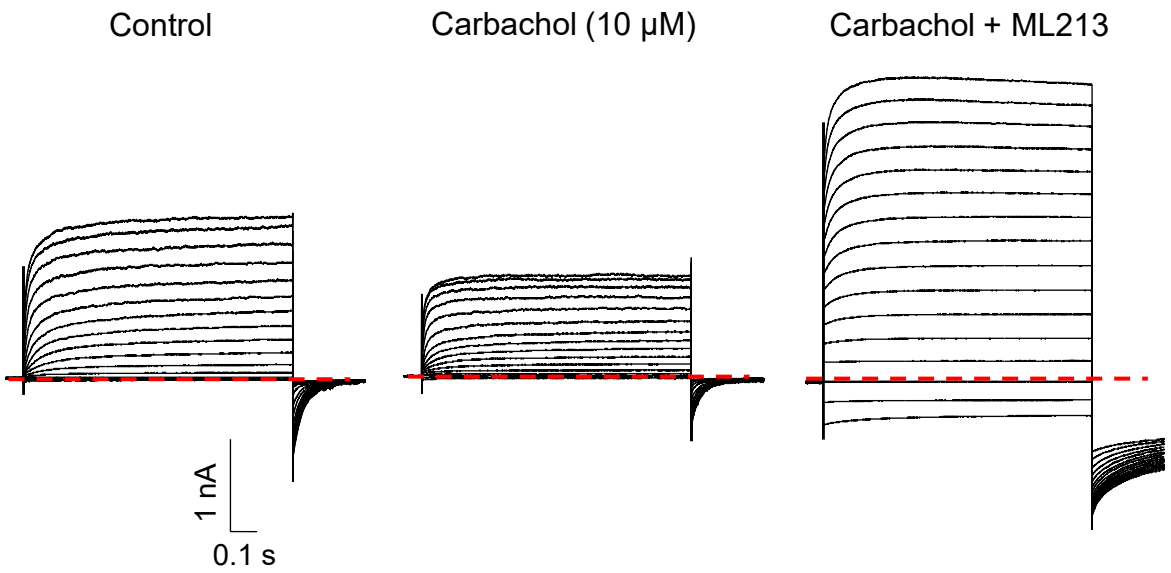

B ML213 (5 µM) on Kv7.5 current

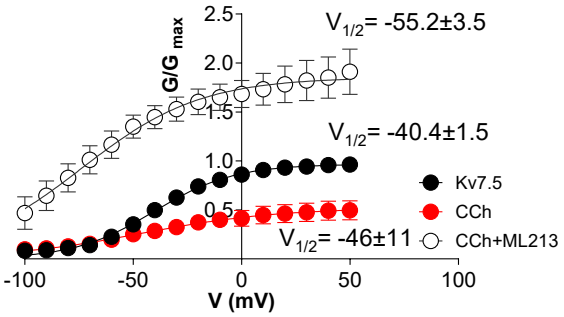

Figure 5.10. Effects of ML213 on M2R and Kv7.5 currents in the presence of carbachol (A) Typical families of currents obtained from HEK293 cells transfected with M2Rs and Kv7.5. CCh reduced the current amplitude and this effect was reversed by ML213 (5 µM). (**B)** Summary activation curves obtained by measuring tail currents before (black circles) and during application of CCh (red circles) and ML213 (open circles; n=6). The curves were fit with the Boltzmann equation.

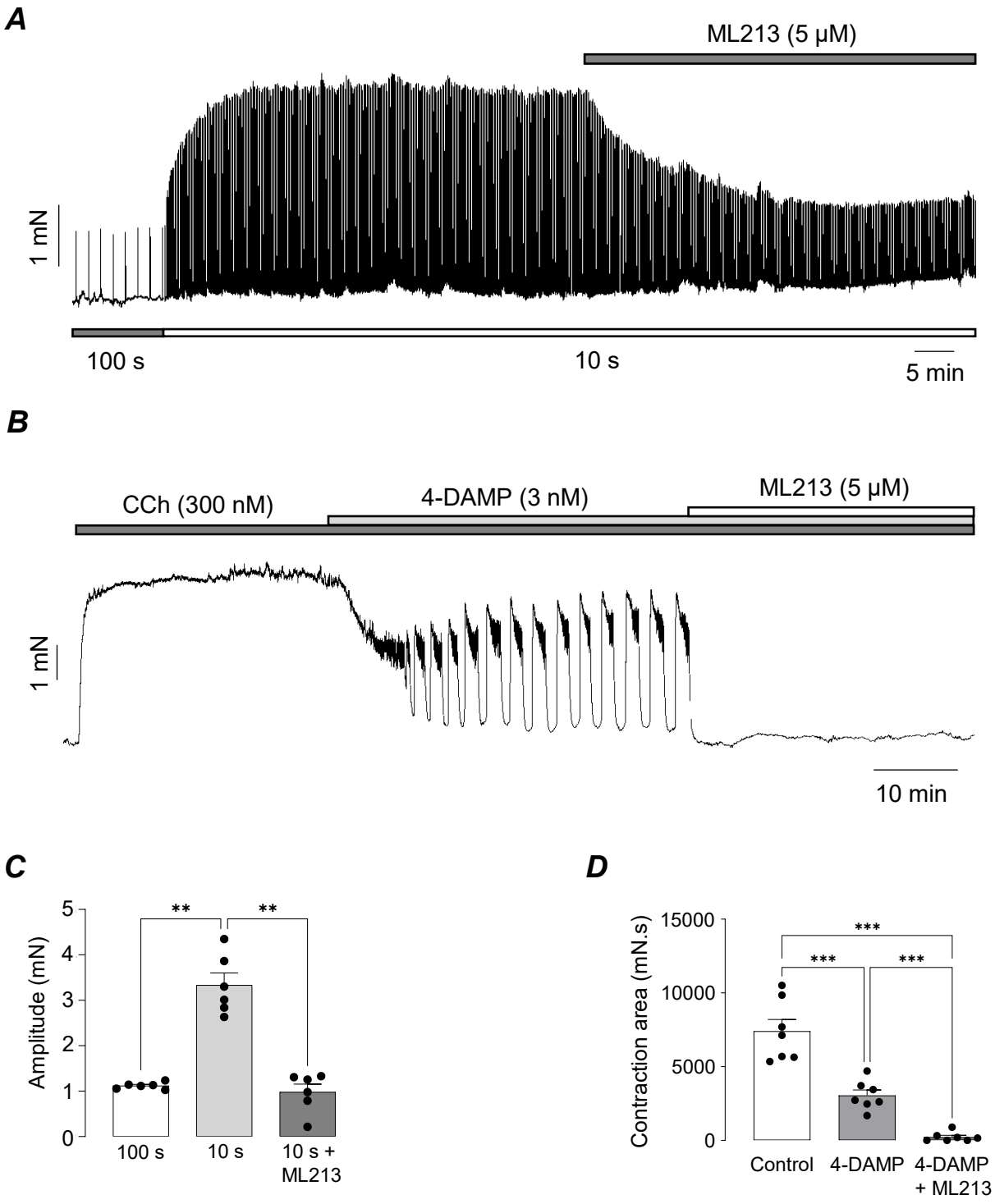

Figure 5.11. Effect of ML213 on EFS and CCh-evoked M2R contractions of ASM. (A) Representative isometric tension trace showing that ML213 (5 μM) attenuated the M2R-mediated enhancement of EFS-evoked contractions at 10 s stimulation intervals. **(B)** Representative trace illustrating that ML213 (5 μM) reduced the CCh-evoked contractions that remained in the presence of 4-DAMP. **(C)** Summary bar chart plotting mean amplitude of contractions evoked by EFS at 100 s and 10 s intervals and at 10 s intervals in the presence of ML213 (**p<0.01, n=6, N=4, one-way ANOVA). **(D)** Summary bar chart showing mean contraction amplitude evoked by CCh before and during 4-DAMP and 4-DAMP plus ML213 (***p<0.001, n=7, N=4, one-way ANOVA).

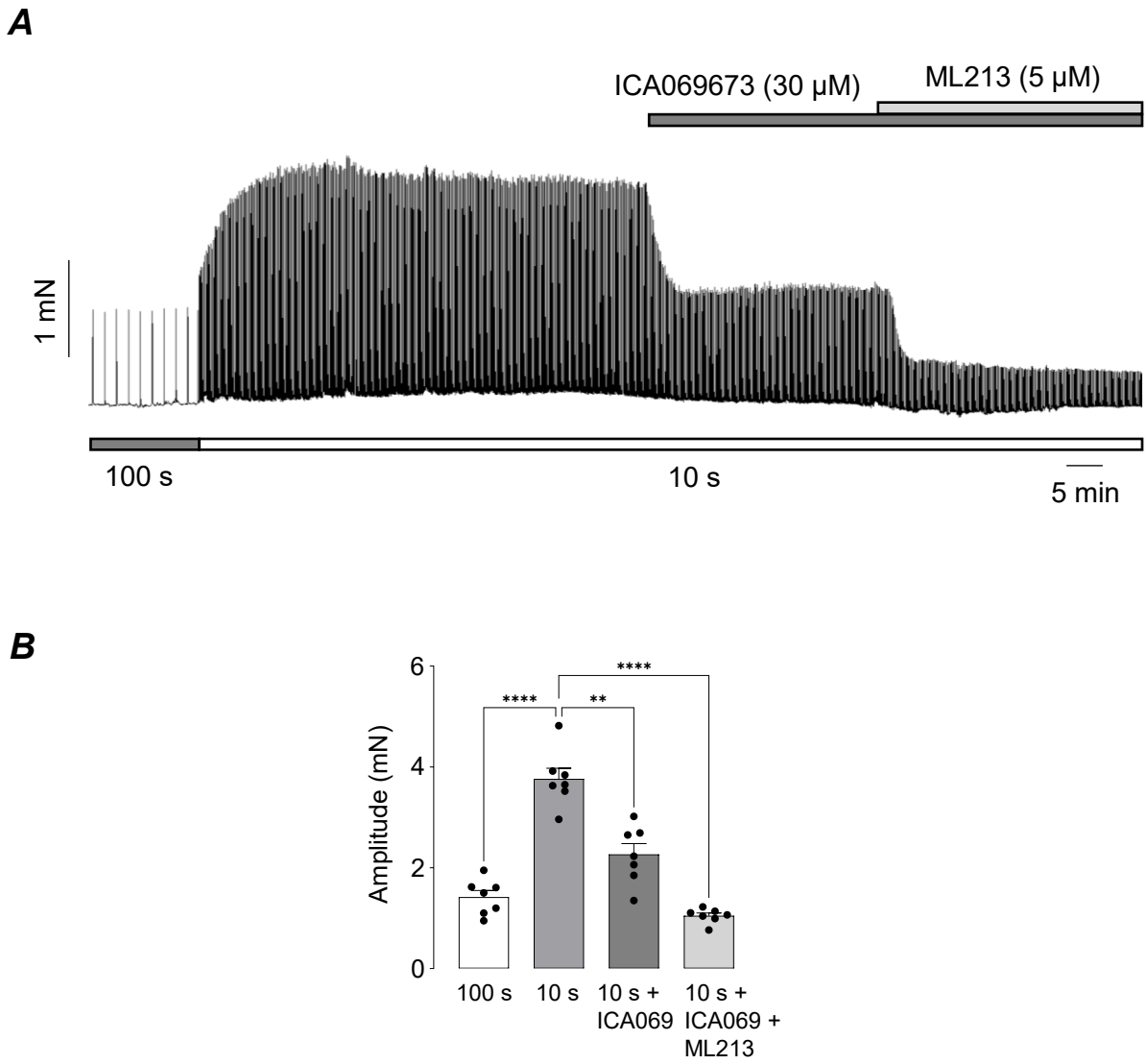

Figure 5.12. Effect of co-administration of ICA069673 and ML213 on EFS-evoked contractions of ASM. (A) Representative isometric tension trace showing that ICA06963 (30 µM) reduced the M2R-mediated enhancement of EFS-evoked contractions at 10 s stimulation intervals. Addition of ML213 (5 µM) further reduced the amplitude of the contractions. **(B)** Summary bar chart showing the effect of ICA069673 and ML213 on EFS contractions at 10 s intervals (**p<0.01, ****p<0.0001, n=7, N=5, one-way ANOVA).

A Control Kv7.4 + Kv7.5 + M2R current

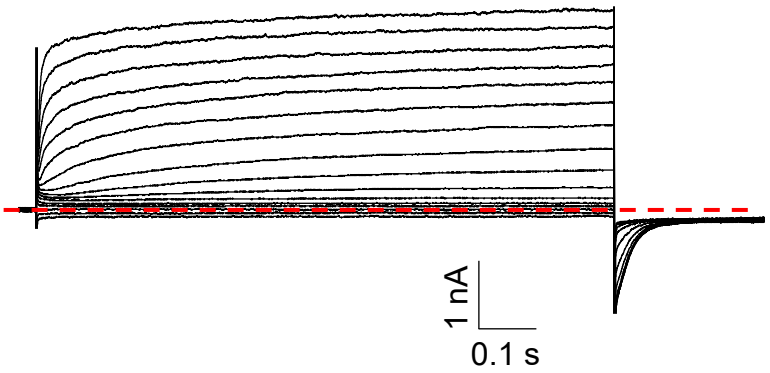

B Carbachol (10 µM) on Kv7.4 + Kv7.5 + M2R current

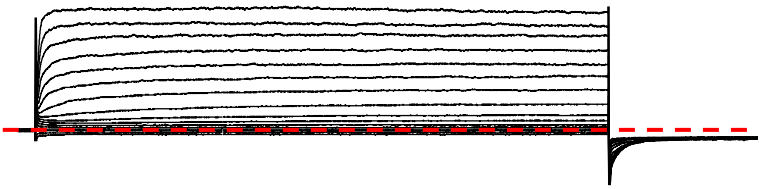

C Summary

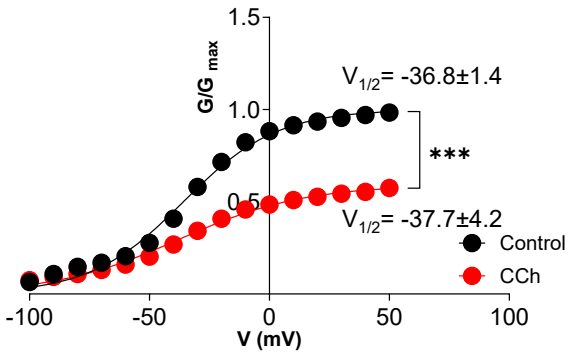

Figure 5.13. Effects of carbachol (10 µM) on M2R and Kv7.4 + Kv7.5 currents.
(A) Families of currents, recorded from HEK293 cells co-expressing M2R with Kv7.4 and Kv7.5 heterotetramer. Dotted lines represent the zero current levels. (**B)** Families of currents, recorded in the presence of carbachol (10 µM) from the same HEK293 cells co-expressing M2R with Kv7.4/7.5 **(C)** Summary activation curves obtained by measuring tail currents before (black circles) and during (red circles) application of carbachol (n=7). The curves were fit with the Boltzmann equation.

A Control Kv7.4 current

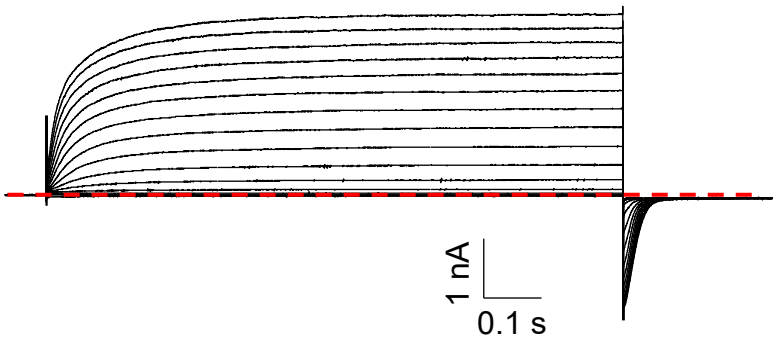

B Carbachol (10 µM) on Kv7.4 current

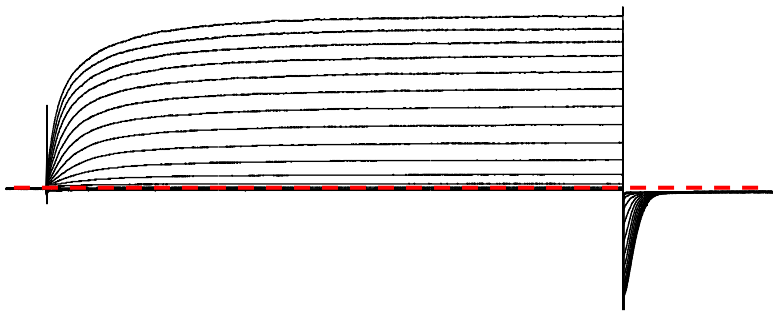

C Summary

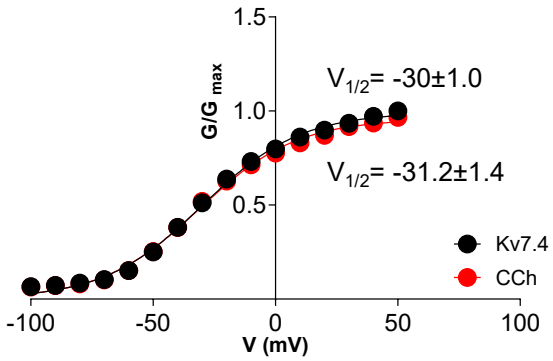

Figure 5.14. Effects of carbachol on Kv7.4 currents recorded from HEK293 cells transfected with Kv7.4. (A) Typical families of currents obtained from wildtype Kv7.4 channels expressed in HEK293 cells. (**B)** Effect of CCh (10 µM) on currents from the same cell. **(C)** Summary activation curves obtained by measuring tail currents in seven cells before (black circles) and during (red circles) application of CCh (n=7). The curves were fit with the Boltzmann equation.

A Control Kv7.5 current

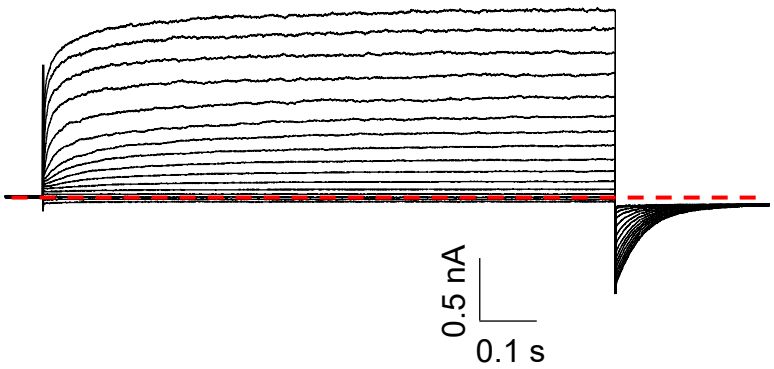

B Carbachol (10 μM) on Kv7.5 current

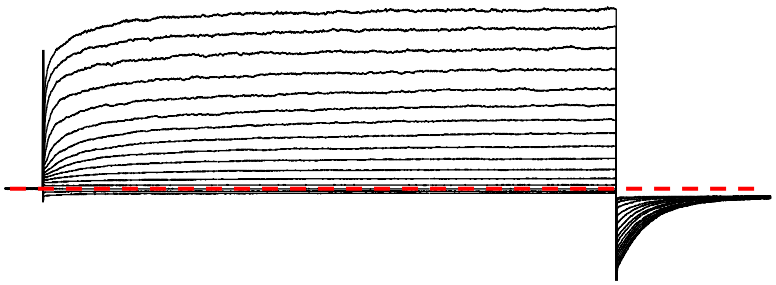

C Summary

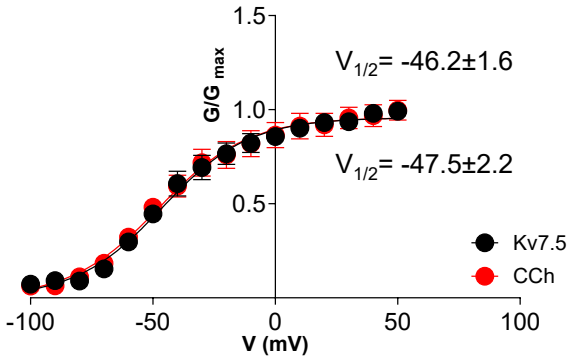

Figure 5.15. Effects of carbachol on Kv7.5 currents recorded from HEK293 cells transfected with Kv7.5. (A) Typical families of currents obtained from wildtype Kv7.5 channels expressed in HEK293 cells. (**B)** Effect of CCh (10 μM) on currents from the same cell. **(C)** Summary activation curves obtained by measuring tail currents in seven cells before (black circles) and during (red circles) application of CCh (n=7). The curves were fit with the Boltzmann equation.

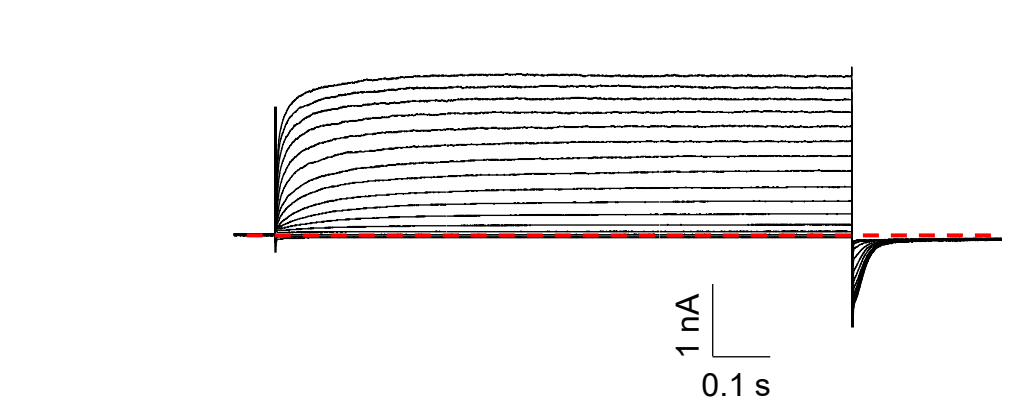

Figure 5.16. Effects of PKA activator, 6MB-cAMP on Kv7.4 currents recorded from HEK293 cells transfected with Kv7.4. (A) Typical families of currents obtained from wildtype Kv7.4 channels expressed in HEK293 cells. (**B)** Effect of 6MB-cAMP (300 µM) on currents from the same cell. **(C)** Summary activation curves obtained by measuring tail currents before (black circles) and during (red circles) application of 6MB-cAMP (n=6). The curves were fit with the Boltzmann equation. **(D)** Summary graph showing the increase in the tau of deactivation following 6MB-cAMP treatment (ns, non-significant, n=6, paired t-test).

A Control Kv7.5 current

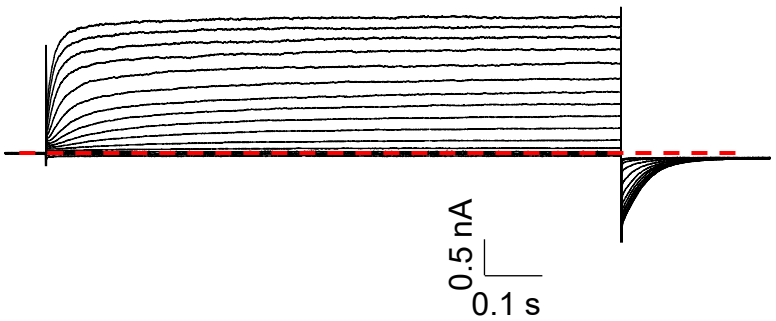

B 6MB-cAMP (300 µM) on Kv7.5 current

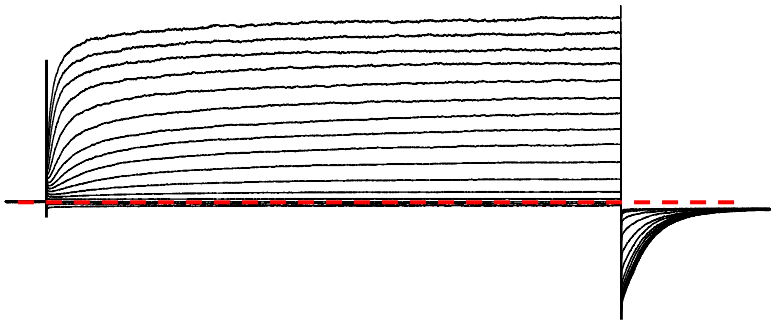

C Summary

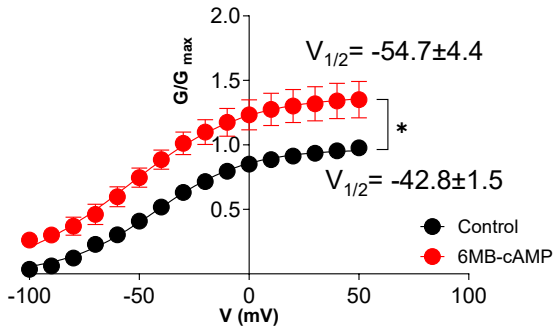

D

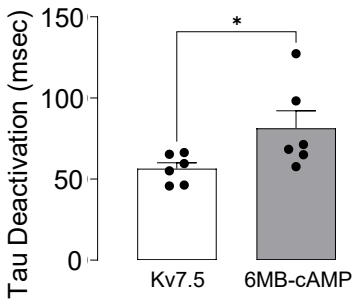

Figure 5.17. Effects of 6MB-cAMP on Kv7.5 currents recorded from HEK293 cells transfected with Kv7.5. (A) Typical families of currents obtained from wildtype Kv7.5 channels expressed in HEK293 cells. (**B)** Effect of 6MB-cAMP (300 µM) on currents from the same cell. **(C)** Summary activation curves obtained by measuring tail currents before (black circles) and during (red circles) application of 6MB-cAMP (n=6). The curves were fit with the Boltzmann equation. **(D)** Summary graph showing the increase in the tau of deactivation following 6MB-cAMP treatment (*p<0.05, n=6, paired t-test).

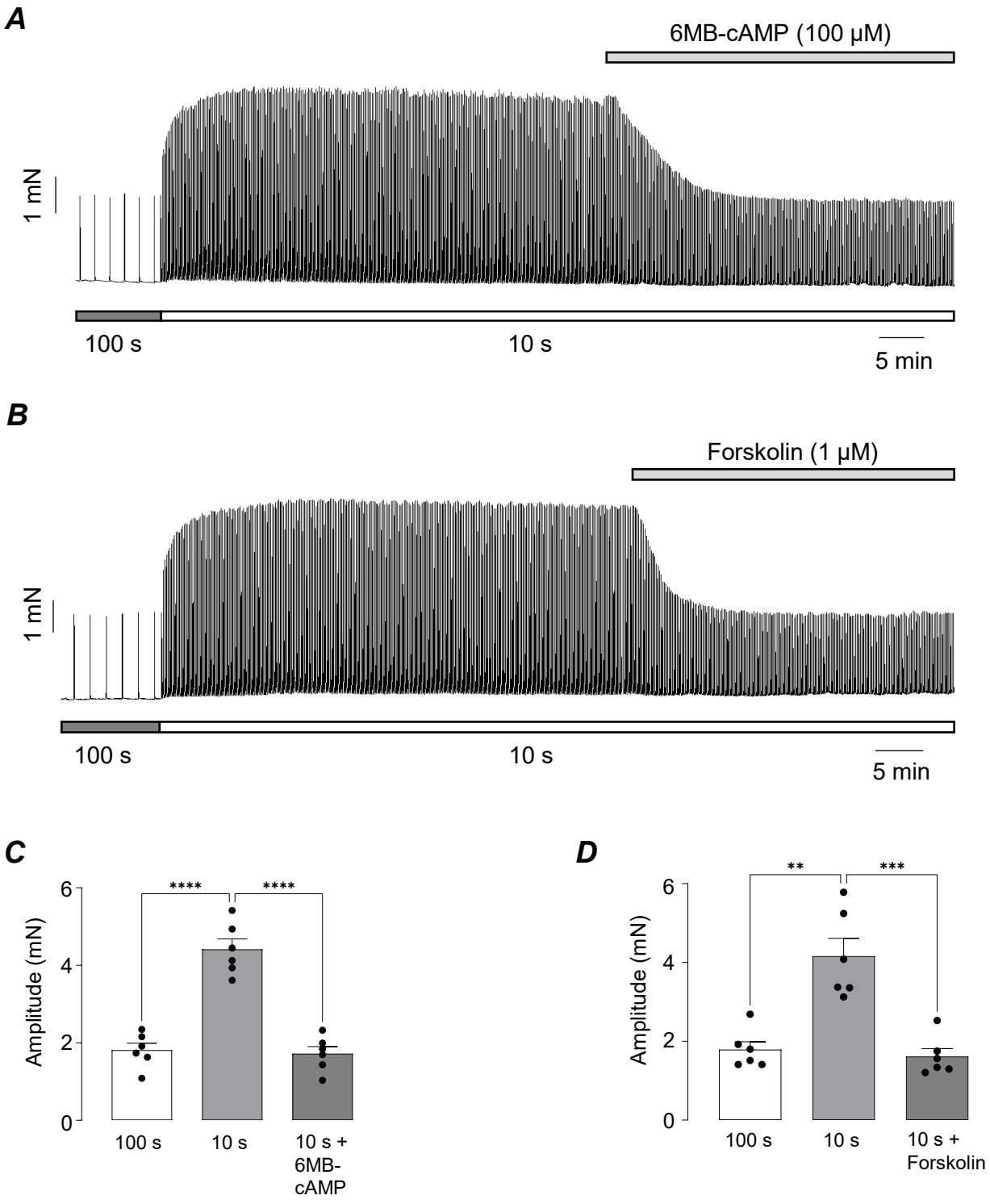

Figure 5.18. Effect of 6MB-cAMP and adenylate cyclase activator, forskolin on EFS-evoked contractions of ASM. (A) Representative isometric tension trace showing that 6MB-cAMP (100 µM) attenuated the M2R-mediated enhancement of EFS-evoked contractions at 10 s stimulation intervals. **(B)** Representative trace illustrating that forskolin (1 µM) reversed the increase in contraction amplitude induced by reducing the stimulation interval from 100 s to 10 s. **(C)** Summary bar chart showing the effect of 6MB-cAMP on EFS contractions at 10 s intervals (****p<0.0001, n=6, N=6, one-way ANOVA). **(D)** Summary bar chart showing the effect of forskolin on EFS contractions at 10 s intervals (**p<0.01, ***p<0.001, n=6, N=5, one-way ANOVA).

A M2R and Kv7.4 control + PIP_2 diC8 in the pipette

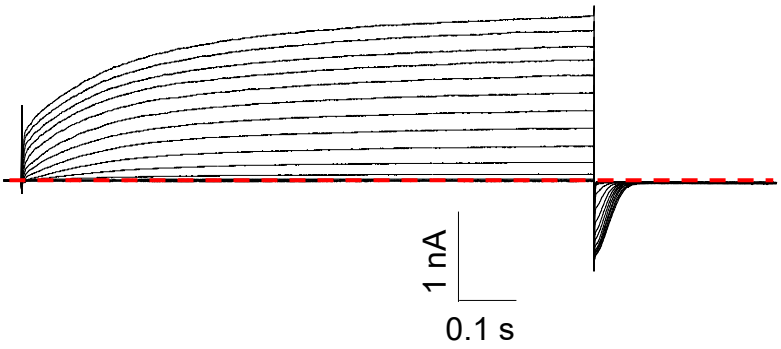

B Carbachol (10 μM) on M2R and Kv7.4 + PIP_2 diC8 in the pipette

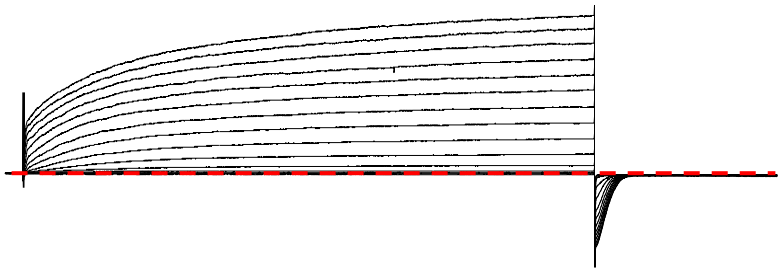

C Summary

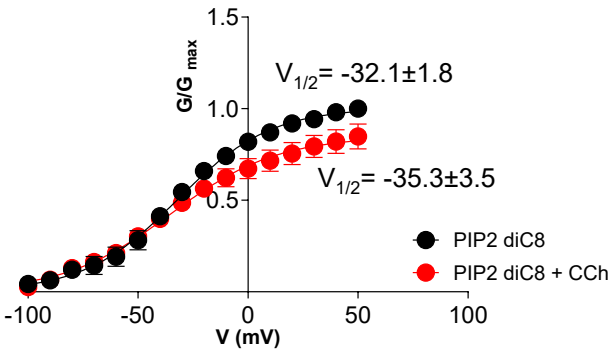

Figure 5.19. Effects of carbachol on Kv7.4 currents recorded from HEK293 cells dialysed with the PIP_2 analogue, PIP_2 diC8. (A) Typical families of currents obtained from Kv7.4 channels in HEK293 cells transfected with M2R and Kv7.4. Potassium pipette solution contained PIP_2 diC8 (200 μM) in it. (**B)** Effect of carbachol (10 μM) on currents from the same cell. **(C)** Summary activation curves obtained by measuring tail currents in six cells before (black circles) and during (red circles) application of CCh (ns, non-significant, n=6). The curves were fit with the Boltzmann equation.

A M2R and Kv7.5 control + PIP2 diC8 in the pipette

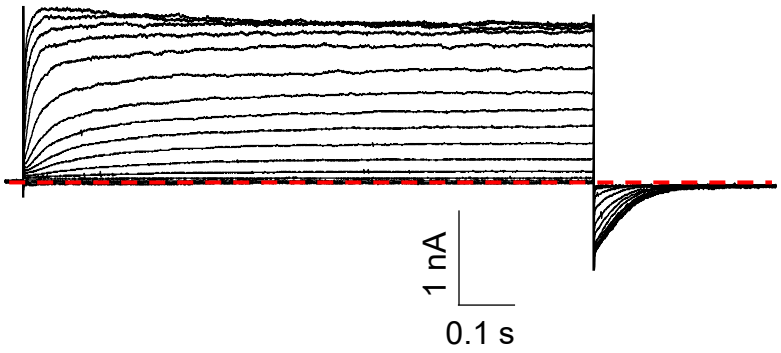

B Carbachol (10 µM) on M2R and Kv7.5 + PIP2 diC8 in the pipette

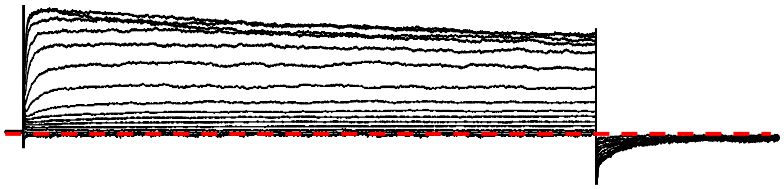

C Summary

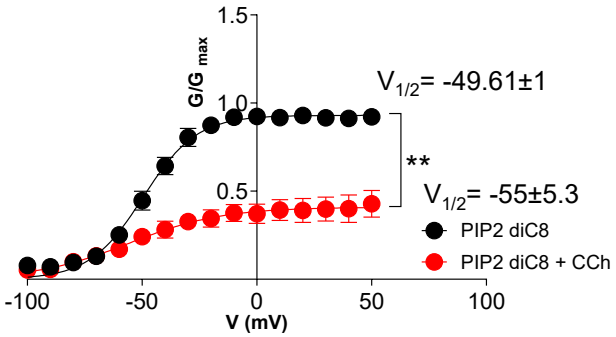

Figure 5.20. Effects of carbachol on M2R and Kv7.5 currents recorded from HEK293 cells dialysed with PIP_2 diC8. (A) Typical families of currents obtained from Kv7.5 channels in HEK293 cells transfected with M2R and Kv7.5. Potassium pipette solution contained PIP_2 diC8 (200 µM) in it. (**B)** Effect of carbachol (10 µM) on currents from the same cell. **(C)** Summary activation curves obtained by measuring tail currents in patches before (black circles) and during (red circles) application of CCh (**p<0.01, n=6, paired t-test). The curves were fit with the Boltzmann equation.

Chapter 6

Involvement of Ca^{2+} buffering by the SERCA pump and Ano1 Ca^{2+}-activated Cl^- channels in M2R-mediated ASM contractions

6.1. Introduction

Data in the previous chapters demonstrated that M2R-dependent contractions of ASM involve Ca^{2+} influx via LTCC, possibly by a mechanism involving inhibition of Kv7.4 and Kv7.5 channels. Janssen et al. (1999) reported that Ca^{2+} influx via LTCC in canine tracheal myocytes was heavily buffered by the activity of SERCA pumps present on the superficial SR located in close proximity to the plasma membrane [355]. This mechanism, whereby the superficial SR is able to remove Ca^{2+} which enters smooth muscle cells before it can reach the myofilaments was referred to as the superficial buffer barrier (SBB) hypothesis [356-358]. In vascular smooth muscle, inhibition of the SBB has been proposed as a mechanism to enhance agonist-induced contractions resulting from the opening of VDCCs [358]; however, it is not yet known if this mechanism contributes to the contraction of ASM. Importantly, Mahn et al. (2009) observed reduced SERCA protein expression in ASM cells isolated from asthmatic patients compared with those from healthy individuals, suggesting a pathophysiological link between impaired Ca^{2+} reuptake and AHR [359].

ASM cells express abundant Ano1 CACC [510]. However, the functional contribution of Ano1 channels to cholinergic contractions of the airways remains controversial. Previous studies reported that CACC blockers, including niclosamide and benzbromarone, could relax ASM [256, 260, 266]. However, it is now recognised that these agents have off-target effects [267]. In contrast, Ani9, a more potent and selective Ano1 inhibitor did not affect CCh-induced contractions of human or mouse ASM [267, 511, 512]. Wang et al. (2018) reported that contractions of ASM induced by MCh (10 μM) remained intact in mice lacking Ano1 channels, but responses induced by lower concentrations (300 nM) were 50% smaller than their wild-type (WT) counterparts [513]. Therefore, it is possible that Ano1 CACC contribute to cholinergic contractions of ASM, but only to responses evoked by low concentrations of cholinergic agonist. The purpose of the experiments contained in the present chapter was to investigate if the M2R-mediated component of cholinergic ASM contractions involves inhibition of SERCA activity and activation of Ano1 CACC.

6.2. Results

6.2.1. Distribution and expression of SERCA in airway smooth muscle cells

Janssen et al. (1999) reported that Ca^{2+} influx via LTCC in canine tracheal myocytes was heavily buffered by the activity of SERCA pumps present on the superficial SR located in close proximity to the plasma membrane [355]. Given the reliance of M2R-dependent contractions of ASM on Ca^{2+} influx via LTCC we investigated the hypothesis that M2R-dependent contractions of ASM involve inhibition of SERCA adjacent to the plasma membrane, leading to reduced buffering of Ca^{2+} influx via LTCC. This concept is contingent on SERCA being located at the periphery of ASM cells; therefore, we examined the cellular distribution of SERCA2 in isolated murine ASM cells using immunocytochemistry with selective SERCA2 antibodies. The reason we looked at only SERCA2 is that it is the dominant SERCA isoform in smooth muscle. In contrast, SERCA1 is almost exclusively expressed in fast-twitch skeletal muscle fibres and is essentially absent from ASM. SERCA3 expression is mainly confined to non-muscle cell types such as endothelial cells, immune cells, and some epithelial tissues, and where it is present, it generally shows much lower expression and activity in contractile smooth muscle compared to SERCA2 [514-517]. The data in Figure 6.1A show dense SERCA2 staining around the periphery of ASM cells, along with some staining around the perinuclear region. The qPCR data in Figure 6.1B indicate that SERCA2B was the most highly expressed SERCA isoform in mice bronchial tissues. This suggests that in ASM cells, SERCA2B is predominantly expressed in the cell periphery near the plasma membrane, allowing it to buffer Ca^{2+} entry via LTCC.

6.2.2. Effect of SERCA inhibition on contractions of ASM evoked by activation of LTCC

To establish if inhibition of SERCA led to enhanced LTCC-dependent contractions of ASM, we investigated if contractions induced by the LTCC activator, FPL 64176 were enhanced by inhibition of SERCA using thapsigargin, which has been shown to be an irreversible inhibitor of the SERCA pump [518]. Figure 6.2A shows that FPL 64176, applied at 300 nM and 1 μM, induced a series of rapid phasic contractions. When reapplied to the same muscle strip in the presence of thapsigargin (1 μM), its effects were dramatically increased. The summary data in

Figure 6.2B shows that mean contraction area induced by FPL 64176 (300 nM) increased from 221.1 ± 172.1 mN.s under control conditions to 1072 ± 662.3 mN.s in the presence of thapsigargin ($p<0.05$, n=6). Contractions induced by FPL 64176 (1 μM) increased from 776 ± 540.5 mN.s under control conditions to 2,686 ± 1574 mN.s in the presence of thapsigargin ($p<0.05$, n=6). These data suggest that Ca^{2+} influx via LTCC in ASM cells is dampened by the Ca^{2+} buffering capacity of SERCA pumps and that inhibition of SERCA enhanced contractions that were induced by Ca^{2+} influx via LTCC.

6.2.3. Effect of SERCA inhibition on EFS and CCh-induced contractions of ASM

We next examined whether inhibition of SERCA enhanced the amplitude of cholinergic nerve-evoked contractions of ASM and, if so, whether these responses were inhibited by blockade of LTCC. The representative trace and summary data in Fig. 6.3A and B show that application of SERCA inhibitor, thapsigargin (1 μM) increased the amplitude of EFS-evoked contractions of ASM, at 100 s intervals, from 1.38 ± 0.1 mN under control conditions to 3.2 ± 0.3 mN ($p<0.01$, n=6). By way of example, reducing the stimulus interval to 10 s in the same muscle strips increased contraction amplitude to 3.5 ± 0.5 mN ($p<0.05$, n=6). Addition of nifedipine reduced the mean amplitude of responses recorded in the presence of thapsigargin to 0.7 ± 0.08 mN ($p<0.01$, n=6; Figure 6.3A and B).

Figure 6.4A shows that thapsigargin (1 μM) enhanced contractions induced by CCh that remained in the presence of 4-DAMP, and this effect was also reversed by 1 μM nifedipine. In 6 preparations, addition of thapsigargin increased mean contraction area from 1312 ± 295 to 2761 ± 312 mN.s ($p<0.001$, n=6) and addition of nifedipine reduced contraction area to 464.7 ± 165.7 mN.s ($p<0.001$, n=6, Figure 6.4B). Experiments were also performed to investigate whether thapsigargin could mimic the M2R effects and restore oscillatory contractions in M2R KO mice. As shown in Figure 6.5A, addition of 4-DAMP (3 nM) in the presence of 300 nM CCh failed to elicit oscillatory contractions, confirming the absence of functional M2R activity. However, subsequent application of thapsigargin (1 μM) induced oscillatory contractions, resembling M2R-mediated responses. This activity was also abolished by nifedipine, indicating LTCC involvement. The summary data in Figure 6.5B show that CCh increased mean contraction area to 3277 ± 386 mN.s, which was reduced

to -36.1 ± 69.2 mN.s ($p<0.01$, n=6) in 4-DAMP. Further addition of thapsigargin increased mean contraction area to 982.4 ± 257.5 ($p<0.05$, n=6) and this effect was sensitive to nifedipine, which reduced mean contraction area to 81.1 ± 47.2 ($p<0.05$, n=6). Therefore, it is evident that inhibition of SERCA enhanced cholinergic nerve-evoked contractions of ASM, similar to the effects of M2R activation, and that this effect was reliant on Ca^{2+} influx via LTCC. It is also noteworthy that nifedipine had a greater effect on EFS responses at 100 s intervals in the presence of thapsigargin than in its absence (Figure 3.1A and C).

6.2.4. Effect of Kv7 channel modulators and thapsigargin on M2R-mediated contractions of ASM

Thus far, our data indicate that thapsigargin and XE991 were both able to potentiate EFS-induced contractions of ASM, albeit to a lesser extent than reducing the stimulus interval to 10 s. Therefore, we next examined whether these effects were cumulative by investigating whether XE991 produced additional stimulatory effects on EFS-evoked contractions of ASM when thapsigargin was already present. Figure 6.6A shows that the addition of a low concentration of thapsigargin (300 nM) elevated the amplitude of EFS-induced contractions at 100 s intervals. Coadministration of 10 μM XE991 caused a further increase in contraction amplitude and also induced an increase in basal contractile activity. These effects were reversed by 1 μM nifedipine. Summary data in Figure 6.6B shows that thapsigargin increased the mean contraction amplitude from 0.72 ± 0.11 under control conditions to 1.1 ± 0.1 mN ($p<0.01$, n=6) and addition of 10 μM XE991 further increased contraction amplitude to 1.71 ± 0.12 mN ($p<0.01$, n=6). The combined effects of thapsigargin and XE991 were comparable to the effects induced by reducing the stimulus interval to 10 s (1.7 ± 0.2 mN). Nifedipine reduced contraction amplitude to 0.47 ± 0.14 mN ($p<0.001$, n=6). Together, these findings suggest that M2R-mediated Kv7 inhibition occurs independently of SERCA inhibition and that both mechanisms can synergistically enhance ASM excitability and contractility.

The experiments shown in Figures 6.7A and C demonstrate that opening of Kv7 channels with zinc pyrithione (3 μM) markedly attenuated the thapsigargin-induced enhancement of EFS-evoked contractions at 100 s intervals, reducing mean contraction amplitude from 3.2 ± 0.3 mN to 1.6 ± 0.2 mN ($p<0.05$, n=6). Figures 6.7B and D show that zinc pyrithione greatly diminished contractions evoked

by CCh in the presence of 4-DAMP and thapsigargin. Thapsigargin increased the mean contraction area recorded in the presence of CCh and 4-DAMP from 1780 ± 170.7 mN.s to 3824 ± 289.1 mN.s ($p<0.01$, n=6) and subsequent addition of zinc pyrithione decreased it to 314.8 ± 124.1 mN.s ($p<0.001$, n=6).

6.2.5. Effect of Ano1 CACC on M2R-mediated contractions of ASM

The results obtained so far indicate that M2R-dependent contractions of ASM may involve inhibition of SERCA and activation of LTCC. We reasoned that SERCA inhibition could increase Ca^{2+} concentration in the subsarcolemmal space between the SR and the plasma membrane, such that it could activate Ca^{2+}-activated channels such as Ano1 CACC. To test this, we examined the effect of a selective Ano1 inhibitor, Ani9 on EFS-induced contractions of ASM in the presence of thapsigargin. As shown in Figure 6.8A, application of 1 μM Ani9 reversed the thapsigargin-mediated enhancement of EFS-evoked contractions at 100 s intervals. The summary data in Figure 6.8B show that 1 μM thapsigargin increased mean contraction amplitude from 0.8 ± 0.1 mN to 1.7 ± 0.1 mN ($p<0.01$, n=7), and subsequent addition of Ani9 reduced the amplitude to 0.65 ± 0.04 mN ($p<0.001$, n=7). Similarly, Ani9 markedly attenuated the effect of thapsigargin on 4-DAMP-resistant contractions induced by CCh (Figures 6.9A and B). Ani9 reduced mean contraction area from 4463 ± 943.3 mN.s to 501.6 ± 340.4 mN.s ($p<0.01$, n=6), supporting a role of Ano1 CACC in thapsigargin-induced contractions of ASM.

We next investigated if activation of Ano1 channels contributed to M2R-dependent contractions of ASM. Data in Figure 6.10A shows that, similar to the effects of nifedipine, Ani9 (1 μM) had little effect on contractions of ASM induced by EFS at 100 s intervals. However, it reversed the enhancement of these contractions elicited by a reduction in stimulus interval to 10 s (from 1.4 ± 0.11 to 0.44 ± 0.08 mN, $p<0.01$, n=6, Figure 6.10B & D). Similarly, Ani9 abolished 4-DAMP-resistant contractions of ASM induced by CCh (Figure 6.11B) but had no effects on CCh responses in the absence of 4-DAMP (Figure 6.11A). Summary data in Figure 6.11D illustrates that addition of Ani9 reduced mean contraction area from 1334 ± 231 mN.s to -11.48 ± 278 mN.s ($p<0.01$, n=7). To rule out the possibility that the inhibitory effects of Ani9 involved an action on nerves, the experiment was repeated in the presence of TTX (1 μM). Figure 6.12A shows that TTX did not affect the oscillatory contractions of ASM induced by CCh or the inhibitory effects of Ani9 on these

responses. The summary data shown in Figure 6.12B demonstrate that 300 nM CCh increased mean contraction area to 6531 ± 659.7 mN.s, which was reduced to 1621 ± 405.6 mN.s upon addition of 4-DAMP ($p<0.01$, n=6). Subsequent application of 1 μM Ani9 further decreased mean contraction area to 156.7 ± 202.1 mN.s ($p<0.05$, n=6). These findings indicate that M2R-dependent contractions of ASM are inhibited by blockade of Ano1 channels.

To further examine the involvement of Ano1 channels in M2R-mediated ASM contractions, we examined the effects of another Ano1 blocker, CaCCinh-A01. As shown in Figure 6.13A, application of 10 μM CaCCinh-A01 abolished the M2R-mediated enhancement of contraction amplitude at EFS 10 s intervals, consistent with the effects observed with Ani9. The summary data in Figure 6.13C indicate that CaCCinh-A01 significantly reduced the mean contraction amplitude from 2.9 ± 0.3 mN to 1.5 ± 0.3 mN ($p<0.001$, n=6). Likewise, CaCCinh-A01 markedly inhibited CCh-induced contractions that persisted in the presence of 4-DAMP (Figure 6.13B), decreasing the mean contraction area from 1775 ± 219.4 mN.s to -39.2 ± 33.86 mN.s ($p<0.001$, n=7; Figure 6.13D). These findings suggest an important role for Ano1 channels in M2R-dependent contractions of ASM.

6.3. Discussion

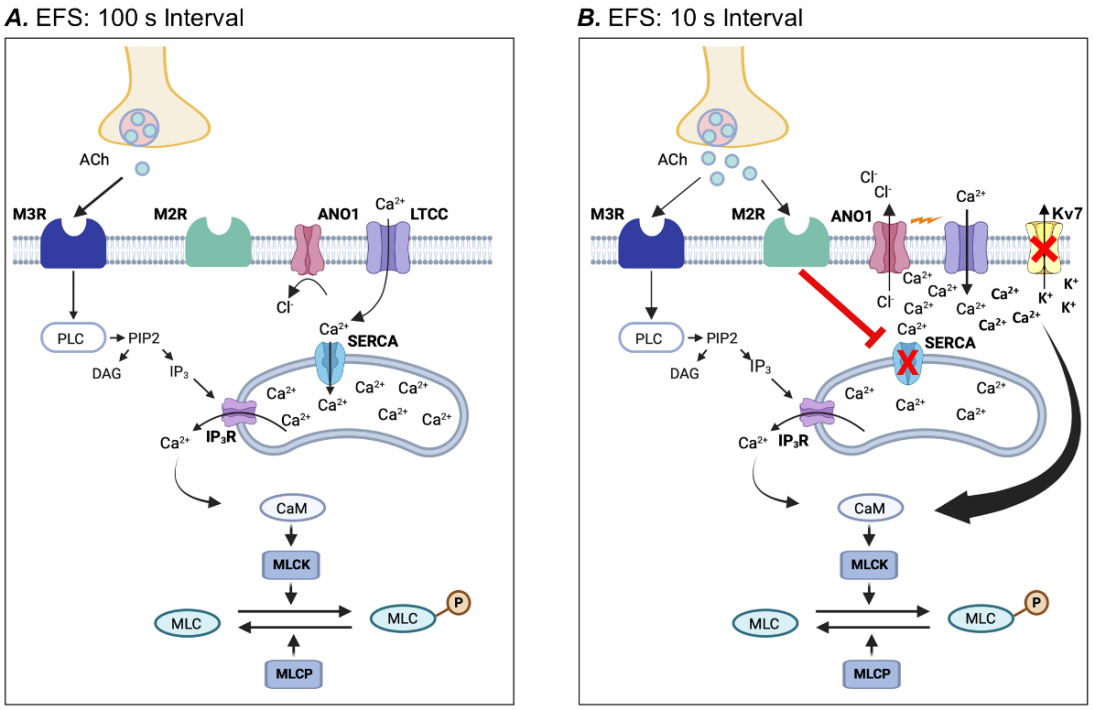

Figure 6.15. Model showing cellular mechanism underlying contractions of ASM induced by EFS at **(A)** 100 s intervals and **(B)** 10 s intervals. At 100 s intervals, EFS-evoked contractions of ASM are mediated by activation of M3Rs leading to release of Ca^{2+} from the sarcoplasmic reticulum via IP_3Rs. Ca^{2+} influx via LTCC is buffered by the activity of SERCA pumps at peripheral sarcoplasmic reticulum. Reducing the stimulus interval to 10 s leads to activation of M2Rs. M2R activation induces inhibition of SERCA, possibly via phosphorylation of phospholamban (PLB), resulting in reduced buffering of Ca^{2+} influx via LTCC. Increased Ca^{2+} levels in the subsarcolemmal space activate Ano1 CACC, leading to Cl^- efflux, inhibit Kv7 channel, causing K^+ accumulation, membrane depolarisation and further activation of LTCC. Increased cytosolic Ca^{2+} levels increase contraction amplitude. Figure created with a licensed version of BioRender.com.

The main findings of this chapter were that: 1) M2R-dependent contractions of ASM were augmented by the SERCA inhibitor, thapsigargin and these effects were inhibited by the LTCC inhibitor, nifedipine; 2) SERCA2 showed abundant distribution at the periphery of isolated ASM cells; 3) contractions of ASM evoked by direct activation of LTCC with FPL were enhanced by thapsigargin; 4) blockade of Kv7 channels with XE991 induced additional stimulatory effects to that of thapsigargin; 5) M2R-dependent contractions of ASM were inhibited by the Ano1 CACC inhibitors, Ani9 and CACCinh-A01; 6) the stimulatory effects of thapsigargin on M2R responses were also reversed by Ani9 (Figure 6.15).

We propose that activation of M2Rs leads to reduced Ca^{2+} buffering by SERCA2 located on SR present at the periphery of ASM cells, which acts as a SBB

[356-358] (Figure 6.1A). Inhibition of the SBB means that Ca^{2+} entry via LTCC is no longer buffered, resulting in accumulation of Ca^{2+} in the cytosol that can access the contractile filaments to augment ASM contraction. In addition, the rise in intracellular Ca^{2+} levels may activate Ano1 channels, resulting in membrane depolarisation and further activation of LTCC. A central tenet of the SBB hypothesis is that Ca^{2+} that enters the cell across the cell membrane is, in part, pumped into the SR before it can induce contraction [356-358]. In contrast to vascular smooth muscle, where this pathway is well recognised, its role in ASM has not been fully established. However, Janssen et al. (1999) reported that Ca^{2+} influx via LTCC in canine tracheal myocytes was heavily buffered by the activity of SERCA pumps present on the superficial SR located in close proximity to the plasma membrane [355]. Further, Janssen et al. (2001) also reported that at low levels of cholinergic stimulation, inhibition of the SERCA pump with CPA enhanced ASM contraction, as SERCA normally functions as a SBB that rapidly sequesters Ca^{2+} near the membrane and limits its access to the contractile apparatus. When this buffering is diminished, due to SERCA inhibition, the Ca^{2+} concentration increases, thereby augmenting contraction [519]. Interestingly, Mahn et al. (2009) found that SERCA protein expression was diminished in native and cultured ASM from endobronchial biopsies of patients with mild and moderate/severe asthma compared with that of healthy subjects and predicted that reduced expression or functionality of SERCA2 would potentiate Ca^{2+} influx-induced elevations of $[Ca^{2+}]_i$ [359]. Therefore, it is recognised that SERCA has the ability to regulate Ca^{2+} influx in ASM.

qPCR studies of the bronchi tissue showed that the SERCA2b isoform was the major SERCA subtype expressed (Figure 6.1B), which is in accordance with Álvarez-Santos et al. (2022) [520]. Clark et al. (2010) demonstrated that SERCA2b is predominantly expressed within 1.5 μm of the plasma membrane in pulmonary arterial smooth muscle cells, co-localising with RyR1, whereas SERCA2a and RyR3 are mainly confined to regions within 1.5 μm of the nucleus [360]. This spatial organisation suggests distinct functional roles for each SERCA subtype. The subplasmalemmal SR, enriched with SERCA2b and RyR1, regulates local Ca^{2+} dynamics associated with BK_{Ca} channel activation or Ca^{2+} extrusion via Na^+/Ca^{2+} exchanger (NCX), thereby mediating smooth muscle relaxation [360, 521]. In contrast, the perinuclear SR, containing SERCA2a together with RyR2 and RyR3,

is more directly involved in contractile Ca^{2+} release leading to smooth muscle contraction. Based on this compartmentalisation, inhibition of SERCA2b could disrupt Ca^{2+} sequestration near the plasma membrane, causing local Ca^{2+} accumulation, membrane depolarisation, and subsequent LTCC activation, resulting in smooth muscle contraction. However, if SERCA2a activity remains functional, Ca^{2+} release via RyR2 and RyR3 in the deeper SR could still elicit contraction independently of LTCC activity. Therefore, for contractions that are strictly LTCC-dependent, inhibition of both SERCA2a and SERCA2b is required, a scenario consistent with M2R activation, since M2R-mediated responses are strongly LTCC-dependent. This finding suggests that M2R activation likely inhibits both SERCA2a and SERCA2b isoforms.

The question arises as to how M2R activation could lead to inhibition of SERCA? SERCA activity is regulated by phospholamban (PLB), a small protein that interacts with SERCA [522]. When PLB is in an unphosphorylated state, it reduces the affinity of SERCA for Ca^{2+} [523, 524]. However, when it is phosphorylated by cAMP-dependent PKA, it dissociates from SERCA and its ability to inhibit SERCA activity is reduced. Therefore, pathways that activate PKA tend to promote Ca^{2+} uptake by SERCA, whereas pathways that reduce PKA activity inhibit SERCA and reduce the buffering capacity of the SR. Since M2Rs are coupled to G_i-proteins that reduce adenylate cyclase activity and cAMP levels, it is likely that M2R activation would reduce phosphorylation of PLB and inhibit SERCA [525]. However, more experiments would be required to test this idea.

We found that the Kv7 activator (zinc pyrithione) diminished the thapsigargin-mediated increase in ASM contraction (Figure 6.7). This effect is likely due to membrane hyperpolarisation caused by Kv7 channel activation, which prevents the membrane potential from reaching the threshold required to open LTCCs, thereby reducing Ca^{2+} influx and contraction. The data in this thesis suggest that stimulation of M2Rs can both inhibit Kv7 channels and SERCA. The twin action of these pathways is to drive Ca^{2+} entry via LTCC to contract ASM.

Ano1 channels and muscarinic receptors are highly expressed in ASM cells [513]. Similar to the disputed role of M2Rs and LTCC in cholinergic contractions of ASM, the contribution of Ano1 CACC has also been controversial. For example,

Danielsson et al. (2015) showed that Ano1 antagonists prevented methacholine-induced ASM contraction [266, 267], whereas Wang et al. (2018) showed that methacholine-induced contractions of ASM were still present in ASM taken from TMEM16A KO mice. Interestingly, however, it was noted that contractions induced by low (30 nmol/L or 100 nmol/L) concentrations of MCh were 50% smaller than WT controls [513]. This implies a role for Ano1 channels in cholinergic responses, but only in responses evoked by low concentrations of agonist. This is reminiscent of the effects of M2R and LTCC blockers which were also more effective against contractions of ASM evoked by low concentrations of agonist [164, 233]. For example, Farley and Miles (1978) reported that verapamil inhibits ACh contractions of dog tracheal smooth muscle at lower concentrations, but had little effect at higher concentrations [233]. Therefore, our data fit with the model that M2R-dependent contractions of ASM rely on activation of LTCC and Ano1 channels, but that these responses may be functionally diminished in experiments using high agonist concentrations that would lead to M3R-dependent Ca^{2+} release from stores and inactivation of LTCC.

Our study demonstrated that Ani9 did not affect EFS responses at 100 s intervals (Figure 6.11A). These responses are exclusively reduced by activation of M3Rs [153]. Therefore, it is apparent that the M3R-dependent contractions of ASM do not involve activation of LTCC or activation of Ano1 channels. Precise reasons as to why CACC channels are not involved in M3R responses require further investigation. However, in most smooth muscles, opening of CACC induces contraction by providing enough depolarisation to activate LTCC. Therefore, under circumstances when LTCC are inactivated by Ca^{2+}, for example, following release of Ca^{2+} from intracellular stores, then the contractile response to CACC activation may be diminished.

We observed a significant augmentation in the contraction amplitude when thapsigargin was added to EFS contractions at 100 s intervals. This increase in amplitude closely resembled EFS contractions occurring at 10 s intervals, which involve activation of M2Rs. This suggests that thapsigargin may mimic responses initiated by activation of M2Rs. Notably, the heightened contraction amplitude in the presence of thapsigargin exhibited sensitivity to both nifedipine (Figure 6.3A) and Ani9 (Figure 6.9A), mirroring the characteristics observed in EFS responses at 10 s

intervals. This is consistent with our hypothesis that inhibiting SERCA pumps, primarily situated in the superficial region adjacent to the plasma membrane, disrupts the SBB, leading to accumulation of Ca^{2+} from LTCC and activation of Ano1 channels, which acts as a positive feedback mechanism to further drive Ca^{2+} influx via LTCC, ultimately triggering ASM contraction.

In conclusion, the findings in this chapter indicate that the enhancement of cholinergic nerve mediated contractions in ASM through M2R activation may involve inhibition of SERCA and activation of Ano1 CACC.

A

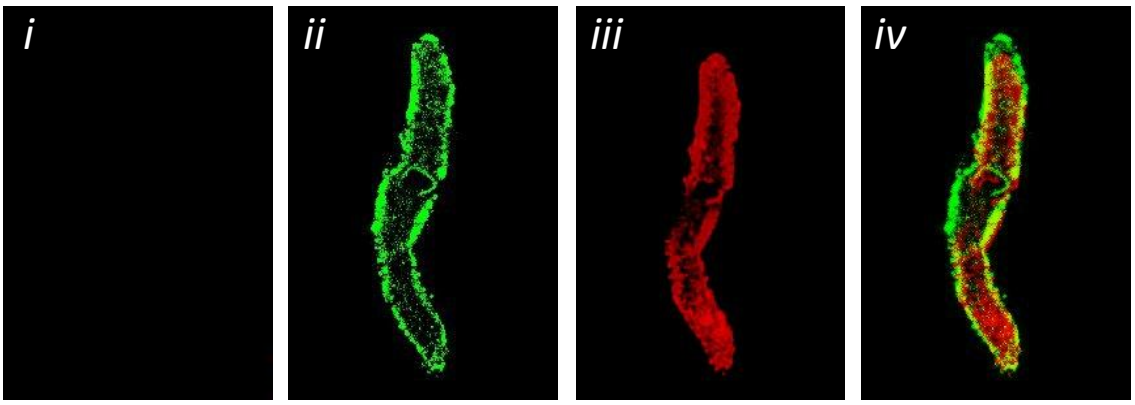

Secondary antibody only	Anti-SERCA2 (1:200) and donkey anti-rabbit Alexa Fluor-488 (1:1000)	Anti-smooth muscle α-actin (1:100) and donkey anti-mouse Alexa Fluor-555 (1:1000)	Two conjugated secondary antibodies

B

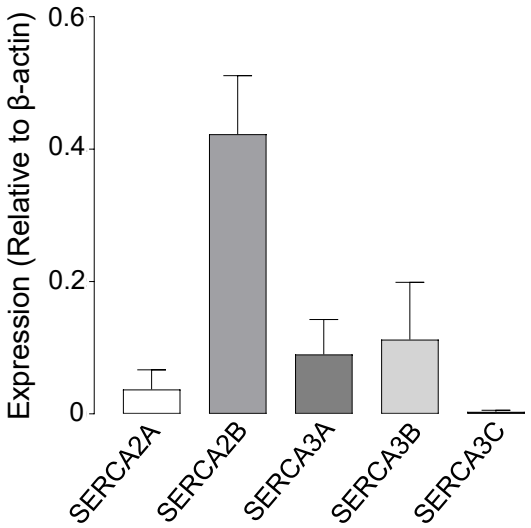

Figure 6.1. Expression of SERCA isoforms in the murine ASM.
(*A*) Representative confocal images of a freshly isolated murine ASM cell treated with antibodies against SERCA2 (*A.ii*) and α-actin (*A.iii*). *A.i* is a negative control showing image of a cell not treated with any primary antibodies and *A.iv* is an overlay image of *A.ii* & *A.iii*, respectively. **(*B*)** Summary bar chart showing relative expression of SERCA2A and B and SERCA3A-C isoforms from murine bronchi using real-time quantitative PCR (n=3, N=9).

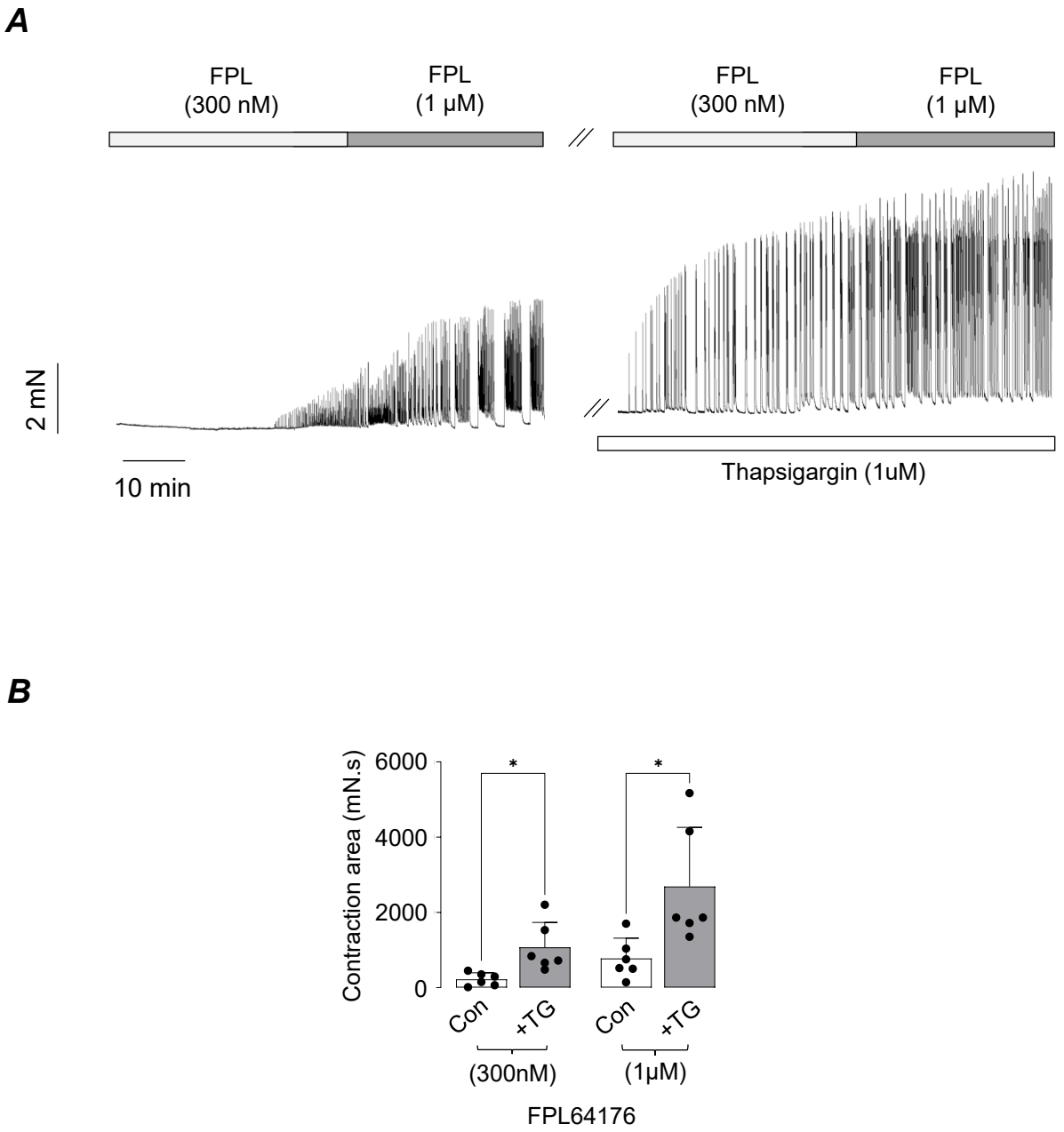

Figure 6.2. Effect of FPL64176 on contractions of ASM the absence and presence of the SERCA inhibitor, thapsigargin. (A) Representative trace showing effects of FPL64176 at 300 nM and 1 μM, before and in the presence of thapsigargin (1 μM). **(B)** Summary bar chart plotting mean contraction area induced by FPL64176 (300 nM and 1 μM) before and during the presence of thapsigargin (shaded bars) (*p<0.05, n=6, N=5, multiple paired t-test).

A

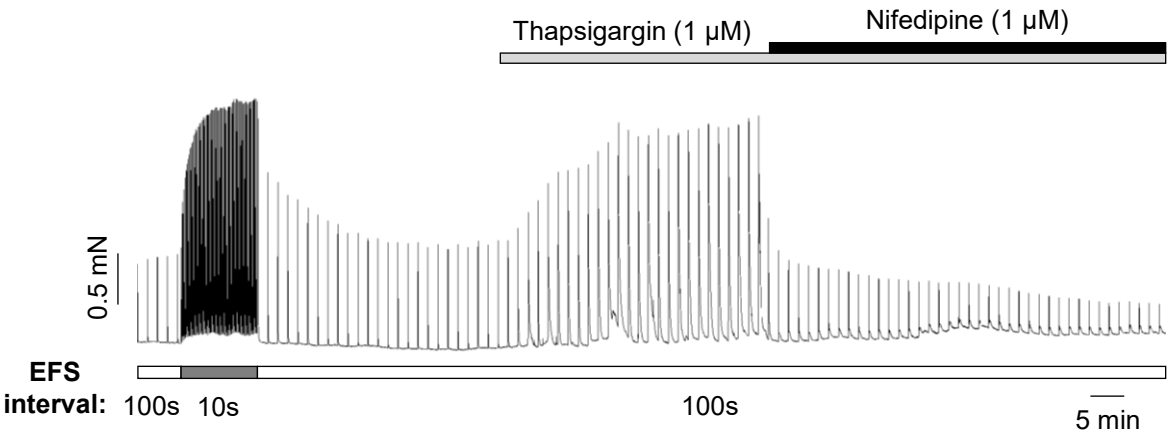

B

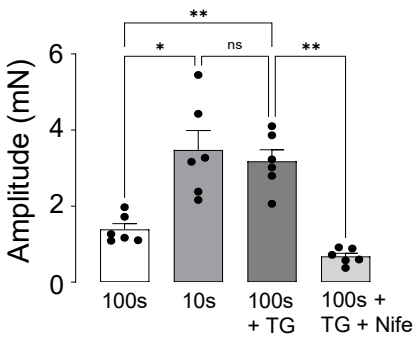

Figure 6.3. Effect of thapsigargin on contractions of ASM evoked by EFS at 100 s intervals. (A) Representative trace showing that EFS-evoked contractions of ASM at 100 s intervals were enhanced by thapsigargin (1 μM), to a similar level as a reduction in stimulus interval to 10 s. Nifedipine (1 μM) abolished the stimulatory effects of thapsigargin on contraction amplitude. **(B)** Summary bar chart showing mean peak contraction amplitude at 100 s and 10 s intervals under control conditions and at 100 s intervals in the presence of thapsigargin and thapsigargin plus nifedipine. (ns, non-significant, *p<0.05, **p<0.01, n=6, N=5, one-way ANOVA).

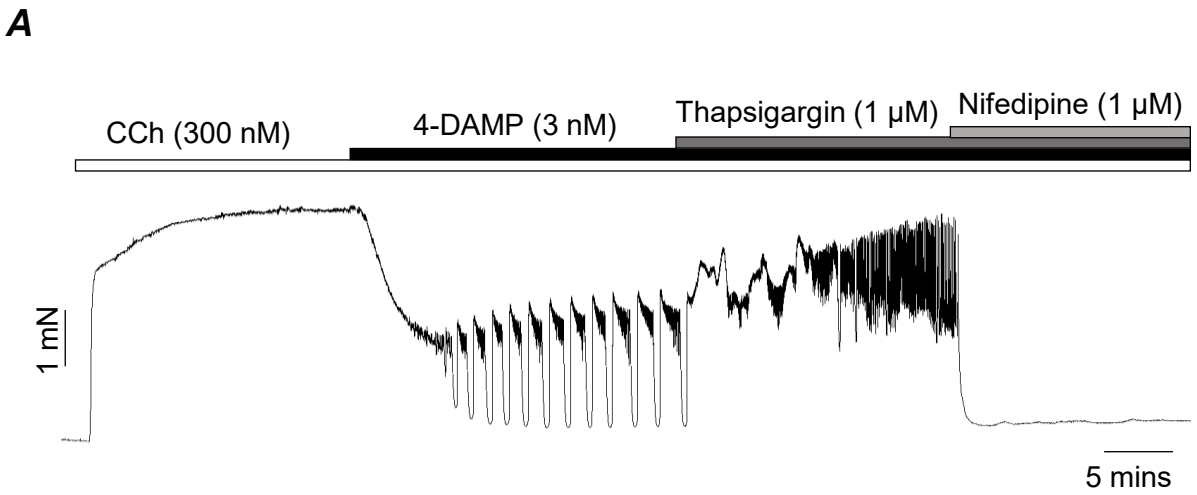

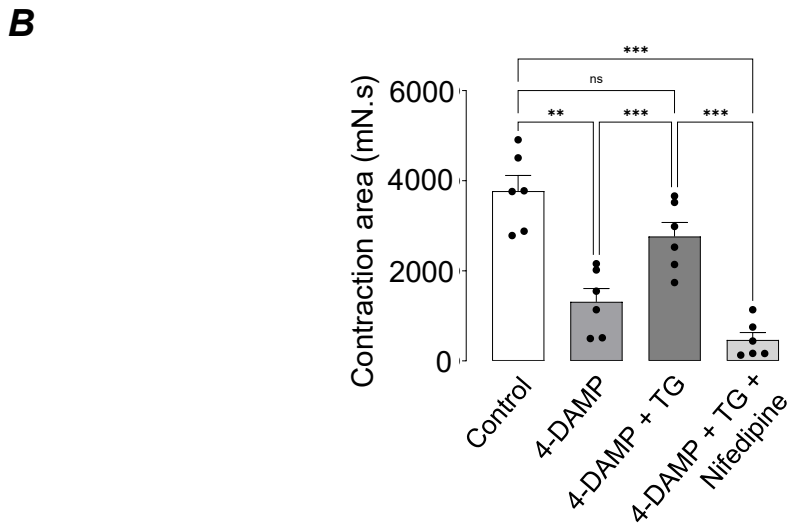

Figure 6.4. Effect of thapsigargin on 4-DAMP resistant contractions of ASM evoked by CCh. (A) Representative trace showing that 4-DAMP resistant contractions of ASM induced by CCh were enhanced by thapsigargin (1 μM) and this effect was abolished by 1 μM nifedipine. **(B)** Summary bar chart plotting mean contraction area induced by CCh before and during 4-DAMP and in the presence of 4-DAMP plus thapsigargin and 4-DAMP plus thapsigargin and nifedipine (ns, non-significant, **p<0.01, ***p<0.001, n=6, N=5, one-way ANOVA).

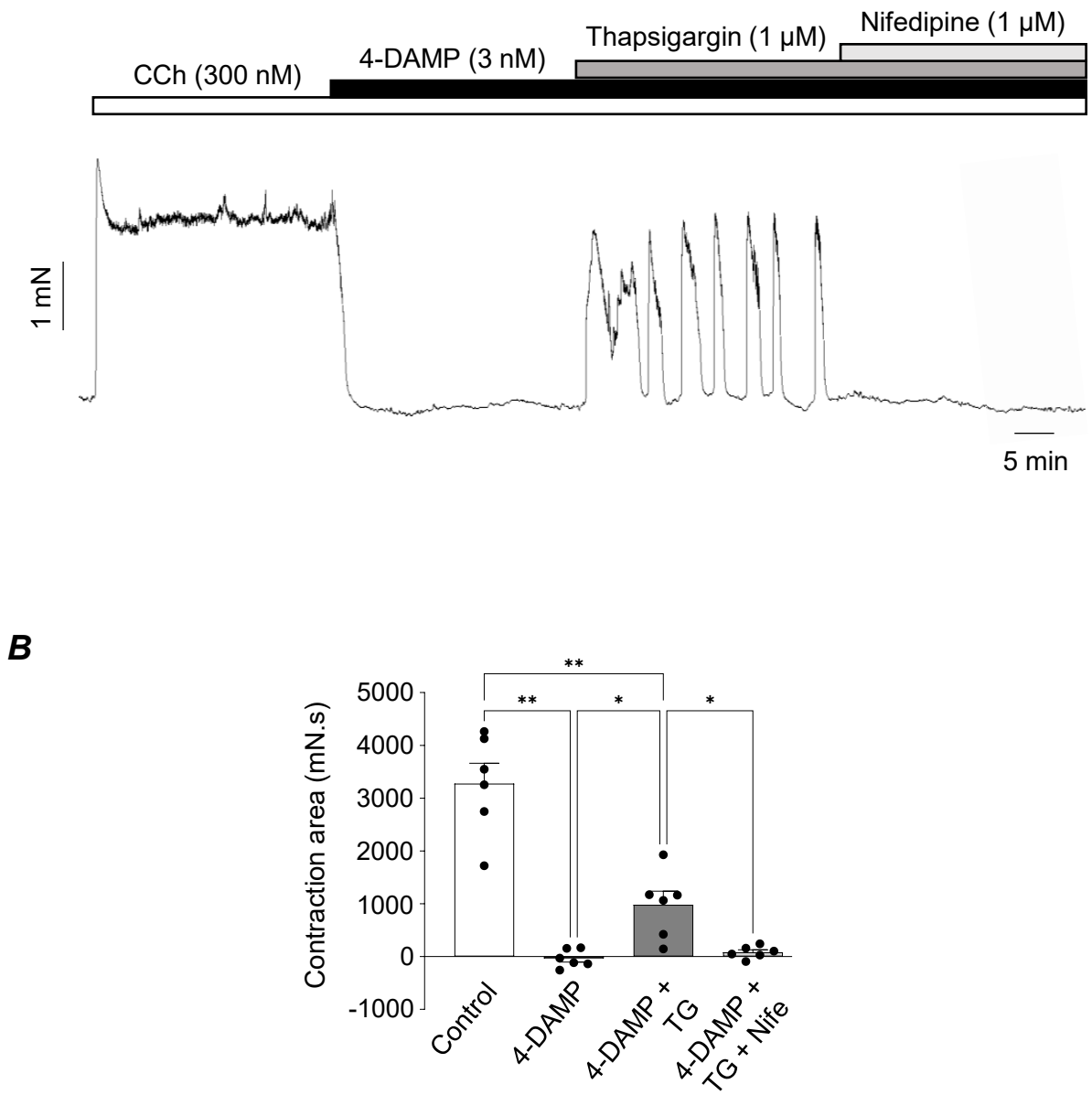

Figure 6.5. Thapsigargin induces nifedipine sensitive contractions in ASM taken from M2R KO mice. (A) Representative tension recording from a bronchial ring taken from an M2R KO mouse. CCh-evoked contractions were abolished by 4-DAMP and subsequent addition of thapsigargin (1 μM) induced phasic contractions that were abolished by nifedipine. **(B)** Summary bar chart plotting mean contraction area induced by CCh before and during 4-DAMP and in the presence of 4-DAMP plus thapsigargin and 4-DAMP plus thapsigargin and nifedipine (*p<0.05, **p<0.01, n=6, N=3, one-way ANOVA).

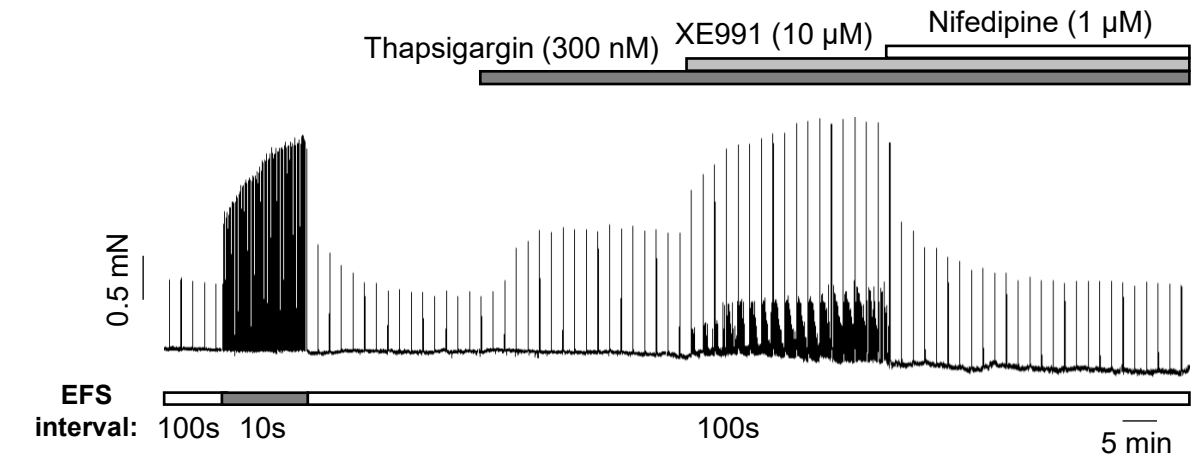

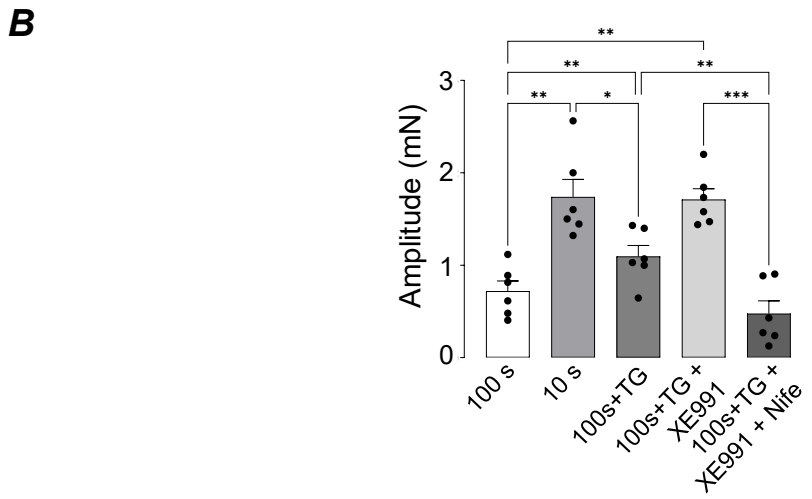

Figure 6.6. Effects of thapsigargin and XE991 on ASM contractions evoked by EFS at 100 s intervals. (A) Representative trace showing that cumulative addition of thapsigargin (300 nM) and XE991 (10 μM) induced contractions of ASM and these responses were abolished by nifedipine (1 μM). **(B)** Summary bar chart showing mean peak contraction amplitude at 100 s and 10 s intervals under control conditions and at 100 s intervals in the presence of thapsigargin, thapsigargin and XE991 and after subsequent addition of nifedipine. (*p<0.05, **p<0.01, ***p<0.001, n=6, N=5, one-way ANOVA).

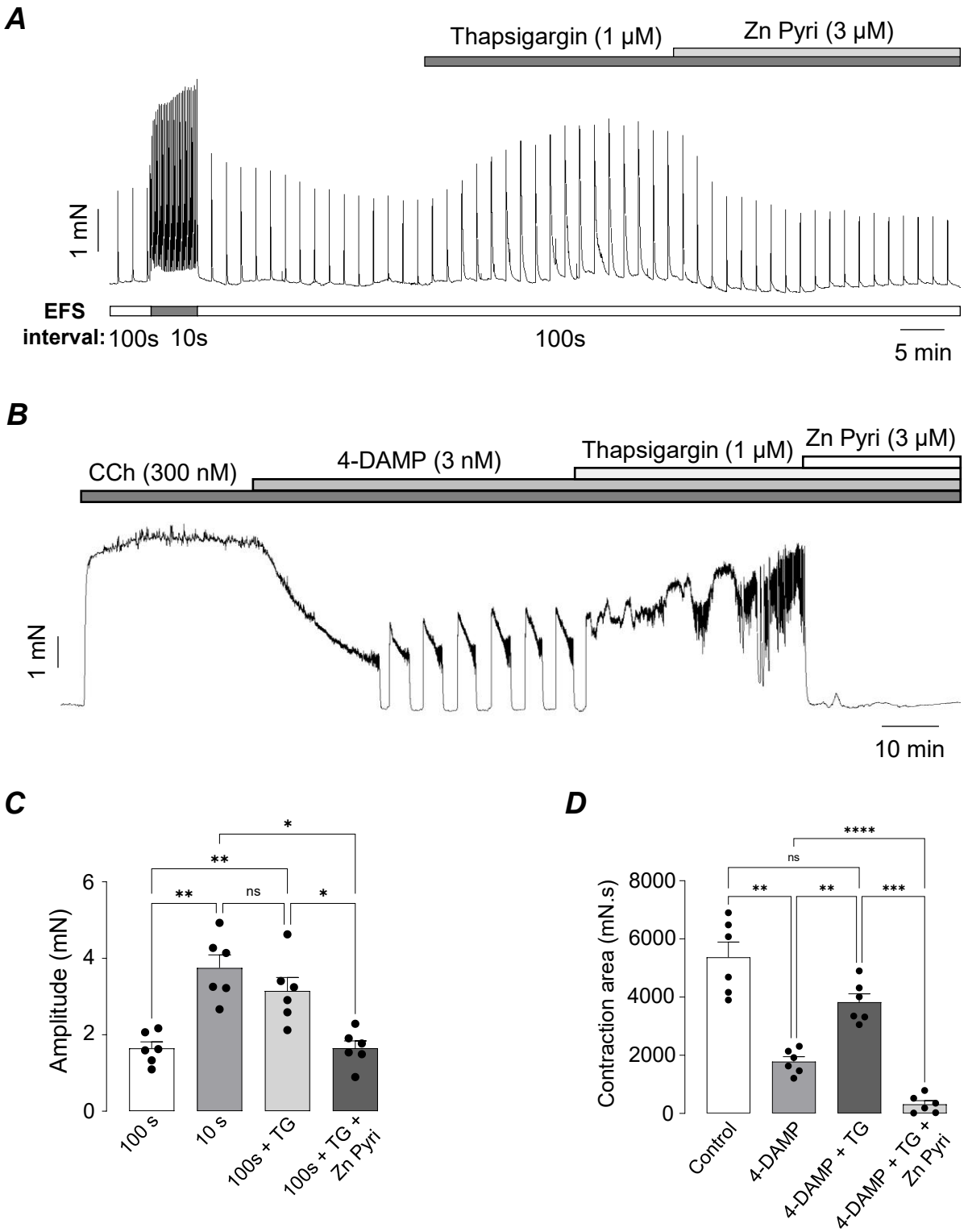

Figure 6.7. Thapsigargin-induced enhancement of cholinergic contractions of ASM are inhibited by zinc pyrithione. (A) Representative trace showing that thapsigargin (1 μM) enhanced EFS-evoked contractions at 100 s intervals, which was abolished by zinc pyrithione (3 μM). **(B)** Representative trace illustrating that thapsigargin increased contractions of ASM induced by CCh in the presence of 4-DAMP and this effect was abolished by zinc pyrithione (3 μM). **(C)** Summary bar chart showing mean peak contraction amplitude at 100 s and 10 s intervals under control conditions and at 100 s intervals in the presence of thapsigargin and thapsigargin plus zinc pyrithione. (ns, non-significant, *p<0.05, **p<0.01, n=6, N=4, one-way ANOVA). **(D)** Summary bar graph showing mean contraction areas under control, 4-DAMP, 4-DAMP plus thapsigargin, and 4-DAMP plus thapsigargin plus zinc pyrithione conditions (ns, non-significant, p<0.01, *p<0.001, **p<0.0001, n=6, N=4, one-way ANOVA).

A

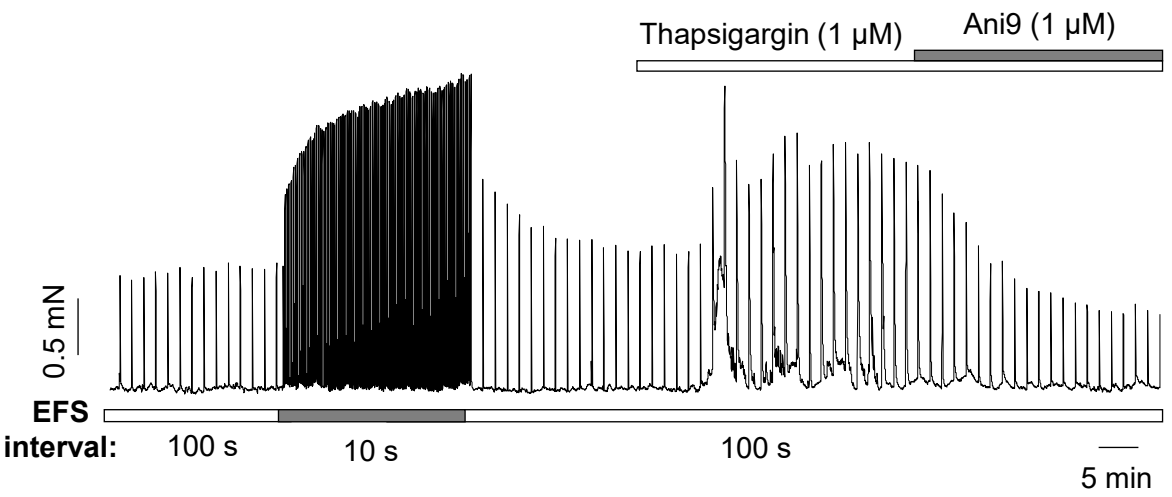

B

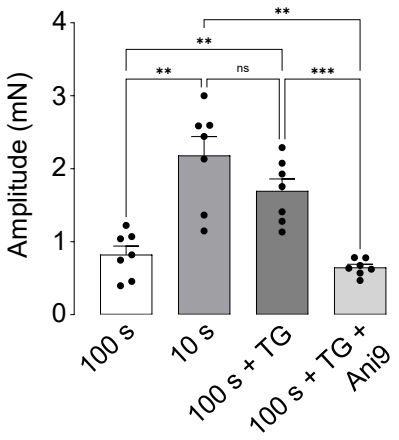

Figure 6.8. Effect of thapsigargin and Ano1 channel blocker, Ani9 on EFS-evoked contractions of ASM at 100 s intervals. (A) Representative trace showing that EFS-evoked contractions of ASM at 100 s intervals were enhanced by thapsigargin (1 μM) and that this effect was reversed by Ani9 (1 μM). **(B)** Summary bar chart showing mean peak contraction amplitude at 100 s and 10 s intervals under control conditions and at 100s intervals in the presence of thapsigargin and thapsigargin plus Ani9. (ns, non-significant, **p<0.01, ***p<0.001, n=7, N=4, one-way ANOVA).

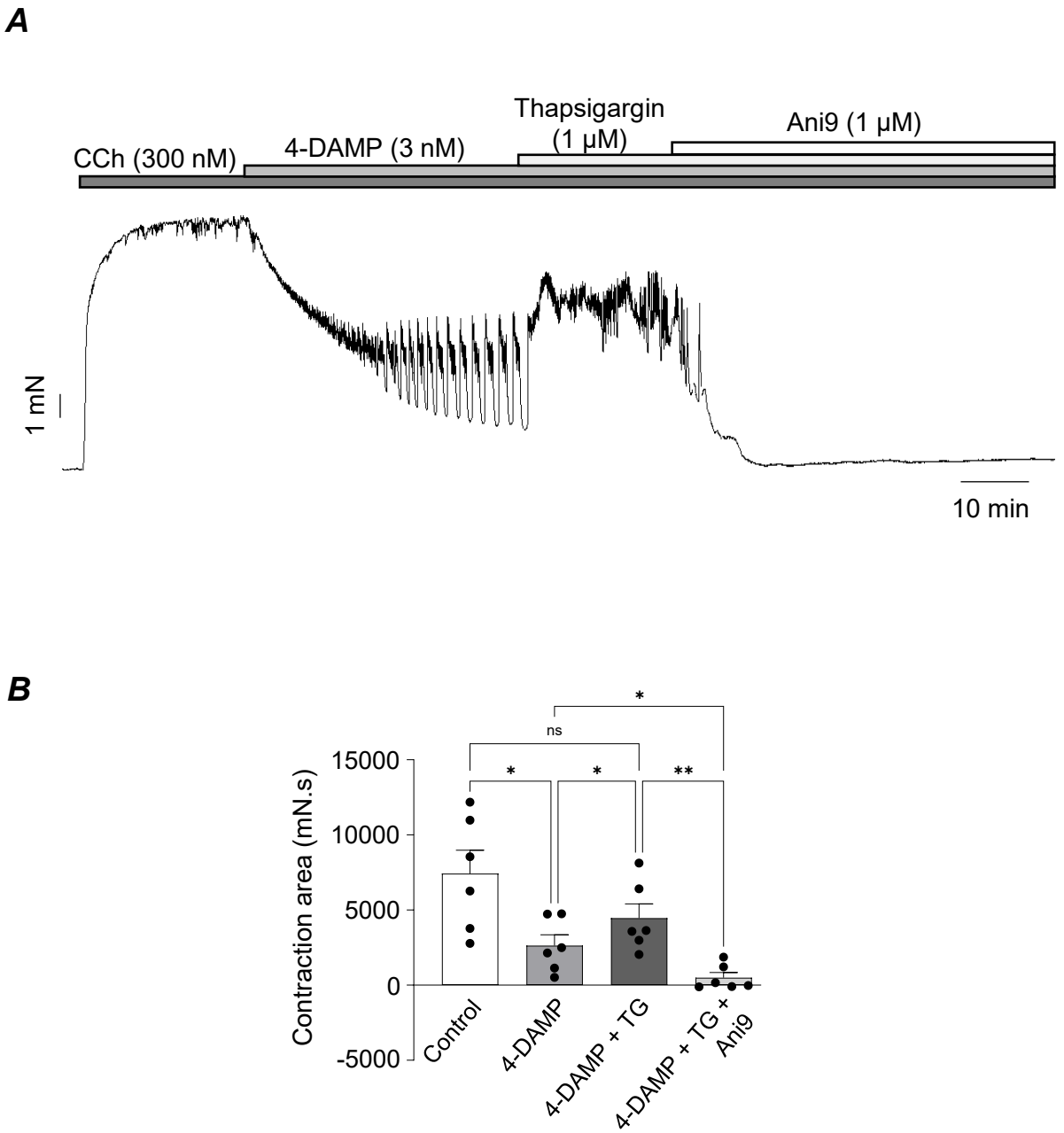

Figure 6.9. Effect of thapsigargin and Ani9 on CCh evoked contractions of ASM that remained in the presence of 4-DAMP. (A) Representative trace showing that thapsigargin (1 μM) enhanced contractions when applied in the presence of CCh and 4-DAMP, and that this effect was subsequently reversed by Ani9 (1 μM). **(B)** Summary bar chart showing the mean contraction area induced by CCh under control conditions, in the presence of 4-DAMP, following addition of thapsigargin in the presence of 4-DAMP, and after subsequent application of Ani9 (ns, non-significant, *p<0.05, **p<0.01, ***p<0.001, n=6, N=5, one-way ANOVA).

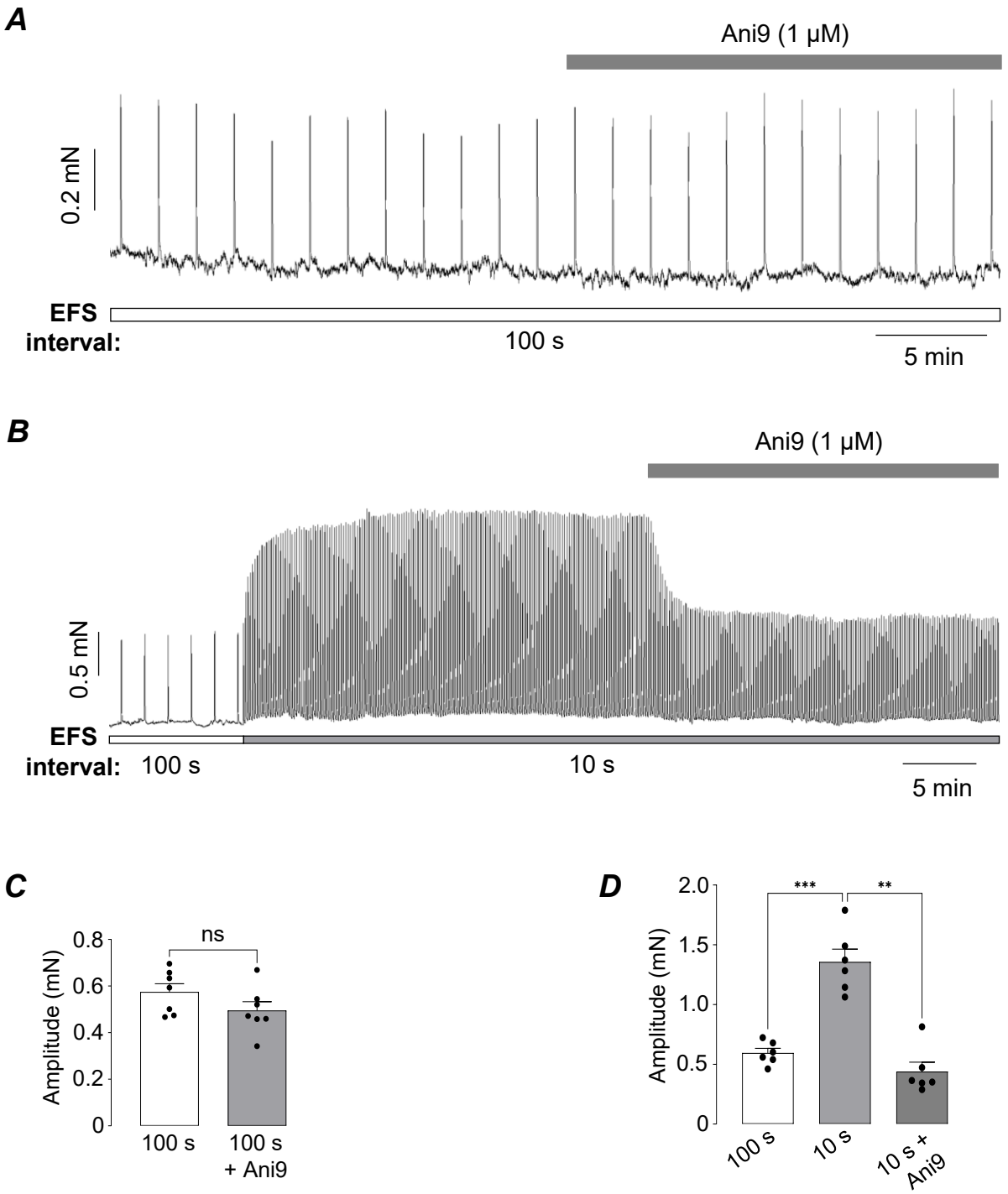

Figure 6.10. Effect of Ani9 on EFS-induced contractions of ASM.
(A) and **(C)** Representative trace and summary bar chart showing that Ani9 (1 μM) did not affect contractions of ASM induced by EFS (2 Hz) at 100 s intervals (ns, non-significant, n=7, N=5, paired t-test). **(B)** Representative trace shows that decreasing the stimulus interval from 100 to 10 s increased contraction amplitude. Application of Ani9 (1 μM) reduced the amplitude of contractions evoked at 10 s intervals. **(D)** Summary plot of mean peak contraction amplitude at 100 s intervals and at 10 s intervals before and during the presence of Ani9 (**p<0.01,***p<0.001, n=6, N=6, one-way ANOVA).

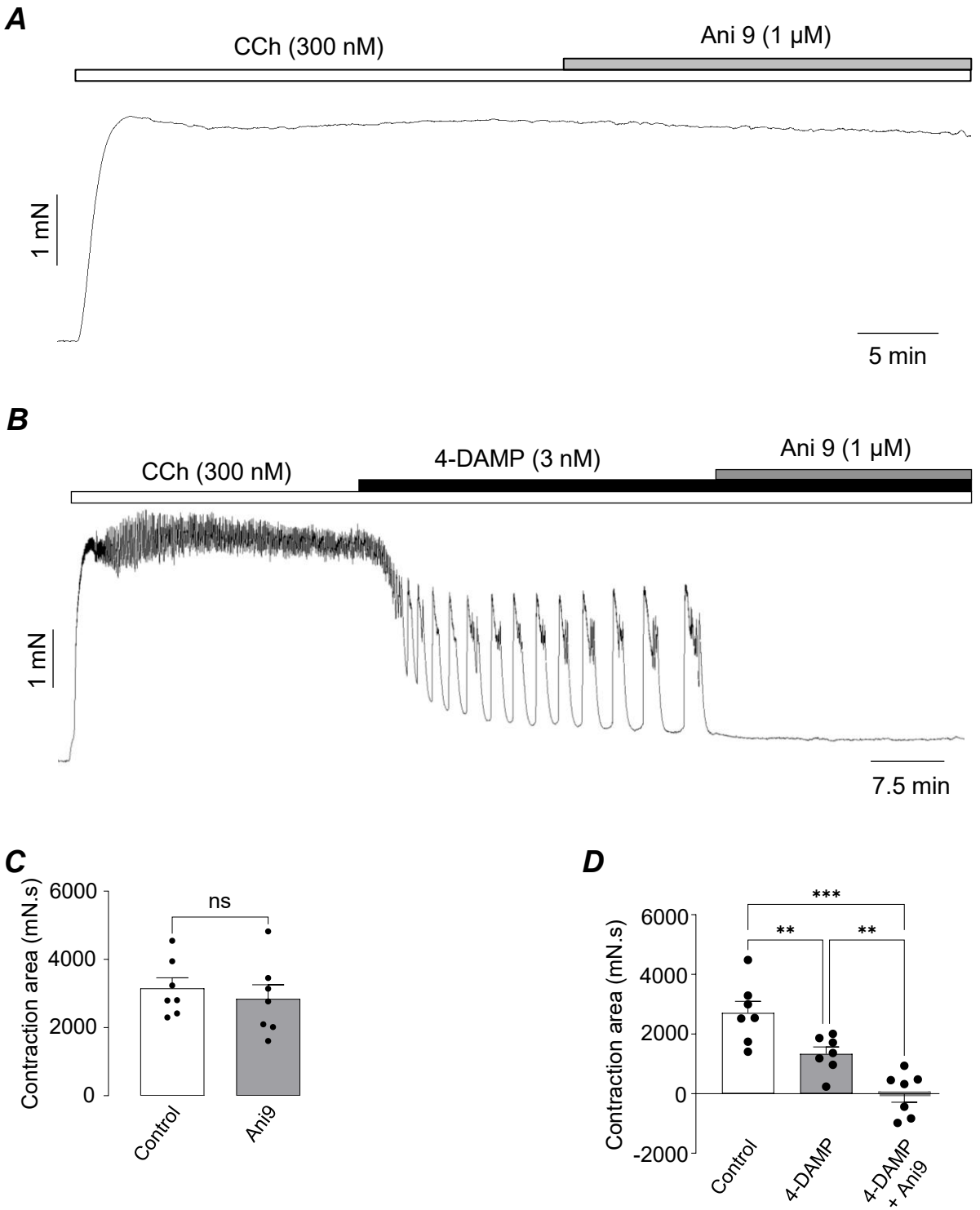

Figure 6.11. Effect of Ani9 on CCh-induced contractions of ASM
(A) Representative trace showing the effect of Ani9 (1 µM) on CCh-induced tonic contractions of ASM. **(B)** Representative trace illustrating that CCh (300 nM)-induced contractions persisting in the presence of 4-DAMP were abolished by Ani9 (1 µM). **(C)** Summary bar graph showing the mean contraction area induced by CCh under control conditions and following addition of Ani9 (ns, non-significant, n=7, N=6, paired t-test). **(D)** Summary bar graph showing the mean contraction area induced by CCh under control conditions, in the presence of 4-DAMP, and in the presence of 4-DAMP plus Ani9 (**p<0.01, ***p<0.001, n=7, N=7, one-way ANOVA).

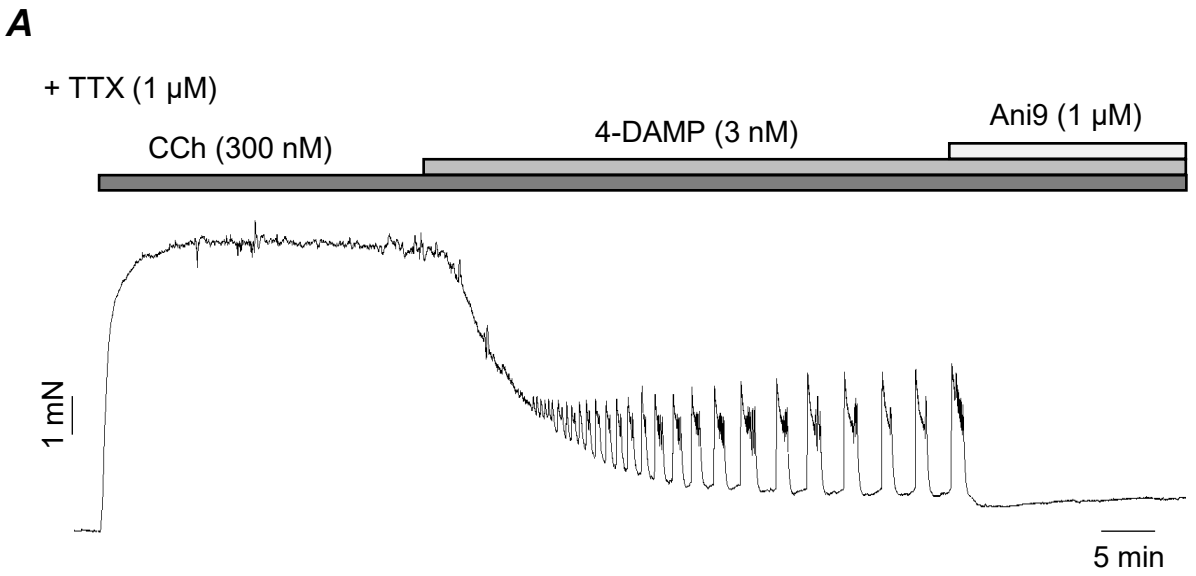

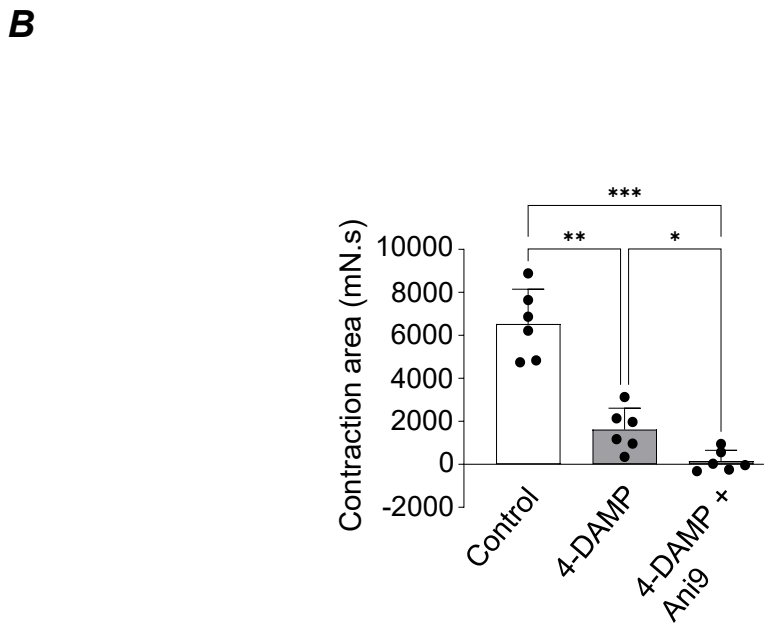

Figure 6.12. Effects of Ani9 on CCh evoked contractions of murine bronchial rings that remained in the presence of 4-DAMP. (A) Representative isometric tension trace showing CCh (300 nM)-induced contractions in the presence of 4-DAMP (3 nM), illustrating the characteristic M2R-mediated oscillatory activity. Subsequent addition of Ani9 (1 µM) abolished these oscillations. TTX (1 µM) was added into bath before start of the experiment. **(B)** Summary bar chart plotting CCh contraction amplitude (measured by area under the curve) before and during the presence of 4-DAMP and 4-DAMP + Ani9 (*p<0.05, **p<0.01, ***p<0.001, n=6, N=6, one-way ANOVA).

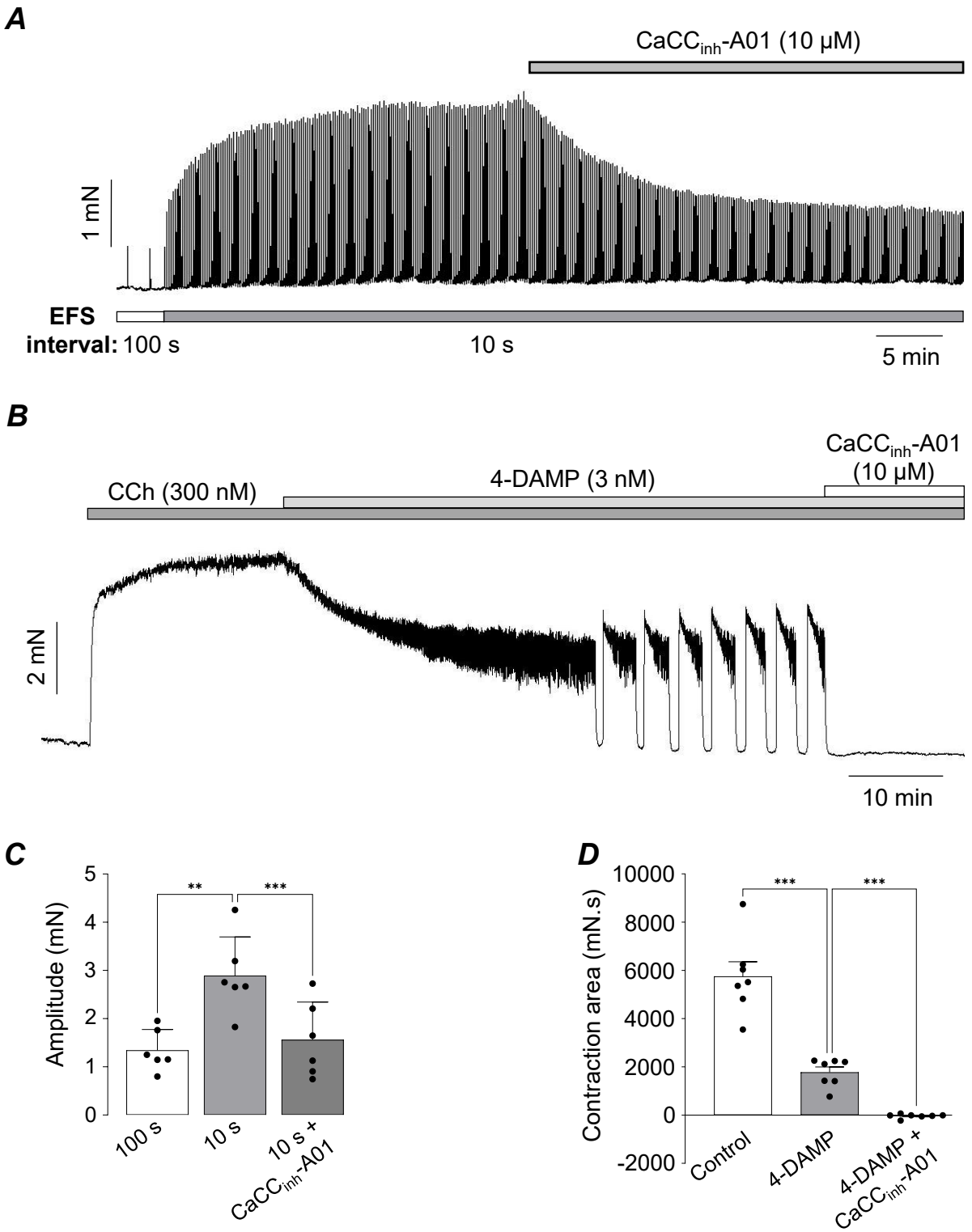

Figure 6.13. Effect of CaCCinh-A01 on EFS and CCh-induced M2R contractions of ASM. (A) Representative trace showing the effect of CaCC$_{inh}$-A01 (10 µM) on EFS-mediated contractions of ASM evoked at 10 s intervals **(B)** Representative trace illustrating that CCh (300 nM)-induced contractions persisting in the presence of 4-DAMP were abolished by CaCC$_{inh}$-A01 (10 µM). **(C)** Summary bar graph showing the mean contraction amplitude induced by EFS under 100 s and 10 s interval and following addition of CaCC$_{inh}$-A01 (**p<0.01, ***p<0.001, n=6, N=6, one-way ANOVA). **(D)** Summary bar graph showing the mean contraction area induced by CCh under control conditions, in the presence of 4-DAMP, and in the presence of 4-DAMP and CaCC$_{inh}$-A01 (***p<0.001, n=7, N=7, one-way ANOVA).

Chapter 7

General discussion

ASM contraction represents a critical determinant of airway tone and AHR in diseases such as asthma and COPD [54, 526, 527]. Parasympathetic activity is enhanced in asthma and COPD and is regarded as the major reversible component of airway obstruction [398-400, 528-530]. Asthmatic patients are hypersensitive to cholinergic agonists and anticholinergics are used to treat both COPD and asthma [397, 531-533]. ACh induces bronchoconstriction primarily by binding to muscarinic receptors on ASM cells [165, 167]. Muscarinic receptors are categorised into five subtypes (M1R-M5R), each encoded by a distinct gene, although ASM cells mainly possess M2Rs and M3Rs [156, 167, 534-536]. The ratio of M2Rs to M3Rs in ASM is approximately 4:1 in most species, yet ACh-induced contractions of ASM are thought to be primarily mediated by M3Rs [537, 538]. M3Rs are coupled to G_q proteins which induce contractions of ASM by activating the PLC signalling cascade to increase IP_3 levels and stimulate Ca^{2+} release from intracellular stores [222, 538, 539]. Despite the abundance of M2Rs in ASM, it was widely thought that they had no direct role in ASM contractions induced by activation of cholinergic nerves [399, 540-542]. However, several studies have shown that cholinergic contractions are still present in M3RKO mice and that knockout of both M2R and M3Rs was required to completely abolish cholinergic responses [145, 166]. Studies in murine ileum and trachea have shown that involvement of M2Rs is evident in contractions evoked by low concentrations of agonists, suggesting that experimental parameters greatly impact these responses [163]. The present thesis systematically explored the mechanisms underlying M2R-dependent contractions of ASM, revealing roles for Ca^{2+} influx via LTCC, inhibition of Kv7 channels, inhibition of SERCA and activation of Ano1 channels (Figure 7.1).

Alkawadri et al. (2022) showed that activation of post-junctional M2Rs made a direct contribution to ASM contraction, rather than merely opposing β-adrenergic effects [153]. They demonstrated that nerve-evoked contractions of ASM evoked by low-frequency EFS (2 Hz) were enhanced when the stimulus interval was reduced from 100 to 10 s. This enhancement was abolished by selective M2R antagonists (methoctramine and AFDX-116) and was absent in M2R KO mice, confirming that the response was mediated by M2Rs. CCh-evoked contractions of ASM that remained in the presence of the M3R antagonist 4-DAMP were also blocked by M2R

antagonists, confirming involvement of M2Rs in cholinergic contractions of ASM [153].

We demonstrated that potentiation of cholinergic, nerve-evoked ASM contractions induced by M2R activation was mediated by Ca^{2+} influx through LTCCs. While ACh-induced contractions have long been attributed to Ca^{2+} release from intracellular stores via IP_3Rs and RyRs, the role of Ca^{2+} entry through LTCCs in these responses is disputed as the effect of blockers of these channels on cholinergic agonist-induced contractions of ASM has been mixed. For example, Farley & Miles (1978) reported that verapamil diminished ACh-induced contractions of canine trachea, but only those responses evoked by low (<1 μM) concentrations of ACh [233]. In contrast, Chen & Sanderson (2017) showed that the LTCC inhibitors, nifedipine and nimodipine only induced a partial relaxation of murine airways precontracted with methacholine [228]. Hirota et al. (2007) reported that nifedipine reduced the amplitude of ACh-induced contractions of bovine trachea by 50% but concluded that this was attributable to an effect on refilling of intracellular Ca^{2+} stores [543]. Byron et al. (2013) comprehensively reviewed this issue, reporting that LTCC blockers such as nifedipine are more effective at inhibiting submaximal cholinergic responses than those induced by maximal agonist concentrations, suggesting that LTCC-mediated Ca^{2+} influx dominates at low agonist levels [234]. Consistent with these observations, we found that nifedipine abolished the enhanced contractile responses observed at short stimulation intervals (10 s) which involve M2R activation, but not those at 100 s intervals which are primarily mediated by M3Rs. Similarly, M2R-dependent phasic contractions induced by low concentrations of CCh (300 nM), in the presence of the M3R antagonist 4-DAMP, were abolished by nifedipine. These findings support the concept that M2R-mediated cholinergic responses rely on Ca^{2+} influx via LTCC, as opposed to the pharmacomechanical coupling that dominates at high agonist concentrations through IP_3-mediated SR Ca^{2+} release [267]. The reliance of M2R-mediated contractions on Ca^{2+} influx via LTCC may provide a mechanistic explanation as to why the contribution of M2Rs to airway cholinergic contractions has been underestimated in earlier studies. LTCCs are known to undergo CDI at high $[Ca^{2+}]_i$, thereby reducing their contribution under conditions of strong M3R stimulation or SR Ca^{2+} release [544]. Unno et al. (2005) proposed a similar phenomenon in ileal smooth muscle, whereby LTCCs are

inactivated following large Ca^{2+} transients [163]. Therefore, M2R-dependent responses could be masked in preparations exposed to high agonist concentrations that promote M3R dominance.

ASM cells express several TRP channel subtypes, including members of the TRPC and TRPV families [241, 246, 450], which have been implicated in cholinergic signalling and AHR associated with asthma and COPD. Pharmacological inhibition of these channels using selective antagonists has demonstrated therapeutic potential in animal models. For instance, Pyr3, a TRPC3/6 antagonist, was shown by Wang et al. (2017) to reduce ASM proliferation and migration in OVA-sensitised mice [545]. Similarly, Mažerik et al. (2023) reported that treatment with the TRPV4 antagonist, HC-067047 alleviated asthmatic symptoms, reducing cough frequency, specific airway resistance (sRaw), and ACh-induced contractions in an experimental guinea pig model of ovalbumin-induced allergic asthma [546]. In contrast, HC-070, a potent and selective TRPC4/5 inhibitor, has not yet been tested in airway or lung models but has been shown to alleviate mechanical hypersensitivity in rodent models of visceral and neuropathic pain, suggesting potential for targeting TRPC4/5-mediated Ca^{2+} entry in respiratory pathophysiology [547]. A major focus of this thesis was to investigate the mechanisms which coupled activation of M2Rs to Ca^{2+} entry via LTCC. As activation of muscarinic receptors has previously been shown to activate mICAT in gastrointestinal smooth muscle cells, mediated by activation of TRP channels [243, 244], we examined the effect of several TRP channel blockers on the M2R responses. However, we observed that the enhancement of nerve-evoked ASM contractions induced by M2R activation was unaffected by Pyr3, HC-070, or HC-067047 (Figure 3.6). These findings indicate that, although M2R-mediated responses depend on voltage-dependent Ca^{2+} entry, they are not mediated through activation of TRPC3/6, TRPC4/5 or TRPV4 channels.

ASM possess BK_{Ca} and Kv7 channels, which are known to be regulated by activation of muscarinic receptors [286, 461, 464]. Therefore, we next investigated if the M2R responses involved inhibition of these channels. Our data revealed that blockade of Kv7 channels with XE991 markedly potentiated nerve-evoked contractions of ASM, mimicking the effects of M2R activation. In contrast, inhibition of BK_{Ca} channels with iberiotoxin produced only minor effects, indicating that BK_{Ca} channels are not the primary targets of M2R signalling. These observations align

with the findings of Semenov et al. (2011), who showed that BK_{Ca} β_1 subunits antagonise M2R-mediated contraction [164]. Using qPCR, we detected prominent expression of Kv7.1, Kv7.4 and Kv7.5 in murine ASM, consistent with expression patterns reported by Brueggemann et al. (2018) and Haick & Byron (2016) [299, 494]. Functionally, selective activation of Kv7.4 with ICA069673 and of Kv7.4/7.5 with ML213 abolished M2R-dependent contractions, confirming that opening these channels could suppress M2R responses. M2R responses were unaffected by Kv7.1 modulators.

This study provides the first direct evidence that M2R activation suppresses Kv7 currents in a heterologous expression system, extending the earlier findings of Shapiro et al. (2000) who showed muscarinic inhibition of M1R-Kv7.2/7.3 currents [468] and Guo and Schofield (2003) who found that activation of M3R with oxotremorine-M produced a robust suppression of the M-current in HEK293 cells expressing M3R and KCNQ2/3 [548]. Importantly, the inhibitory effects of M2R activation on Kv7.4, but not Kv7.5, was suppressed in cells dialysed with PIP_2 diC8, suggesting that the inhibitory effects of M2R activation on Kv7.4 may involve depletion of PIP_2. In contrast, the PKA activator 6-Mb-cAMP potentiated Kv7.5 but not Kv7.4 currents, suggesting that the effects of M2R activation on Kv7.5 could be associated with decreased cAMP/PKA signalling. Unlike M3Rs, which couple to G_q proteins and activate PLC, M2Rs are coupled to G_i proteins which inhibit adenylate cyclase. Therefore, it is not immediately intuitive as to how M2R activation could lead to depletion of PIP_2. However, Pfeil et al. (2020) showed that $G_{\beta\gamma}$ subunits released from Gi proteins can activate PLC_β following priming by G_q subunits, suggesting a molecular basis for M2R-M3R crosstalk [134]. In the context of ASM, this could mean that M3R-mediated G_q signalling initiates contraction, while concurrent M2R activation sustains depolarisation by inhibiting Kv7 channels, thereby maintaining LTCC activity. Collectively, these findings provide a new mechanistic framework in which M2R activation enhances ASM contractility by inhibiting Kv7.4 and Kv7.5 channels via PIP_2 depletion and down-regulation of cAMP/PKA, respectively [549]. Inhibition of Kv7 channels could depolarise membrane potential and promote LTCC-mediated Ca^{2+} influx, thereby coupling M2R signalling directly to excitation-contraction mechanisms.

Experiments in chapter 6 revealed that M2R-dependent contractions of ASM were potentiated by the SERCA inhibitor thapsigargin. These effects were abolished by nifedipine, and thapsigargin was also able to enhance contractions induced by direct activation of LTCC with FPL. SERCA was found to be primarily located around the periphery of the ASM cell, indicating that inhibition of SERCA pumps could diminish Ca^{2+} buffering of Ca^{2+} entry across the plasma membrane. We propose that activation of M2Rs disrupts SERCA activity that would normally limit access of Ca^{2+} influx via LTCC to the contractile machinery [355]. Consequently, during M2R stimulation, we propose that inhibition of Kv7 currents enhances Ca^{2+} entry via LTCC to initiate contraction and that this process is potentiated by reduced buffering of Ca^{2+} influx by SERCA pumps.

Clark et al. (2010) demonstrated distinct spatial segregation of SERCA2 isoforms in pulmonary arterial smooth muscle cells, with SERCA2b enriched in the subplasmalemmal SR and SERCA2a localised more perinuclearly [360]. Thapsigargin is more lipophilic and exhibits higher affinity (1000 times) toward SERCA2b than CPA. Our data are consistent with the idea that M2R activation inhibits SERCA2b, disrupting the SBB, allowing Ca^{2+} to access the contractile machinery of the cell and also activate plasmalemmal Ano1 channels, to further depolarise membrane potential and drive Ca^{2+} influx via LTCC. Thapsigargin also inhibits SERCA2a, and if this isoform remains active, Ca^{2+} release via RyR2 and RyR3 in the deeper SR could still drive contraction independently of LTCCs. Thus, a purely LTCC-dependent contraction requires inhibition of both SERCA2a and SERCA2b, consistent with the effects of M2R activation. These observations suggest that M2R activation likely suppresses both SERCA2a and SERCA2b activity.

Mechanistically, it is possible that the G_i-coupled nature of M2Rs contributes to SERCA inhibition via reduced cAMP/PKA signalling and consequent dephosphorylation of PLB, a negative regulator of SERCA activity [524]. Reduced phosphorylation of PLB would decrease SERCA Ca^{2+} affinity, thus impairing SR Ca^{2+} uptake and enhancing cytosolic Ca^{2+} accumulation. Danielsson et al. (2015) and Wang et al. (2018) provided contrasting reports on the role of Ano1 in cholinergic contraction; however, both noted that its contribution was most evident at low agonist concentrations, conditions under which M2R-LTCC signalling predominates

[265, 266]. In agreement with these findings, our study showed that inhibition of Ano1 with Ani9 abolished thapsigargin enhanced and M2R-dependent contractions, suggesting that Ano1 could participate in a positive feedback mechanism sustaining depolarisation and Ca^{2+} entry.

The findings presented in this thesis could have important physiological and therapeutic implications. Firstly, we suggest that M2Rs act as amplifiers of ASM responsiveness under conditions of modest ACh elevation, such as during airway inflammation when non-neuronal ACh release occurs [550-552]. Secondly, we identified Kv7.4/7.5 channels and SERCA2 as potential pharmacological targets for modulating ASM tone. Kv7 activators or drugs that enhance SERCA function could represent novel therapeutic strategies for reducing airway hyperreactivity. Finally, the interplay between M2R activation, PIP_2 depletion and cAMP suppression highlights potential molecular convergence points that could be targeted to attenuate excessive ASM excitability in obstructive airway diseases.

The clinical relevance of the mechanisms identified in the present study will ultimately be contingent upon the degree to which they apply in human ASM. The present study was performed on mice, which may be useful for the investigation of airway physiology [553], but are limited in modelling airway disease, as mouse models of asthma and COPD do not fully replicate the inflammatory, immune and histological changes that occur in humans [554]. In the future, we would like to repeat these experiments in human bronchi, with intact cholinergic responses [554] but suggest that the present study provides a basis for these investigations. Interestingly, Mahn et al. (2009) showed that SERCA protein expression was diminished in native and cultured ASM from endobronchial biopsies of patients with mild and moderate/severe asthma compared with that of healthy subjects [359]. Therefore, it is possible that dysregulation of the SBB and enhanced $[Ca^{2+}]_i$ levels following Ca^{2+} entry via LTCC contribute to AHR in asthmatic patients.

In summary, this thesis puts forward several mechanisms by which post-junctional M2R activation enhances ASM excitability, including inhibition of Kv7.4/7.5 channels, suppression of SERCA-mediated Ca^{2+} buffering and activation of Ano1 and LTCC. These pathways operate in concert to sustain depolarisation and Ca^{2+} influx, leading to enhanced contraction. The findings advance our understanding of

cholinergic control of airway tone and provide a foundation for developing targeted interventions to alleviate AHR in asthma and COPD.

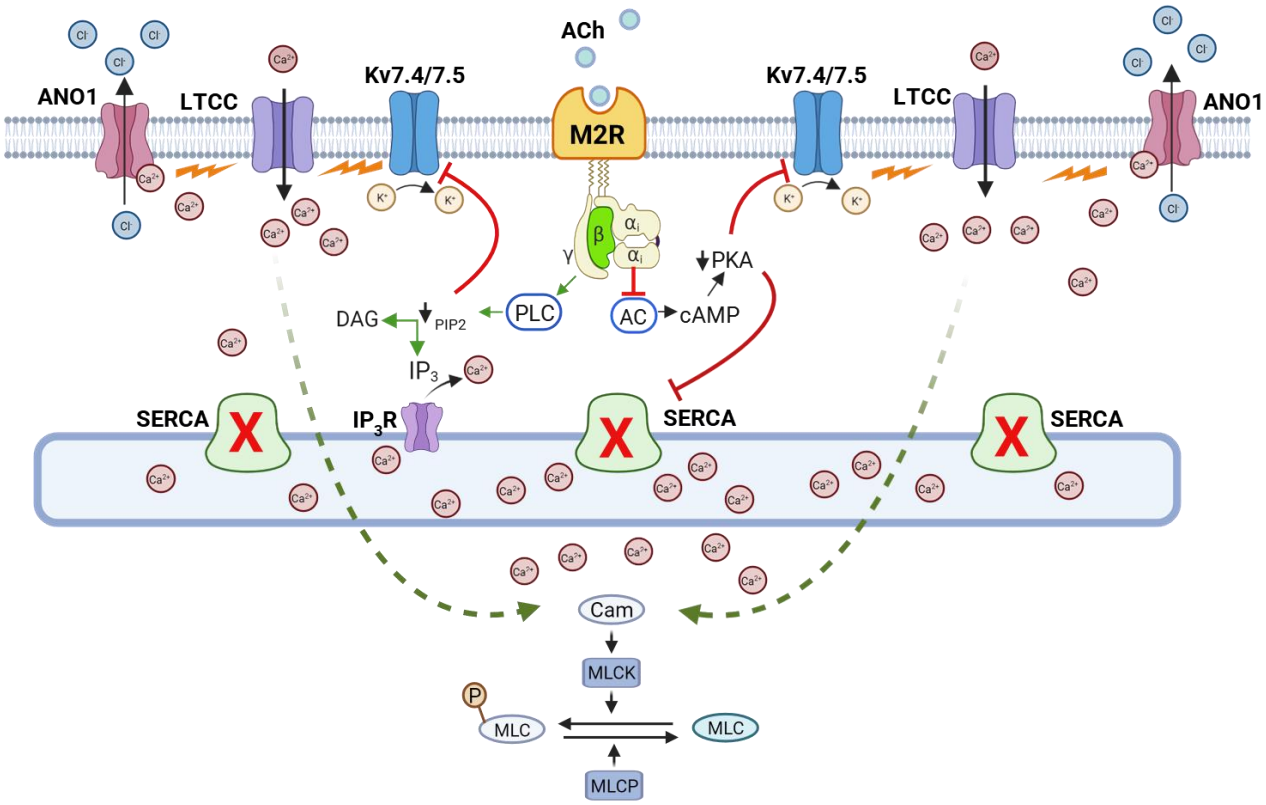

Figure 7.1. Model illustrating M2R-mediated ASM contraction. M2R activation via $G_{\alpha i}$ reduces cAMP/PKA signalling, inhibiting Kv7.5 channels, while $G_{\beta\gamma}$-mediated activation of PLC depletes PIP_2, inhibiting Kv7.4 channels. Concurrently, M2R signalling suppresses SERCA function, likely via phospholamban (PLB), reducing Ca^{2+} reuptake and enhancing subsarcolemmal Ca^{2+} accumulation. Elevated Ca^{2+} activates Ano1 Ca^{2+}-activated Cl^- channels (CACC), promoting Cl^- efflux, membrane depolarisation, and further LTCC activation. The resulting increase in intracellular Ca^{2+} enhances calmodulin (CaM) dependent activation of MLCK, promoting myosin light chain (MLC) phosphorylation and augmented ASM contraction. Figure created with a licensed version of BioRender.com.

Future experiments

Building upon the findings of this thesis, several experimental approaches can be undertaken to validate and extend the proposed mechanisms in physiologically relevant models and clinical settings. These studies will help determine the translational potential of M2R signalling pathways in AHR and identify novel therapeutic targets for asthma and COPD.

1. **Murine models of asthma and COPD**

   The mechanisms identified in this thesis should be validated *in vivo* using ovalbumin and LPS-induced asthma models and cigarette smoke-induced COPD models in mice. These studies will determine whether M2R-mediated inhibition of Kv7 channels and SERCA, and activation of LTCC/Ano1, contribute to bronchoconstriction and alteration of functional respiratory parameters. Furthermore, targeting these pathways pharmacologically or genetically could reveal whether modulating these mechanisms can reverse disease severity and improve airway function.

2. **Human bronchial tissue validation**

   Functional and molecular analyses should be extended to human bronchial rings obtained from healthy donors and COPD patients through clinical collaborations. Comparative evaluation of M2R signalling, Kv7 expression and LTCC dependence will help to assess the translational relevance of the proposed pathways to human disease.

3. **Conditional knockout or knockdown of Kv7.4 and Kv7.5**

   To dissect isoform-specific contributions, conditional Kv7.4 and Kv7.5 knockout mice or morpholino-induced knockdown in bronchial tissue could be employed. Such models will confirm whether the loss of either subtype alters M2R-dependent depolarisation and ASM contractility *in vivo*.

4. **Influence of inflammatory cytokines on M2R and Ano1 function**

   Inflammatory cytokines such as IL-4, IL-5, and IL-13 (known to be elevated in asthma and COPD) should be examined for their ability to modulate M2R signalling and upregulate Ano1 expression, as shown by Huang et al. (2012)

[256]. Understanding cytokine-dependent amplification of M2R-Ano1 coupling will link inflammatory signalling to enhanced ASM excitability.

5. Cigarette smoke extract (CSE) and M2R signalling

CSE at different concentrations should be tested for its ability to alter muscarinic receptor expression and function, G-protein coupling, and Kv7/LTCC function in cultured ASM cells or bronchial tissues. My preliminary findings indicate that CSE augments sensitivity to carbachol.

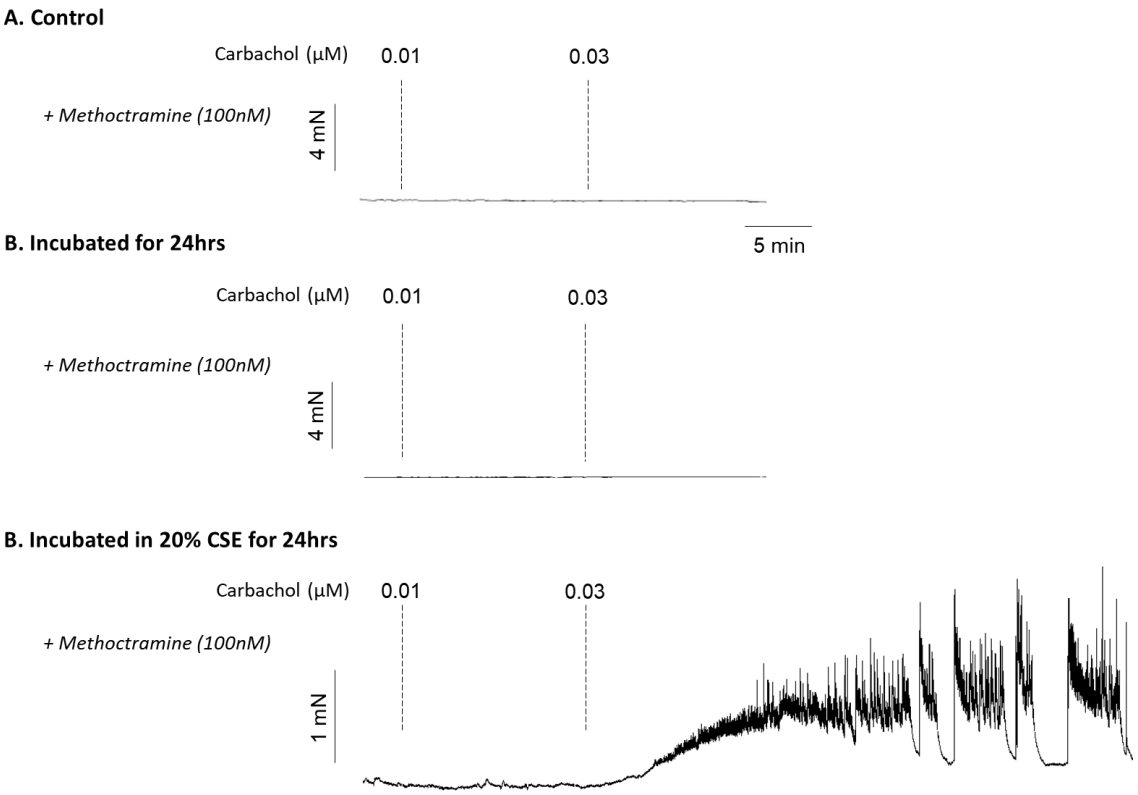

6. M2R regulation of Kv7.4/7.5 heterotetramers

Since Kv7.4 and Kv7.5 also assemble as heterotetramers, future patch-clamp experiments in co-transfected HEK293 cells should assess whether M2R activation differentially inhibits heteromeric versus homomeric channels. This will clarify whether channel composition determines sensitivity to muscarinic inhibition and pharmacological modulators.

7. **M2R crosstalk with the RhoA/ROCK pathway**

   While M3R-driven Ca^{2+} sensitisation via the RhoA/ROCK cascade is well established [477], the potential of M2R activation to modulate this pathway remains unexplored. Studies using ROCK inhibitors (e.g., Y-27632) could determine whether M2R-induced contractions involve secondary activation of Rho kinase or PKC-dependent Ca^{2+} sensitisation mechanisms.

8. **Real-time Ca^{2+} and membrane potential imaging**

   High-resolution Ca^{2+} imaging and voltage-sensitive dye studies in live ASM preparations could visualise dynamic M2R-mediated depolarisation and LTCC activation. Combining this with optogenetic or biosensor approaches will yield mechanistic insight into temporal coordination of ion channel activity during cholinergic stimulation.

9. **Single-cell transcriptomic and proteomic profiling**

   Integration of single-cell RNA sequencing (scRNA-seq) and proteomics on human ASM and immune cells from COPD lungs could delineate co-expression networks linking M2R, Kv7 subunits, SERCA2 isoforms and Ano1. This will identify patient-specific regulatory signatures relevant to airway hyperreactivity.

10. **Design of selective M2R antagonists**

    Collaboration with medicinal chemists could facilitate the design of selective M2R antagonists with minimal cardiac or presynaptic side-effects. Such agents could represent next-generation bronchodilators by selectively targeting post-junctional M2Rs to reduce airway tone without compromising M3R-mediated physiological functions.

References

1. Clancy, J. and A. McVicar, *The respiratory system and homeostasis.* Br J Theatre Nurs, 1996. **6**(8): p. 16-20, 22.
2. Butler, J.P. and A. Tsuda, *Transport of gases between the environment and alveoli--theoretical foundations.* Compr Physiol, 2011. **1**(3): p. 1301-16.
3. Powers, K.A. and A.S. Dhamoon, *Physiology, pulmonary ventilation and perfusion*, in *StatPearls [Internet]*. 2023, Treasure Island (FL): StatPearls Publishing; 2025 Jan. Available from: https://www.ncbi.nlm.nih.gov/books/NBK539907/.
4. Patwa, A. and A. Shah, *Anatomy and physiology of respiratory system relevant to anaesthesia.* Indian J Anaesth, 2015. **59**(9): p. 533-41.
5. Downey, R.P. and N.S. Samra, *Anatomy, thorax, tracheobronchial tree*, in *StatPearls [Internet]*. 2020, Treasure Island (FL): StatPearls Publishing. Available from: https://www.ncbi.nlm.nih.gov/books/NBK556044/.
6. Watson AY, B.R., Kennedy D, *Biological Disposition of Airborne Particles: Basic Principles and Application to Vehicular Emissions*. Air Pollution, the Automobile, and Public Health. 1988: National Academies Press (US).
7. Mahabadi, N., A.A. Goizueta, and B. Bordoni, *Anatomy, thorax, lung pleura and mediastinum*, in *StatPearls [Internet]*. 2018, Treasure Island (FL): StatPearls Publishing. Available from: https://www.ncbi.nlm.nih.gov/books/NBK519048/.
8. Breul, R., *1.7 - The deeper fasciae of the neck and ventral torso*, in *Fascia: The Tensional Network of the Human Body*, R. Schleip, et al., Editors. 2012, Churchill Livingstone: Oxford. p. 45-52.
9. D'Agostino, H.P. and M.A. Edens, *Physiology, pleural fluid*, in *StatPearls [Internet]*. 2018, Treasure Island (FL): StatPearls Publishing. Available from: https://www.ncbi.nlm.nih.gov/books/NBK513353/.
10. Krishna, R., et al., *Pleural effusion*, in *StatPearls [Internet]*. 2024, Treasure Island (FL): StatPearls Publishing. Available from: https://www.ncbi.nlm.nih.gov/books/NBK448189/.
11. Albertine, K.H. and B.A. Yoder, *Chapter 17 - Pulmonary Consequences of Preterm Birth*, in *The Lung (Second Edition)*, R. Harding and K.E. Pinkerton, Editors. 2014, Academic Press: Boston. p. 311-327.
12. Townsley, M.I., *Structure and composition of pulmonary arteries, capillaries, and veins.* Compr Physiol, 2012. **2**(1): p. 675-709.
13. Robinson, N.E. and P.W. Furlow, *1 - Anatomy of the Respiratory System*, in *Equine Respiratory Medicine and Surgery*, B.C. McGorum, et al., Editors. 2007, W.B. Saunders: Edinburgh. p. 3-17.
14. Hopkins, S.R., *Ventilation/Perfusion Relationships and Gas Exchange: Measurement Approaches.* Compr Physiol, 2020. **10**(3): p. 1155-1205.
15. Seadler, B.D., F. Toro, and S. Sharma, *Physiology, Alveolar Tension*, in *StatPearls [Internet]*. 2023, Treasure Island (FL): StatPearls Publishing. Available from: https://www.ncbi.nlm.nih.gov/books/NBK539825/.

16. Brandt, J.P. and P. Mandiga, *Histology, alveolar cells*, in *StatPearls [Internet]*. 2020, Treasure Island (FL): StatPearls Publishing. Available from: https://www.ncbi.nlm.nih.gov/books/NBK557542/.

17. Pittman, R., *The Circulatory System and Oxygen Transport*. 2011: Morgan & Claypool Life Sciences.

18. Brinkman, J.E., F. Toro, and S. Sharma, *Physiology, Respiratory Drive*, in *StatPearls [Internet]*. 2023, Treasure Island (FL): StatPearls Publishing. Available from: https://www.ncbi.nlm.nih.gov/books/NBK482414/.

19. Scanlon, V.C. and T. Sanders, *Essentials of anatomy and physiology (8th ed.).* 2018: F.A. Davis Company.

20. Gold, W.M. and L.L. Koth, *Pulmonary Function Testing*. Murray and Nadel's Textbook of Respiratory Medicine. 2016:407-435.e18. doi: 10.1016/B978-1-4557-3383-5.00025-7. Epub 2015 Apr 3.

21. Bains, K.N.S., S. Kashyap, and S.L. Lappin, *Anatomy, thorax, diaphragm*, in *StatPearls [Internet]*. 2018, Treasure Island (FL): StatPearls Publishing. Available from: https://www.ncbi.nlm.nih.gov/books/NBK519558/.

22. Aliverti, A., *The respiratory muscles during exercise.* Breathe (Sheff), 2016. **12**(2): p. 165-8.

23. Park, H. and D. Han, *The effect of the correlation between the contraction of the pelvic floor muscles and diaphragmatic motion during breathing.* J Phys Ther Sci, 2015. **27**(7): p. 2113-5.

24. Donley, E.R., M.R. Holme, and J.W. Loyd, *Anatomy, thorax, wall movements*, in *StatPearls [Internet]*. 2018, Treasure Island (FL): StatPearls Publishing. Available from: https://www.ncbi.nlm.nih.gov/books/NBK526023/

25. Van Scott, M.R., et al., *Airway Anatomy, Physiology, and Inflammation*. The Toxicant Induction of Irritant Asthma, Rhinitis, and Related Conditions. 2013 Nov 11:19-61. doi: 10.1007/978-1-4614-9044-9_2.

26. Block, D.R. and J.R. Genzen, *Chapter 27 - Diagnostic body fluid testing*, in *Contemporary Practice in Clinical Chemistry (Fourth Edition)*, W. Clarke and M.A. Marzinke, Editors. 2020, Academic Press. p. 469-486.

27. Mentzer, S.J., A. Tsuda, and S.H. Loring, *Pleural mechanics and the pathophysiology of air leaks.* J Thorac Cardiovasc Surg, 2018. **155**(5): p. 2182-2189.

28. Burstiner, L. and Y. Al Khalili, *Anatomy, thorax, pleurae*, in *StatPearls [Internet]*. 2025, Treasure Island (FL): StatPearls Publishing. Available from: https://www.ncbi.nlm.nih.gov/books/NBK541079/.

29. Hall, J.E., *Guyton and Hall Textbook of Medical Physiology*. 13th ed. 2016: Elsevier.

30. Reid, S.H., F. Toro, and J.V. Ashurst, *Physiology, tidal volume*, in *StatPearls [Internet]*. 2023, Treasure Island (FL): StatPearls Publishing. Available from: https://www.ncbi.nlm.nih.gov/books/NBK482502/.

31. Lofrese, J.J., et al., *Physiology, residual volume*, in *StatPearls [Internet]*. 2023, Treasure Island (FL): StatPearls Publishing. Available from: https://www.ncbi.nlm.nih.gov/books/NBK493170/.

32. Gilday, C., A. Odunayo, and A.-M. Hespel, *Spontaneous Pneumothorax: Pathophysiology, Clinical Presentation and Diagnosis.* Topics in Companion Animal Medicine, 2021. **45**: p. 100563.

33. Sahetya, S.K. and R.G. Brower, *The promises and problems of transpulmonary pressure measurements in acute respiratory distress syndrome.* Curr Opin Crit Care, 2016. **22**(1): p. 7-13.

34. Neupane, K. and R.T. Jamil, *Physiology, transpulmonary pressure*, in *StatPearls [Internet]*. 2020, Treasure Island (FL): StatPearls Publishing. Available from: https://www.ncbi.nlm.nih.gov/books/NBK559004/.

35. Edwards, Z. and P. Annamaraju, *Physiology, Pulmonary Compliance*, in *StatPearls [Internet]*. 2023, Treasure Island (FL): StatPearls Publishing. Available from: https://www.ncbi.nlm.nih.gov/books/NBK554517/.

36. Desai, J.P. and F. Moustarah, *Pulmonary compliance*, in *StatPearls [Internet]*. 2022, Treasure Island (FL): StatPearls Publishing. Available from: https://www.ncbi.nlm.nih.gov/books/NBK538324/.

37. Leeman, K.T., C.M. Fillmore, and C.F. Kim, *Lung stem and progenitor cells in tissue homeostasis and disease.* Curr Top Dev Biol, 2014. **107**: p. 207-233.

38. Singh, S., et al., *Airway Epithelium: A Neglected but Crucial Cell Type in Asthma Pathobiology.* Diagnostics (Basel), 2023. **13**(4).

39. Hyde, D.M., Q. Hamid, and C.G. Irvin, *Anatomy, pathology, and physiology of the tracheobronchial tree: emphasis on the distal airways.* J Allergy Clin Immunol, 2009. **124**(6 Suppl): p. S72-7.

40. Amatngalim, G.D. and P.S. Hiemstra, *Airway Epithelial Cell Function and Respiratory Host Defense in Chronic Obstructive Pulmonary Disease.* Chin Med J (Engl), 2018. **131**(9): p. 1099-1107.

41. Johnston, S.L., et al., *Airway Epithelial Innate Immunity.* Front Physiol, 2021. **12**: p. 749077.

42. Panettieri, R.A., Jr., et al., *Airway smooth muscle in bronchial tone, inflammation, and remodeling: basic knowledge to clinical relevance.* Am J Respir Crit Care Med, 2008. **177**(3): p. 248-52.

43. Shi, W. and Y. Luo, *The Origin of Stem Cells in Developmental Lungs*, in *Encyclopedia of Tissue Engineering and Regenerative Medicine*, R.L. Reis, Editor. 2019, Academic Press: Oxford. p. 313-318.

44. AY, B.R.W. and D. Kennedy, *Air pollution, the automobile, and public health*. 1988: National Academies Press (US).

45. Kia'i, N. and T. Bajaj, *Histology, respiratory epithelium*, in *StatPearls [Internet]*. 2019, Treasure Island (FL): StatPearls Publishing. Available from: https://www.ncbi.nlm.nih.gov/books/NBK541061/.

46. Herbert, R.A., et al., *Chapter 22 - Nose, Larynx, and Trachea*, in *Boorman's Pathology of the Rat (Second Edition)*, A.W. Suttie, Editor. 2018, Academic Press: Boston. p. 391-435.

47. Lust, R.M., *The Pulmonary System*, in *xPharm: The Comprehensive Pharmacology Reference*, S.J. Enna and D.B. Bylund, Editors. 2007, Elsevier: New York. p. 1-6.

48. Mason, R.J., *EPITHELIAL CELLS | Type II Cells*, in *Encyclopedia of Respiratory Medicine*, G.J. Laurent and S.D. Shapiro, Editors. 2006, Academic Press: Oxford. p. 138-142.

49. Ruaro, B., et al., *The History and Mystery of Alveolar Epithelial Type II Cells: Focus on Their Physiologic and Pathologic Role in Lung.* Int J Mol Sci, 2021. **22**(5).

50. Knight, D.A. and S.T. Holgate, *The airway epithelium: structural and functional properties in health and disease.* Respirology, 2003. **8**(4): p. 432-46.

51. Crystal, R.G., et al., *Airway epithelial cells: current concepts and challenges.* Proc Am Thorac Soc, 2008. **5**(7): p. 772-7.

52. Gunst, S.J., *Chapter 104 - Airway Smooth Muscle and Asthma*, in *Muscle*, J.A. Hill and E.N. Olson, Editors. 2012, Academic Press: Boston/Waltham. p. 1359-1369.

53. Carroll, R.C. and E.G. Peralta, *The m3 muscarinic acetylcholine receptor differentially regulates calcium influx and release through modulation of monovalent cation channels.* Embo j, 1998. **17**(11): p. 3036-44.

54. Ozier, A., et al., *The pivotal role of airway smooth muscle in asthma pathophysiology.* J Allergy (Cairo), 2011. **2011**: p. 742710.

55. Eglen, R.M., et al., *Muscarinic acetylcholine receptor subtypes in smooth muscle.* Trends Pharmacol Sci, 1994. **15**(4): p. 114-9.

56. Billington, C.K. and R.B. Penn, *Signaling and regulation of G protein-coupled receptors in airway smooth muscle.* Respir Res, 2003. **4**(1): p. 2.

57. Evseev, A.I., et al., *Kcnq Channels in Airway Smooth Muscle.* Biophysical Journal, 2013. **104**(2): p. 269a.

58. Mondejar-Parreño, G., F. Perez-Vizcaino, and A. Cogolludo, *Kv7 Channels in Lung Diseases.* Front Physiol, 2020. **11**: p. 634.

59. Guntur, D., et al., *Revisiting the Large-Conductance Calcium-Activated Potassium (BKCa) Channels in the Pulmonary Circulation.* Biomolecules, 2021. **11**(11).

60. Liu, C., et al., *Regulation of Rho/ROCK signaling in airway smooth muscle by membrane potential and [Ca2+]i.* Am J Physiol Lung Cell Mol Physiol, 2005. **289**(4): p. L574-82.

61. Mahavadi, S., et al., *Inhibition of MLC20 phosphorylation downstream of Ca2+ and RhoA: A novel mechanism involving phosphorylation of myosin phosphatase interacting protein (M-RIP) by PKG and stimulation of MLC phosphatase activity.* Cell Biochem Biophys, 2014. **68**(1): p. 1-8.

62. Chetty, A. and H.C. Nielsen, *Targeting Airway Smooth Muscle Hypertrophy in Asthma: An Approach Whose Time Has Come.* J Asthma Allergy, 2021. **14**: p. 539-556.

63. Damera, G. and R.A. Panettieri, Jr., *Does airway smooth muscle express an inflammatory phenotype in asthma?* Br J Pharmacol, 2011. **163**(1): p. 68-80.

64. Tliba, O. and Y. Amrani, *Airway smooth muscle cell as an inflammatory cell: lessons learned from interferon signaling pathways.* Proc Am Thorac Soc, 2008. **5**(1): p. 106-12.

65. Howarth, P.H., et al., *Synthetic responses in airway smooth muscle.* Journal of Allergy and Clinical Immunology, 2004. **114**(2): p. S32-S50.

66. Kolahian, S. and R. Gosens, *Cholinergic regulation of airway inflammation and remodelling.* J Allergy (Cairo), 2012. **2012**: p. 681258.

67. Mio, T., et al., *Cigarette smoke induces interleukin-8 release from human bronchial epithelial cells.* Am J Respir Crit Care Med, 1997. **155**(5): p. 1770-6.

68. Johnson, P.R., et al., *Extracellular matrix proteins modulate asthmatic airway smooth muscle cell proliferation via an autocrine mechanism.* J Allergy Clin Immunol, 2004. **113**(4): p. 690-6.

69. Lee, Y.C., et al., *Collagen-rich airway smooth muscle cells are a metastatic niche for tumor colonization in the lung.* Nat Commun, 2019. **10**(1): p. 2131.

70. Parameswaran, K., et al., *Role of extracellular matrix and its regulators in human airway smooth muscle biology.* Cell Biochem Biophys, 2006. **44**(1): p. 139-46.

71. White, E.S., *Lung extracellular matrix and fibroblast function.* Ann Am Thorac Soc, 2015. **12 Suppl 1**(Suppl 1): p. S30-3.

72. Lendahl, U., L. Muhl, and C. Betsholtz, *Identification, discrimination and heterogeneity of fibroblasts.* Nature Communications, 2022. **13**(1): p. 3409.

73. Ghonim, M.A., et al., *Pulmonary inflammation and fibroblast immunoregulation: from bench to bedside.* J Clin Invest, 2023. **133**(17).

74. Tsukui, T., et al., *Collagen-producing lung cell atlas identifies multiple subsets with distinct localization and relevance to fibrosis.* Nature Communications, 2020. **11**(1): p. 1920.

75. Zhang, X., et al., *Dissecting pulmonary fibroblasts heterogeneity in lung development, health and diseases.* Heliyon, 2023. **9**(9).

76. Ushakumary, M.G., M. Riccetti, and A.T. Perl, *Resident interstitial lung fibroblasts and their role in alveolar stem cell niche development, homeostasis, injury, and regeneration.* Stem Cells Transl Med, 2021. **10**(7): p. 1021-1032.

77. Michalik, M., et al., *Fibroblast-to-myofibroblast transition in bronchial asthma.* Cell Mol Life Sci, 2018. **75**(21): p. 3943-3961.

78. Zabihi, M., et al., *Understanding myofibroblast origin in the fibrotic lung.* Chinese Medical Journal Pulmonary and Critical Care Medicine, 2024. **2**(3): p. 142-150.

79. Lingampally, A., et al., *Use of the Reversible Myogenic to Lipogenic Transdifferentiation Switch for the Design of Pre-clinical Drug Screening in Idiopathic Pulmonary Fibrosis.* Front Bioeng Biotechnol, 2020. **8**: p. 569865.

80. Tsukui, T., P.J. Wolters, and D. Sheppard, *Alveolar fibroblast lineage orchestrates lung inflammation and fibrosis.* Nature, 2024. **631**(8021): p. 627-634.

81. Ojiaku, C.A., E.J. Yoo, and R.A. Panettieri, Jr., *Transforming Growth Factor β1 Function in Airway Remodeling and Hyperresponsiveness. The Missing Link?* Am J Respir Cell Mol Biol, 2017. **56**(4): p. 432-442.

82. Shi, X., et al., *The novel molecular mechanism of pulmonary fibrosis: insight into lipid metabolism from reanalysis of single-cell RNA-seq databases.* Lipids Health Dis, 2024. **23**(1): p. 98.

83. Halwani, R., et al., *Role of transforming growth factor-β in airway remodeling in asthma.* Am J Respir Cell Mol Biol, 2011. **44**(2): p. 127-33.

84. Al-Alawi, M., T. Hassan, and S.H. Chotirmall, *Transforming growth factor β and severe asthma: a perfect storm.* Respir Med, 2014. **108**(10): p. 1409-23.

85. Wnuk, D., et al., *Enhanced asthma-related fibroblast to myofibroblast transition is the result of profibrotic TGF-β/Smad2/3 pathway intensification and antifibrotic TGF-β/Smad1/5/(8)9 pathway impairment.* Scientific Reports, 2020. **10**(1): p. 16492.

86. Hogg, J.C., et al., *The nature of small-airway obstruction in chronic obstructive pulmonary disease.* N Engl J Med, 2004. **350**(26): p. 2645-53.

87. Hogg, J.C., P.D. Paré, and T.-L. Hackett, *The Contribution of Small Airway Obstruction to the Pathogenesis of Chronic Obstructive Pulmonary Disease.* Physiological Reviews, 2017. **97**(2): p. 529-552.

88. Kraik, K., et al., *The Role of Transforming Growth Factor-β (TGF-β) in Asthma and Chronic Obstructive Pulmonary Disease (COPD).* Cells, 2024. **13**(15).

89. Kilinc, M., et al., *Elevated Urotensin-II and TGF-β Levels in COPD: Biomarkers of Fibrosis and Airway Remodeling in Smokers.* Medicina (Kaunas), 2024. **60**(11).

90. Wang, R.D., J.L. Wright, and A. Churg, *Transforming growth factor-beta1 drives airway remodeling in cigarette smoke-exposed tracheal explants.* Am J Respir Cell Mol Biol, 2005. **33**(4): p. 387-93.

91. Churg, A., et al., *Cigarette smoke drives small airway remodeling by induction of growth factors in the airway wall.* Am J Respir Crit Care Med, 2006. **174**(12): p. 1327-34.

92. Green, C.E. and A.M. Turner, *The role of the endothelium in asthma and chronic obstructive pulmonary disease (COPD).* Respir Res, 2017. **18**(1): p. 20.

93. Gillich, A., et al., *Capillary cell-type specialization in the alveolus.* Nature, 2020. **586**(7831): p. 785-789.

94. Green, C.E. and A.M. Turner, *The role of the endothelium in asthma and chronic obstructive pulmonary disease (COPD).* Respiratory Research, 2017. **18**(1): p. 20.

95. Ricciardolo, F.L., F.P. Nijkamp, and G. Folkerts, *Nitric oxide synthase (NOS) as therapeutic target for asthma and chronic obstructive pulmonary disease.* Curr Drug Targets, 2006. **7**(6): p. 721-35.

96. Moncada, S. and A. Higgs, *The L-arginine-nitric oxide pathway.* N Engl J Med, 1993. **329**(27): p. 2002-12.

97. Förstermann, U. and W.C. Sessa, *Nitric oxide synthases: regulation and function.* Eur Heart J, 2012. **33**(7): p. 829-37, 837a-837d.

98. Brindicci, C., et al., *Exhaled nitric oxide from lung periphery is increased in COPD.* Eur Respir J, 2005. **26**(1): p. 52-9.

99. Malerba, M., et al., *Exhaled nitric oxide as a biomarker in COPD and related comorbidities.* Biomed Res Int, 2014. **2014**: p. 271918.

100. Ogoshi, T., et al. *Role of Nitric Oxide Synthases in Respiratory Health and Disease: Insights from Triple Nitric Oxide Synthases Knockout Mice*. International Journal of Molecular Sciences, 2024. **25**, DOI: 10.3390/ijms25179317.

101. Alves-Lopes, R., K.B. Neves, and R.M. Touyz, *Muscarinic Receptor Type-3 in Hypertension and Cholinergic-Adrenergic Crosstalk: Genetic Insights and Potential for New Antihypertensive Targets.* Canadian Journal of Cardiology, 2019. **35**(5): p. 555-557.

102. Folino, A., et al., *Muscarinic receptor M3 contributes to vascular and neural growth factor up-regulation in severe asthma.* Allergy, 2020. **75**(3): p. 717-720.

103. Li, D., J. Wu, and X. Xiong *The Role of the Acetylcholine System in Common Respiratory Diseases and COVID-19*. Molecules, 2023. **28**, DOI: 10.3390/molecules28031139.

104. Ahmed, M., et al., *Effects of novel muscarinic M3 receptor ligand C1213 in pulmonary arterial hypertension models.* Physiol Rep, 2016. **4**(24).

105. Song, Q., P. Chen, and X.M. Liu, *The role of cigarette smoke-induced pulmonary vascular endothelial cell apoptosis in COPD.* Respir Res, 2021. **22**(1): p. 39.

106. Voelkel, N.F., J. Gomez-Arroyo, and S. Mizuno, *COPD/emphysema: The vascular story.* Pulm Circ, 2011. **1**(3): p. 320-6.

107. Bhattarai, P., et al., *Endothelial to mesenchymal transition is an active process in smokers and patients with early COPD contributing to pulmonary arterial pathology.* ERJ Open Res, 2024. **10**(1).

108. Hartl, D., et al., *Innate Immunity of the Lung: From Basic Mechanisms to Translational Medicine.* J Innate Immun, 2018. **10**(5-6): p. 487-501.

109. Hiemstra, P.S., P.B. McCray, Jr., and R. Bals, *The innate immune function of airway epithelial cells in inflammatory lung disease.* Eur Respir J, 2015. **45**(4): p. 1150-62.

110. Arora, S., et al., *Macrophages: Their role, activation and polarization in pulmonary diseases.* Immunobiology, 2018. **223**(4-5): p. 383-396.

111. Branchett, W.J., et al., *Airway macrophage-intrinsic TGF-β1 regulates pulmonary immunity during early-life allergen exposure.* J Allergy Clin Immunol, 2021. **147**(5): p. 1892-1906.

112. Palestra, F., et al., *Histamine as a mediator of cross-talk between human lung mast cells and macrophages.* Scientific Reports, 2025. **15**(1): p. 31969.

113. Zhou, B.-w., et al., *The role of macrophage polarization and cellular crosstalk in the pulmonary fibrotic microenvironment: a review.* Cell Communication and Signaling, 2024. **22**(1): p. 172.

114. Cheetham, C.J., et al. *Neutrophil-Derived Proteases in Lung Inflammation: Old Players and New Prospects*. International Journal of Molecular Sciences, 2024. **25**, DOI: 10.3390/ijms25105492.

115. Li, Y., T. Yang, and B. Jiang, *Neutrophil and neutrophil extracellular trap involvement in neutrophilic asthma: A review.* Medicine, 2024. **103**(34).

116. Januskevicius, A., et al., *Integrative Cross-Talk in Asthma: Unraveling the Complex Interactions Between Eosinophils, Immune, and Structural Cells in the Airway Microenvironment.* Diagnostics (Basel), 2024. **14**(21).

117. Whetstone, C.E., et al., *Pathobiology and Regulation of Eosinophils, Mast Cells, and Basophils in Allergic Asthma.* Immunol Rev, 2025. **331**(1): p. e70018.

118. Pavón-Romero, G.F., et al., *Neuroimmune Pathophysiology in Asthma.* Front Cell Dev Biol, 2021. **9**: p. 663535.

119. Toyoshima, S. and Y. Okayama, *Neuro-allergology: Mast cell–nerve cross-talk*. Allergology International, 2022. **71**(3): p. 288-293.

120. Xie, C., et al., *Immunologic aspects of asthma: from molecular mechanisms to disease pathophysiology and clinical translation.* Front Immunol, 2024. **15**: p. 1478624.

121. Radhouani, M. and P. Starkl, *Adjuvant-independent airway sensitization and infection mouse models leading to allergic asthma.* Front Allergy, 2024. **5**: p. 1423938.

122. Chiba, Y., et al., *Interleukin-13 augments bronchial smooth muscle contractility with an up-regulation of RhoA protein.* Am J Respir Cell Mol Biol, 2009. **40**(2): p. 159-67.

123. Risse, P.A., et al., *Interleukin-13 inhibits proliferation and enhances contractility of human airway smooth muscle cells without change in contractile phenotype.* Am J Physiol Lung Cell Mol Physiol, 2011. **300**(6): p. L958-66.

124. Pelaia, C., et al., *Interleukin-5 in the Pathophysiology of Severe Asthma.* Front Physiol, 2019. **10**: p. 1514.

125. Roufosse, F., *Targeting the Interleukin-5 Pathway for Treatment of Eosinophilic Conditions Other than Asthma.* Front Med (Lausanne), 2018. **5**: p. 49.

126. Sahnoon, L., et al., *Targeting IL-13 and IL-4 in Asthma: Therapeutic Implications on Airway Remodeling in Severe Asthma.* Clin Rev Allergy Immunol, 2025. **68**(1): p. 44.

127. Nelson, A.J., et al., *Lung-resident memory B cells maintain allergic IgE responses in the respiratory tract.* Immunity, 2025. **58**(4): p. 875-888.e8.

128. An, S.S., et al., *Airway smooth muscle dynamics: a common pathway of airway obstruction in asthma.* Eur Respir J, 2007. **29**(5): p. 834-60.

129. Black, J.L., et al., *Airway smooth muscle in asthma: just a target for bronchodilation?* Clin Chest Med, 2012. **33**(3): p. 543-58.

130. Billups, D., et al., *Modulation of Gq-protein-coupled inositol trisphosphate and Ca2+ signaling by the membrane potential.* J Neurosci, 2006. **26**(39): p. 9983-95.

131. Zaagsma, J., A.F. Roffel, and H. Meurs, *Muscarinic control of airway function.* Life Sci, 1997. **60**(13-14): p. 1061-8.

132. Chiba, Y., H. Sakai, and M. Misawa, *Possible involvement of G(i3) protein in augmented contraction of bronchial smooth muscle from antigen-induced airway hyperresponsive rats.* Biochem Pharmacol, 2001. **61**(7): p. 921-4.

133. Hirshman, C.A. and C.W. Emala, *Actin reorganization in airway smooth muscle cells involves Gq and Gi-2 activation of Rho.* Am J Physiol, 1999. **277**(3): p. L653-61.

134. Pfeil, E.M., et al., *Heterotrimeric G Protein Subunit Gαq Is a Master Switch for Gβγ-Mediated Calcium Mobilization by Gi-Coupled GPCRs.* Molecular Cell, 2020. **80**(6): p. 940-954.e6.

135. Fisher, I.J., et al., *Activation of Phospholipase C β by Gβγ and Gα(q) Involves C-Terminal Rearrangement to Release Autoinhibition.* Structure, 2020. **28**(7): p. 810-819.e5.

136. Sanchez, G.A., et al., *Coincident Regulation of PLCβ Signaling by Gq-Coupled and μ-Opioid Receptors Opposes Opioid-Mediated Antinociception.* Mol Pharmacol, 2022. **102**(6): p. 269-279.

137. Hakim, A. and O.S. Usmani, *Structure of the Lower Respiratory Tract*, in *Reference Module in Biomedical Sciences*. 2014, Elsevier.

138. Kistemaker, L.E.M. and Y.S. Prakash, *Airway Innervation and Plasticity in Asthma.* Physiology (Bethesda), 2019. **34**(4): p. 283-298.

139. Barnes, P.J., *Chapter 41 - Autonomic Control of the Lower Airways*, in *Primer on the Autonomic Nervous System (Third Edition)*, D. Robertson, et al., Editors. 2012, Academic Press: San Diego. p. 201-204.

140. Wine, J.J., *Parasympathetic control of airway submucosal glands: central reflexes and the airway intrinsic nervous system.* Auton Neurosci, 2007. **133**(1): p. 35-54.

141. Vaillancourt, M., et al., *Autonomic nervous system involvement in pulmonary arterial hypertension.* Respir Res, 2017. **18**(1): p. 201.

142. Thirstrup, S., F. Nielsen-Kudsk, and R. Dahl, *Effects of five different airway smooth muscle relaxants on inhibitory neurotransmission in isolated guinea-pig trachea in vitro.* European Journal of Pharmacology, 1998. **345**(3): p. 289-297.

143. Belvisi, M.G., et al., *Inhibitory NANC nerves in human tracheal smooth muscle: a quest for the neurotransmitter.* J Appl Physiol (1985), 1992. **73**(6): p. 2505-10.

144. Karakiulakis, G. and M. Roth, *Muscarinic receptors and their antagonists in COPD: anti-inflammatory and antiremodeling effects.* Mediators Inflamm, 2012. **2012**: p. 409580.

145. Struckmann, N., et al., *Role of muscarinic receptor subtypes in the constriction of peripheral airways: studies on receptor-deficient mice.* Mol Pharmacol, 2003. **64**(6): p. 1444-51.

146. Milara, J., et al., *Aclidinium inhibits human lung fibroblast to myofibroblast transition.* Thorax, 2012. **67**(3): p. 229-37.

147. Profita, M., et al., *Cigarette smoke extract activates human bronchial epithelial cells affecting non-neuronal cholinergic system signalling in vitro.* Life Sci, 2011. **89**(1-2): p. 36-43.

148. Kistemaker, L.E., et al., *Regulation of airway inflammation and remodeling by muscarinic receptors: perspectives on anticholinergic therapy in asthma and COPD.* Life Sci, 2012. **91**(21-22): p. 1126-33.

149. Oenema, T.A., et al., *Cross-talk between transforming growth factor-β_1 and muscarinic M_2 receptors augments airway smooth muscle proliferation.* Am J Respir Cell Mol Biol, 2013. **49**(1): p. 18-27.

150. Jacoby, D.B., G.J. Gleich, and A.D. Fryer, *Human eosinophil major basic protein is an endogenous allosteric antagonist at the inhibitory muscarinic M2 receptor.* J Clin Invest, 1993. **91**(4): p. 1314-8.

151. Minette, P.A. and P.J. Barnes, *Prejunctional inhibitory muscarinic receptors on cholinergic nerves in human and guinea pig airways.* J Appl Physiol (1985), 1988. **64**(6): p. 2532-7.

152. Henrot, P., et al., *Muscarinic receptor M3 activation promotes fibrocytes contraction.* Front Pharmacol, 2022. **13**: p. 939780.

153. Alkawadri, T., et al., *Contribution of Postjunctional M2 Muscarinic Receptors to Cholinergic Nerve-Mediated Contractions of Murine Airway Smooth Muscle.* Function (Oxf), 2022. **3**(1): p. zqab053.

154. Mak, J.C., J.N. Baraniuk, and P.J. Barnes, *Localization of muscarinic receptor subtype mRNAs in human lung.* Am J Respir Cell Mol Biol, 1992. **7**(3): p. 344-8.

155. Kruse, A.C., et al., *Structure and dynamics of the M3 muscarinic acetylcholine receptor.* Nature, 2012. **482**(7386): p. 552-6.

156. Fryer, A.D. and D.B. Jacoby, *Muscarinic receptors and control of airway smooth muscle.* Am J Respir Crit Care Med, 1998. **158**(5 Pt 3): p. S154-60.

157. Ehlert, F.J., *Contractile role of M2 and M3 muscarinic receptors in gastrointestinal, airway and urinary bladder smooth muscle.* Life Sci, 2003. **74**(2-3): p. 355-66.

158. Ehlert, F.J., R.S. Ostrom, and G.W. Sawyer, *Subtypes of the muscarinic receptor in smooth muscle.* Life Sci, 1997. **61**(18): p. 1729-40.

159. Wettschureck, N. and S. Offermanns, *Mammalian G proteins and their cell type specific functions.* Physiol Rev, 2005. **85**(4): p. 1159-204.

160. Locht, C., L. Coutte, and N. Mielcarek, *The ins and outs of pertussis toxin.* The FEBS journal, 2011. **278**(23): p. 4668-4682.

161. Kume, H., et al., *Role of G proteins and KCa channels in the muscarinic and beta-adrenergic regulation of airway smooth muscle.* Am J Physiol, 1995. **268**(2 Pt 1): p. L221-9.

162. Hirshman, C.A., B. Lande, and T.L. Croxton, *Role of M2 muscarinic receptors in airway smooth muscle contraction.* Life sciences, 1999. **64**(6-7): p. 443-448.

163. Unno, T., et al., *M2 and M3 muscarinic receptor-mediated contractions in longitudinal smooth muscle of the ileum studied with receptor knockout mice.* British journal of pharmacology, 2005. **146**(1): p. 98-108.

164. Semenov, I., et al., *BK channel β1 subunits regulate airway contraction secondary to M2 muscarinic acetylcholine receptor mediated depolarization.* J Physiol, 2011. **589**(Pt 7): p. 1803-17.

165. Schlenz, H., et al., *Muscarinic receptor-mediated bronchoconstriction is coupled to caveolae in murine airways.* American Journal of Physiology-Lung Cellular and Molecular Physiology, 2010. **298**(5): p. L626-L636.

166. Stengel, P.W., et al., *M3-receptor knockout mice: muscarinic receptor function in atria, stomach fundus, urinary bladder, and trachea.* American Journal of Physiology-Regulatory, Integrative and Comparative Physiology, 2002. **282**(5): p. R1443-R1449.

167. Fryer, A.D. and J. Maclagan, *Muscarinic inhibitory receptors in pulmonary parasympathetic nerves in the guinea-pig.* British journal of pharmacology, 1984. **83**(4): p. 973.

168. Fryer, A.D. and D.B. Jacoby, *Parainfluenza virus infection damages inhibitory M2 muscarinic receptors on pulmonary parasympathetic nerves in the guinea-pig.* Br J Pharmacol, 1991. **102**(1): p. 267-71.

169. Fryer, A.D. and M. Wills-Karp, *Dysfunction of M2-muscarinic receptors in pulmonary parasympathetic nerves after antigen challenge.* J Appl Physiol (1985), 1991. **71**(6): p. 2255-61.

170. Larsen, G.L., et al., *Increased acetylcholine release in tracheas from allergen-exposed IgE-immune mice.* Am J Physiol, 1994. **266**(3 Pt 1): p. L263-70.

171. Schultheis, A.H., D.J. Bassett, and A.D. Fryer, *Ozone-induced airway hyperresponsiveness and loss of neuronal M2 muscarinic receptor function.* J Appl Physiol (1985), 1994. **76**(3): p. 1088-97.

172. Enweasor, C., C.H. Flayer, and A. Haczku, *Ozone-Induced Oxidative Stress, Neutrophilic Airway Inflammation, and Glucocorticoid Resistance in Asthma.* Front Immunol, 2021. **12**: p. 631092.

173. Dyring-Andersen, B., et al., *Interleukin (IL)-17A and IL-22-producing neutrophils in psoriatic skin.* Br J Dermatol, 2017. **177**(6): p. e321-e322.

174. Ray, A. and J.K. Kolls, *Neutrophilic Inflammation in Asthma and Association with Disease Severity.* Trends Immunol, 2017. **38**(12): p. 942-954.

175. Gambone, L.M., C.L. Elbon, and A.D. Fryer, *Ozone-induced loss of neuronal M2 muscarinic receptor function is prevented by cyclophosphamide.* J Appl Physiol (1985), 1994. **77**(3): p. 1492-9.

176. Nickel, K., et al., *Neutrophil response to cyclophosphamide predicts resilience to age-related learning impairment.* Aging Pathobiol Ther, 2020. **2**(4): p. 230-231.

177. Ayala, L.E. and T. Ahmed, *Is There Loss of a Protective Muscarinic Receptor Mechanism in Asthma?* CHEST, 1989. **96**(6): p. 1285-1291.

178. Okayama, M., et al., *Effect of pilocarpine on propranolol-induced bronchoconstriction in asthma.* Am J Respir Crit Care Med, 1994. **149**(1): p. 76-80.

179. Ghosh, S., et al., *A review on the effect of COVID-19 in type 2 asthma and its management.* Int Immunopharmacol, 2021. **91**: p. 107309.

180. Nakagome, K. and M. Nagata, *Involvement and Possible Role of Eosinophils in Asthma Exacerbation.* Front Immunol, 2018. **9**: p. 2220.

181. Costello, R.W., D.B. Jacoby, and A.D. Fryer, *Pulmonary neuronal M2 muscarinic receptor function in asthma and animal models of hyperreactivity.* Thorax, 1998. **53**(7): p. 613-6.

182. Fryer, A.D. and D.B. Jacoby, *Function of pulmonary M2 muscarinic receptors in antigen-challenged guinea pigs is restored by heparin and poly-L-glutamate.* J Clin Invest, 1992. **90**(6): p. 2292-8.

183. Elbon, C.L., D.B. Jacoby, and A.D. Fryer, *Pretreatment with an antibody to interleukin-5 prevents loss of pulmonary M2 muscarinic receptor function in antigen-challenged guinea pigs.* Am J Respir Cell Mol Biol, 1995. **12**(3): p. 320-8.

184. Evans, C.M., et al., *Pretreatment with antibody to eosinophil major basic protein prevents hyperresponsiveness by protecting neuronal M2 muscarinic receptors in antigen-challenged guinea pigs.* J Clin Invest, 1997. **100**(9): p. 2254-62.

185. Fryer, A.D., et al., *Antibody to VLA-4, but not to L-selectin, protects neuronal M2 muscarinic receptors in antigen-challenged guinea pig airways.* J Clin Invest, 1997. **99**(8): p. 2036-44.

186. Fryer, A.D., E.E. el-Fakahany, and D.B. Jacoby, *Parainfluenza virus type 1 reduces the affinity of agonists for muscarinic receptors in guinea-pig lung and heart.* Eur J Pharmacol, 1990. **181**(1-2): p. 51-8.

187. Jacoby, D.B., et al., *Virus- and interferon-induced loss of inhibitory M2 muscarinic receptor function and gene expression in cultured airway parasympathetic neurons.* J Clin Invest, 1998. **102**(1): p. 242-8.

188. Luo, J., J.M. Busillo, and J.L. Benovic, *M3 muscarinic acetylcholine receptor-mediated signaling is regulated by distinct mechanisms.* Mol Pharmacol, 2008. **74**(2): p. 338-47.

189. Liu, Q.-H., et al., *Membrane depolarization causes a direct activation of G protein-coupled receptors leading to local Ca²⁺ release in smooth muscle.* Proceedings of the National Academy of Sciences, 2009. **106**(27): p. 11418-11423.

190. Ong, H.L., L.B. de Souza, and I.S. Ambudkar, *Role of TRPC Channels in Store-Operated Calcium Entry.* Adv Exp Med Biol, 2016. **898**: p. 87-109.

191. Xiao, J.H., et al., *Functional role of canonical transient receptor potential 1 and canonical transient receptor potential 3 in normal and asthmatic airway smooth muscle cells.* Am J Respir Cell Mol Biol, 2010. **43**(1): p. 17-25.

192. Kang, H., et al., *Direct modulation of TRPC ion channels by Gα proteins.* Front Physiol, 2024. **15**: p. 1362987.

193. Gonzalez-Cobos, J.C. and M. Trebak, *TRPC channels in smooth muscle cells.* Front Biosci (Landmark Ed), 2010. **15**(3): p. 1023-39.

194. Yoo, E.J., et al., *Gα12 facilitates shortening in human airway smooth muscle by modulating phosphoinositide 3-kinase-mediated activation in a RhoA-dependent manner.* British Journal of Pharmacology, 2017. **174**(23): p. 4383-4395.

195. Gosens, R., et al., *Muscarinic M3 receptor stimulation increases cigarette smoke-induced IL-8 secretion by human airway smooth muscle cells.* Eur Respir J, 2009. **34**(6): p. 1436-43.

196. Kistemaker, L.E., et al., *Muscarinic M_3 receptors contribute to allergen-induced airway remodeling in mice.* Am J Respir Cell Mol Biol, 2014. **50**(4): p. 690-8.

197. Hollenhorst, M.I. and G. Krasteva-Christ, *Nicotinic Acetylcholine Receptors in the Respiratory Tract.* Molecules, 2021. **26**(20).

198. Khalfaoui, L., et al., *Functional α7 nicotinic receptors in human airway smooth muscle increase intracellular calcium concentration and contractility in asthmatics.* Am J Physiol Lung Cell Mol Physiol, 2023. **325**(1): p. L17-l29.

199. Borkar, N.A., et al., *Nicotinic receptors in airway disease.* Am J Physiol Lung Cell Mol Physiol, 2024. **326**(2): p. L149-l163.

200. Gundavarapu, S., et al., *Role of nicotinic receptors and acetylcholine in mucous cell metaplasia, hyperplasia, and airway mucus formation in vitro and in vivo.* J Allergy Clin Immunol, 2012. **130**(3): p. 770-780.e11.

201. Maouche, K., et al., *Contribution of α7 nicotinic receptor to airway epithelium dysfunction under nicotine exposure.* Proceedings of the National Academy of Sciences, 2013. **110**(10): p. 4099-4104.

202. van der Velden, V.H. and A.R. Hulsmann, *Autonomic innervation of human airways: structure, function, and pathophysiology in asthma.* Neuroimmunomodulation, 1999. **6**(3): p. 145-59.

203. Bottasso, E., *Toward the Existence of a Sympathetic Neuroplasticity Adaptive Mechanism Influencing the Immune Response. A Hypothetical View-Part II.* Front Endocrinol (Lausanne), 2019. **10**: p. 633.

204. Carbajal-García, A., J. Reyes-García, and L.M. Montaño, *Androgen Effects on the Adrenergic System of the Vascular, Airway, and Cardiac Myocytes and Their Relevance in Pathological Processes.* Int J Endocrinol, 2020. **2020**: p. 8849641.

205. Abosamak, N.R., P. Patel, and M.H. Shahin, *Beta2-Receptor Agonists and Antagonists*, in *StatPearls [Internet]*. 2025, Treasure Island (FL): StatPearls Publishing. Available from: https://www.ncbi.nlm.nih.gov/books/NBK559069/.

206. Godinho, R.O., T. Duarte, and E.S. Pacini, *New perspectives in signaling mediated by receptors coupled to stimulatory G protein: the emerging significance of cAMP efflux and extracellular cAMP-adenosine pathway.* Front Pharmacol, 2015. **6**: p. 58.

207. Bertin, B., et al., *Cellular signaling by an agonist-activated receptor/Gs alpha fusion protein.* Proc Natl Acad Sci U S A, 1994. **91**(19): p. 8827-31.

208. DeBernardi, M.A., T. Seki, and G. Brooker, *Inhibition of cAMP accumulation by intracellular calcium mobilization in C6-2B cells stably transfected with substance K receptor cDNA.* Proc Natl Acad Sci U S A, 1991. **88**(20): p. 9257-61.

209. Kuo, I.Y. and B.E. Ehrlich, *Signaling in muscle contraction.* Cold Spring Harb Perspect Biol, 2015. **7**(2): p. a006023.

210. Li, L., et al., *Phosphorylation of phospholamban and troponin I in beta-adrenergic-induced acceleration of cardiac relaxation.* Am J Physiol Heart Circ Physiol, 2000. **278**(3): p. H769-79.

211. Wehbe, N., et al., *EPAC in Vascular Smooth Muscle Cells.* Int J Mol Sci, 2020. **21**(14).

212. Roscioni, S.S., et al., *Epac as a novel effector of airway smooth muscle relaxation.* Journal of Cellular and Molecular Medicine, 2011. **15**(7): p. 1551-1563.

213. Chen, Y.-f., et al., *Exchange protein directly activated by cAMP (Epac) protects against airway inflammation and airway remodeling in asthmatic mice.* Respiratory Research, 2019. **20**(1): p. 285.

214. Alkawadri, T., et al., *M2 Muscarinic Receptor-Dependent Contractions of Airway Smooth Muscle are Inhibited by Activation of β-Adrenoceptors.* Function (Oxf), 2022. **3**(6): p. zqac050.

215. Bean, B.P., *Classes of calcium channels in vertebrate cells.* Annu Rev Physiol, 1989. **51**: p. 367-84.

216. Hirota, S. and L.J. Janssen, *Store-refilling involves both L-type calcium channels and reverse-mode sodium-calcium exchange in airway smooth muscle.* Eur Respir J, 2007. **30**(2): p. 269-78.

217. Janssen, L.J., *T-type and L-type Ca2+ currents in canine bronchial smooth muscle: characterization and physiological roles.* Am J Physiol, 1997. **272**(6 Pt 1): p. C1757-65.

218. Kamp, T.J. and J.W. Hell, *Regulation of cardiac L-type calcium channels by protein kinase A and protein kinase C.* Circ Res, 2000. **87**(12): p. 1095-102.

219. Sang, L., et al., *The molecular basis of the inhibition of Ca(V)1 calcium-dependent inactivation by the distal carboxy tail.* J Biol Chem, 2021. **296**: p. 100502.

220. Zamponi, M.T.A.a.G.W., *Voltage-Dependent Inactivation of Voltage Gated Calcium Channels*. Madame Curie Bioscience Database [Internet]. 2000-2013, Austin (TX): Landes Bioscience.

221. Liu, Z. and R.A. Khalil, *Evolving mechanisms of vascular smooth muscle contraction highlight key targets in vascular disease.* Biochem Pharmacol, 2018. **153**: p. 91-122.

222. Grandordy, B.M., et al., *Phosphatidylinositol response to cholinergic agonists in airway smooth muscle: relationship to contraction and muscarinic receptor occupancy.* J Pharmacol Exp Ther, 1986. **238**(1): p. 273-9.

223. Yang, C.M., Y.L. Yo, and Y.Y. Wang, *Intracellular calcium in canine cultured tracheal smooth muscle cells is regulated by M3 muscarinic receptors.* Br J Pharmacol, 1993. **110**(3): p. 983-8.

224. Liu, Q.H., Y.M. Zheng, and Y.X. Wang, *Two distinct signaling pathways for regulation of spontaneous local Ca2+ release by phospholipase C in airway smooth muscle cells.* Pflugers Arch, 2007. **453**(4): p. 531-41.

225. Bai, Y., M. Edelmann, and M.J. Sanderson, *The contribution of inositol 1,4,5-trisphosphate and ryanodine receptors to agonist-induced Ca(2+) signaling of airway smooth muscle cells.* Am J Physiol Lung Cell Mol Physiol, 2009. **297**(2): p. L347-61.

226. Janssen, L.J., *Ionic mechanisms and Ca(2+) regulation in airway smooth muscle contraction: do the data contradict dogma?* Am J Physiol Lung Cell Mol Physiol, 2002. **282**(6): p. L1161-78.

227. Perez-Zoghbi, J.F., et al., *Ion channel regulation of intracellular calcium and airway smooth muscle function.* Pulm Pharmacol Ther, 2009. **22**(5): p. 388-97.

228. Chen, J. and M.J. Sanderson, *Store-operated calcium entry is required for sustained contraction and Ca(2+) oscillations of airway smooth muscle.* J Physiol, 2017. **595**(10): p. 3203-3218.

229. Kajita, J. and H. Yamaguchi, *Calcium mobilization by muscarinic cholinergic stimulation in bovine single airway smooth muscle.* Am J Physiol, 1993. **264**(5 Pt 1): p. L496-503.

230. Mátyás, S., V. Pucovský, and V. Bauer, *Involvement of different Ca2+ sources in changes of responsiveness of guinea-pig trachea to repeated administration of histamine and acetylcholine.* Gen Physiol Biophys, 1995. **14**(1): p. 51-60.

231. Flores-Soto, E., et al., *Sarcoplasmic reticulum Ca(2+) refilling is determined by L-type Ca(2+) and store operated Ca(2+) channels in guinea pig airway smooth muscle.* Eur J Pharmacol, 2013. **721**(1-3): p. 21-8.

232. Ahmed, F., R.W. Foster, and R.C. Small, *Some effects of nifedipine in guinea-pig isolated trachealis.* Br J Pharmacol, 1985. **84**(4): p. 861-9.

233. Farley, J.M. and P.R. Miles, *The sources of calcium for acetylcholine-induced contractions of dog tracheal smooth muscle.* J Pharmacol Exp Ther, 1978. **207**(2): p. 340-6.

234. Byron, K.L., et al., *Kv7 (KCNQ) potassium channels and L-type calcium channels in the regulation of airway diameter*, in *Calcium Signaling in Airway Smooth Muscle Cells*. 2013, Springer. p. 21-33.

235. Shieh, C.-C., et al., *Cromakalim effects of acetylcholine-induced changes in cytosolic calcium and tension in swine trachealis.* The Journal of pharmacology and experimental therapeutics, 1992. **260**(1): p. 261-268.

236. Unno, T., et al., *M(2) and M(3) muscarinic receptor-mediated contractions in longitudinal smooth muscle of the ileum studied with receptor knockout mice.* Br J Pharmacol, 2005. **146**(1): p. 98-108.

237. Flockerzi, V., *Non-selective Cation Channels*, in *Encyclopedia of Molecular Pharmacology*, S. Offermanns and W. Rosenthal, Editors. 2008, Springer Berlin Heidelberg: Berlin, Heidelberg. p. 870-871.

238. Samanta, A., T.E.T. Hughes, and V.Y. Moiseenkova-Bell, *Transient Receptor Potential (TRP) Channels.* Subcell Biochem, 2018. **87**: p. 141-165.

239. Himmel, N.J. and D.N. Cox, *Transient receptor potential channels: current perspectives on evolution, structure, function and nomenclature.* Proc Biol Sci, 2020. **287**(1933): p. 20201309.

240. White, T.A., et al., *Role of transient receptor potential C3 in TNF-alpha-enhanced calcium influx in human airway myocytes.* Am J Respir Cell Mol Biol, 2006. **35**(2): p. 243-51.

241. Wang, Y.X. and Y.M. Zheng, *Molecular expression and functional role of canonical transient receptor potential channels in airway smooth muscle cells.* Adv Exp Med Biol, 2011. **704**: p. 731-47.

242. Ong, H.L., et al., *Evidence for the expression of transient receptor potential proteins in guinea pig airway smooth muscle cells.* Respirology, 2003. **8**(1): p. 23-32.

243. Ambudkar, I.S., *Unraveling smooth muscle contraction: the TRP link.* Gastroenterology, 2009. **137**(4): p. 1211-4.

244. Zholos, A.V., *Regulation of TRP-like muscarinic cation current in gastrointestinal smooth muscle with special reference to PLC/InsP3/Ca2+ system.* Acta Pharmacologica Sinica, 2006. **27**(7): p. 833-842.

245. Huynh, K.W., et al., *Structural insight into the assembly of TRPV channels.* Structure, 2014. **22**(2): p. 260-8.

246. Jia, Y., et al., *Functional TRPV4 channels are expressed in human airway smooth muscle cells.* Am J Physiol Lung Cell Mol Physiol, 2004. **287**(2): p. L272-8.

247. Lalloo, U.G., et al., *Capsazepine inhibits cough induced by capsaicin and citric acid but not by hypertonic saline in guinea pigs.* J Appl Physiol (1985), 1995. **79**(4): p. 1082-7.

248. Fuller, R.W., C.M. Dixon, and P.J. Barnes, *Bronchoconstrictor response to inhaled capsaicin in humans.* J Appl Physiol (1985), 1985. **58**(4): p. 1080-4.

249. Grace, M.S., et al., *Transient receptor potential (TRP) channels in the airway: role in airway disease.* Br J Pharmacol, 2014. **171**(10): p. 2593-607.

250. S. J. Bonvini, J.J.A., M. S. Grace, K. E. Baker, M. A. Birrell, M. G. Belvisi *Activation of TRPV4 causes bronchoconstriction: A possible role in respiratory disease?* in *ERS Congress, Barcelona*. 2013.

251. Huang, Y., et al., *A structural overview of the ion channels of the TRPM family.* Cell Calcium, 2020. **85**: p. 102111.

252. Zhang, M., et al., *TRP (transient receptor potential) ion channel family: structures, biological functions and therapeutic interventions for diseases.* Signal Transduction and Targeted Therapy, 2023. **8**(1): p. 261.

253. Gosling, M., C. Poll, and S. Li, *TRP channels in airway smooth muscle as therapeutic targets.* Naunyn-Schmiedeberg's Archives of Pharmacology, 2005. **371**(4): p. 277-284.

254. Earley, S., *TRPM4 channels in smooth muscle function.* Pflugers Arch, 2013. **465**(9): p. 1223-31.

255. Kunzelmann, K., et al., *TMEM16A in Cystic Fibrosis: Activating or Inhibiting?* Front Pharmacol, 2019. **10**: p. 3.

256. Huang, F., et al., *Calcium-activated chloride channel TMEM16A modulates mucin secretion and airway smooth muscle contraction.* Proc Natl Acad Sci U S A, 2012. **109**(40): p. 16354-9.

257. Liang, P., et al., *Niclosamide potentiates TMEM16A and induces vasoconstriction.* bioRxiv, 2023.

258. Anagnostopoulou, P., et al., *Allergic airway inflammation induces a pro-secretory epithelial ion transport phenotype in mice.* Eur Respir J, 2010. **36**(6): p. 1436-47.

259. Danielsson, J., et al., *Agonism of the TMEM16A calcium-activated chloride channel modulates airway smooth muscle tone.* Am J Physiol Lung Cell Mol Physiol, 2020. **318**(2): p. L287-l295.

260. Zhang, C.H., et al., *The transmembrane protein 16A Ca(2+)-activated Cl- channel in airway smooth muscle contributes to airway hyperresponsiveness.* Am J Respir Crit Care Med, 2013. **187**(4): p. 374-81.

261. Cabrita, I., et al., *Niclosamide repurposed for the treatment of inflammatory airway disease.* JCI Insight, 2019. **4**(15).

262. Chipperfield, A.R., J.P. Davis, and A.A. Harper, *An acetazolamide-sensitive inward chloride pump in vascular smooth muscle.* Biochem Biophys Res Commun, 1993. **194**(1): p. 407-12.

263. Bulley, S. and J.H. Jaggar, *Cl^- channels in smooth muscle cells.* Pflugers Arch, 2014. **466**(5): p. 861-72.

264. Chipperfield, A.R. and A.A. Harper, *Chloride in smooth muscle.* Prog Biophys Mol Biol, 2000. **74**(3-5): p. 175-221.

265. Wang, P., et al., *Inflammatory mediators mediate airway smooth muscle contraction through a G protein-coupled receptor–transmembrane protein 16A–voltage-dependent Ca2+ channel axis and contribute to bronchial hyperresponsiveness in asthma.* Journal of Allergy and Clinical Immunology, 2018. **141**(4): p. 1259-1268. e11.

266. Danielsson, J., et al., *Antagonists of the TMEM16A calcium-activated chloride channel modulate airway smooth muscle tone and intracellular calcium.* Anesthesiology, 2015. **123**(3): p. 569-81.

267. Dwivedi, R., et al., *The TMEM16A blockers benzbromarone and MONNA cause intracellular Ca(2+)-release in mouse bronchial smooth muscle cells.* Eur J Pharmacol, 2023. **947**: p. 175677.

268. Li, M., et al., *Potassium channels: Novel targets for tumor diagnosis and chemoresistance.* Front Oncol, 2022. **12**: p. 1074469.

269. Guéguinou, M., et al., *KCa and Ca2+ channels: The complex thought.* Biochimica et Biophysica Acta (BBA) - Molecular Cell Research, 2014. **1843**(10): p. 2322-2333.

270. Sancho, M. and B.D. Kyle, *The Large-Conductance, Calcium-Activated Potassium Channel: A Big Key Regulator of Cell Physiology.* Front Physiol, 2021. **12**: p. 750615.

271. Adams, P.R., et al., *Intracellular Ca2+ activates a fast voltage-sensitive K+ current in vertebrate sympathetic neurones.* Nature, 1982. **296**(5859): p. 746-9.

272. Contet, C., et al., *BK Channels in the Central Nervous System.* Int Rev Neurobiol, 2016. **128**: p. 281-342.

273. Kotlikoff, M.I., *Potassium channels in airway smooth muscle: a tale of two channels.* Pharmacol Ther, 1993. **58**(1): p. 1-12.

274. Kshatri, A.S., A. Gonzalez-Hernandez, and T. Giraldez, *Physiological Roles and Therapeutic Potential of Ca(2+) Activated Potassium Channels in the Nervous System.* Front Mol Neurosci, 2018. **11**: p. 258.

275. Bradley, E., et al., *Inhibitory effects of openers of large-conductance Ca2+-activated K+ channels on agonist-induced phasic contractions in rabbit and mouse bronchial smooth muscle.* American Journal of Physiology-Cell Physiology, 2018. **315**(6): p. C818-C829.

276. Macmillan, S., et al., *A comparison of the effects of SCA40, NS 004 and NS 1619 on large conductance Ca(2+)-activated K+ channels in bovine tracheal smooth muscle cells in culture.* Br J Pharmacol, 1995. **116**(1): p. 1656-60.

277. McCann, J.D. and M.J. Welsh, *Calcium-activated potassium channels in canine airway smooth muscle.* J Physiol, 1986. **372**: p. 113-27.

278. Saunders, H.M. and J.M. Farley, *Spontaneous transient outward currents and Ca(++)-activated K+ channels in swine tracheal smooth muscle cells.* Journal of Pharmacology and Experimental Therapeutics, 1991. **257**(3): p. 1114.

279. Lee, S.H. and Y.E. Earm, *Caffeine induces periodic oscillations of Ca(2+)-activated K+ current in pulmonary arterial smooth muscle cells.* Pflugers Arch, 1994. **426**(3-4): p. 189-98.

280. Jackson, W.F., *Potassium Channels in Regulation of Vascular Smooth Muscle Contraction and Growth.* Adv Pharmacol, 2017. **78**: p. 89-144.

281. Barman, S.A., S. Zhu, and R.E. White, *Protein kinase C inhibits BKCa channel activity in pulmonary arterial smooth muscle.* Am J Physiol Lung Cell Mol Physiol, 2004. **286**(1): p. L149-55.

282. Liu, B., A.M. Freyer, and I.P. Hall, *Bradykinin activates calcium-dependent potassium channels in cultured human airway smooth muscle cells.* Am J Physiol Lung Cell Mol Physiol, 2007. **292**(4): p. L898-907.

283. Amrani, Y. and C. Bronner, *Tumor necrosis factor alpha potentiates the increase in cytosolic free calcium induced by bradykinin in guinea-pig tracheal smooth muscle cells.* C R Acad Sci III, 1993. **316**(12): p. 1489-94.

284. Schmidlin, F., et al., *Interleukin-1beta induces bradykinin B2 receptor gene expression through a prostanoid cyclic AMP-dependent pathway in human bronchial smooth muscle cells.* Mol Pharmacol, 1998. **53**(6): p. 1009-15.

285. Zhang, Y., M. Adner, and L.O. Cardell, *Up-regulation of bradykinin receptors in a murine in-vitro model of chronic airway inflammation.* Eur J Pharmacol, 2004. **489**(1-2): p. 117-26.

286. Zhou, X.B., et al., *M2 muscarinic receptors induce airway smooth muscle activation via a dual, Gbetagamma-mediated inhibition of large conductance Ca2+-activated K+ channel activity.* J Biol Chem, 2008. **283**(30): p. 21036-44.

287. Goldklang, M.P., et al., *Treatment of experimental asthma using a single small molecule with anti-inflammatory and BK channel-activating properties.* Faseb j, 2013. **27**(12): p. 4975-86.

288. Nieves-Cintrón, M., et al., *Regulation of voltage-gated potassium channels in vascular smooth muscle during hypertension and metabolic disorders.* Microcirculation, 2018. **25**(1).

289. Huang, Y., et al., *Voltage-gated potassium channels KCNQs: Structures, mechanisms, and modulations.* Biochemical and Biophysical Research Communications, 2023. **689**: p. 149218.

290. Mondéjar-Parreño, G., et al., *Uncovered Contribution of Kv7 Channels to Pulmonary Vascular Tone in Pulmonary Arterial Hypertension.* Hypertension, 2020. **76**(4): p. 1134-1146.

291. Brueggemann, L.I., L.L. Cribbs, and K.L. Byron, *Heteromeric Channels Formed From Alternating Kv7.4 and Kv7.5 α-Subunits Display Biophysical, Regulatory, and Pharmacological Characteristics of Smooth Muscle M-Currents.* Front Physiol, 2020. **11**: p. 992.

292. Brueggemann, L.I., et al., *Kv7 potassium channels in airway smooth muscle cells: signal transduction intermediates and pharmacological targets for bronchodilator therapy.* Am J Physiol Lung Cell Mol Physiol, 2012. **302**(1): p. L120-32.

293. Kreir, M., et al., *Role of Kv7.2/Kv7.3 and M(1) muscarinic receptors in the regulation of neuronal excitability in hiPSC-derived neurons.* Eur J Pharmacol, 2019. **858**: p. 172474.

294. Wang, J.-j. and Y. Li, *KCNQ potassium channels in sensory system and neural circuits.* Acta Pharmacologica Sinica, 2016. **37**(1): p. 25-33.

295. Jones, F., N. Gamper, and H. Gao, *Kv7 Channels and Excitability Disorders.* Handb Exp Pharmacol, 2021. **267**: p. 185-230.

296. Zhang, H., et al., *PIP2 Activates KCNQ Channels, and Its Hydrolysis Underlies Receptor-Mediated Inhibition of M Currents.* Neuron, 2003. **37**(6): p. 963-975.

297. Li, Y., et al., *Regulation of Kv7 (KCNQ) K+ channel open probability by phosphatidylinositol 4,5-bisphosphate.* J Neurosci, 2005. **25**(43): p. 9825-35.

298. van der Horst, J., I.A. Greenwood, and T.A. Jepps, *Cyclic AMP-Dependent Regulation of Kv7 Voltage-Gated Potassium Channels.* Front Physiol, 2020. **11**: p. 727.

299. Brueggemann, L.I., et al., *Mechanisms of PKA-dependent potentiation of Kv7. 5 channel activity in human airway smooth muscle cells.* International Journal of Molecular Sciences, 2018. **19**(8): p. 2223.

300. Elliott, D.J., et al., *Molecular mechanism of voltage sensor movements in a potassium channel.* Embo j, 2004. **23**(24): p. 4717-26.

301. Jepps, T.A., V. Barrese, and F. Miceli, *Editorial: Kv7 Channels: Structure, Physiology, and Pharmacology.* Front Physiol, 2021. **12**: p. 679317.

302. Alaimo, A., et al., *Lack of correlation between surface expression and currents in epileptogenic AB-calmodulin binding domain Kv7.2 potassium channel mutants.* Channels (Austin), 2018. **12**(1): p. 299-310.

303. Baculis, B.C., J. Zhang, and H.J. Chung, *The Role of K(v)7 Channels in Neural Plasticity and Behavior.* Front Physiol, 2020. **11**: p. 568667.

304. Brueggemann, L.I., L.L. Cribbs, and K.L. Byron, *Structural Determinants of Kv7.5 Potassium Channels That Confer Changes in Phosphatidylinositol 4,5-Bisphosphate (PIP2) Affinity and Signaling Sensitivities in Smooth Muscle Cells.* Molecular Pharmacology, 2020. **97**(3): p. 145-158.

305. Greene, D.L. and N. Hoshi, *Modulation of Kv7 channels and excitability in the brain.* Cell Mol Life Sci, 2017. **74**(3): p. 495-508.

306. Zaydman, M.A. and J. Cui, *PIP2 regulation of KCNQ channels: biophysical and molecular mechanisms for lipid modulation of voltage-dependent gating.* Front Physiol, 2014. **5**: p. 195.

307. Zhang, Q., et al., *Dynamic PIP2 interactions with voltage sensor elements contribute to KCNQ2 channel gating.* Proc Natl Acad Sci U S A, 2013. **110**(50): p. 20093-8.

308. Pant, S., et al., *PIP2-dependent coupling of voltage sensor and pore domains in Kv7.2 channel.* Communications Biology, 2021. **4**(1): p. 1189.

309. Rohacs, T., *Phosphoinositide regulation of non-canonical transient receptor potential channels.* Cell Calcium, 2009. **45**(6): p. 554-65.

310. Haick, J.M., et al., *PKC-dependent regulation of Kv7.5 channels by the bronchoconstrictor histamine in human airway smooth muscle cells.* Am J Physiol Lung Cell Mol Physiol, 2017. **312**(6): p. L822-l834.

311. Salzer, I., et al., *Phosphorylation regulates the sensitivity of voltage-gated Kv7.2 channels towards phosphatidylinositol-4,5-bisphosphate.* J Physiol, 2017. **595**(3): p. 759-776.

312. Shvetsova, A.A., et al., *Potassium channel-mediated NO-induced vasodilation during maturation: Dominance of Kv7 channels.* FASEB Bioadv, 2025. **7**(3): p. e1490.

313. Tykocki, N.R., E.M. Boerman, and W.F. Jackson, *Smooth Muscle Ion Channels and Regulation of Vascular Tone in Resistance Arteries and Arterioles.* Compr Physiol, 2017. **7**(2): p. 485-581.

314. Battefeld, A., et al., *Heteromeric Kv7.2/7.3 channels differentially regulate action potential initiation and conduction in neocortical myelinated axons.* J Neurosci, 2014. **34**(10): p. 3719-32.

315. Stewart, A.P., et al., *The Kv7.2/Kv7.3 heterotetramer assembles with a random subunit arrangement.* J Biol Chem, 2012. **287**(15): p. 11870-7.

316. Brueggemann, L.I., et al., *Differential Protein Kinase C-dependent Modulation of Kv7.4 and Kv7.5 Subunits of Vascular Kv7 Channels *.* Journal of Biological Chemistry, 2014. **289**(4): p. 2099-2111.

317. Chadha, P.S., et al., *Contribution of kv7.4/kv7.5 heteromers to intrinsic and calcitonin gene-related peptide-induced cerebral reactivity.* Arterioscler Thromb Vasc Biol, 2014. **34**(4): p. 887-93.

318. Oliveras, A., et al., *Functional assembly of Kv7.1/Kv7.5 channels with emerging properties on vascular muscle physiology.* Arterioscler Thromb Vasc Biol, 2014. **34**(7): p. 1522-30.

319. Soh, H., et al., *KCNQ2 and KCNQ5 form heteromeric channels independent of KCNQ3.* Proc Natl Acad Sci U S A, 2022. **119**(13): p. e2117640119.

320. Howard, R.J., et al., *Structural Insight into KCNQ (Kv7) Channel Assembly and Channelopathy.* Neuron, 2007. **53**(5): p. 663-675.

321. Etxeberria, A., et al., *Three mechanisms underlie KCNQ2/3 heteromeric potassium M-channel potentiation.* J Neurosci, 2004. **24**(41): p. 9146-52.

322. McCrossan, Z.A. and G.W. Abbott, *The MinK-related peptides.* Neuropharmacology, 2004. **47**(6): p. 787-821.

323. Nakajo, K. and G. Kasuya, *Modulation of potassium channels by transmembrane auxiliary subunits via voltage-sensing domains.* Physiological Reports, 2024. **12**(6): p. e15980.

324. Kanda, V.A. and G.W. Abbott, *KCNE Regulation of K(+) Channel Trafficking - a Sisyphean Task?* Front Physiol, 2012. **3**: p. 231.

325. Gofman, Y., et al., *How does KCNE1 regulate the Kv7.1 potassium channel? Model-structure, mutations, and dynamics of the Kv7.1-KCNE1 complex.* Structure, 2012. **20**(8): p. 1343-52.

326. Lundby, A., G.N. Tseng, and N. Schmitt, *Structural basis for K(V)7.1-KCNE(x) interactions in the I(Ks) channel complex.* Heart Rhythm, 2010. **7**(5): p. 708-13.

327. Seebohm, G., et al., *Pharmacological activation of normal and arrhythmia-associated mutant KCNQ1 potassium channels.* Circ Res, 2003. **93**(10): p. 941-7.

328. Roura-Ferrer, M., et al., *Functional implications of KCNE subunit expression for the Kv7.5 (KCNQ5) channel.* Cell Physiol Biochem, 2009. **24**(5-6): p. 325-34.

329. Abbott, G.W., *KCNE1 and KCNE3: The yin and yang of voltage-gated K(+) channel regulation.* Gene, 2016. **576**(1 Pt 1): p. 1-13.

330. Tinel, N., et al., *KCNE2 confers background current characteristics to the cardiac KCNQ1 potassium channel.* Embo j, 2000. **19**(23): p. 6326-30.

331. Dedek, K. and S. Waldegger, *Colocalization of KCNQ1/KCNE channel subunits in the mouse gastrointestinal tract.* Pflugers Arch, 2001. **442**(6): p. 896-902.

332. Barro-Soria, R., M.E. Perez, and H.P. Larsson, *KCNE3 acts by promoting voltage sensor activation in KCNQ1.* Proceedings of the National Academy of Sciences, 2015. **112**(52): p. E7286-E7292.

333. Grunnet, M., et al., *KCNE4 is an inhibitory subunit to the KCNQ1 channel.* J Physiol, 2002. **542**(Pt 1): p. 119-30.

334. Strutz-Seebohm, N., et al., *Functional coassembly of KCNQ4 with KCNE-beta- subunits in Xenopus oocytes.* Cell Physiol Biochem, 2006. **18**(1-3): p. 57-66.

335. Jepps, T.A., et al., *Fundamental role for the KCNE4 ancillary subunit in Kv7.4 regulation of arterial tone.* J Physiol, 2015. **593**(24): p. 5325-40.

336. Angelo, K., et al., *KCNE5 induces time- and voltage-dependent modulation of the KCNQ1 current.* Biophys J, 2002. **83**(4): p. 1997-2006.

337. Seebohm, G., M.C. Sanguinetti, and M. Pusch, *Tight coupling of rubidium conductance and inactivation in human KCNQ1 potassium channels.* J Physiol, 2003. **552**(Pt 2): p. 369-78.

338. Reddish, F.N., et al., *Calcium Dynamics Mediated by the Endoplasmic/Sarcoplasmic Reticulum and Related Diseases.* Int J Mol Sci, 2017. **18**(5).

339. Hill-Eubanks, D.C., et al., *Calcium signaling in smooth muscle.* Cold Spring Harb Perspect Biol, 2011. **3**(9): p. a004549.

340. Narayanan, D., A. Adebiyi, and J.H. Jaggar, *Inositol trisphosphate receptors in smooth muscle cells.* Am J Physiol Heart Circ Physiol, 2012. **302**(11): p. H2190-210.

341. Hall, I.P., *Second messengers, ion channels and pharmacology of airway smooth muscle.* Eur Respir J, 2000. **15**(6): p. 1120-7.

342. Gambardella, J., et al., *The discovery and development of IP3 receptor modulators: an update.* Expert Opin Drug Discov, 2021. **16**(6): p. 709-718.

343. Ashkenazi, A., et al., *An M2 Muscarinic Receptor Subtype Coupled to Both Adenylyl Cyclase and Phosphoinositide Turnover.* Science, 1987. **238**(4827): p. 672-675.

344. Tao, F.C., et al., *Inositol (1,4,5)trisphosphate metabolism and enhanced calcium mobilization in airway smooth muscle of hyperresponsive rats.* Am J Respir Cell Mol Biol, 2000. **23**(4): p. 514-20.

345. Guerrero-Hernández, A., et al., *Ryanodine receptors in smooth muscle.* Front Biosci, 2002. **7**: p. d1676-88.

346. Woll, K.A. and F. Van Petegem, *Calcium-release channels: structure and function of IP(3) receptors and ryanodine receptors.* Physiol Rev, 2022. **102**(1): p. 209-268.

347. Lanner, J.T., et al., *Ryanodine receptors: structure, expression, molecular details, and function in calcium release.* Cold Spring Harb Perspect Biol, 2010. **2**(11): p. a003996.

348. Takeshima, H., *Primary structure and expression from cDNAs of the ryanodine receptor.* Ann N Y Acad Sci, 1993. **707**: p. 165-77.

349. Hyvelin, J.M., et al., *Human isolated bronchial smooth muscle contains functional ryanodine/caffeine-sensitive Ca-release channels.* Am J Respir Crit Care Med, 2000. **162**(2 Pt 1): p. 687-94.

350. Wang, Y., et al., *[Expression of ryanodine receptor isoforms in airway smooth muscle cells of rats].* Zhongguo Ying Yong Sheng Li Xue Za Zhi, 2004. **20**(2): p. 181-4.

351. Lifshitz, L.M., et al., *Spatial organization of RYRs and BK channels underlying the activation of STOCs by Ca(2+) sparks in airway myocytes.* J Gen Physiol, 2011. **138**(2): p. 195-209.

352. Du, W., et al., *Ryanodine receptors in muscarinic receptor-mediated bronchoconstriction.* J Biol Chem, 2005. **280**(28): p. 26287-94.

353. Wu, K.-D., D. Bungard, and J. Lytton, *Regulation of SERCA Ca2+ pump expression by cytoplasmic [Ca2+] in vascular smooth muscle cells.* American Journal of Physiology-Cell Physiology, 2001. **280**(4): p. C843-C851.

354. Tong, X., A. Evangelista, and R.A. Cohen, *Targeting the redox regulation of SERCA in vascular physiology and disease.* Curr Opin Pharmacol, 2010. **10**(2): p. 133-8.

355. Janssen, L.J., et al., *Superficial buffer barrier and preferentially directed release of Ca2+ in canine airway smooth muscle.* Am J Physiol, 1999. **276**(5): p. L744-53.

356. Chen, Q., M. Cannell, and C. van Breemen, *The superficial buffer barrier in vascular smooth muscle.* Can J Physiol Pharmacol, 1992. **70**(4): p. 509-14.

357. Chen, Q. and C. van Breemen, *The superficial buffer barrier in venous smooth muscle: sarcoplasmic reticulum refilling and unloading.* Br J Pharmacol, 1993. **109**(2): p. 336-43.

358. van Breemen, C., Q. Chen, and I. Laher, *Superficial buffer barrier function of smooth muscle sarcoplasmic reticulum.* Trends Pharmacol Sci, 1995. **16**(3): p. 98-105.

359. Mahn, K., et al., *Diminished sarco/endoplasmic reticulum Ca2+ ATPase (SERCA) expression contributes to airway remodelling in bronchial asthma.* Proc Natl Acad Sci U S A, 2009. **106**(26): p. 10775-80.

360. Clark, J.H., et al., *Identification of functionally segregated sarcoplasmic reticulum calcium stores in pulmonary arterial smooth muscle.* J Biol Chem, 2010. **285**(18): p. 13542-9.

361. Prakriya, M. and R.S. Lewis, *Store-Operated Calcium Channels.* Physiol Rev, 2015. **95**(4): p. 1383-436.

362. Ghosh, D., et al., *Calcium Channels in Vascular Smooth Muscle.* Adv Pharmacol, 2017. **78**: p. 49-87.

363. Figueiredo, I.A.D., et al., *A review of the pathophysiology and the role of ion channels on bronchial asthma.* Front Pharmacol, 2023. **14**: p. 1236550.

364. Johnson, M. and M. Trebak, *ORAI channels in cellular remodeling of cardiorespiratory disease.* Cell Calcium, 2019. **79**: p. 1-10.

365. Spinelli, A.M., et al., *Airway smooth muscle STIM1 and Orai1 are upregulated in asthmatic mice and mediate PDGF-activated SOCE, CRAC currents, proliferation, and migration.* Pflugers Arch, 2012. **464**(5): p. 481-92.

366. Duke, J., *CHAPTER 9 - Pulmonary Function Testing*, in *Anesthesia Secrets (Fourth Edition)*, J. Duke, Editor. 2011, Mosby: Philadelphia. p. 68-74.

367. Yan, F., et al., *Roles of airway smooth muscle dysfunction in chronic obstructive pulmonary disease.* J Transl Med, 2018. **16**(1): p. 262.

368. Doeing, D.C. and J. Solway, *Airway smooth muscle in the pathophysiology and treatment of asthma.* J Appl Physiol (1985), 2013. **114**(7): p. 834-43.

369. Lauzon, A.M., et al., *A multi-scale approach to airway hyperresponsiveness: from molecule to organ.* Front Physiol, 2012. **3**: p. 191.

370. Eschenbacher, W.L. and D. Sheppard, *Respiratory heat loss is not the sole stimulus for bronchoconstriction induced by isocapnic hyperpnea with dry air.* Am Rev Respir Dis, 1985. **131**(6): p. 894-901.

371. Aggarwal, B., A. Mulgirigama, and N. Berend, *Exercise-induced bronchoconstriction: prevalence, pathophysiology, patient impact, diagnosis and management.* NPJ Prim Care Respir Med, 2018. **28**(1): p. 31.

372. Caggiano, S., et al., *Exercise-Induced Bronchospasm and Allergy.* Front Pediatr, 2017. **5**: p. 131.

373. Del Giacco, S.R., et al., *Exercise and asthma: an overview.* Eur Clin Respir J, 2015. **2**: p. 27984.

374. Buels, K.S. and A.D. Fryer, *Muscarinic receptor antagonists: effects on pulmonary function.* Handb Exp Pharmacol, 2012(208): p. 317-41.

375. Li, L., et al., *Possible involvement of the novel CPI-17 protein in protein kinase C signal transduction of rabbit arterial smooth muscle.* J Physiol, 1998. **508 (Pt 3)**(Pt 3): p. 871-81.

376. Pang, H., et al., *RhoA-Rho kinase pathway mediates thrombin- and U-46619-induced phosphorylation of a myosin phosphatase inhibitor, CPI-17, in vascular smooth muscle cells.* Am J Physiol Cell Physiol, 2005. **289**(2): p. C352-60.

377. Mahn, K., et al., *Ca(2+) homeostasis and structural and functional remodelling of airway smooth muscle in asthma.* Thorax, 2010. **65**(6): p. 547-52.

378. Xiong, D.J.P., J.G. Martin, and A.M. Lauzon, *Airway smooth muscle function in asthma.* Front Physiol, 2022. **13**: p. 993406.

379. Mazzone, S.B. and B.J. Undem, *Vagal Afferent Innervation of the Airways in Health and Disease.* Physiol Rev, 2016. **96**(3): p. 975-1024.

380. *Chronic Obstructive Pulmonary Disease (COPD)*. Centers for Disease Control and Prevention (CDC); Available from: https://www.cdc.gov/copd/index.html#:~:text=Chronic%20obstructive%20pulmonary%20disease%2C%20or,Americans%20who%20have%20this%20disease.

381. Chung, K.F., *The role of airway smooth muscle in the pathogenesis of airway wall remodeling in chronic obstructive pulmonary disease.* Proc Am Thorac Soc, 2005. **2**(4): p. 347-54; discussion 371-2.

382. Jones, R.L., et al., *Airway remodelling in COPD: It's not asthma!* Respirology, 2016. **21**(8): p. 1347-1356.

383. Benayoun, L., et al., *Airway structural alterations selectively associated with severe asthma.* Am J Respir Crit Care Med, 2003. **167**(10): p. 1360-8.

384. Hogg, J.C., J.E. McDonough, and M. Suzuki, *Small airway obstruction in COPD: new insights based on micro-CT imaging and MRI imaging.* Chest, 2013. **143**(5): p. 1436-1443.

385. Loring, S.H., M. Garcia-Jacques, and A. Malhotra, *Pulmonary characteristics in COPD and mechanisms of increased work of breathing.* J Appl Physiol (1985), 2009. **107**(1): p. 309-14.

386. Seow, C.Y., *Passive stiffness of airway smooth muscle: the next target for improving airway distensibility and treatment for asthma?* Pulm Pharmacol Ther, 2013. **26**(1): p. 37-41.

387. Jindal, S.K., *Remodeling in asthma and COPD-recent concepts.* Lung India, 2016. **33**(1): p. 1-2.

388. Rossi, A., et al., *Chronic obstructive pulmonary disease with mild airflow limitation: current knowledge and proposal for future research - a consensus document from six scientific societies.* Int J Chron Obstruct Pulmon Dis, 2017. **12**: p. 2593-2610.

389. Dekkers, B.G.J., et al., *Basement membranes in obstructive pulmonary diseases.* Matrix Biol Plus, 2021. **12**: p. 100092.

390. Higham, A., et al., *The pathology of small airways disease in COPD: historical aspects and future directions.* Respir Res, 2019. **20**(1): p. 49.

391. Qaisar, R., et al., *Sarcopenia in pulmonary diseases is associated with elevated sarcoplasmic reticulum stress and myonuclear disorganization.* Histochemistry and Cell Biology, 2022. **157**(1): p. 93-105.

392. Nguyen, T., et al., *Effect of chronic obstructive pulmonary disease on calcium pump ATPase expression in human diaphragm.* J Appl Physiol (1985), 2005. **98**(6): p. 2004-10.

393. Hanania, N.A., et al., *Treatments for COPD.* Respir Med, 2005. **99 Suppl B**: p. S28-40.

394. Alagha, K., et al., *Long-acting muscarinic receptor antagonists for the treatment of chronic airway diseases.* Ther Adv Chronic Dis, 2014. **5**(2): p. 85-98.

395. *Global Initiative for Chronic Obstructive Lung Disease Global Strategy for the Diagnosis, Management, and Prevention of Chronic Obstructive Lung Disease: 2022 Report*. 2022; Available from: https://goldcopd.org/wp-content/uploads/2021/12/GOLD-REPORT-2022-v1.1-22Nov2021_WMV.pdf.

396. Maia, I.S., et al., *Long-acting muscarinic antagonists vs. long-acting β 2 agonists in COPD exacerbations: a systematic review and meta-analysis.* J Bras Pneumol, 2017. **43**(4): p. 302-312.

397. Jacoby, D.B. and A.D. Fryer, *Anticholinergic therapy for airway diseases.* Life Sci, 2001. **68**(22-23): p. 2565-72.

398. Cazzola, M., et al., *Pharmacology and therapeutics of bronchodilators.* Pharmacological reviews, 2012. **64**(3): p. 450-504.

399. Coulson, F.R. and A.D. Fryer, *Muscarinic acetylcholine receptors and airway diseases.* Pharmacology & therapeutics, 2003. **98**(1): p. 59-69.

400. Gosens, R., et al., *Muscarinic receptor signaling in the pathophysiology of asthma and COPD.* Respiratory research, 2006. **7**(1): p. 73.

401. Whicker, S., et al., *Effect of sensitization and aerosol antigen challenge in guinea-pigs—studies of airway receptor function and characteristics.* Pulmonary Pharmacology, 1990. **3**(3): p. 129-136.

402. Haddad, E.B., et al., *Muscarinic and beta-adrenergic receptor expression in peripheral lung from normal and asthmatic patients.* Am J Physiol, 1996. **270**(6 Pt 1): p. L947-53.

403. Donfack, J., et al., *Sequence variation in the promoter region of the cholinergic receptor muscarinic 3 gene and asthma and atopy.* Journal of allergy and clinical immunology, 2003. **111**(3): p. 527-532.

404. Hakonarson, H., D.J. Herrick, and M.M. Grunstein, *Mechanism of impaired beta-adrenoceptor responsiveness in atopic sensitized airway smooth muscle.* American Journal of Physiology-Lung Cellular and Molecular Physiology, 1995. **269**(5): p. L645-L652.

405. Chiba, Y., H. Sakai, and M. Misawa, *Possible involvement of Gi3 protein in augmented contraction of bronchial smooth muscle from antigen-induced airway hyperresponsive rats.* Biochemical pharmacology, 2001. **61**(7): p. 921-924.

406. Hamblin, A.S., *The role of cytokines in asthma.* Ann N Y Acad Sci, 1991. **629**: p. 250-61.

407. Kips, J.C., J. Tavernier, and R.A. Pauwels, *Tumor necrosis factor causes bronchial hyperresponsiveness in rats.* Am Rev Respir Dis, 1992. **145**(2 Pt 1): p. 332-6.

408. Broide, D.H., et al., *Cytokines in symptomatic asthma airways.* J Allergy Clin Immunol, 1992. **89**(5): p. 958-67.

409. Barnes, P.J., K.F. Chung, and C.P. Page, *Inflammatory mediators and asthma.* Pharmacological reviews, 1988. **40**(1): p. 49-84.

410. Hakonarson, H., et al., *Mechanism of cytokine-induced modulation of beta-adrenoceptor responsiveness in airway smooth muscle.* The Journal of clinical investigation, 1996. **97**(11): p. 2593-2600.

411. Bhatt, S., et al., *Targeting Molecular and Cellular Mechanisms in Chronic Obstructive Pulmonary Disease*, in *Targeting Cellular Signalling Pathways in Lung Diseases*, K. Dua, et al., Editors. 2021, Springer Singapore: Singapore. p. 127-146.

412. Ghosh, S., et al., *Role of voltage-gated Ca2+ channels and Ano1 Ca2+-activated Cl− channels in M2 muscarinic receptor-dependent contractions of murine airway smooth muscle.* American Journal of Physiology-Lung Cellular and Molecular Physiology, 2025. **328**(2): p. L301-L312.

413. Fransen, P., et al., *Contractile Behavior of Mouse Aorta Depends on SERCA2 Isoform Distribution: Effects of Replacing SERCA2a by SERCA2b.* Front Physiol, 2020. **11**: p. 282.

414. Mercer, M., et al., *K(V)7 channels modulate tension and calcium signaling in mouse corpus cavernosum.* Am J Physiol Cell Physiol, 2025. **328**(3): p. C729-c742.

415. Pluteanu, F., et al., *Inward Rectifier K(+) Currents Contribute to the Proarrhythmic Electrical Phenotype of Atria Overexpressing Cyclic Adenosine Monophosphate Response Element Modulator Isoform CREM-IbΔC-X.* J Am Heart Assoc, 2020. **9**(23): p. e016144.

416. Roepke, T.K., et al., *Genetic dissection reveals unexpected influence of beta subunits on KCNQ1 K+ channel polarized trafficking in vivo.* Faseb j, 2011. **25**(2): p. 727-36.

417. Baldi, L., et al., *Recombinant protein production by large-scale transient gene expression in mammalian cells: state of the art and future perspectives.* Biotechnol Lett, 2007. **29**(5): p. 677-84.

418. Dalton, A.C. and W.A. Barton, *Over-expression of secreted proteins from mammalian cell lines.* Protein Sci, 2014. **23**(5): p. 517-25.

419. Wurm, F.M., *Production of recombinant protein therapeutics in cultivated mammalian cells.* Nat Biotechnol, 2004. **22**(11): p. 1393-8.

420. Thomas, P. and T.G. Smart, *HEK293 cell line: a vehicle for the expression of recombinant proteins.* J Pharmacol Toxicol Methods, 2005. **51**(3): p. 187-200.

421. Lemtiri-Chlieh, F. and R. Ali, *Characterization of heterologously expressed transporter genes by patch- and voltage-clamp methods: application to cyclic nucleotide-dependent responses.* Methods Mol Biol, 2013. **1016**: p. 67-93.

422. *Useful Numbers for Cell Culture*. 2021; Available from: https://www.thermofisher.com/ie/en/home/references/gibco-cell-culture-basics/cell-culture-protocols/cell-culture-useful-numbers.html.

423. Zavaritskaya, O., et al., *Vasodilation of rat skeletal muscle arteries by the novel BK channel opener GoSlo is mediated by the simultaneous activation of BK and K(v) 7 channels.* Br J Pharmacol, 2020. **177**(5): p. 1164-1186.

424. Ogden, D., *Microelectrode techniques. The Plymouth workshop handbook*. 1994: The Company of Biologists Ltd.

425. Hamill, O.P., et al., *Improved patch-clamp techniques for high-resolution current recording from cells and cell-free membrane patches.* Pflugers Arch, 1981. **391**(2): p. 85-100.

426. Roffel, A.F., et al., *Muscarinic M2 receptors in bovine tracheal smooth muscle: discrepancies between binding and function.* Eur J Pharmacol, 1988. **153**(1): p. 73-82.

427. Fernandes, L.B., A.D. Fryer, and C.A. Hirshman, *M2 muscarinic receptors inhibit isoproterenol-induced relaxation of canine airway smooth muscle.* J Pharmacol Exp Ther, 1992. **262**(1): p. 119-26.

428. Jude, J.A., et al., *Calcium signaling in airway smooth muscle.* Proc Am Thorac Soc, 2008. **5**(1): p. 15-22.

429. De Moudt, S., et al., *GSK-7975A, an inhibitor of Ca(2+) release-activated calcium channels, depresses isometric contraction of mouse aorta.* Eur J Pharmacol, 2021. **906**: p. 174197.

430. Sankary, R.M., et al., *Muscarinic cholinergic inhibition of cyclic AMP accumulation in airway smooth muscle. Role of a pertussis toxin-sensitive protein.* Am Rev Respir Dis, 1988. **138**(1): p. 145-50.

431. Milligan, G. and F.M. Mitchell, *An arginine residue is the site of receptor-stimulated, cholera toxin-catalysed ADP-ribosylation of pertussis toxin-sensitive G-proteins.* Cell Signal, 1993. **5**(4): p. 485-93.

432. Yamashita, T. and S. Kokubun, *Nonselective cationic currents activated by acetylcholine in swine tracheal smooth muscle cells.* Can J Physiol Pharmacol, 1999. **77**(10): p. 796-805.

433. Song, T., et al., *Inositol 1,4,5-trisphosphate activates TRPC3 channels to cause extracellular Ca2+ influx in airway smooth muscle cells.* Am J Physiol Lung Cell Mol Physiol, 2015. **309**(12): p. L1455-66.

434. Dietrich, A., D. Steinritz, and T. Gudermann, *Transient receptor potential (TRP) channels as molecular targets in lung toxicology and associated diseases.* Cell Calcium, 2017. **67**: p. 123-137.

435. Behringer, E.J. and S.S. Segal, *Membrane potential governs calcium influx into microvascular endothelium: integral role for muscarinic receptor activation.* The Journal of Physiology, 2015. **593**(20): p. 4531-4548.

436. Kiyonaka, S., et al., *Selective and direct inhibition of TRPC3 channels underlies biological activities of a pyrazole compound.* Proc Natl Acad Sci U S A, 2009. **106**(13): p. 5400-5.

437. Kiyonaka, S., et al., *[Pharmacological properties of novel TRPC channel inhibitors].* Yakugaku Zasshi, 2010. **130**(3): p. 303-11.

438. Polat, O.K., et al., *Contribution of Coiled-Coil Assembly to Ca(2+)/Calmodulin-Dependent Inactivation of TRPC6 Channel and its Impacts on FSGS-Associated Phenotypes.* J Am Soc Nephrol, 2019. **30**(9): p. 1587-1603.

439. Cole, B.A. and E.B.E. Becker, *Modulation and Regulation of Canonical Transient Receptor Potential 3 (TRPC3) Channels.* Cells, 2023. **12**(18).

440. Hasan, R. and X. Zhang, *Ca(2+) Regulation of TRP Ion Channels.* Int J Mol Sci, 2018. **19**(4).

441. Sanz-Salvador, L., et al., *Agonist- and Ca2+-dependent desensitization of TRPV1 channel targets the receptor to lysosomes for degradation.* J Biol Chem, 2012. **287**(23): p. 19462-71.

442. Ishii, K., et al., *Effects of neostigmine on bronchoconstriction with continuous electrical stimulation in rats.* J Anesth, 2012. **26**(1): p. 80-4.

443. Saito, M., et al., *Effects of ketamine on neostigmine-induced contractile and phosphatidylinositol responses of the rat trachea.* Journal of Anesthesia, 2003. **17**(2): p. 104-107.

444. Bergner, A. and M.J. Sanderson, *Acetylcholine-induced calcium signaling and contraction of airway smooth muscle cells in lung slices.* J Gen Physiol, 2002. **119**(2): p. 187-98.

445. Ann Twiss, M., et al., *Efficacy of calcium channel blockers as maintenance therapy for asthma.* Br J Clin Pharmacol, 2002. **53**(3): p. 243-9.

446. Ozenne, G., et al., *Nifedipine in chronic bronchial asthma: a randomized double-blind crossover trial against placebo.* Eur J Respir Dis, 1985. **67**(4): p. 238-43.

447. Soldatov, N.M., *Ca2+ channel moving tail: link between Ca2+-induced inactivation and Ca2+ signal transduction.* Trends Pharmacol Sci, 2003. **24**(4): p. 167-71.

448. Unno, T., S. Komori, and H. Ohashi, *Inhibitory effect of muscarinic receptor activation on Ca2+ channel current in smooth muscle cells of guinea-pig ileum.* J Physiol, 1995. **484 (Pt 3)**(Pt 3): p. 567-81.

449. Dwivedi, R., et al., *Excitatory cholinergic responses in mouse primary bronchial smooth muscle require both Ca(2+) entry via l-type Ca(2+) channels and store operated Ca(2+) entry via Orai channels.* Cell Calcium, 2023. **112**: p. 102721.

450. Jiang, Y., et al., *TRPC channels mediated calcium entry is required for proliferation of human airway smooth muscle cells induced by nicotine-nAChR.* Biochimie, 2019. **158**: p. 139-148.

451. Nassini, R., et al., *Transient receptor potential ankyrin 1 channel localized to non-neuronal airway cells promotes non-neurogenic inflammation.* PLoS One, 2012. **7**(8): p. e42454.

452. Zhang, X., et al., *The effects of transient receptor potential channel (TRPC) on airway smooth muscle cell isolated from asthma model mice.* J Cell Biochem, 2018. **119**(7): p. 6033-6044.

453. Belvisi, M.G., et al., *Capsazepine as a selective antagonist of capsaicin-induced activation of C-fibres in guinea-pig bronchi.* Eur J Pharmacol, 1992. **215**(2-3): p. 341-4.

454. Trebak, M., et al., *Signaling Mechanism for Receptor-activated Canonical Transient Receptor Potential 3 (TRPC3) Channels*.* Journal of Biological Chemistry, 2003. **278**(18): p. 16244-16252.

455. Venkatachalam, K., F. Zheng, and D.L. Gill, *Regulation of canonical transient receptor potential (TRPC) channel function by diacylglycerol and protein kinase C.* J Biol Chem, 2003. **278**(31): p. 29031-40.

456. Kummer, W. and G. Krasteva-Christ, *Non-neuronal cholinergic airway epithelium biology.* Current Opinion in Pharmacology, 2014. **16**: p. 43-49.

457. Wilson, C., M.D. Lee, and J.G. McCarron, *Acetylcholine released by endothelial cells facilitates flow-mediated dilatation.* J Physiol, 2016. **594**(24): p. 7267-7307.

458. Wessler, I. and C. Kirkpatrick, *Acetylcholine beyond neurons: the non‐neuronal cholinergic system in humans.* British journal of pharmacology, 2008. **154**(8): p. 1558-1571.

459. Kolahian, S. and R. Gosens, *Cholinergic Regulation of Airway Inflammation and Remodelling.* Journal of Allergy, 2012. **2012**(1): p. 681258.

460. Snetkov, V.A. and J.P. Ward, *Ion currents in smooth muscle cells from human small bronchioles: presence of an inward rectifier K+ current and three types of large conductance K+ channel.* Exp Physiol, 1999. **84**(5): p. 835-846.

461. Brown, D.A. and P.R. Adams, *Muscarinic suppression of a novel voltage-sensitive K+ current in a vertebrate neurone.* Nature, 1980. **283**(5748): p. 673-6.

462. Constanti, A. and D.A. Brown, *M-Currents in voltage-clamped mammalian sympathetic neurones.* Neurosci Lett, 1981. **24**(3): p. 289-94.

463. Brueggemann, L.I., et al., *KCNQ (Kv7) potassium channel activators as bronchodilators: combination with a β2-adrenergic agonist enhances relaxation of rat airways.* Am J Physiol Lung Cell Mol Physiol, 2014. **306**(6): p. L476-86.

464. Evseev, A.I., et al., *Functional effects of KCNQ K(+) channels in airway smooth muscle.* Front Physiol, 2013. **4**: p. 277.

465. Mani, B.K., et al., *Kv7.5 Potassium Channel Subunits Are the Primary Targets for PKA-Dependent Enhancement of Vascular Smooth Muscle Kv7 Currents.* Mol Pharmacol, 2016. **89**(3): p. 323-34.

466. Xiong, Q., H. Sun, and M. Li, *Zinc pyrithione-mediated activation of voltage-gated KCNQ potassium channels rescues epileptogenic mutants.* Nat Chem Biol, 2007. **3**(5): p. 287-96.

467. Eid, B.G. and A.M. Gurney, *Zinc pyrithione activates K+ channels and hyperpolarizes the membrane of rat pulmonary artery smooth muscle cells.* PLoS One, 2018. **13**(2): p. e0192699.

468. Shapiro, M.S., et al., *Reconstitution of muscarinic modulation of the KCNQ2/KCNQ3 K(+) channels that underlie the neuronal M current.* J Neurosci, 2000. **20**(5): p. 1710-21.

469. Suzuki, Y., et al., *Caveolin-1 facilitates the direct coupling between large conductance Ca2+-activated K+ (BKCa) and Cav1.2 Ca2+ channels and their clustering to regulate membrane excitability in vascular myocytes.* J Biol Chem, 2013. **288**(51): p. 36750-61.

470. Kyle, B., et al., *Contribution of Kv2.1 channels to the delayed rectifier current in freshly dispersed smooth muscle cells from rabbit urethra.* Am J Physiol Cell Physiol, 2011. **301**(5): p. C1186-200.

471. Brueggemann, L.I., et al., *Differential activation of vascular smooth muscle Kv7.4, Kv7.5, and Kv7.4/7.5 channels by ML213 and ICA-069673.* Mol Pharmacol, 2014. **86**(3): p. 330-41.

472. Jepps, T.A., S.P. Olesen, and I.A. Greenwood, *One man's side effect is another man's therapeutic opportunity: targeting Kv7 channels in smooth muscle disorders.* Br J Pharmacol, 2013. **168**(1): p. 19-27.

473. Pyne, S. and N.J. Pyne, *Bradykinin-stimulated phosphatidylcholine hydrolysis in airway smooth muscle: the role of Ca2+ and protein kinase C.* Biochem J, 1995. **311 (Pt 2)**(Pt 2): p. 637-42.

474. Kim, R.Y., et al., *Atomic basis for therapeutic activation of neuronal potassium channels.* Nature Communications, 2015. **6**(1): p. 8116.

475. Kim, R.Y., S.A. Pless, and H.T. Kurata, *PIP2 mediates functional coupling and pharmacology of neuronal KCNQ channels.* Proc Natl Acad Sci U S A, 2017. **114**(45): p. E9702-e9711.

476. Al-Shboul, O., *The role of the RhoA/ROCK pathway in gender-dependent differences in gastric smooth muscle contraction.* J Physiol Sci, 2016. **66**(1): p. 85-92.

477. Murthy, K.S., *Signaling for contraction and relaxation in smooth muscle of the gut.* Annu Rev Physiol, 2006. **68**: p. 345-74.

478. Betrie, A.H., et al., *Zinc drives vasorelaxation by acting in sensory nerves, endothelium and smooth muscle.* Nature Communications, 2021. **12**(1): p. 3296.

479. Kosenko, A., et al., *Coordinated signal integration at the M-type potassium channel upon muscarinic stimulation.* Embo j, 2012. **31**(14): p. 3147-56.

480. Suh, B.C. and B. Hille, *Recovery from muscarinic modulation of M current channels requires phosphatidylinositol 4,5-bisphosphate synthesis.* Neuron, 2002. **35**(3): p. 507-20.

481. Winks, J.S., et al., *Relationship between membrane phosphatidylinositol-4,5-bisphosphate and receptor-mediated inhibition of native neuronal M channels.* J Neurosci, 2005. **25**(13): p. 3400-13.

482. Falkenburger, B.H., J.B. Jensen, and B. Hille, *Kinetics of PIP2 metabolism and KCNQ2/3 channel regulation studied with a voltage-sensitive phosphatase in living cells.* J Gen Physiol, 2010. **135**(2): p. 99-114.

483. Gamper, N., et al., *Phosphatidylinositol [correction] 4,5-bisphosphate signals underlie receptor-specific Gq/11-mediated modulation of N-type Ca2+ channels.* J Neurosci, 2004. **24**(48): p. 10980-92.

484. Caulfield, M.P., *Muscarinic receptors--characterization, coupling and function.* Pharmacol Ther, 1993. **58**(3): p. 319-79.

485. Wess, J., *Molecular biology of muscarinic acetylcholine receptors.* Crit Rev Neurobiol, 1996. **10**(1): p. 69-99.

486. Wickenden, A.D., et al., *Characterization of KCNQ5/Q3 potassium channels expressed in mammalian cells.* Br J Pharmacol, 2001. **132**(2): p. 381-4.

487. Brown, D.A., *Regulation of neural ion channels by muscarinic receptors.* Neuropharmacology, 2018. **136**(Pt C): p. 383-400.

488. Alkawadri, T., *Mechanisms underlying cholinergic contractions of airway smooth muscle and their regulation by beta-adrenoreceptor agonists*. 2022, Dundalk Institute of Technology.

489. Sun, J. and R. MacKinnon, *Structural Basis of Human KCNQ1 Modulation and Gating.* Cell, 2020. **180**(2): p. 340-347.e9.

490. Zaydman, M.A., et al., *Kv7.1 ion channels require a lipid to couple voltage sensing to pore opening.* Proc Natl Acad Sci U S A, 2013. **110**(32): p. 13180-5.

491. Suh, B.C., et al., *Rapid chemically induced changes of PtdIns(4,5)P2 gate KCNQ ion channels.* Science, 2006. **314**(5804): p. 1454-7.

492. Delmas, P. and D.A. Brown, *Pathways modulating neural KCNQ/M (Kv7) potassium channels.* Nat Rev Neurosci, 2005. **6**(11): p. 850-62.

493. Brueggemann, L.I., L.L. Cribbs, and K.L. Byron, *Structural Determinants of Kv7.5 Potassium Channels That Confer Changes in Phosphatidylinositol 4,5-Bisphosphate (PIP(2)) Affinity and Signaling Sensitivities in Smooth Muscle Cells.* Mol Pharmacol, 2020. **97**(3): p. 145-158.

494. Haick, J.M. and K.L. Byron, *Novel treatment strategies for smooth muscle disorders: Targeting Kv7 potassium channels.* Pharmacol Ther, 2016. **165**: p. 14-25.

495. Chadha, P.S., et al., *Pharmacological dissection of K(v)7.1 channels in systemic and pulmonary arteries.* Br J Pharmacol, 2012. **166**(4): p. 1377-87.

496. Yu, H., et al., *Discovery, Synthesis, and Structure Activity Relationship of a Series of N-Aryl- bicyclo[2.2.1]heptane-2-carboxamides: Characterization of ML213 as a Novel KCNQ2 and KCNQ4 Potassium Channel Opener.* ACS Chem Neurosci, 2011. **2**(10): p. 572-577.

497. Provence, A., J. Malysz, and G.V. Petkov, *The Novel KV7.2/KV7.3 Channel Opener ICA-069673 Reveals Subtype-Specific Functional Roles in Guinea Pig Detrusor Smooth Muscle Excitability and Contractility.* J Pharmacol Exp Ther, 2015. **354**(3): p. 290-301.

498. Higashida, H., et al., *Protein kinase C bound with A-kinase anchoring protein is involved in muscarinic receptor-activated modulation of M-type KCNQ potassium channels.* Neurosci Res, 2005. **51**(3): p. 231-4.

499. Taylor, K.C. and C.R. Sanders, *Regulation of KCNQ/Kv7 family voltage-gated K(+) channels by lipids.* Biochim Biophys Acta Biomembr, 2017. **1859**(4): p. 586-597.

500. Barrese, V., J.B. Stott, and I.A. Greenwood, *KCNQ-Encoded Potassium Channels as Therapeutic Targets.* Annu Rev Pharmacol Toxicol, 2018. **58**: p. 625-648.

501. Ford, C.P., et al., *Experiments to test the role of phosphatidylinositol 4,5-bisphosphate in neurotransmitter-induced M-channel closure in bullfrog sympathetic neurons.* J Neurosci, 2003. **23**(12): p. 4931-41.

502. Boyer, J.L., G.L. Waldo, and T.K. Harden, *Beta gamma-subunit activation of G-protein-regulated phospholipase C.* J Biol Chem, 1992. **267**(35): p. 25451-6.

503. Blank, J.L., K.A. Brattain, and J.H. Exton, *Activation of cytosolic phosphoinositide phospholipase C by G-protein beta gamma subunits.* J Biol Chem, 1992. **267**(32): p. 23069-75.

504. Smrcka, A.V. and P.C. Sternweis, *Regulation of purified subtypes of phosphatidylinositol-specific phospholipase C beta by G protein alpha and beta gamma subunits.* J Biol Chem, 1993. **268**(13): p. 9667-74.

505. Philip, F., et al., *Synergistic activation of phospholipase C-beta3 by Galpha(q) and Gbetagamma describes a simple two-state coincidence detector.* Curr Biol, 2010. **20**(15): p. 1327-35.

506. Rebres, R.A., et al., *Synergistic Ca2+ responses by G{alpha}i- and G{alpha}q-coupled G-protein-coupled receptors require a single PLC{beta} isoform that is sensitive to both G{beta}{gamma} and G{alpha}q.* J Biol Chem, 2011. **286**(2): p. 942-51.

507. Mizuta, K., et al., *Gi-coupled γ-aminobutyric acid-B receptors cross-regulate phospholipase C and calcium in airway smooth muscle.* Am J Respir Cell Mol Biol, 2011. **45**(6): p. 1232-8.

508. Rhee, S.G., *Regulation of phosphoinositide-specific phospholipase C.* Annu Rev Biochem, 2001. **70**: p. 281-312.

509. Stott, J.B., et al., *G-protein βγ subunits are positive regulators of Kv7.4 and native vascular Kv7 channel activity.* Proc Natl Acad Sci U S A, 2015. **112**(20): p. 6497-502.

510. Huang, F., et al., *Studies on expression and function of the TMEM16A calcium-activated chloride channel.* Proc Natl Acad Sci U S A, 2009. **106**(50): p. 21413-8.

511. Seo, Y., et al., *Ani9, A Novel Potent Small-Molecule ANO1 Inhibitor with Negligible Effect on ANO2.* PLoS One, 2016. **11**(5): p. e0155771.

512. Danahay, H., et al., *Potentiating TMEM16A does not stimulate airway mucus secretion or bronchial and pulmonary arterial smooth muscle contraction.* FASEB Bioadv, 2020. **2**(8): p. 464-477.

513. Wang, P., et al., *Inflammatory mediators mediate airway smooth muscle contraction through a G protein-coupled receptor-transmembrane protein 16A-voltage-dependent Ca(2+) channel axis and contribute to bronchial hyperresponsiveness in asthma.* J Allergy Clin Immunol, 2018. **141**(4): p. 1259-1268.e11.

514. Baba-Aissa, F., et al., *Distribution and isoform diversity of the organellar Ca2+ pumps in the brain.* Molecular and Chemical Neuropathology, 1998. **33**(3): p. 199-208.

515. Wray, S. and T. Burdyga, *Sarcoplasmic Reticulum Function in Smooth Muscle.* Physiological Reviews, 2010. **90**(1): p. 113-178.

516. Lipskaia, L., et al., *Expression of sarco (endo) plasmic reticulum calcium ATPase (SERCA) system in normal mouse cardiovascular tissues, heart failure and atherosclerosis.* Biochim Biophys Acta, 2014. **1843**(11): p. 2705-18.

517. Periasamy, M. and A. Kalyanasundaram, *SERCA pump isoforms: Their role in calcium transport and disease.* Muscle & Nerve, 2007. **35**(4): p. 430-442.

518. Thastrup, O., et al., *Thapsigargin, a tumor promoter, discharges intracellular Ca2+ stores by specific inhibition of the endoplasmic reticulum Ca2(+)-ATPase.* Proceedings of the National Academy of Sciences, 1990. **87**(7): p. 2466-2470.

519. Janssen, L.J., et al., *Muscarinic excitation-contraction coupling mechanisms in tracheal and bronchial smooth muscles.* Journal of Applied Physiology, 2001. **91**(3): p. 1142-1151.

520. Álvarez-Santos, M.D., et al., *Role of airway smooth muscle cell phenotypes in airway tone and obstruction in guinea pig asthma model.* Allergy, Asthma & Clinical Immunology, 2022. **18**(1): p. 3.

521. Boittin, F.X., et al., *Vasodilation by the calcium-mobilizing messenger cyclic ADP-ribose.* J Biol Chem, 2003. **278**(11): p. 9602-8.

522. James, P., et al., *Nature and site of phospholamban regulation of the Ca2+ pump of sarcoplasmic reticulum.* Nature, 1989. **342**(6245): p. 90-2.

523. Colyer, J., *Phosphorylation states of phospholamban.* Ann N Y Acad Sci, 1998. **853**: p. 79-91.

524. Simmerman, H.K. and L.R. Jones, *Phospholamban: protein structure, mechanism of action, and role in cardiac function.* Physiol Rev, 1998. **78**(4): p. 921-47.

525. Ghosh, S., et al., *Unravelling the Role of Post-Junctional M2 Muscarinic Receptors in Cholinergic Nerve-Mediated Contractions of Airway Smooth Muscle.* Int J Mol Sci, 2025. **26**(12).

526. Amrani, Y. and R.A. Panettieri, *Airway smooth muscle: contraction and beyond.* Int J Biochem Cell Biol, 2003. **35**(3): p. 272-6.

527. Ford, M.L., et al., *Integrative Roles of Pro-Inflammatory Cytokines on Airway Smooth Muscle Structure and Function in Asthma.* Immunological Reviews, 2025. **330**(1): p. e70007.

528. Gross, N.J., E. Co, and M.S. Skorodin, *Cholinergic bronchomotor tone in COPD: estimates of its amount in comparison with that in normal subjects.* Chest, 1989. **96**(5): p. 984-987.

529. Gross, N.J. and M.S. Skorodin, *Role of the parasympathetic system in airway obstruction due to emphysema.* New England Journal of Medicine, 1984. **311**(7): p. 421-425.

530. Matera, M., et al., *Pharmacology and therapeutics of bronchodilators revisited.* Pharmacological reviews, 2020. **72**(1): p. 218-252.

531. Cazzola, M., P. Rogliani, and M.G. Matera, *The latest on the role of LAMAs in asthma.* Journal of Allergy and Clinical Immunology, 2020. **146**(6): p. 1288-1291.

532. Cazzola, M., L. Calzetta, and M.G. Matera, *Long-acting muscarinic antagonists and small airways in asthma: Which link?* Allergy, 2021. **76**(7): p. 1990-2001.

533. Agache, I., et al., *The Bronchodilator and Anti-Inflammatory Effect of Long-Acting Muscarinic Antagonists in Asthma: An EAACI Position Paper.* Allergy, 2025. **80**(2): p. 380-394.

534. Caulfield, M.P. and N.J. Birdsall, *International Union of Pharmacology. XVII. Classification of Muscarinic Acetylcholine Receptorsa.* Pharmacological reviews, 1998. **50**(2): p. 279-290.

535. Zaagsma, J., A. Roffel, and H. Meurs, *Muscarinic control of airway function.* Life sciences, 1997. **60**(13-14): p. 1061-1068.

536. Barnes, P.J., *The role of anticholinergics in chronic obstructive pulmonary disease.* Am J Med, 2004. **117 Suppl 12A**: p. 24s-32s.

537. Belmonte, K.E., *Cholinergic pathways in the lungs and anticholinergic therapy for chronic obstructive pulmonary disease.* Proceedings of the American Thoracic Society, 2005. **2**(4): p. 297-304.

538. Roffel, A., et al., *Characterization of the muscarinic receptor subtype involved in phosphoinositide metabolism in bovine tracheal smooth muscle.* British journal of pharmacology, 1990. **99**(2): p. 293-296.

539. Chilvers, E.R., et al., *Formation of inositol polyphosphates in airway smooth muscle after muscarinic receptor stimulation.* J Pharmacol Exp Ther, 1990. **252**(2): p. 786-91.

540. Watson, N., H. Magnussen, and K.F. Rabe, *Pharmacological characterization of the muscarinic receptor subtype mediating contraction of human peripheral airways.* The Journal of pharmacology and experimental therapeutics, 1995. **274**(3): p. 1293-1297.

541. Barnes, P.J., *Muscarinic receptor subtypes in airways.* Life sciences, 1993. **52**(5-6): p. 521-527.

542. Roux, E., M. Molimard, and R. Marthan, *Muscarinic stimulation of airway smooth muscle cells.* General Pharmacology: The Vascular System, 1998. **31**(3): p. 349-356.

543. Hirota, S., P. Helli, and L.J. Janssen, *Ionic mechanisms and Ca2+ handling in airway smooth muscle.* Eur Respir J, 2007. **30**(1): p. 114-33.

544. Grandi, E., et al., *Interplay of voltage and Ca-dependent inactivation of L-type Ca current.* Prog Biophys Mol Biol, 2010. **103**(1): p. 44-50.

545. Wang, L., et al., *Inhibition of TRPC3 downregulates airway hyperresponsiveness, remodeling of OVA-sensitized mouse.* Biochemical and Biophysical Research Communications, 2017. **484**(1): p. 209-217.

546. Mažerik, J., et al., *Effects of TRPV4 channel blocker on airway inflammation and airway defense reflexes in experimentally induced model of allergic asthma.* Respir Physiol Neurobiol, 2023. **316**: p. 104123.

547. Jalava, N., et al., *Inhibition of Canonical Transient Receptor Potential Channels 4/5 with Highly Selective and Potent Small-Molecule HC-070 Alleviates Mechanical Hypersensitivity in Rat Models of Visceral and Neuropathic Pain.* International Journal of Molecular Sciences, 2023. **24**(4): p. 3350.

548. Guo, J. and G.G. Schofield, *Activation of muscarinic m5 receptors inhibits recombinant KCNQ2/KCNQ3 K+ channels expressed in HEK293T cells.* European Journal of Pharmacology, 2003. **462**(1): p. 25-32.

549. Ghosh, S., et al., *M2 muscarinic receptor-dependent contractions of airway smooth muscle are mediated by inhibition of Kv7 channels.* Am J Physiol Cell Physiol, 2026. **330**(4): p. C926-c942.

550. Yajima, T., et al., *Non-neuronal release of ACh plays a key role in secretory response to luminal propionate in rat colon.* J Physiol, 2011. **589**(Pt 4): p. 953-62.

551. Fujii, T., et al., *Expression and Function of the Cholinergic System in Immune Cells.* Front Immunol, 2017. **8**: p. 1085.

552. Knights, A.J., et al., *Acetylcholine-synthesizing macrophages in subcutaneous fat are regulated by β(2) -adrenergic signaling.* Embo j, 2021. **40**(24): p. e106061.

553. Semenov, I., J.T. Herlihy, and R. Brenner, *In vitro measurements of tracheal constriction using mice.* J Vis Exp, 2012(64).

554. Calzetta, L., et al., *Use of human airway smooth muscle in vitro and ex vivo to investigate drugs for the treatment of chronic obstructive respiratory disorders.* Br J Pharmacol, 2024. **181**(5): p. 610-639.